Silver based catalysts for the selective oxidation of cyclic hydrocarbons under mild conditions

Baozhai Han

A thesis submitted in partial fulfilment of the requirements for the degree of Doctor of Philosophy

The University of Sheffield
Faculty of Science
Department of Chemistry

11/09/2021

Author's Declaration

I, the author, confirm that the Thesis is my own work. I am aware of the University's Guidance on the Use of Unfair Means (www.sheffield.ac.uk/ssid/unfair-means). This work has not been previously been presented for an award at this, or any other, university.

Foreword

“Spend a straw-cloaked life in mist and rain”.

“Impervious to wind, rain or shine, I'll have my will.”

- Shi Su (1037-1101), Tune: Calming the Wave

Acknowledgments

Upon the completion of this thesis, I would like to dedicate my research work to all of those who have offered me tremendous assistance during these four years.

Firstly and importantly, I would like to express my sincere thanks to my supervisor, Dr. Marco Conte, a nice, dedicated and patient supervisor, for giving me this great opportunity and offering his professional support and encouragement in my PhD research. I do appreciate that the guide he offered for my research and the kind concerns for me, especially when I was in a low mood at some time, to inspire and encourage me with a passion into research and life. Thank you very much and give you my best wishes.

I am always feeling so grateful and lucky to be one member of Conte group, not only because we have a kind supervisor, but also the members within the group. I would like to give my sincere thanks to: James, Changyan, Prea, Dedi, Mohammod, Rebecca, Mengyuan, Ghadeer, Bahaj. It is a wonderful experience to work with all of you guys and thanks for making my four years research period being pleasure and meaningful. I do wish you enjoy your research and life.

I would also like to acknowledge the support from the staff in the department (past and present): Neil and Heather for the ICP analysis, Simon for GC-MS, Craig for XRD and NMR, etc., a lot of people who I want to give my sincere thanks. Meanwhile, thanks for the XPS analysis by Dr. David Morgan from the UK Catalysis Hub, Harwell, UK and TEM by Prof. Xi Liu who is from Shanghai Jiaotong University. Thank all of you for your assistance throughout my study period here, making me feel I was always supported not alone. I would also like to

express my thanks to my funding body, China Scholarship Council and the University of Sheffield, for their support to complete this research project.

Finally yet importantly, I would like to thank my big family and friends. My eternal gratitude would go to my parents and grandparents who are always standing with me tighter, giving me unconditional and endless love all the same. Without all of you, I would not go far away here, and I want to say I love you as much as you love me. In addition, I want to say to my loved grandfather, although you are not in this world, I can feel you never leave us alone and hopefully you will be pride of what I have acquired. Thanks to Changyan, it is quite a coincidence and luck to be a friend and co-worker with you and thank you for listening and sharing as well as support all the time. Thanks to Yu, it would be unforgettable time to spend with you during this abroad studying period in Sheffield. A lot of friends from China or UK I would like to express my gratitude, thank you and I wish all of you enjoy what you are doing and become who you want to be.

Abstract

This research work is centred on the selective oxidation of alkanes or cyclic alkanes by using molecular oxygen, and developing supported metal nanoparticles catalysts in a solvent-free system under mild conditions. It aims to design of novel supported metal nanoparticles for the direct oxidation of hydrocarbons to synthesize the corresponding oxygen-containing products like alcohols and ketones, which are valuable precursors for the manufacture of fibres, nylon and their derivatives. To this scope, Ag supported metal particles were developed, and these catalysts were capable of activating O_2 and the organic substrate.

In particular, a novel supported metal catalyst Ag/Nb_2O_5 was developed for the oxidation of cyclooctane and cyclohexane, which to the best of our knowledge it is firstly reported, developed and applied for catalytic purposes. A systematic study was conducted to investigate both the catalytic activity of Ag and Nb_2O_5 in cyclooctane oxidation, as well as the possibility of existence of other active species in the parent Nb_2O_5 or cyclooctane. This included a systematic evaluation on the effect of traces of water or alkyl hydroperoxides in cyclooctane and characterization of metal and support by means of XPS, XRD and TEM.

By using this new catalyst, it was possible to achieve conversion values of 81%, 13% for the substrates, cyclooctane, cyclohexane, respectively. With a total selectivity of ~70%, ~75% to the combination of ketone and alcohol (mainly ketone) generating from these substrates, posing a potential application of this catalyst in the production of oxygen containing products, especially for ketone. Given these promising results, the roles of supported Ag particles and Nb_2O_5 in the oxidation process were systematically investigated. It was found that Ag species

(Ag^0, Ag^+) could activate molecular oxygen to give reactive superoxide species, or Ag^+ was responsible for the direct dissociation of C-H bond, whereas metallic Ag^0 was proved to be effective for the abstraction of α-H in the crucial intermediates alkyl hydroperoxide to generate the corresponding ketones as a higher selectivity to ketones was found in comparison with Nb_2O_5 in the oxidation of cyclooctane and cyclohexane. Nb_2O_5 was also having an active role in the decomposition of alkyl hydroperoxides. In addition, based on the studies about the different reaction performance of Ag/Nb_2O_5 prepared by different methods: wet impregnation(WI), deposition precipitation(DP) and sol immobilization(SI), the impregnation protocol was the one that exhibited the highest catalytic activity towards C-H activation, which was probably because the method led to a relatively larger amount of Ag^+ species versus Ag^0 and correlated to a higher Ag loading. Moreover, in view of these results, a bimetallic supported catalyst with the incorporation of Fe was developed, with the aim to have a metallic partner promoting the initiation of the reaction and a metallic partner promoting the selectivity of the reaction, and therefore in practical terms to have a bifunctional catalyst. In this case supported $Ag\text{-}Fe/Nb_2O_5$ prepared by wet impregnation method exhibited a superior reactivity with an enhanced selectivity to ketone (~60%) and a higher K/A (ketone to alcohol) molar ratio (3.0) in comparison with supported monometallic Ag/Nb_2O_5.

According to the collected results, a simplified reaction scheme was proposed for the understanding of the catalytic performances of Ag/Nb_2O_5 to provide insight of the effects of active species in the oxidation process, laying foundation for the further exploitation of this catalyst into the oxidation of other hydrocarbons or alcohols.

Thesis contents

Chapter 1: Introduction

With the aims for the development of supported metal nanoparticles catalysts applied for the selective oxidation of alkanes or cyclic alkanes to produce the corresponding alcohols or ketones that are valuable building blocks for the manufacture of industrial materials, this chapter mainly involves several aspects: i) a fundamental understanding about the reaction mechanism of alkanes or cyclic alkanes oxidation and the challenging issues (the activation of O_2 and dissociation of C-H bond) to be solved for the achievement of selective oxidation; ii) on the ground of point i), the catalysts systems that can be applied for the oxidation were investigated, based on which we aimed for the development of supported metal nanoparticles catalysts and further the effects of properties of these catalysts on catalytic activity were discussed to provide insights for the designing of catalysts; iii) given a sufficient literature review about the supported metal catalysts in hydrocarbons oxidation and previous research work within our group, Nb_2O_5 was selected as support or active phase and supported Ag particles was expected to facilitate the activation of molecular oxygen. In view of all these discussions, a novel supported metal nanoparticle Ag/Nb_2O_5 was proposed to be applied in the oxidation of hydrocarbons in our thesis work.

1.1 Selective oxidation of hydrocarbons

The directly selective oxidation of hydrocarbons is an important process both in industry and academia to produce oxygen containing compounds by the transformation of petrochemical feedstocks[1-4], like methane, cyclohexane, ethylbenzene, cyclooctane. In the oxidation process, molecular oxygen or air are often employed for the partial oxidation of aryl

and cyclic hydrocarbons (e.g., cyclohexane, ethylbenzene) to desired corresponding alcohols or ketones with relatively low selectivity for undesired by products in comparison with other oxygen donor oxidants[3, 5-7], e.g. hydrogen peroxide, nitric acid. The use of molecular oxygen is because it is cheap, nontoxic from economic and environmental-friendly perspectives, and the by-product is usually water from O_2. Nowadays, more than 90% of organic compounds are derived from petrochemicals that are saturated hydrocarbons[6] and numerous efforts have been put into the selective oxidation for the manufacture of precursors like alcohols or ketones that are among the major building blocks for the polymer industry, such as fibres, plastics and coatings. For example, several million tons of terephthalic acid (TPA) are produced every year, which is an important precursor to produce polyester (PET) used to make clothing and plastic bottles[8]. A large amount of TPA is produced via the oxidation of *p*-xylene catalysed by cobalt, manganese, and bromide compounds (hydrobromic acid HBr, sodium bromide NaBr) in acid acetic medium and using air as oxidant (AMOCO process)[8-10]. Besides, the liquid phase oxidation of cyclohexane for the yield of cyclohexanol and cyclohexanone (K/A oil, ca. 10^6 tonne per year), both of which are important precursors of adipic acid or ε-caprolactam that are building blocks for the commercial manufacture of nylon-6 and nylon-6,6[2, 11]. The formed K/A oil from the direct oxidation of cyclohexane can be furtherly converted into adipic acid or ε-caprolactam in the presence of acid catalysts, as demonstrated in Fig. 1.1[2]. It should be noted in the industrial scale, the manufacture of K/A oil is achieved via an autoxidation process, as discussed in the following part.

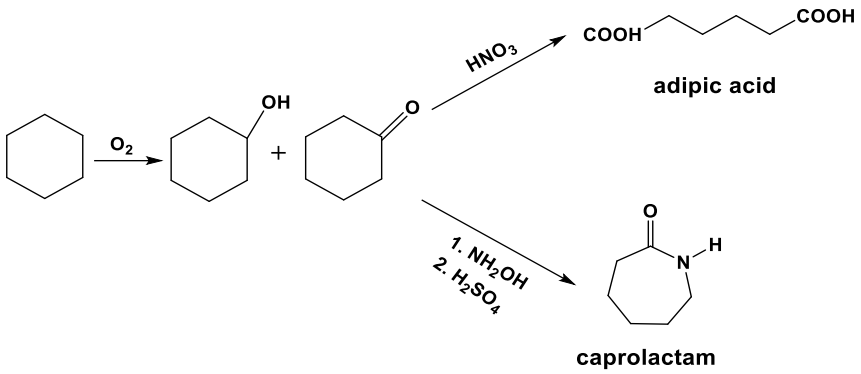

Fig. 1.1 Schematics for the oxidation process for the conversion of cyclohexane to adipic acid or ε-caprolactam[2]. Reprinted from ref. 2 with permission from Elsevier.

1.1.1 Autoxidation

Autoxidation is an ever-present process in the oxidation of hydrocarbons. This process involves the oxygenation of hydrocarbons by means of ground state (triplet) molecular oxygen in the liquid phase, leading to the formation of organic hydroperoxides as primary intermediates through a free-radical chain pathway, followed by the decomposition of alkyl hydroperoxides to other products (i.e., alcohols, ketones, acids)[12]. The autoxidation process is usually uncontrolled, leading to a large number of undesired products, even at a low conversion, but it still receives much attention as it plays an important role in the chemistry for the manufacture of valuable oxygenated compounds. For example, there are two large scale process where this series of reactions are used deliberately: cyclohexane oxidation to produce cyclohexanol and cyclohexanone (K/A oils, $6 \cdot 10^6$ tons/per year)[13] and terephthalic acid ($3 \cdot 10^7$ tons/per year) from *p*-xylene oxidation[8]. It is because of the extreme significance of these processes, both at industrial level and the nature as well as a very large demand for the products that are obtained from this process, that many studies were, and are carried out in

literature to exploit the use of molecular oxygen as oxidant for other hydrocarbon oxidation processes.

Autoxidation process can be illustrated by radical chain mechanism, as displayed in scheme 1.1. In an initiation step (eq. 1.1), C-H bond undergoes homolytic cleavage to generate free-radicals. The initiation of autoxidation can be triggered by the presence of an initiator which is minor amount of alkyl hydroperoxide residues (eq. 1.2) in the starting materials[14], or even promoter like the metal walls of a reactor (and any trace of metal that can be found even in glassware) when there is no additional initiator added. The formed R· radicals interact with ground state oxygen O_2 to form alkyl peroxy radicals, which is considered as energetically barrierless step practically controlled by diffusion-limitation only[15]. Subsequently peroxy radicals abstract H atoms from the substrate to regenerate R· and alkyl hydroperoxides, which could undergo homolytic cleavage to give RO· and ·OH, both of which are reactive radicals to propagate the autoxidation process. This is in fact a branching reaction, that generates more and more radicals during the process, and unless termination occurs it can, in principle, carry on indefinitely up to consumption of the reagents. The termination step involves the interaction of two alkyl peroxides to yield an equal amount of alcohol and ketone. Consequently, the molar ratio of alcohol and ketone for a given hydrocarbon substrate would be expected to be 1 at low conversion (i.e., absence of parallel reaction routes) and absence of any catalyst capable to induce any kind of selectivity control.[13, 16]

Initiation:

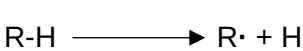

(eq. 1.1)

R-H + iniator (ROO· as example) ⟶ R· + ROOH **(eq. 1.2)**

Propagation:

R· + O_2 ⟶ R-OO· **(eq. 1.3)**

ROO· + R-H ⟶ ROOH + R· **(eq. 1.4)**

R-OOH ⟶ RO· + ·OH **(eq. 1.5)**

RO· + R-H ⟶ R-OH + R· **(eq. 1.6)**

·OH + R-H ⟶ H_2O + R· **(eq. 1.7)**

ROO· + ROOH ⟶ ROOH + (R·)OOH **(eq. 1.8)**

(R·)OOH ⟶ R=O + ·OH **(eq. 1.9)**

Termination:

ROO· + ROO· ⟶ R-O + R=O + O_2 **(eq. 1.10)**

Scheme 1.1 A simplified process of hydrocarbons autoxidation in the absence of added initiator or catalysts. The initiation of reaction can be achieved by the presence of initiator (alkyl hydroperoxides in this case, eq. 1.2). The cleavage of O-O bond (eq. 1.5) of alkyl hydroperoxides would give alcohols and the abstraction of α-H (eq. 1.8) from alkyl hydroperoxide generates ketones.

However, despite its popularity, the simplified scheme does not account for additional interactions within the various intermediates generated during the process or interactions with the walls of the reactors, and practically any reaction mixture originated from autoxidation always has an excess of ketone - usually with a molar ration of 2:1 - with respect to the alcohol.[11, 17, 18] For example, literature studies for cyclohexane autoxidation, revealed that the rate constant of initiation was proportional to an initially added ketone concentration, which also agreed with arising increase of initiation rates with the proceeding of reaction, suggesting a bimolecular reaction between cyclohexyl hydroperoxide and cyclohexanone.[17, 19] From this

perspective, the formed ·OH radicals from the dissociation of cyclohexyl peroxide (Cy-OOH) possibly abstracts a weakly bonded α-H of cyclohexanone (Cy=O), as shown in eq. 1.11.

$$CyOOH + Cy{=}O \longrightarrow CyO\cdot + \cdot Cy{=}O + H_2O \quad \textbf{(eq. 1.11)}$$

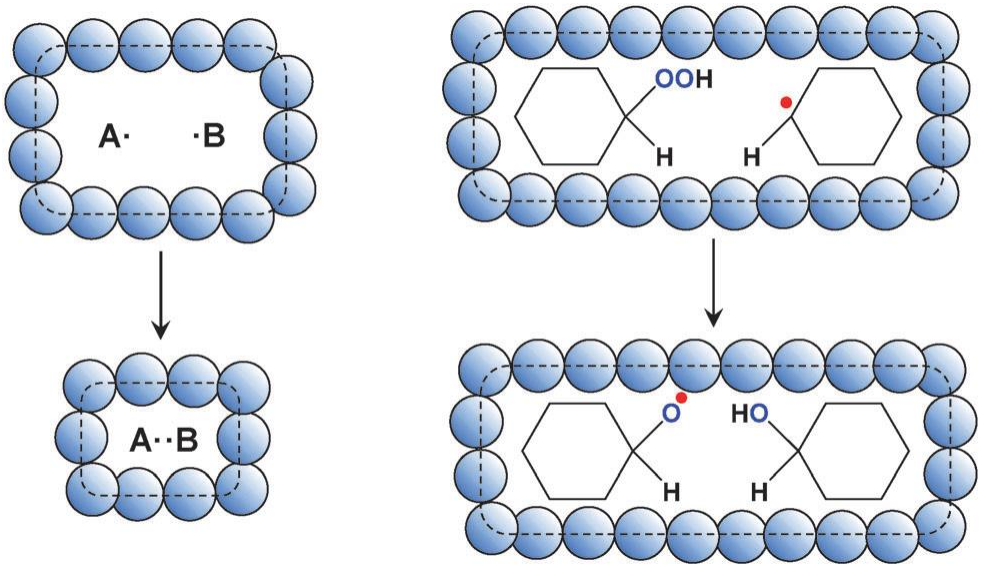

Fig. 1.2 Radical recombination in the solvent cage (shown on the left) and the radical recombination reaction of alkyl peroxide and alkyl radical (the right part) to give alkoxyl radical and alcohol.[20] Reproduced from Ref. 20 with permission from the PCCP Owner Societies.

In addition, the presence of solvent cage (a phenomenon that the possibility of recombination of generated radical pairs is higher in solution than that in gas phase) might affect the autoxidation by constraining the radical intermediates (Fig. 1.2), especially for the oxidation process taking place in liquid phase[20]. By considering this, there is then an alternative reaction pathway capable of generating ketone and alcohol before the termination step[21], which can then affect the final selectivity of the reaction. It should be mentioned that the characterization of reaction products needs to be taken into account in order to unveil reaction mechanisms. This is not a trivial exercise, as tens (> 40%) of by-products can be

formed during the autoxidation of hydrocarbons including acids, esters[22], which can also react among them, for example the dehydration of an alcohol by an acid with subsequence double bond formation and this can further react to further by-products and so on. Furthermore, under autoxidation conditions, the reaction is controlled by the diffusion of O_2, making the oxidation take place in a diffusion regime rather than kinetic regime, which can further affect the product distribution in an undesired manner.

According to the above discussion, the complexity of autoxidation makes this process proceed in an unselective way, leading to a complex reaction mixture, and in turn product distribution, which has to be taken into account if to be used for structure activity correlations for catalyst development and design. Thus, the manipulation of catalytic decomposition of alkyl hydroperoxides can be an important tool to modify selectivity patterns in autoxidation reactions.[19] In our case, the autoxidation of cyclic hydrocarbons (mainly cyclooctane and cyclohexane) in the absence of initiators or catalysts will be investigated firstly, as a benchmark for the evaluation of catalysts on conversion and selectivity and to minimize the effects of blank autoxidation to distinguish the reaction performances of catalysts. Given the types of catalysts, that is usually classified into heterogenous catalysts, homogeneous catalysts or enzymes, and their applications in various reactions, we mainly discuss about the homogeneous and heterogeneous catalysts in the next part to explore an appropriate catalyst type in the oxidation of hydrocarbons according to our aims in this project.

1.1.2 Homogeneous catalysis

In the oxidation of hydrocarbons to corresponding alcohols and carbonyl compounds, homogeneous catalysts can play an important role in selectively converting the reactants to desired products. Homogeneous catalysts are normally well-structured complexes, e.g. transition metal complexes, heteropoly acid[23]. Heteropoly acids are widely used for the reactions in homogeneous liquid phase, which have higher catalytic activity than mineral acids[24]. For example, the hydration of propene to propanol that can be used in paints, coatings and dyes, catalysed by heteropoly acids is an important industrial process[25]. Many industrial manufacture processes, such as hydrogenation, isomerization, polymerization, carbonylation and epoxidation, have been achieved by transition metal (mostly by using Rh, Co, Cr, Mo, V, Ni) complexes[23, 26, 27]. For instance, the production of terephthalic acid (TPA) from the oxidation of *p*-xylene is catalysed by cobalt (Co), manganese (Mn) acetates and bromide ions (Br^-) with acetic acid medium, which is a homogeneous catalysis process[8]. Research indicates that the initiation was done by hydrogen abstraction from the hydrocarbon by bromine radicals generated through bromide ion oxidation by the metals, and the decomposition of peroxides to form oxygenate products was catalysed by Co and Mo[9]. However, the major problem with this process is the use of highly corrosive bromide salts, which not only increases the running costs largely but also poses environmental threat. The oxidation of cyclohexane in industrial scale is achieved without or in the presence of transition cobalt salts Co(II)-naphthenate, Co(II)-$(acac)_2$ or Fe(III)-$(acac)_3$ [20] for the production of cyclohexanol and cyclohexanone (K/A oil). During the oxidation, cyclohexyl hydroperoxide (CyOOH, Cy denotes C_6H_5) undergoes

homolytic cleavage in the presence of transition metals and these metals take parts in this process through a one electron switch (e.g., Co^{2+}, Mn^{2+},and Cr^{2+}), which is called Haber-Weiss cycle[13, 28], as shown in scheme 1.2.

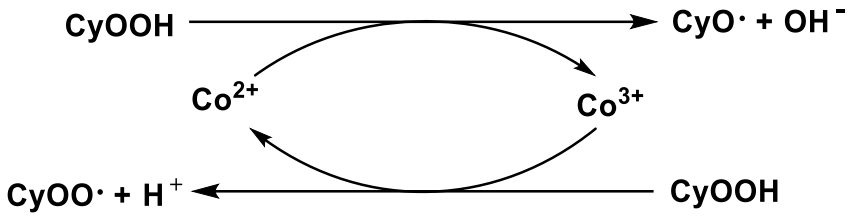

Scheme 1.2 Decomposition of cyclohexyl hydroperoxide (CyOOH) by cobalt-based catalysts in Haber-Weiss cycle.[13] Transition metal Co^{2+} undergoes a one-electron switch to catalyse the decomposition of CyOOH to initiate the process.

As the homogeneous catalysts are soluble in reaction media and no carriers are utilised as support, there aren't, practically, mass transfer limitations induced by diffusion phenomena to/from the surface or pores of a catalyst. While bulk mass transfer might affect the reaction especially for the reaction process involve gases, such as the starvation of O_2 in the liquid phase in *p*-xylene oxidation with gaseous molecular oxygen[29]. In this case, the dissolution of gases into the liquid phase can be enhanced by using high pressure or vigorous stirring to strengthen mass transfer. Moreover, the separation or recovery of catalysts is quite challenging in the field of homogeneous catalysis. It is reported that distillation can be employed as long as there is obvious difference in vapor pressure of the products and catalyst; and ion exchange with an appropriate sequestering agent like amine compounds proves to be effective for the recovery of catalysts[30]. However, from an economic perspective, the recovery (if any) and reuse of homogeneous catalysis is a complex process that adds to the costs of the process, and in the assumption that a recovery is possible.

In general, homogeneous catalysis exhibits the advantages of higher activity or selectivity, efficient heat transfer and milder reaction conditions, compared with heterogeneous catalysis[31]. However, the shortcomings in separation of the products and the catalyst from the reaction mixture, and issues associated to the regeneration and recovery of the catalysts, as well as continuous processing, limit the further commercial applicability of these systems and current researches are focused on the development of heterogeneous catalysts instead[32]. By considering all these factors, heterogeneous catalysis could address these issues to some extent. Consequently, in our case, we mainly focused on the study and development of heterogeneous catalysis in this thesis work.

1.1.3 Heterogeneous catalysis

According to the discussion about the applications of homogeneous and heterogeneous catalysis, a comparison is drawn as illustrated in Fig. 1.3. Although homogeneous catalysts display high activity with more accessible active sites for the interaction with reactants, from the industrial perspective for economic consideration, heterogeneous catalysis exhibits the advantages of easier separation and recovery and can be used for continuous flow processes. However, heterogeneous catalysis can be affected by some drawbacks that could limit the further application, such as the sintering of supported metal species, loss of active species in solution[33], mass transfer limitation[34], undesired changes of oxidation state or phase transitions, the difficulty to study and identify the mechanism due to the multiphase of reaction[35]. These are all factors that should be addressed in the application and design of heterogeneous catalysts, especially if aimed at preserving a high reactivity and selectivity at the same time.

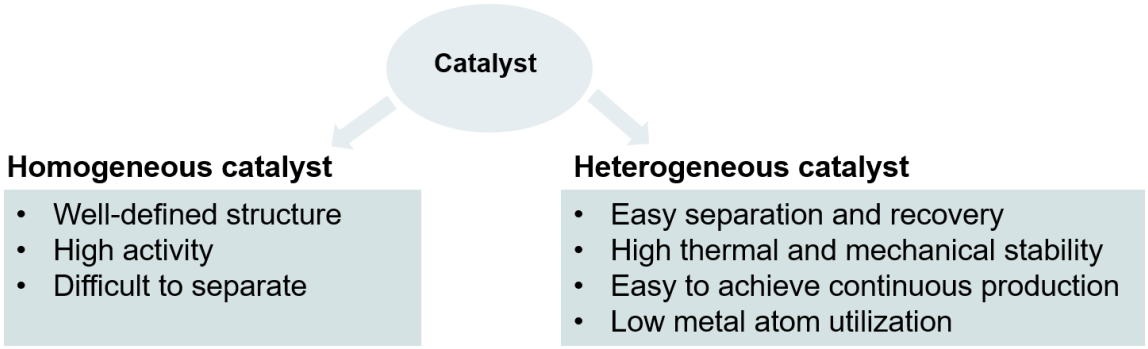

Fig. 1.3 Advantages and disadvantages of heterogeneous and homogeneous catalysts.[31, 36]

Almost 90% of the chemical processes proceed with the presence of catalysts and the usage ratio between heterogeneous and homogeneous catalysis among these processes is around 75:25.[35, 37] As explained in the previous section, one of the most important reasons for the preference of heterogeneous catalysts, especially for scale up or industrial applications, is the easier separation from the reactants and products after reaction. Furthermore if the reaction is carried out in a continuous flow (i.e. in our context is batch to batch) the use of a catalytic bed allows for this option, which is precluded when a homogenous catalyst is used.[38] In general, a heterogeneous catalytic cycle can be divided into the following steps (as shown in scheme 1.3): i) diffusion of the reactant(s) from a fluid phase to the surface; ii) adsorption of the reactant(s) to the catalytic surface; iii) chemical reaction and product(s) formation; iv) desorption of the product(s) from the surface; v) diffusion of the product(s) to the fluid phase. It should be noted however, that often porous materials are used to provide high surface area for the deposition of catalytically active species (mostly metal centres) and enhance the interaction between reactants and active sites. On the other hand, this can also create issues of internal diffusion of reactants and products. Heterogeneous catalysis is constantly playing a significant role in the oil refining and the production of bulk chemicals, such as the production

of ethylene oxide, acrylonitrile and maleic anhydride[31]. Sheldon *et al.*,[39] divided the heterogeneous catalysis into five categories in the organic synthesis field: solid-acid catalysis, solid-base catalysis, catalytic hydrogenation and dehydrogenation, catalytic oxidation, and catalytic C-C bond formation, among which the selectivity catalytic oxidation, e.g. hydrocarbons oxidation, alcohol oxidation, are pivotal reactions in fine chemistry.

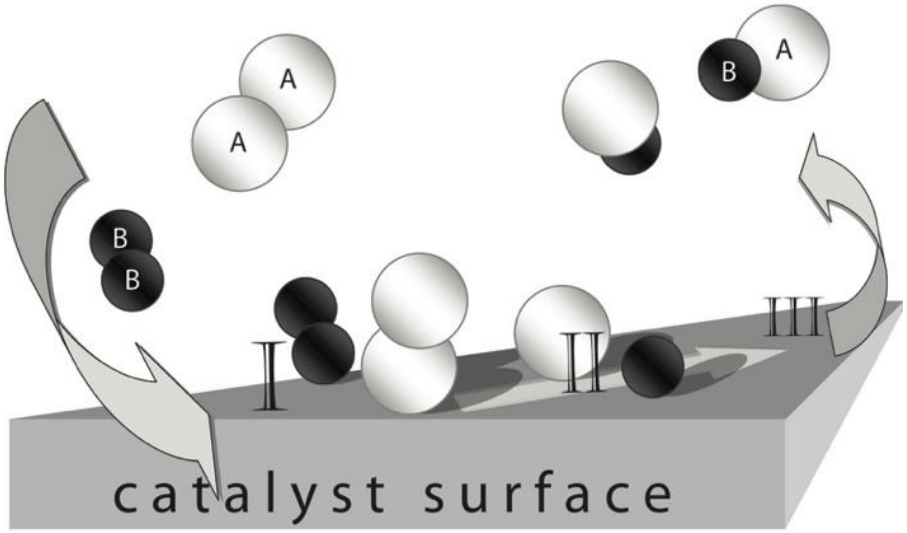

Scheme 1.3 A simplified elemental steps in a heterogeneously catalytic cycle[40]. This diagram illustrates a heterogeneous catalytic cycle involving the steps: adsorption of reactants on the catalyst surface; interaction between reactants; desorption process of product(s).

Among the heterogeneous catalysts, supported metal catalysts have been widely applied and studied in the oxidation of hydrocarbons or corresponding alcohols. There are numerous noble metals and transition metals that have been applied for oxidation processes, such as Au, Pt, Pd, Co, Fe, Mn, as they display unique properties when supported as metal or metal oxide nanoparticle. For example, supported gold catalysts with the supported particle size below 5 nm can display remarkable activity for selective oxidation reactions like the propene epoxidation[41], or higher alkanes (cyclohexane, styrene, cyclooctene)[42, 43]. Co-based catalysts

have shown high activity in the alkenes oxidation and a lot of researches focusing on the cobalt oxide supported on different supports (Co/MCM-41, Co/SBA-15) have been made to improve the activity[44, 45]. In this perspective Ag represents an attractive catalytic system, which has been utilised in some reactions, like ethylene epoxidation[46, 47], styrene epoxidation[48-50], carbon monoxide[51], soot[52, 53], but receives limited studies for the oxidation of cycloalkanes like cyclohexane or cyclooctane, which will be investigated in this thesis work for a novel application. To date Ag is industrially employed for ethylene epoxidation to produce ethylene oxide (up to 80% selectivity) that is a valuable intermediate for the manufacture of ethylene glycol (an ingredient in antifreeze), poly(ethylene oxide) as well as surfactants[54] and dehydrogenation of methanol to formaldehyde[55], which poses an industrial prospect of supported Ag catalysts. In view of the promising results in the application of Ag based catalysts, a further literature investigation about the effects of Ag nanoparticles is demonstrated in section 1.4, based on which we will mainly focus on the development of supported Ag nanoparticles in hydrocarbons oxidation.

1.1.4 Challenges and prospects of hydrocarbons oxidation

The selective oxidation of hydrocarbons plays a significant role in the modern chemical industry to provide many essential intermediates and precursors for high-value chemical products.[56, 57] During the process, the chemoselective activation of C-H bonds is one of the foremost challenges[58]. However, due to the high activation energy of C-H bond of hydrocarbons (table 1.1), typically in the range of 395-470 $kJ \cdot mol^{-1}$ [59, 60], the cleavage of C-H bonds generally requires harsh reaction conditions, such as high temperature and pressure,

corrosive and expensive media[61]. For instance, the production of terephthalic acid is achieved via *p*-xylene oxidation with air in acetic acid as a solvent, which is carried out at 175 - 225 °C and 15 - 30 bar[8]. It should be noted, however, that the oxidation of hydrocarbons leads to products (alkyl hydroperoxides, ketones, alcohols) for which C-H bonds in alpha to oxygenated groups have a lower bond dissociation energy and in turn a higher reactivity – than the correspondent saturate hydrocarbons, over the consequence is then these products are actually easier to oxidise than saturated parent hydrocarbons[62]. The conditions often make the reaction difficult to be controlled and finally leads to the generation of thermodynamically stable undesired products, e.g., CO_2 and H_2O. In view of this, the selective functionalisation of C-H bond with high yields and selectivity for generation of oxfunctionalised products under mild reaction conditions (relatively lower temperature and pressure) is of great significance. Generally, the challenges in a selective oxidation process are reflected in[61]: it is difficult to obtain a high selectivity for desired products in the presence of free-radical pathways; generally saturated hydrocarbons exhibit no basic or acidic properties and they tend to be unreactive with nucleophiles or electrophiles, except some reactive species like super acids[63, 64] (e.g. antimony pentafluoride in the oxidation of benzene). With this framework in mind, the direct aerobic oxidation of hydrocarbons by using O_2 or air as oxidants is in principle an environmentally friendly process and it is cheaper in comparison with other oxygen transfer reagents like H_2O_2 and *tert*-butyl hydroperoxide, which usually are costly to limit the industrial application and tend to lead to the generation of undesirable by-products.[65, 66] In view of these aspects, the development of an efficiently catalytic process for the aerobic oxidation of

hydrocarbons by employing molecular oxygen and the preferential use of heterogeneous catalysts is a challenging and important research area.

An important parameter to be considered in the oxidation of hydrocarbons is the activation of both C-H bond and O_2, which should be achieved in catalytic process. A parameter often used to quantify these reactivity aspects is the C-H bond dissociation energy (as shown in table 1.1). This is relevant because in the presence of transition metal catalysts, (either homogenous or heterogeneous) the activation of a C-H bond generally includes two steps[67]: i) the coordination of C-H bond on a transition metal centre; and ii) the formation of a metal carbon bond by the cleavage of C-H bond. From literature studies the main pathways for C-H bond activation systems are[67]: sigma bond metathesis, oxidative addition, and electrophilic substitution. However, although the activation of a C-H bond is a fundamental pre-requisite for the reactivity of a hydrocarbon, it does also worthy to bear in mind that for our applications a high selectivity to a desired product is also an important parameter in catalysts and process developments.[62, 68] This is especially true in hydrocarbon oxidation, various products, can be formed from the reactants by involving processes like: chain or cyclic hydrocarbons cleavage, oxygen insertion for the formation of alcohols, ketones and the dehydrogenation, which is related to the catalysts and reaction conditions[62]. By considering this, the use of catalysts should be able to enhance the oxidation in a more selective way under mild reaction conditions and to minimize the generation of undesirable by-products and minimize waste. In our case, we mainly focus on the application of supported metal catalysts to drive the oxidation process selectively. On the other hand, the activation of O_2 represents a big challenge as O_2 in the

ground triplet state is kinetically inert towards the oxidation of saturated hydrocarbons, but if activated it can then end up to highly reactive species (e.g., hydroxyl radicals, hydroperoxides, or peroxides) that react very quickly and are difficult to control instead[66]. A method to activate triplet state oxygen but in a 'controlled' way is by using transition metals at a specific oxidation state, where oxygen superoxide is formed by the electron transfer from metal centre to a triplet state oxygen (eq. 1.12)[20, 69]. The commonly used transition metals to achieve this process usually contain unpaired electrons, such as Fe, Cu, Mo, Co. In addition, it should be mentioned that in some cases by using supported metal catalysts in which metal oxides (e.g., CeO_2, TiO_2) act as support, O_2 serves the roles for the regeneration of metal oxides, as the surface lattice of oxygen in metal oxide is partially involved in the reaction[70].

$$M^{n+} + {}^{\bullet}O\text{-}O^{\bullet} \longrightarrow M^{(n+1)+} - O\text{-}O^{\bullet -} \qquad \textbf{(eq.1.12)}$$

Table 1.1 C-H and O-H bond dissociation energy of some relevant organic compounds[60].

Compound	Formula	C-H bond energy (kcal·mol^{-1})	C-H bond energy (kJ·mol^{-1})
Methane	CH_4	105	439
Methylene	CH_2	101	423
Methine	C-**H**	81	339
Benzene	C_6H_5-**H**	113	473
Toluene	$C_6H_5CH_2$-**H**	90	377
Tert-Butanol	$(CH_3)_3CO$-**H**	106	443
Phenol	C_6H_5O-**H**	90	377
Hydrogen peroxide	HOO-**H**	88	368
Cyclohexane	C_6H_{11}-**H**	99	414
Cyclooctane	C_8H_{15}-**H**	92	385
Ethylbenzene	C_6H_5-C**H**$_2$-CH_3	85	356

1.2 Supported metal nanoparticles catalyst

1.2.1 Development and applications in catalysis

As in this thesis work, we have mainly focused on the development of supported metal nanoparticle catalysts, the properties of these materials will be described in this introduction. Metal nanoparticles with the particle size range of 1-100 nm show unique properties that are different from bulk metal, especially high reactivity of some nanostructured noble and transition metals[71]. For instance, although bulk gold is inert, gold nanoparticles catalysts with particle size below 5 nm have shown a great application in many reactions, e.g., CO oxidation, hydrogenation, selective oxidation of hydrocarbons and alcohols, water gas shift reaction[50, 72-75]. However, due to the stability of gold under normal conditions in the earlier days, it was thought to be a catalytically inert metal, and some earlier research showed that gold as a catalyst was not superior to others[76]. In 1973, Bond et al. investigated about the hydrogenation of olefins by using supported gold catalysts, and it was proved that supported gold as a heterogeneous catalyst could be active in the hydro chlorination of ethyne[77] and CO oxidation[78] afterwards. Based on these pioneering studies, gold nanoparticle was considered to be catalytically active in some reactions with excellent performances. Metals like Pd, Pt, Ni, Ru can also exhibit a similar behaviour when in nanoparticulate form, by displaying new catalytic properties, if compared to their bulk counterpart. For example, Pt in bulk state is a reducing or inert metal, but supported Pt nanoparticles are used in the selective oxidation of alcohols to the corresponding carbonyl compounds [79], aerobic epoxidation of alkenes[80], and CO to CO_2[81]. Supported Pd nanoparticles exhibited reactivity in C-C bond formation properties,

as described by the Suzuki, Heck and Sonogashira reactions[82]. Supported bimetallic and multimetallic nanoparticles were developed, and still in progress, in recent years to improve the catalytic performance of catalysts and for an economic perspective[83]. Currently, supported metal nanoparticles are attracting more and more attention in academic research and their application in industry field needs to be more exploited.

The preparation of supported nanoparticles can, generally speaking, be achieved by two distinct ways[83], which are: i) subdivision of bulk metals to smaller units by a physical route; ii) the growth and deposition of nanoparticles from molecular or ionic precursors, that is, a chemical method. It should be underlined, however, that the control of the atom aggregation is one of the most challenging steps, and because of these challenges an array of preparation methods with the aim to obtain uniformly dispersed nanoparticles were developed over the years including impregnation, deposition-precipitation, coprecipitation, sol immobilization protocol (see section 2.2.1), all of which are commonly used for the preparation of supported metal nanoparticles that exhibits different properties and catalytic reactivity. The control of metal nanoparticles properties, such as: particle size, shape, composition, oxidation state, is a central research topic on its own, because all these are important factors to drive the reactivity of these clusters towards a chemical reaction. Therefore, the investigation about the effects of these factors on nanoparticles is quite important to tailor certain catalyst for reactions. These aspects will be described in detail in chapters 5 and 6, for the establishment of a structure activity relationship in the oxidation of cyclooctane and cyclohexane, providing for the design of this supported metal catalyst.

1.2.2 Influencing factors on catalytic reactivity

There are many factors which have significant effects on the catalytic reactivity of supported metal catalysts, such as: particle size, type of support, oxidation state of active metals, chemical composition and crystallographic phase of a catalyst, and shape of supported particles. In this section, we will discuss the correlation of these factors and their implications in terms of catalytic activity. It should also be stressed though, that some of these factors could mutually affect each other [84], consequently, the interrelated contribution of these factors to the reactivity of nanocatalysts, although often difficult to unveil, should be considered if aimed to the design of new materials.

1.2.2.1 Particle size

Haruta et al.,[41, 78] firstly observed significant changes in the catalytic activity and selectivity for the CO oxidation when the size of supported gold particles was below 5 nm, demonstrating the effects of nanoparticle size on catalytic properties and arousing the study about the influence of metal nanoparticle size. Ono et al.,[85] revealed that the catalytic activity increased with the reduction of gold nanoparticle size, leading to the increase of low-coordinated sites[86], and it was found the observed catalytic reactivity for CO oxidation was mainly determined by particle size while the charge transfer from metal oxide support to the nanoparticle surface and the interaction between reactants with nanoparticle support perimeter surfaces exhibited no obvious effect on reactivity[86]. In addition, supported Pd over silica-alumina for the oxidation of various alcohols was found that the particle size in the range of 3.6 nm to 4.3 nm exhibited the highest turnover frequency (TOF, refers to the number of reacted molecules per surface

active site per time in a reaction) for benzyl alcohol conversion[87]. Silica-supported phosphine-stabilized Au nanoparticles displayed effects of size of Au nanoparticles on the catalytic activity in cyclohexane oxidation, demonstrating that the Au(0) nanoparticles with size > 2 nm were active in the cyclohexane oxidation, and the increase of nanoparticles size led to the decrease of conversion[88]. Similarly, catalytically active Ag nanoparticles in the range of 2-10 nm supported over ZrO_2 were found to be mostly active for soot oxidation, whereas Ag clusters and larger particles were observed no obvious correlation with catalytic activity and the amount of adsorbed oxygen on Ag nanoparticles played a significant role in reaction rate[89]. It is also reported that particle size of supported Ag catalysts could affect the relative populations of the nucleophilic and electrophilic oxygen species in ethylene epoxidation, and nucleophilic oxygen is only observed in the particle with size larger than 30 nm[90]. The particle size of Ag can be controlled by the preparation method, which furtherly affects the activity and selectivity for the oxidation of ammonia to nitrogen[91]. The size of supported Ag nanoparticles over Al_2O_3 prepared by impregnation method falls in the range of 3.5-25 nm in diameter and larger size is found from 12-50 nm in the catalyst prepared by solgel methods. The former Ag/Al_2O_3 with smaller Ag nanoparticles affords a higher activity with a poor selectivity for the formation of N_2 while larger Ag nanoparticles result in a high N_2 selectivity with lower activity in comparison. From this perspective, in the aerobic oxidation by using molecular oxygen, the particle size of Ag appears to be an important parameter to influence the catalytic activity. Thus, in our case, the particle size of supported Ag will be controlled and the effect on the oxidation of cyclooctane and cyclohexane will be investigated (see section 5.6.2 in chapter 5).

Many models have been established for the explanation of high activity of metals on nanoscale, which can be described as Fig. 1.4[92]. Herein, it is proposed that the size dependent reactivity can be attributed to several factors: i) non-metallic behaviour (quantum size effects) of metal nanoparticles; ii) the increased number of low coordinated atoms; iii) extra electronic charge between the nanoparticles and support; iv) the presence active perimeter sites due to the interaction of nanoparticles and support. However, it should be noted that although the decrease of nanoparticle size can result in the increase of low coordinated atoms for the accessible interaction with reactants, smaller size is not always favoured as the dominating factor for reactivity might be other aspects like oxidation state, support instead of size, and selectivity of desirable product could be decreased because smaller nanoparticles may enhance the formation of undesired products. For example, Ag/ZrO_2 prepared by impregnation method with Ag particles smaller than 5 nm shows low activity for the complete oxidation of methane and the conversion improves with the size increase from 5 to 10 nm, while the catalytic activity mainly depends on Ag state and dispersion[55]. Therefore, it is essential to take all these factors into account when investigating about the size effect on catalytic reactivity during the process of tailoring a catalyst for specific reaction.

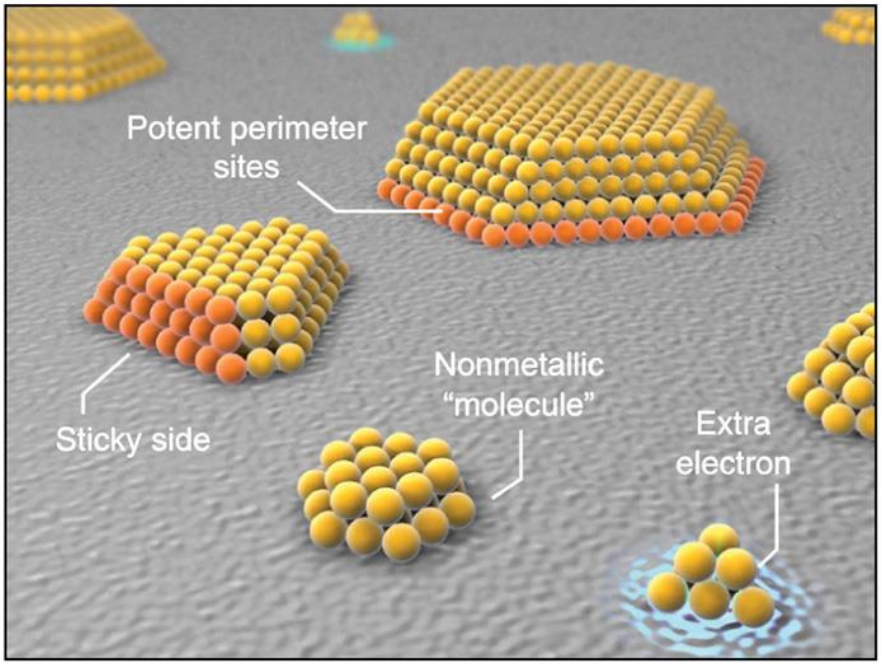

Fig. 1.4 Depiction of the possible active sites responsible for the enhanced activity in nanoparticle scale.[92] From A. Cho, Science, 299 (2003) 1684. Reprinted with permission from AAAS.

1.2.2.2 Support

Generally, supports to be used in heterogeneous catalysis needs some 'physical' requirements such as: high specific surface area to promote the formation of highly dispersed metal supported nanoparticles, to be stable at high temperature and pressure, mechanical resistant to friction, especially for batch-to-batch applications under stirring, reasonably cheap. It should be noted however, that the support can also have an active role in some chemical reactions, for example the total combustion of volatile organic compounds to CO_2 and water by CeO_2[93]. In the preparation of supported metal nanoparticle catalysts, metal oxides have been broadly utilized as the supported and exhibit various effects on the properties of catalysts as well as reaction performances. Laursen and Linic[94] proposed that there was electron charge transfer process from oxygen vacancies at interface (TiO_2) to supported Au nanoparticles to

alter the electronic structure of nanoparticles, facilitating the activation of O_2 and oxidation. Defects sites like surface oxygen vacancies of metal oxide support display effects on the adsorption energy, particle shape and electronic structure of supported metal nanoparticles, which furtherly contributes to the catalytic activity[94-96]. Consequently, it is found that the supported metals (Au, Pt) over reducible oxides (e.g., TiO_2, CeO_2, MoO_3) exhibit a higher activity than that on irreducible oxide (e.g., SiO_2, Al_2O_3)[94].

Of particular relevance as Ag has been extensively used and investigated in this thesis work, are metal support interactions between Ag and metal oxides supports. For example, synergetic interactions were observed between Ag and support (manganese oxides) to promote the reducibility of catalysts and formation of abundant active lattice oxygen, which furtherly strengthened catalytic reactivity in the complete oxidation of toluene for the purpose of removing hazardous organic compounds[97]. Herein, interactions between supported Ag nanoparticle and support could affect the distribution of oxygen vacancies (bulk and surface oxygen vacancies) and the activity of supported Ag/CeO_2 was controlled by surface vacancies near nanoparticles at rich oxygen atmosphere whereas bulk oxygen vacancies had a dominating role in poor oxygen conditions[98]. It was also found that the support could affect the shape of gold nanoparticles. More circular particles on TiO_2 and highly faceted particles on ZnO were discovered respectively, as shown in Fig.1.5[99], while more rounded morphology of gold particles were discovered over TiO_2 with more low-coordinate surface sites[100].

Another relevance for Ag based catalysts is the relative proportion of supported Ag/Ag_2O. This is for multiple reasons: surface Ag can evolve to Ag_2O but on the other hand Ag_2O can

also relatively easily convert back to Ag by thermal decomposition, and Ag and Ag^{+} species may have different reactivity. As for other heterogeneous catalysts the actual oxidation state of the active metal is dependent on the nature of support. For instance, Ag_2O is richly dispersed over the surface of CeO_2 while metallic Ag is preferentially formed on ZrO_2 and Al_2O_3, because the strong interaction between Ag and CeO_2 may hamper the decomposition of Ag_2O particle to Ag[53]. Similarly, the oxidation state and stability of metallic Pt nanoparticles are influenced by the support, where Pt^{2+} is mainly distributed in Pt/ZrO_2 and Pt/SiO_2, while Pt/CeO_2 exhibits a highly oxidized state (Pt^{4+}) and a strong interaction between CeO_2 and Pt nanoparticles is depicted by a higher binding energies[101].

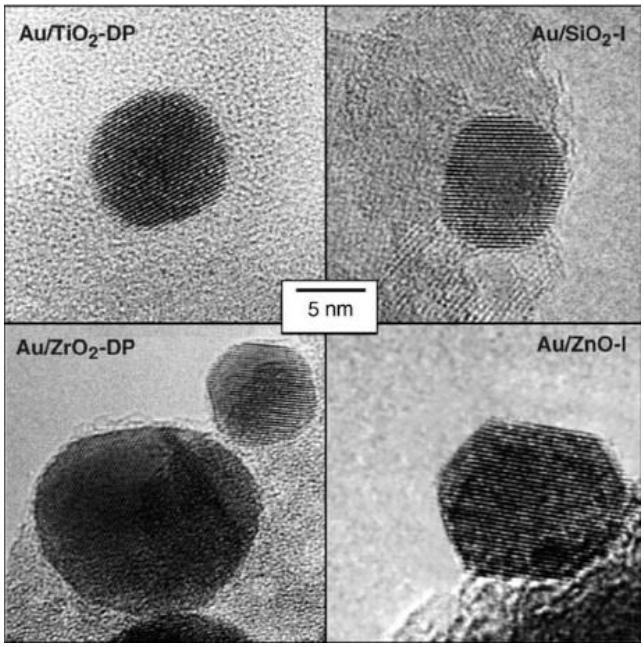

Fig. 1.5 Morphology of gold particles on different supports (DP: deposition-precipitation method, I: impregnation method)[99]. Reproduced/Adapted from ref. 99 with permission from the PCCP Owner Societies.

Based on the researches about catalyst supports, Beatriz [84]summarized the effects of support on the reaction activity of catalyst: i) improving the stability of metal nanoparticles

against sintering, i.e. their aggregation to inactive macroparticles; ii) affecting the physical properties of nanoparticles, like structure and morphology; iii) providing oxygen vacancies for reaction (e.g., MoO_3, CeO_2); iv) stabilising the active species of nanoparticles during the reaction; vi) influencing the interactions between nanoparticles and support. Although the effects of support on reaction process have been investigated much, a major challenge for the study of heterogeneous catalyst is the identification of active sites on the surface[102].

1.2.2.3 Oxidation state of active metals

There is a vast literature reporting that the actual active species of supported metal catalysts is not the pure metal itself but its correspondent metal oxide (e.g., RuO_2, PtO_x in the CO oxidation to CO_2 under O_2 rich conditions) [103-105], implying that it is an important aspect of the identification of reactive species in supported metal catalysts, which is something very relevant for the area of catalyst development by design. For example, Gong et al.[106, 107] found that the oxides were more reactive than metals by comparing the CO oxidation energetics and pathways catalysed by Ru, Rh, Pd, Pt and the corresponding oxides RuO_2, RhO_2, PdO_2, PtO_2. Jason R. et.[108] observed that Pt oxides on Pt/ZrO_2 nanoparticle catalyst were active for the methanol oxidation, suggesting that the reduction process of catalysts might not be necessary. Investigation about the reaction of propane on PdO (101) film suggested that the dissociation of C-H bond was much easier, which could facilitate propane oxidation process because propane molecules interacted strongly with the PdO film surface by a donor-acceptor process, serving as a precursor to initiate the cleavage of C-H bond[109]. In view of these findings, the

identification of mechanism driven by metal oxides (MeO_x) or metallic metals should be considered in the practical oxidation process.

For the scope of this thesis work, Ag is no exception to these phenomena. In fact, in the oxidation process of cyclooctane and cyclohexane by using supported Ag based catalysts, it is found that the valence of Ag plays an important role affecting the reaction performances. For instance, it is discovered that Ag^0 in Ag/Al_2O_3 is mainly responsible for the oxidation of ammonia at temperature below 140 °C, whereas Ag^+ is possibly the active species at a higher temperature above 140 °C, which is probably because of the oxidation of Ag^0 at a higher temperature[91]. Moreover, the distribution of various valance of Ag species (Ag^{2+}, Ag^+, Ag^0) is observed in supported Ag/CeO_2 prepared by impregnation protocol whereas Ag^{2+} is absent in the catalyst prepared by deposition precipitation method, which explains a better reaction performance by impregnated catalyst in the oxidation of propylene, CO and soot, due to three redox couples, Ag^{2+}/Ag^+, Ag^{2+}/Ag^0, and Ag^+/Ag^0.[110] Different reaction performances of the supported Ag or Ag_2O nanoparticles on cyclohexane oxidation is also discovered, caused by the preparation method that Ag_2O over MgO is presented in impregnated catalyst and deposited Ag^0 is mainly found in so-immobilized catalyst[3]. According to the literature, the oxidation state of supported nanoparticles can be controlled by the preparation conditions (e.g., calcination temperature, reduction process by H_2), preparation methods, the types of support. In our studies about supported Ag nanoparticles, different metal oxides, mainly Nb_2O_5 and then other metal oxides like CeO_2, MgO, TiO_2, SiO_2 for comparison, were used as support and an array of preparation methods (wet impregnation, deposition precipitation, sol immobilization

method, discussed in chapter 2) were employed. So the presence of surface and interfacial metallic metal or oxides on support should be considered for the description of catalytic reactivity.

1.2.2.4 Other factors (effects of particles shape, composition)

Except the factors discussed above, there are some other aspects that have influences on the properties of catalysis which further affect the activity and selectivity for reaction. For example, the oxidation of styrene catalysed by different shapes of Ag nanoparticles (cubic, truncated triangular nanoplates, and near-spherical) shows that the nanocube particles have the highest reaction rate, which is fourteen times than that of nanoplates, and four times than that of near-spherical particles. It is more related with the different reaction activity of facets, and (100) facets on nanotube nanoparticles is higher than (111) facets on nanoplates[111]. Haruta et al.[112] found that the shapes of supported gold nanoparticles can be controlled by preparation methods and hemispherical gold particles over TiO_2 generated by deposition precipitation method had better performance than spherical gold particles by impregnation protocol for CO oxidation. These results imply that the effects on catalytic reactivity are probably correlated with the perimeter interfaces around gold nanoparticles. The effect of preparation method on the shape of supported Ag nanoparticles on ZrO_2 is also observed[52]. Hemispherical Ag particles disperse non-uniformly on the surface of ZrO_2 while spherically shaped Ag nanoparticles are relatively homogeneously formed by chemical reduction method, and the latter catalyst exhibits higher activity for soot oxidation. In addition, the composition of the catalyst is also widely studied, including the bimetallic and multimetallic catalytic systems,

for the economical consideration to reduce the number of noble metals, promote activity and selectivity. It has been found that CeO_2 could act as the promoter in the supported Ag nanoparticle catalyst for the oxidation of alcohols[113].

Catalytic properties of bimetallic catalysts can be improved in comparison with monometallic catalysts, and the electronic effect due to the charge transfer plays a prominent role[83, 114-116]. Bimetallic catalysts have been investigated for many reactions, such as, liquid phase oxidation of cyclohexane by bimetallic Au-Pd/MgO[115], Ag-Pd/MgO, Au-Pd catalyst for selective oxidation of methane to methanol[117], and Au-Ag catalyst for CO oxidation[118], Pd-Ag catalyst for the selective oxidation of benzyl alcohol[119]. It should be underlined though that, two or more metals in the catalyst could have synergistic effects which may change the electronic properties of the nanoparticles catalysts to improve the reaction activity, but they can also have no net effect, or even have a detrimental effect (for the same reason to alter the electron density in a non-productive manner). In our project, a bimetallic supported Ag based catalyst (Ag+Fe) was investigated for the oxidation of cyclohexane, as a comparison with monometallic supported Ag to furtherly optimize the catalytic reactivity of Ag based catalysts. It should be noted however that in our case we aimed not just to a bimetallic catalyst but a bifunctional one. That is a region of the catalyst promoting the initiation and a region of the catalyst promoting selectivity control.

According to the above discussion, supported metal nanoparticles catalyst has exhibited extraordinary performance in the oxidation field. And the catalytic properties of nanoparticles are influenced by size, the type of support, oxidation stats of active metals, morphology,

composition, and the chemical environment of metal atoms. Fig. 1.6 displays the changes of optical properties of Ag nanoparticles with the size[120]. Therefore, the development of a highly active, selective, recyclable and environmentally friendly supported meal nanoparticles catalysts can be achieved by manipulating these parameters.

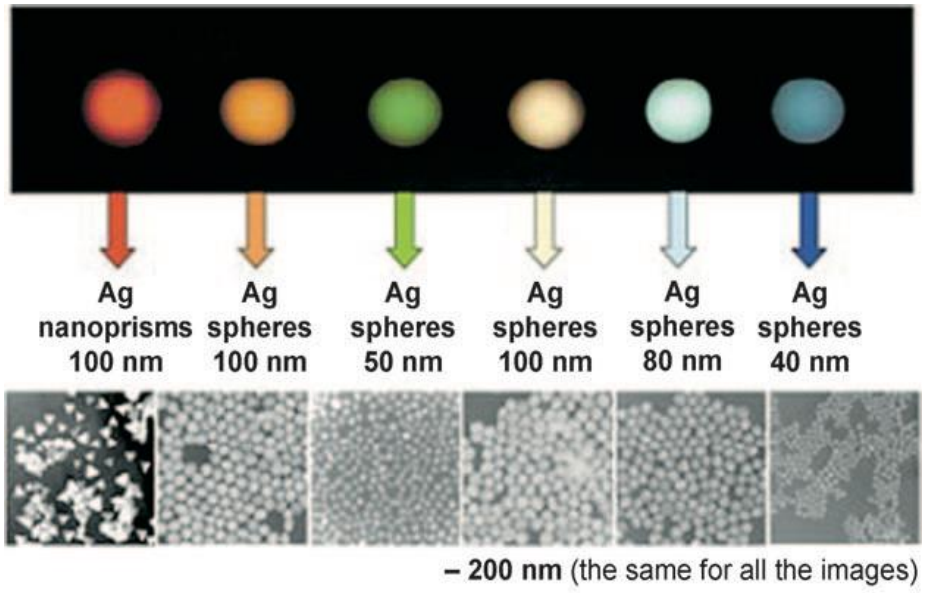

Fig. 1.6 Typical size and shape of Ag nanoparticles[120]. The size and shape of nanoparticles could influence optical, chemical properties at nanometre scale. Copyright (2004) Wiley. Used with permission from C. A. Mirkin.

1.2.3 Challenges in the exploitation of supported metal catalysts

Although supported metal nanoparticles exhibit unique properties and superior reaction performances in comparison with bulk metals, they still suffer from some issues which cannot be neglected for practical applications. The deactivation or the decrease of catalytic reactivity and selectivity over time is a great concern and the classification of deactivation is illustrated in table 1.2[33, 121, 122]. Specifically, it has been reported that Pt based catalysts are poisoned by adsorbed side products (e.g., from aldol condensation, oligomerization of carbonyl compound

products) in the oxidation of alcohol[123, 124], and formation of an inactive surface oxide layer on supported Pd/C catalysts hammers the reactivity because the high affinity of Pd nanoparticles for oxygen, which could be avoided by the addition of bismuth[125]. As nanoparticles are thermodynamically unstable, the aggregation of metal nanoparticles in the preparation or reaction process is also an issue to cause the loss of activity, especially in the case that uniformly dispersed nanoparticles exhibit better reaction performances[126]. This has been reported in the sintering of Ag nanoparticles in Ag/ZrO_2, which is responsible for the loss of activity in soot oxidation[52]. For example, the migration of supported cobalt particles to the external surface, sintering tighter to form large particles, which results in the loss in reactivity[127]. Herein, the aggregation should be prevented in some cases by enhancing the dispersion of particles on the support with high surface area, using robust support to make the active surface sites accessible for substrates molecules, or conducting the reaction under a milder condition (lower temperature) [128].

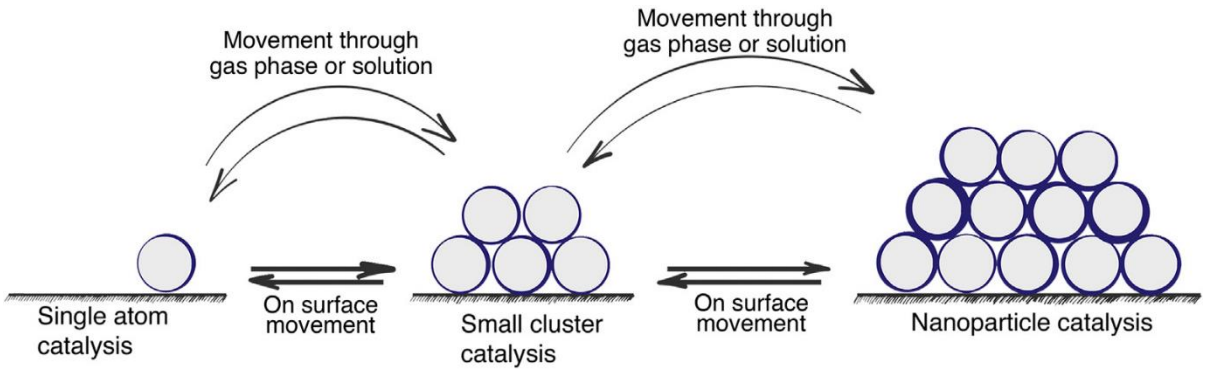

Fig. 1.7 Surface dynamics in supported metal nanoparticle catalysts to elucidate the aggregation of nanoparticles to form cluster.[129] Reprinted from D. B. Eremin and V. P. Ananikov, Copyright (2017), with permission from Elsevier.

Table 1.2 Various types of catalyst deactivation. [33, 123, 124] The reasons for catalyst deactivation are classified by type and mechanism. In our case, metal leaching is our main concerns as it is a quite common phenomenon and one of the major parameters for the loss of activity in supported metal nanoparticles catalysts.

Type of deactivation	Mechanism	Brief description
Mechanical	Fouling	The physical deposition of species in reaction causing the inaccessible of active metal sits.
	Attrition/ crushing	Abrasion leads to the loss of catalytic materials. Crushing causes the loss of internal surface area.
	Erosion	Collisions between the particles or the particles with reactor walls.
Chemical	Poisoning	Chemisorption of species on catalytic sites.
	Leaching	Loss of active metals into the fluid stream.
Thermal	Phase transformation	Transferring from catalytic phase into noncatalytic phase.
	Sintering	The aggregation of metal particles or the loss of catalytic surface area.

Furthermore, among the studies about the deactivation of supported metal catalysts, it is discovered that metal leaching into liquid phase media is a common phenomenon observed for both metal and metal oxide catalysts and a critical issue leading to the instability of catalysts[129]. In fact, it has been investigated in detail for all of the reactions that were investigated in this thesis work. The leaching of metals could result in the consequences, such as: i) the loss of reactivity of catalysts as the proceeding of reaction; ii) the failure for the regeneration and recycling of catalysts; iii) contamination of products[130, 131]; iv) occurrence of the homogeneous reaction pathway if the leaching species is active. A notable example very often cited in the literature, which caused an argument to recognize the reaction mechanism is the C-C Suzuki cross-coupling reaction by palladium catalysts.[132-134] A high catalytic reactivity of leached Pd is found in Suzuki–Miyaura cross-coupling reaction and suggesting that both of the supported Pd nanoparticles and soluble Pd^{2+} species are responsible for the

catalytic process[135]. From an industrial perspective, the leaching of metal limits the practical reusability whether the leached species are active or inert, which should be avoided. On the other hand, it is important to identify the effect of leached metal on reaction if it occurs, and the cooperating activity might lead to debate about the mechanism in a mixed catalytic process containing homogeneous and heterogeneous catalysis due to the complexity of reaction.

Gruber-Wölfler et. al.[136] reported the methods for the observation of metal leaching and effects on reaction, as shown in table 1.3. With regard to this thesis work, the analysis for metal leaching (Ag) was determined by ICP-MS and the control tests to investigate about the effects of leached Ag species in Ag^+ state on the oxidation process were conducted in the presence of $AgNO_3$. Moreover, supported catalysts were recycled from the reaction mixture and the dried solids were continually applied for the oxidation under the same reaction conditions for the assessment of catalytic stability.

Table 1.3 The analysis for the extent of Pd leaching and effect of leached species on reaction by various methods.[136] Based on this table, the quantitative analysis for metal leaching into reaction mixture was achieved by ICP and a series of tests for catalyst reusability were conducted in our research.

Methods	Description of process	Results
Hot filtration test	Active particles are removed by filtration and observe the activity of filtrate.	Observed conversion might be an implication that leached species are active, while it cannot justify the reaction only occurs in heterogeneous catalysis as the leached species can redeposit on support, making it undetected by this method[137, 138].
ICP/OES analysis	Reaction mixture is dried and the residue is dissolved into nitric acid, which is analysed for the concentration of metal species.	Quantitative analysis for the leached metal in reaction mixture if obvious leaching occurs during reaction.

Three-phase test	Covalently immobilized reaction partner is added into the soluble reagent with the presence of supported catalyst.[139, 140]	This method can provide reliable evidence for the monitor of active homogeneous metal species. The covalently immobilized reagent will be converted if leaching occurs.
Catalyst reusability	Recycling the catalyst from reaction mixture after reaction, and then conducting the tests with fresh substrate.	Reusability is an important factor for the valuation of catalysts stability. An obvious decrease of catalytic activity caused by leaching would be observed after many runs of test if the activity is influenced by the amount of present active species.
Tests in various solvent	Testing the catalysts for same model reaction in the presence of various solvent	Catalytic reactivity and the amount of leached metals can be influenced by the nature of solvent.[141, 142] It is suggested that the polarity of solvent and a high temperature might have no effect on Pd leaching.
Catalyst poisoning	Adding catalysts poisoning to the reaction system in the existence of catalysts.	The deactivation of catalyst will be observed if metal leaching occurs as the leached species can be deactivated by poisons.

1.3 Application of bulk niobium oxides in supported metal catalysts

Metal oxides like CeO_2, MgO, SiO_2, Al_2O_3, TiO_2, are widely applied as the support for the preparation of supported metal nanoparticles due to their special properties: i) thermal and mechanical stability are useful and important for long term use and scale up; ii) high surface area is a parameter associated with the dispersion of metal nanoparticles, and the interaction between support and deposited nanoparticles is able to prevent the sintering or aggregation of particles; iii) presence of oxygen vacancies might affect partial oxidation reaction. For example, it is found that the oxygen vacancies of CeO_2 tend to facilitate the activity as oxygen can be chemically adsorbed and activated on these sites to form superoxide (O_2^-) species[143, 144] (a new pathway suggests that O_2 is adsorbed on Au-Ce^{3+} bride sites in CO oxidation[145]) and the oxidation of CO in the absence of O_2 indicates the participation of lattice oxygen from CeO_2[146, 147]. The oxygen vacancies in Co/MgO also display the ability of enhancing the

chemisorption of O_2 in the liquid phase oxidation of cyclohexane.[148] However, it should be noted that the presence of neutral oxygen vacancies could probably trap the radicals, this effect being observed in MoO_3[149] and ZnO[150] that acts as quencher for peroxy radicals to suppress the oxidation. In view of these, the vacancies in surface and bulk might play a decisive role in the catalytic process.

A support however, that received limited attention so far, and that has been widely used in this thesis work is Nb_2O_5 in the concept of designing a novel catalyst system for hydrocarbons oxidation. This support has been reported capable of strong metal-support interaction (SMSI) in case of Pt nanoparticles, and it was able to influence the dispersion of metal nanoparticles (a uniform loading of Pt nanoparticles with smaller size[151]) and catalytic reactivity in the enhancing or supressing way[152]. An enhanced selectivity towards *n*-hexane and 1-hexanol in the hydrodeoxygenation of f 1,6-hexanediol is observed due to a SMSI effect from the charge transfer from Nb_2O_5 to Pt nanoparticles reducing the electron density of Pt[153]. Whereas, it is also found that this interaction is not always playing a promoting role, as evidenced that nickel supported over Nb_2O_5 suppress the activity in hydrogenation reaction[152].

Niobium oxides materials have attracted much attention and exhibited of importance potentiality in many fields such as, catalysis, solid electrolytic capacitors, photochromic devices, due to their unique optical, electronic and chemical properties.[154] Whereas the understanding about these oxygen compounds and their applications are still insufficient. There are three oxidation state of niobium, 2+, 4+ and 5+ in the oxides NbO, NbO_2, and Nb_2O_5. Among these Nb_2O_5 is the most thermodynamically state[154]. The properties of niobium oxides

with various oxidation state are highly controlled by the phase, polymorphism as well as stoichiometry, e.g., generally octahedral coordinated NbO_6 structure is presented while NbO_7 and NbO_8 can be found[155], and various phases of Nb_2O_5 (TT-pseudohexagonal, T-orthorhombic, M-tetragonal, B-monoclinic, H-monoclinic) can be obtained with the changes of temperature[155], indicating that a combination of different phases in a niobium oxide sample may exist. In our project, aiming for the purpose of designing a novel material for the selective oxidation of hydrocarbons, and given the fact that Nb_2O_5 is the most thermodynamically state that is an essential property as support, herein we used Nb_2O_5 for hydrocarbons oxidation as an active species or a support for the deposition of nanoparticles.

1.3.1 Fundamental properties of bulk niobium pentoxide (Nb_2O_5)

Given the large use we did of this metal oxide, it is appropriate to describe the properties of this material more in detail. Nb_2O_5 has a conduction band from an empty Nb^{5+} 4d orbitals and a band gap value is around 3.4 eV that is higher than that of titanium dioxide (TiO_2) by 0.2-0.4 eV, which implies that it can still adsorb light in UV regions, posing a potential application as a photo catalyst under UV illumination, although at present this has been virtually unexplored.[154, 156] Furthermore, Nb_2O_5 mainly comprises of NbO_6 octahedral unit cell where Nb atom is linked with six oxygen atoms connected by corner and edge sharing, whereas NbO_7 and NbO_8 is also observed in some phases (amorphous, TT and T phase of Nb_2O_5)[155, 156]. Highly distorted NbO_6 has Nb=O double bond units that are correlated to Lewis acid sites, while slightly distorted NbO_6 as well as NbO_7 and NbO_8 structure only has Nb-O bond which is connected with Brønsted acid sites[155]. And Lewis acid can be found in all

supported Nb_2O_5 catalysis while in some specific catalysis systems there is only Brønsted acid present, such as Nb_2O_5/Al_2O_3, Nb_2O_5/SiO_2[157, 158]. In view of this, there is a promising application of Nb_2O_5 in acid catalysed reaction (e.g., isomerization of 1-buetene[159], hydration of ethylene oxide to give monoethylene glycol[160]) by tailoring acid properties.

Schäfer et al.,[161] pointed that an O/Nb ratio at 2.5 can be created by several combinations of octahedral linkages, resulting in the multiple crystal structure of Nb_2O_5. Nb_2O_5 exhibits a variety of different polymorphisms from the amorphous state to form into various polymorphs during the crystallization process with the increase of temperature, as shown in Fig. 1.8. There are several common polymorphisms, TT-Nb_2O_5 in pseudohexagonal crystal, T-Nb_2O_5 in orthorhombic crystal and monoclinic H-Nb_2O_5. TT or T phase is usually formed with a crystallization temperature at about 500 °C from amorphous Nb_2O_5, followed by the transformation into M phase with tetragonal crystal and monoclinic B-Nb_2O_5 at ~800 °C, and monoclinic H phase is obtained at a higher temperature than 1000 °C[156, 162]. Among these polymorphisms, it is found that the crystal structure of bulk Nb_2O_5 formed at high temperature is more ordered than that at lower temperature[162]. Amorphous Nb_2O_5 possesses slightly distorted NbO_6, NbO_7, NbO_8, and it is capable of facilitating the formation of radical peroxo specie by the interaction with hydrogen peroxide[163]. TT and T phases display similar X-ray diffraction patterns while some refection peaks are split in T-Nb_2O_5 in comparison with peak shown from TT-Nb_2O_5[155]. For example, the peaks at $2\theta = 29°$ (180) plane and 37° (181) plane are split in XRP patterns of T phase of Nb_2O_5[164]. TT phase is less crystallized than T and normally is stabilized by impurities like OH^-, Cl^- or oxygen vacancies and the occupancy of

Nb atoms in T-Nb_2O_5 is in separate, closely-spaced and equivalent sites, which probably cause the broader peaks comparing the same splitting peaks in T-Nb_2O_5[156, 162]. H-Nb_2O_5 is the most thermodynamically stable phase that can be obtained by a heat treatment at the temperature above 1000 °C from any Nb_2O_5 polymorph, whereas TT or T phase of Nb_2O_5 are more metastable as comparison[156, 162]. Moreover, it should stress that preparation methods, properties of starting material, existed impurities and the interactions with other compositions can affect the crystal structure of Nb_2O_5[161, 162].

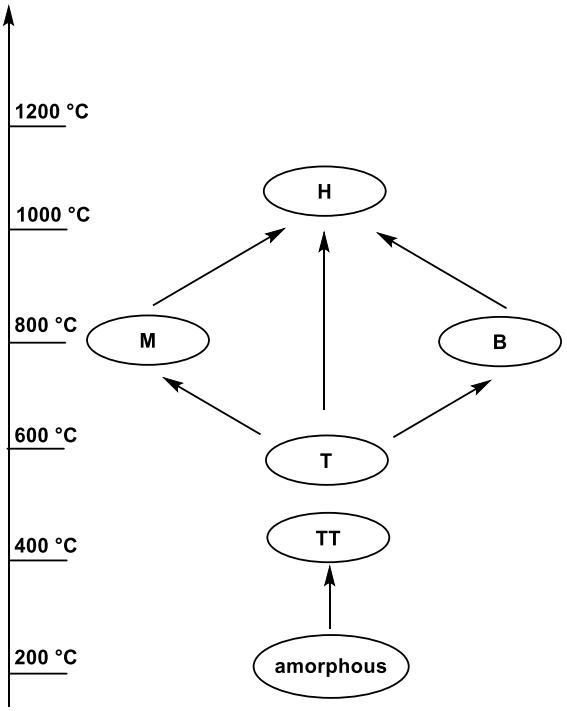

Fig. 1.8 Polymorphism of Nb_2O_5 and transformation state with the increase of temperature.[155]

These considerations are reported here as the interactions are able to influence physical and chemical properties (e.g., reducibility and acidity) in the application of catalysis process. In view of this, it is probably different polymorphisms presented in Nb_2O_5 would affect its reaction performances when using in catalysis. In our project, we investigated the reactivity of

Nb_2O_5 of different grade (99.9% and 99.99%) in the oxidation of cyclooctane and the polymorphisms were considered for analysis of the reaction performance.

1.3.2 Application of bulk Nb_2O_5 in catalysis

There are, however, some rare examples for the use of Nb_2O_5 as it is for chemical reactions. For example, Tanabe et al.,[159] and Wachs et al., [157, 165] pioneered the works of niobium species applied in catalysis, illustrating that niobium compounds can act as promoter or active species, support and solid acid catalyst in the area of catalysis. As for Nb_2O_5, it displays promising results as a promoter or support in heterogeneous catalysts for many various reactions, e.g., esterification[159], alcohols oxidation, photooxidation of hydrocarbons in the presence of solvent[166, 167]. Although Nb_2O_5 has some promising prospects applied as catalysts by playing the role of promoter, active phase or support, Nb_2O_5 gains less attention in comparison with other transition metal oxides, e.g., CeO_2, MoO_3, TiO_2, MgO, and the understanding about the roles of Nb_2O_5 is still insufficient[156], which poses a great potential for the investigation of Nb_2O_5 in catalysis field. Moreover, there is less attention to the direct oxidation of hydrocarbons by molecular oxygen in the presence of niobium oxide-based catalysts without any initiator or solvent, suggesting an exploitation of Nb_2O_5 applied into hydrocarbons oxidation. Thus, in our case, the research about the application of Nb_2O_5 as active phase or support in the direct oxidation of hydrocarbons was conducted with the aim to provide insight about the feasibility of Nb_2O_5 in this field.

Herein, a summary about the application of Nb_2O_5 in oxidation field is developed, as displayed in table 1.4. According to the literature, several roles of Nb_2O_5 on the properties of

catalysts and catalytic reactivity can be summarised as: i) Nb_2O_5 displays a potential application in photooxidation as active phase or support in the oxidation of hydrocarbons or alcohols and the radicals are formed through the electron transfer from the surface electron donor to the conduction band by photo irradiation[168]; ii) bulk amorphous Nb_2O_5 is able to interact with oxidizing agent (e.g., H_2O_2, TBHP) to give peroxy species ($Nb(O)_2$), usually accompanied by the colour changes from white to yellow, which is an active intermediates for the reaction[163]; iii) strong metal-support interaction shows effects on the dispersion and size of metal nanoparticles over the surface of Nb_2O_5, contributing to the activity of catalysts[151]; iv) supported nanoparticle Nb_2O_5 can act as active species in the photo oxidation of saturated and unsaturated hydrocarbons in the presence of initiator[166]. According to the literature and our own investigations, although Nb_2O_5 as active phase or support is applied for the oxidation of hydrocarbons, the reactions are usually conducted by photo-irradiation or in the presence of initiator, which limits the scale up production. Thus, we will investigate about the reactivity of bulk Nb_2O_5 in hydrocarbons (mainly cyclooctane, cyclohexane, ethylbenzene in our case) oxidation and the design of novel catalyst system using Nb_2O_5 as support to selectively catalyse the oxidation for desired products.

Table 1.4 Various roles of Nb_2O_5 and its effects on reaction. Give the promising results of Nb_2O_5 applied as support or active phase and its SMSI with supported metals, a potential application of Nb_2O_5 in the oxidation of cyclic alkanes will be developed within our research.

Catalyst	Results	Ref.
Pt/Nb_2O_5	Nb_2O_5 was used as support and a SMSI was observed between Pt nanoparticles with Nb_2O_5. The interaction could induce electron deficient Pt species to create new interfacial active sites and lead to a relatively uniform dispersion of particles, contributing to a high activity in the dehydrogenation process.	153, 169, 170
Cu/Nb_2O_5, Nb_2O_5	Nb_2O_5 acted as active phase or support and the catalysts were applied for the solvent-free photooxidation of alcohols with molecular oxygen. The radicals were formed by the direct electron transfer from the surface electron donor to the conduction band, and alcohol molecules was adsorbed on the Lewis acid site (Nb^V) to give alkoxide species. The addition of Cu obviously enhanced the photoactivity.	168, 171
Nb_2O_5, TiO_2	The photooxidation of hydrocarbons with molecular oxygen was catalysed by Nb_2O_5 in the absence of solvent. An obvious enhancing conversion of ethylbenzene was observed, even higher than that of TiO_2. While the reactivity for cyclohexane oxidation was limited. Alkyl radical was given by photogenerated positive hole adsorbed oxygen was reduced by a photogenerated electron. The results indicated a promising application of Nb_2O_5 as a photocatalyst.	166
Amorphous and crystalline Nb_2O_5	Amorphous and crystalline Nb_2O_5 were employed for glycerol and cyclohexene oxidation with H_2O_2. The interaction between Nb_2O_5 and H_2O_2 gave peroxo species, which was responsible for the conversion of substrate while the absence of peroxo species in crystalline Nb_2O_5 and H_2O_2 explained the inactivity or less active for reaction.	163, 172
TiO_2/SiO_2, V_2O_5/SiO_2, Nb_2O_5/SiO_2	Nb_2O_5 was deposited over the surface of SiO_2 as active species applied for the oxidation of 1-hexene, cyclohexene and cyclohexane by using *tert*-Butyl hydroperoxide (TBHP) as oxidizing agent. The niobium catalyst was less active than the titanium and vanadium oxide catalysts, but it shows a higher selectivity for alcohols, which can be attributed to the higher amount of Lewis acid sites jointly with metallic centres in Nb_2O_5.	173
Nb species as promoter	The incorporation of small amounts of Nb^{5+} could results in the active metal-Nb-O_x, which furtherly improve the selectivity and stability of the catalysts structure. Whereas the doped Nb species probably interact with active metals to create poisonous phases in some case. (e.g., V-$VNbO_4$ and $VNbO_5$ phases in V/Nb mixed oxides catalysts.	174-177

1.4 Supported Ag nanoparticle catalysts

Silver and silver-based compounds are known to play an important role in the antimicrobial field due to their antiseptic properties, and a substantial amount of research about silver metal is related to biological areas and optoelectronics[178]. Nevertheless, supported Ag nanoparticles are attracting more and more attention applied into heterogeneous catalysis and displaying a promising prospect in the selective oxidation of alkanes and alkenes for the production of oxygen containing compounds[179-181]. However, in comparison with other supported metal nanoparticles, such as, Au, Pt, Cu, Ni, applications of supported Ag nanoparticles are still in their infancy, but for one notable application suggesting a potential development of this catalyst into various reactions and a sufficient understanding about reaction mechanism involving supported Ag nanoparticles as well as the interaction with oxygen or metal oxide support are interesting and challenging field to be investigated[182].

The most known use of Ag based catalysts is the industrially employment for ethylene epoxidation to produce ethylene oxide (up to 80% selectivity), which is used for produce ethylene glycol (an ingredient in antifreeze), poly(ethylene oxide) as well as surfactants[54], and the dehydrogenation of methanol to formaldehyde[55, 183], which is widely used for the production of resins for wood panel industry[184]. Previous reports, however highlighted that the catalytic reactivity of supported Ag catalysts can be controlled by the oxidation state of Ag, size and morphologies of nanoparticles, these factors being influenced by preparation methods and support. For example, silver is found to be stabilized mainly in the oxide state on CeO_2 while metallic is preferentially formed on Al_2O_3 due to the reducibility of CeO_2, and the distribution

of Ag/Ag_2O nanoparticles indicates a different activity in soot oxidation[53]. There are three Ag species (Ag^{2+}, Ag^{+}, Ag^{0}) Ag observed in supported Ag/CeO_2 prepared by impregnation method while no Ag^{2+} is found the catalyst prepared by deposition precipitation as the formation of Ag^{2+} species requires the simultaneous presence of nitrate in the precursor and the migration of oxygen from support at a calcination process above 400 °C[110]. The nitrate from precursor is removed by filtration when catalyst is prepared using deposition precipitation method, which also explains a lower loading of metal is probably observed in comparison with impregnation method. A strong metal-support interaction (SMSI) between Ag and CeO_2 is illustrated to facilitate the catalytic activity in ethanol oxidation by enhancing the electron transfer between Ag nanoparticles and ceria[185]. This SMSI is also observed when employing Nb_2O_5 as support, possibly occurring when Ag nanoparticles is deposited on Nb_2O_5. Thus, considering the effects of preparation methods and type of support on the properties of Ag nanoparticles, which furtherly affects catalytic performances, we will focus on the study about the tailing of supported Ag nanoparticles properties (mainly oxidation state, size, dispersion on support) controlled by preparation methods and the support used for the selectively direct oxidation of cyclic hydrocarbons.

Moreover, it should be noted that a significant role that Ag nanoparticles plays is for the activation of O_2. In the oxidation process involving O_2, two reaction mechanisms are proposed for the formation of reactive oxygenated species[186, 187]: i) O_2 molecule is activated on active sites (e.g., metal particle surface, oxygen vacancies or metal/oxide junction) to give the species like superoxide (O_2^{-}), peroxide (O_2^{2-}); ii) the release of O from the lattice of metal oxide

(Mars-van Kravelen mechanism). It has been reported that supported Ag nanoparticle is able to activate molecular oxygen to form superoxide by the adsorbing of oxygen over Ag species[52, 182, 186]. Recently, Luca et al.[186] pointed that oxygen molecules weakly adsorb on silver particles as a superoxide or strongly adsorb at the oxygen vacancies sites of CeO_2/TiO_2 to form peroxide (scheme 1.4). The electron storage or release ability of CeO_2 is able to facilitate the dissociation of O-O bond by lowering the activation barriers for oxygen reduction through charge transfer from the vacancies to O_2. The addition of supported Ag particles leads to the formation of oxygen vacancies on the surface, which promotes the reductive adsorption of O_2. Thus, the activation of O_2 can occur on silver particles and the oxygen vacancies created due to the interaction between Ag nanoparticles and reducible support. As O_2 is utilised as oxidant for cyclic alkanes oxidation without any initiator in our research project, in view of this effect of Ag on the activation for O_2, it is expected that the Ag species (Ag^0 or Ag^+) could play the role of converting ground triplet molecular oxygen to form reactive oxygen species.

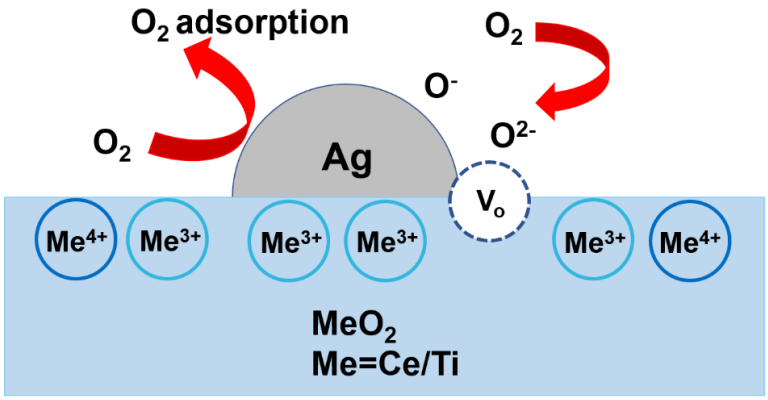

Scheme 1.4 Activation of O_2 by supported Ag nanoparticles over the surface of metal oxides.[186] V_o denotes the oxygen vacancies in metal oxide due to the deposition of Ag nanoparticles. Reproduced/Adapted from ref. 186 with permission from American Chemistry Society.

Herein, the application of supported Ag over metal oxide in the oxidation fields is summarized, shown in table 1.5. Based on these studies, the effects of supported Ag nanoparticles can be ascertained as: i) superior performances for the activation of molecular oxygen by the adsorbing over particles and oxygen vacancies formed from the interaction between particles and metal oxide support[95, 186]; ii) interactions between supported Ag nanoparticle and support could affect the distribution of oxygen vacancies of support which furtherly influences the reaction performances[98]; iii) the presence of various valance of Ag (Ag^{2+}, Ag^{+}, Ag^{0}) in catalyst enhances the redox couples to improve the activity[110]. In addition, Ag is favoured from economic perspective as it is less expensive than other noble metals like Au, Pd, Pt. Therefore, based on the above discussion, Ag indicates a potential development into the selective oxidation of hydrocarbons by molecular oxygen without initiator as the activated oxygen species is probably active to trigger the reaction under proper reaction conditions.

Table 1.5 Applications of supported Ag metal nanoparticles catalysts in the oxidation field. As discussed above, the properties of supported Ag nanoparticles, like particle size, oxidation state of Ag can be affected by the support or preparation method, which will be discussed in our research.

Supported Ag Catalyst	Preparation	Reaction	Ref.
Ag/SiO_2	Impregnation method	CO oxidation	188, 189
Au-Ag/MCM	One-pot approach		51, 190
Ag/CeO_2	Impregnation and deposition precipitation		110
Ag/SiO_2 (Al_2O_3, MgO)	Impregnation method	Alcohols oxidation	113
Ag/ZrO_2	Sol immobilization	Soot oxidation	52
Ag/CeO_2	Impregnation method		53, 98
Ag/Al_2O_3	Impregnation method	Benzene oxidation	191
Ag/SiO_2	Sol immobilization	Ethylbenzene oxidation	192

Ag/Al_2O_3, MgO	Impregnation and sol immobilization	Styrene oxidation	[193, 194]
Ag/Al_2O_3 (TiO_2, CeO_2)	Impregnation method	Ethylene oxidation	[50, 195, 196]
Ag/MCM-41	One-pot synthesis method	Cyclohexane oxidation	[179]
Ag-Pd/MgO	Impregnation and sol immobilization		[3]

1.5 Aims of the research project

In this thesis work, we aim to design appropriate catalysts for the achievement of selective oxidation of cyclic hydrocarbons (mainly cyclooctane and cyclohexane) by molecular oxygen to synthesize corresponding alcohols or ketones under mild conditions. Autoxidation of hydrocarbons in the absence of catalysts proceeds in an unselective way. Thus, a major challenge is how to increase the selectivity, and in turn the yield, to specific products by minimizing waste and improving the energy efficiency of these processes. Supported metal nanoparticles catalysts have been widely applied in the oxidation fields, and among them Ag nanoparticles exhibits promising prospects results in the reaction mainly through the activation of O_2 as well as the interactions with support[182], while the application is still limited to be furtherly explored and the sufficient understanding about reaction mechanism involving the interaction with support or size effect are challenging. It is reported that the activity of supported Ag catalysts mainly depends on the oxidation state, particles size and influences of support[91, 110, 197].

In view of these aspects, our research will focus on the design of a novel silver-based catalysts applied in hydrocarbons oxidation and providing insight into the roles of Ag species plays during the oxidation process. In addition, according to the literature about metal oxide

as support and previous research work within our group, Nb_2O_5 displays a strong metal-support interaction that influences the properties of supported nanoparticles, which furtherly affects the reaction. And the application of Nb_2O_5 in oxidation field as active phase or support (as shown in table 1.4) elucidates the way of Nb_2O_5 affecting the reaction with promising results. However, Nb_2O_5 based catalysts are largely unused for the directly selective oxidation of hydrocarbons by molecular oxygen without any initiator and an understanding about the mechanism involving the C-H bond activation or decomposition of alkyl hydroperoxides by Nb_2O_5 is absent during the oxidation. According to the discussion concerning their properties as well as application of Ag nanoparticles and Nb_2O_5, a novel catalyst system with great potentials in hydrocarbon oxidation field is tentatively developed.

Thus, this project will make use of novel metal and metal nanoparticles, mainly based on Ag, but also extended to species incorporating Fe, firstly applied in the oxidation of cyclic hydrocarbons (mainly, cyclooctane, cyclohexane, ethylbenzene) by molecular oxygen. The supported Ag nanoparticles over metal oxide will be prepared by different methods, impregnation, deposition-precipitation as well as sol-immobilization method to tailor the properties of catalysts (e.g., metal loadings, size, oxidation state of metal). Characterization techniques, such as ICP-MS, XRD, TEM, XPS, will be employed as tools to screen the properties of supported nanoparticles catalysts, for the establishment of structure-activity relationship, which could provide useful information for the optimized design of catalyst. Moreover, the reaction mechanism will be tentatively proposed for our oxidation process accordingly.

1.6 References

1. M. Eichelbaum, R. Glaum, M. Hävecker, K. Wittich, C. Heine, H. Schwarz, C.-K. Dobner, C. Welker-Nieuwoudt, A. Trunschke and R. Schlögl, *ChemCatChem,* 2013, **5**, 2318-2329.
2. U. Schuchardt, D. Cardoso, R. Sercheli, R. Pereira, R. S. Da Cruz, M. C. Guerreiro, D. Mandelli, E. V. Spinacé and E. L. Pires, *Appl. Catal. A: Gen.*, 2001, **211**, 1-17.
3. X. Liu, M. Conte, Q. He, D. Knight, D. Murphy, S. Taylor, K. Whiston, C. Kiely and G. J. Hutchings, *Chem. Eur. J.*, 2017.
4. W. Trakarnpruk, A. Wannatem and J. Kongpeth, *J. Serbian Chem. Soc.* , 2012, **77**, 1599-1607.
5. J.-M. Brégeault, *Dalton Trans.*, 2003, 3289-3302.
6. Y. Ishii, S. Sakaguchi and T. Iwahama, *Adv. Synth. Catal.*, 2001, **343**, 393-427.
7. A. E. Shilov and G. B. Shul'pin, *Chem. Rev.*, 1997, **97**, 2879-2932.
8. R. r. A. Tomás, J. o. C. Bordado and J. F. Gomes, *Chem. Rev.*, 2013, **113**, 7421-7469.
9. Q. Wang, Y. Cheng, L. Wang and X. Li, *Ind. Eng. Chem. Res.*, 2007, **46**, 8980-8992.
10. W. Sun, Y. Pan, L. Zhao and X. Zhou, *Chemical Engineering & Technology: Industrial Chemistry‐Plant Equipment‐Process Engineering‐Biotechnology*, 2008, **31**, 1402-1409.
11. I. Hermans, T. L. Nguyen, P. A. Jacobs and J. Peeters, *ChemPhysChem*, 2005, **6**, 637-645.

12. G. A. Olah, Á. Molnár and G. S. Prakash, *Hydrocarbon Chemistry, 2 Volume Set*, John Wiley & Sons, 2017, p 593-596.

13. B. P. Hereijgers and B. M. Weckhuysen, *J. Catal.*, 2010, **270**, 16-25.

14. D. G. Hendry, C. W. Gould, D. Schuetzle, M. G. Syz and F. R. Mayo, *J. Org. Chem.*, 1976, **41**, 1-10.

15. M. S. Stark, *J. Am. Chem. Soc.*, 2000, **122**, 4162-4170.

16. L. M. Slaughter, J. P. Collman, T. A. Eberspacher and J. I. Brauman, *Inorg. Chem.*, 2004, **43**, 5198-5204.

17. I. Hermans, J. Peeters and P. A. Jacobs, *Top. Catal.*, 2008, **50**, 124-132.

18. I. Hermans, P. A. Jacobs and J. Peeters, *Chem. Eur. J.*, 2006, **12**, 4229-4240.

19. C. Futter, E. Prasetyo and S. A. Schunk, *Chem. Ing. Tech.*, 2013, **85**, 420-436.

20. X. Liu, Y. Ryabenkova and M. Conte, *Phys. Chem. Chem. Phys.*, 2015, **17**, 715-731.

21. I. Hermans, J. Peeters, L. Vereecken and P. A. Jacobs, *ChemPhysChem*, 2007, **8**, 2678-2688.

22. C. J. Hammond, J. R. L. Smith, E. Nagatomi, M. S. Stark and D. J. Waddington, *New J. Chem.*, 2006, **30**, 741-750.

23. P. W. Van Leeuwen, *Homogeneous catalysis: understanding the art*, Springer Science & Business Media, 2006, p 6-9.

24. I. V. Kozhevnikov, *Chem. Rev.*, 1998, **98**, 171-198.

25. M. Misono and N. Nojiri, *Appl. Catal.*, 1990, **64**, 1-30.

26. J. Hagen, *Industrial Catalysis: A Practical Approach, Second Edition*, 2006, 59-82.

27. C. Rangheard, C. de Julián Fernández, P.-H. Phua, J. Hoorn, L. Lefort and J. G. de Vries, *Dalton Trans.*, 2010, **39**, 8464-8471.

28. R. P. Houghton and C. R. Rice, *Polyhedron*, 1996, **15**, 1893-1897.

29. M. Li, F. Niu, D. H. Busch and B. Subramaniam, *Ind. Eng. Chem. Res.*, 2014, **53**, 9017-9026.

30. D. J. Cole-Hamilton, *Science*, 2003, **299**, 1702-1706.

31. R. Sheldon, in *Stud. Surf. Sci. Catal.*, Elsevier, 1991, vol. 59, pp. 33-54.

32. Z. Li, S. Wu, C. Yang, Y. Ma, X. Fu, L. Peng, J. Guan and Q. Kan, *Mol. Catal.*, 2017, **432**, 267-273.

33. M. D. Argyle and C. H. Bartholomew, *Catalysts*, 2015, **5**, 145-269.

34. S. E. Davis, M. S. Ide and R. J. Davis, *Green Chem.*, 2013, **15**, 17-45.

35. B. Cornils and W. A. Herrmann, *J. Catal.*, 2003, **216**, 23-31.

36. A. Wang, J. Li and T. Zhang, *Nat. Rev. Chem.*, 2018, **2**, 65-81.

37. I. Fechete, Y. Wang and J. C. Védrine, *Catal. Today*, 2012, **189**, 2-27.

38. J. K. Nørskov, F. Studt, F. Abild-Pedersen and T. Bligaard, *Fundamental concepts in heterogeneous catalysis*, John Wiley & Sons, 2014, p 4-5.

39. R. A. Sheldon and H. Van Bekkum, *Fine chemicals through heterogeneous catalysis*, John Wiley & Sons, 2008, p 5-7.

40. B. P. C. Hereijgers, Utrecht University, 2011, p 7-8.

41. M. Haruta, *Catal. Today*, 1997, **36**, 153-166.

42. M. D. Hughes, Y.-J. Xu, P. Jenkins, P. McMorn, P. Landon, D. I. Enache, A. F. Carley, G. A. Attard, G. J. Hutchings and F. King, *Nature*, 2005, **437**, 1132.

43. Y.-J. Xu, P. Landon, D. Enache, A. F. Carley, M. Roberts and G. J. Hutchings, *Catal. Lett.*, 2005, **101**, 175-179.

44. Q. Tang, Q. Zhang, H. Wu and Y. Wang, *J. Catal.*, 2005, **230**, 384-397.

45. H. Cui, Y. Zhang, Z. Qiu, L. Zhao and Y. Zhu, *Appl. Catal. B: Environ.*, 2010, **101**, 45-53.

46. M. Ozbek, I. Onal and R. Van Santen, *J. Catal.*, 2011, **284**, 230-235.

47. M. Özbek and R. Van Santen, *Catal. Lett.*, 2013, **143**, 131-141.

48. P. Zhenyan, H. Li, Q. Yunxiang, Y. Hanmin, Z. Xiuge, F. Bo, Z. Wenwen and H. Zhenshan, *Chinese J. Catal.*, 2011, **32**, 428-435.

49. C.-F. Mao and M. A. Vannice, *Appl. Catal. A: Gen.*, 1995, **122**, 61-76.

50. S. Rojluechai, S. Chavadej, J. W. Schwank and V. Meeyoo, *Catal. Commun.*, 2007, **8**, 57-64.

51. A.-Q. Wang, C.-M. Chang and C.-Y. Mou, *J. Phys. Chem. B*, 2005, **109**, 18860-18867.

52. M. Haneda and A. Towata, *Catal. Today*, 2015, **242**, 351-356.

53. E. Aneggi, J. Llorca, C. de Leitenburg, G. Dolcetti and A. Trovarelli, *Appl. Catal. B: Environ.*, 2009, **91**, 489-498.

54. H. H. Lou, J. Chandrasekaran and R. A. Smith, *Comput. Chem. Eng.*, 2006, **30**, 1102-1118.

55. L. Kundakovic and M. Flytzani-Stephanopoulos, *Appl. Catal. A: Gen.*, 1999, **183**, 35-51.

56. J. A. Labinger and J. E. Bercaw, *Nature*, 2002, **417**, 507-514.

57. H. M. Davies and J. R. Manning, *Nature*, 2008, **451**, 417-424.

58. A. A. Fokin and P. R. Schreiner, *Chem. Rev.*, 2002, **102**, 1551-1594.

59. R. H. Crabtree, *Chem. Rev.*, 1995, **95**, 987-1007.

60. S. J. Blanksby and G. B. Ellison, *Acc. Chem. Res.*, 2003, **36**, 255-263.

61. P. J. Pérez, *Alkane CH activation by single-site metal catalysis*, Springer Science & Business Media, 2012, p 1-2.

62. G. B. Shul'pin, *Org. Biomol. Chem.*, 2010, **8**, 4217-4228.

63. G. Brilmyer and R. Jasinski, *J. Electrochem. Soc*, 1982, **129**, 1950.

64. J. W. Larsen, *J. Am. Chem. Soc.*, 1977, **99**, 4379-4383.

65. D. Munz and T. Strassner, *Inorg. Chem.*, 2015, **54**, 5043-5052.

66. E. Roduner, W. Kaim, B. Sarkar, V. B. Urlacher, J. Pleiss, R. Gläser, W. D. Einicke, G. A. Sprenger, U. Beifuß and E. Klemm, *ChemCatChem*, 2013, **5**, 82-112.

67. B. L. Conley, W. J. Tenn III, K. J. Young, S. K. Ganesh, S. K. Meier, V. R. Ziatdinov, O. Mironov, J. Oxgaard, J. Gonzales and W. A. Goddard III, *J. Mol. Catal. A Chem.*, 2006, **251**, 8-23.

68. N. M. Emanuel', *Russ. Chem. Rev.*, 1978, **47**, 705-741.

69. M. H. Dickman and M. T. Pope, *Chem. Rev.*, 1994, **94**, 569-584.

70. D. Widmann and R. J. Behm, *Acc. Chem. Res.*, 2014, **47**, 740-749.

71. M. J. Ndolomingo, N. Bingwa and R. Meijboom, *J. Mater. Sci.*, 2020, **55**, 6195-6241.

72. M. Haruta, *Gold Bull.*, 2004, **37**, 27-36.

73. H. Kung, M. Kung and C. Costello, *J. Catal.*, 2003, **216**, 425-432.

74. J. A. Rodriguez, P. Liu, J. Hrbek, J. Evans and M. Pérez, *Angew. Chem. Int. Ed.*, 2007, **46**, 1329-1332.

75. P. Claus, H. Hofmeister and C. Mohr, *Gold Bull.*, 2004, **37**, 181-186.

76. G. Bond, *Gold Bull.*, 1972, **5**, 11-13.

77. G. J. Hutchings, *J. Catal.*, 1985, **96**, 292-295.

78. M. Haruta, T. Kobayashi, H. Sano and N. Yamada, *Chem. Lett.*, 1987, **16**, 405-408.

79. Y. Yamada, T. Arakawa, H. Hocke and Y. Uozumi, *Angew. Chem.*, 2007, **119**, 718-720.

80. G. Maayan and R. Neumann, *Chem. Commun.*, 2005, 4595-4597.

81. A. Fukuoka, J.-i. Kimura, T. Oshio, Y. Sakamoto and M. Ichikawa, *J. Am. Chem. Soc.*, 2007, **129**, 10120-10125.

82. L. Djakovitch, K. Köhler and J. G. d. Vries, *Nanoparticles and Catalysis*, 2008, 303-348.

83. N. Toshima and T. Yonezawa, *New J. Chem.*, 1998, **22**, 1179-1201.

84. B. R. Cuenya, *Thin Solid Films*, 2010, **518**, 3127-3150.

85. L. Ono, D. Sudfeld and B. R. Cuenya, *Surf. Sci.*, 2006, **600**, 5041-5050.

86. N. Lopez, T. Janssens, B. Clausen, Y. Xu, M. Mavrikakis, T. Bligaard and J. K. Nørskov, *J. Catal.*, 2004, **223**, 232-235.

87. J. Chen, Q. Zhang, Y. Wang and H. Wan, *Adv. Synth. Catal.*, 2008, **350**, 453-464.

88. B. G. Donoeva, D. S. Ovoshchnikov and V. B. Golovko, *ACS Catal.*, 2013, **3**, 2986-2991.

89. T. Nanba, S. Masukawa, A. Abe, J. Uchisawa and A. Obuchi, *Catal. Sci. Technol.*, 2012, **2**, 1961-1966.

90. V. Bukhtiyarov, A. Carley, L. Dollard and M. Roberts, *Surf. Sci.*, 1997, **381**, L605-L608.

91. L. Zhang, C. Zhang and H. He, *J. Catal.*, 2009, **261**, 101-109.

92. A. Cho, *Science*, 2003.

93. Z. Feng, Q. Ren, R. Peng, S. Mo, M. Zhang, M. Fu, L. Chen and D. Ye, *Catal. Today*, 2019, **332**, 177-182.

94. S. Laursen and S. Linic, *Phys. Rev. Lett.*, 2006, **97**, 026101.

95. S. Chang, M. Li, Q. Hua, L. Zhang, Y. Ma, B. Ye and W. Huang, *J. Catal.*, 2012, **293**, 195-204.

96. M. Chen and D. W. Goodman, *Acc. Chem. Res.*, 2006, **39**, 739-746.

97. Z. Qu, Y. Bu, Y. Qin, Y. Wang and Q. Fu, *Appl. Catal. B: Environ.*, 2013, **132**, 353-362.

98. S. Wu, Y. Yang, C. Lu, Y. Ma, S. Yuan and G. Qian, *Eur. J. Inorg. Chem.*, 2018, **2018**, 2944-2951.

99. J. Radnik, C. Mohr and P. Claus, *Phys. Chem. Chem. Phys.*, 2003, **5**, 172-177.

100. C. Mohr, H. Hofmeister and P. Claus, *J. Catal.*, 2003, **213**, 86-94.

101. J. R. Croy, S. Mostafa, J. Liu, Y. Sohn, H. Heinrich and B. R. Cuenya, *Catal. Lett.*, 2007, **119**, 209-216.

102. G. Zhao, F. Yang, Z. Chen, Q. Liu, Y. Ji, Y. Zhang, Z. Niu, J. Mao, X. Bao and P. Hu, *Nat. Commun.*, 2017, **8**, 14039.

103. M. Chen and D. Goodman, *Science*, 2004, **306**, 252-255.

104. H. Over, Y. D. Kim, A. Seitsonen, S. Wendt, E. Lundgren, M. Schmid, P. Varga, A. Morgante and G. Ertl, *Science*, 2000, **287**, 1474-1476.

105. B. Hendriksen and J. Frenken, *Phys. Rev. Lett.*, 2002, **89**, 046101.

106. X.-Q. Gong, R. Raval and P. Hu, *Phys. Rev. Lett.*, 2004, **93**, 106104.

107. X.-Q. Gong, Z.-P. Liu, R. Raval and P. Hu, *J. Am. Chem. Soc.*, 2004, **126**, 8-9.

108. J. R. Croy, S. Mostafa, H. Heinrich and B. R. Cuenya, *Catal. Lett.*, 2009, **131**, 21-32.

109. J. F. Weaver, S. P. Devarajan and C. Hakanoglu, *J. Phys. Chem. C*, 2009, **113**, 9773-9782.

110. M. Skaf, S. Aouad, S. Hany, R. Cousin, E. Abi-Aad and A. Aboukaïs, *J. Catal.*, 2014, **320**, 137-146.

111. R. Xu, D. Wang, J. Zhang and Y. Li, *Chem. Asian J.*, 2006, **1**, 888-893.

112. M. Haruta, *ChemInform*, 2004, **35**.

113. M. J. Beier, T. W. Hansen and J.-D. Grunwaldt, *J. Catal.*, 2009, **266**, 320-330.

114. G. Sharma, A. Kumar, S. Sharma, M. Naushad, R. P. Dwivedi, Z. A. ALOthman and G. T. Mola, *J. King Saud Univ. Sci.*, 2019, **31**, 257-269.

115. X. Liu, M. Conte, M. Sankar, Q. He, D. M. Murphy, D. Morgan, R. L. Jenkins, D. Knight, K. Whiston and C. J. Kiely, *Appl. Catal. A: Gen.*, 2015, **504**, 373-380.

116. Z.-Q. Zhang, J. Huang, L. Zhang, M. Sun, Y.-C. Wang, Y. Lin and J. Zeng, *Nanotechnology*, 2014, **25**, 435602.

117. C. Williams, J. H. Carter, N. F. Dummer, Y. K. Chow, D. J. Morgan, S. Yacob, P. Serna, D. J. Willock, R. J. Meyer and S. H. Taylor, *ACS Catal.*, 2018, **8**, 2567-2576.

118. Y. Iizuka, R. Inoue, T. Miura, N. Morita, N. Toshima, T. Honma and H. Oji, *Appl. Catal. A: Gen.*, 2014, **483**, 63-75.

119. L. Liotta, A. Venezia, G. Deganello, A. Longo, A. Martorana, Z. Schay and L. Guczi, *Catal. Today*, 2001, **66**, 271-276.

120. C. A. Mirkin, *Small*, 2005, **1**, 14-16.

121. S. Kim, Y. F. Tsang, E. E. Kwon, K.-Y. A. Lin and J. Lee, *Korean J. Chem. Eng.*, 2019, **36**, 1-11.

122. C. H. Bartholomew, *Appl. Catal. A: Gen.*, 2001, **212**, 17-60.

123. T. Mallat and A. Baiker, *Chem. Rev.*, 2004, **104**, 3037-3058.

124. T. Mallat, Z. Bodnar, P. Hug and A. Baiker, *J. Catal.*, 1995, **153**, 131-143.

125. M. Besson, F. Lahmer, P. Gallezot, P. Fuertes and G. Fleche, *J. Catal.*, 1995, **152**, 116-121.

126. J. A. Widegren and R. G. Finke, *J. Mol. Catal. A Chem.*, 2003, **198**, 317-341.

127. P. Munnik, P. E. De Jongh and K. P. De Jong, *J. Am. Chem. Soc.*, 2014, **136**, 7333-7340.

128. J. Liu, *ACS Catal.*, 2017, **7**, 34-59.

129. D. B. Eremin and V. P. Ananikov, *Coord. Chem. Rev.*, 2017, **346**, 2-19.

130. S. Schauermann, J. Hoffmann, V. Johánek, J. Hartmann, J. Libuda and H. J. Freund, *Angew. Chem. Int. Ed.*, 2002, **41**, 2532-2535.

131. L. D. Pachon and G. Rothenberg, *Appl. Organomet. Chem.*, 2008, **22**, 288-299.

132. A. V. Gaikwad, A. Holuigue, M. B. Thathagar, J. E. ten Elshof and G. Rothenberg, *Chem. Eur. J.*, 2007, **13**, 6908-6913.

133. Z. Niu, Q. Peng, Z. Zhuang, W. He and Y. Li, *Chem. Eur. J.*, 2012, **18**, 9813-9817.

134. J.-S. Chen, A. N. Vasiliev, A. P. Panarello and J. G. Khinast, *Appl. Catal. A: Gen.*, 2007, **325**, 76-86.

135. T. Borkowski, J. Dobosz, W. Tylus and A. M. Trzeciak, *J. Catal.*, 2014, **319**, 87-94.

136. H. Gruber-Wölfler, P. Radaschitz, P. Feenstra, W. Haas and J. Khinast, *J. Catal.*, 2012, **286**, 30-40.

137. M. Lamblin, L. Nassar-Hardy, J. C. Hierso, E. Fouquet and F. X. Felpin, *Adv. Synth. Catal.*, 2010, **352**, 33-79.

138. N. T. Phan, M. Van Der Sluys and C. W. Jones, *Adv. Synth. Catal.*, 2006, **348**, 609-679.

139. J. Rebek and F. Gavina, *J. Am. Chem. Soc.* , 1974, **96**, 7112-7114.

140. J. Rebek, D. Brown and S. Zimmerman, *J. Am. Chem. Soc.*, 1975, **97**, 454-455.

141. Y. Ji, S. Jain and R. J. Davis, *J. Phys. Chem. B*, 2005, **109**, 17232-17238.

142. A. Corma, H. García and A. Leyva, *Appl. Catal. A: Gen.*, 2002, **236**, 179-185.

143. Z.-Y. Pu, X.-S. Liu, A.-P. Jia, Y.-L. Xie, J.-Q. Lu and M.-F. Luo, *J. Phys. Chem. C*, 2008, **112**, 15045-15051.

144. C. Bozo, N. Guilhaume and J.-M. Herrmann, *J. Catal.*, 2001, **203**, 393-406.

145. H. Y. Kim, H. M. Lee and G. Henkelman, *J. Am. Chem. Soc.*, 2012, **134**, 1560-1570.

146. G. Sedmak, S. Hočevar and J. Levec, *J. Catal.*, 2004, **222**, 87-99.

147. G. Sedmak, S. Hočevar and J. Levec, *J. Catal.*, 2003, **213**, 135-150.

148. M. Wu, Y. Fu, W. Zhan, Y. Guo, Y. Guo, Y. Wang and G. Lu, *Catalysts*, 2017, **7**, 155.

149. L. Dall'Acqua, I. Nova, L. Lietti, G. Ramis and E. Giamello, *Phys. Chem. Chem. Phys.*, 2000, **2**, 4991-4998.

150. M. Conte, H. Miyamura, S. Kobayashi and V. Chechik, *Chem. Commun.*, 2010, **46**, 145-147.

151. S. Shanmugapriya, P. Zhu, C. Yan, A. M. Asiri, X. Zhang and R. K. Selvan, *Adv. Mater. Interfaces*, 2019, **6**, 1900565.

152. R. Wojcieszak, A. Jasik, S. Monteverdi, M. Ziolek and M. Bettahar, *J. Mol. Catal. A Chem.*, 2006, **256**, 225-233.

153. J.-W. Jun, Y.-W. Suh, D. J. Suh and Y.-K. Lee, *Catal. Today*, 2018, **302**, 108-114.

154. C. Nico, T. Monteiro and M. P. Graça, *Prog. Mater. Sci.*, 2016, **80**, 1-37.

155. I. Nowak and M. Ziolek, *Chem. Rev.*, 1999, **99**, 3603-3624.

156. R. A. Rani, A. S. Zoolfakar, A. P. O'Mullane, M. W. Austin and K. Kalantar-Zadeh, *J. Mater. Chem.*, 2014, **2**, 15683-15703.

157. J.-M. Jehng and I. E. Wachs, *Catal. Today*, 1990, **8**, 37-55.

158. J. M. Jehng and I. E. Wachs, *J. Phys. Chem.*, 1991, **95**, 7373-7379.

159. T. Iizuka, K. Ogasawara and K. Tanabe, *Bull. Chem. Soc. Jpn.*, 1983, **56**, 2927-2931.

160. Y. Li, S. Yan, W. Yang, Z. Xie, Q. Chen, B. Yue and H. He, *J. Mol. Catal. A Chem.*, 2005, **226**, 285-290.

161. H. Schäfer, R. Gruehn and F. Schulte, *Angew. Chem., Int. Ed. Engl.*, 1966, **5**, 40-52.

162. E. Ko and J. Weissman, *Catal. Today*, 1990, **8**, 27-36.

163. M. Ziolek, I. Sobczak, P. Decyk and L. Wolski, *Catal. Commun.*, 2013, **37**, 85-91.

164. S. H. Siddiki, M. N. Rashed, M. A. Ali, T. Toyao, P. Hirunsit, M. Ehara and K. i. Shimizu, *ChemCatChem*, 2019, **11**, 383-396.

165. J. M. Jehng and I. E. Wachs, *J. Phys. Chem*, 1991, **95**, 7373-7379.

166. S. Furukawa, T. Shishido, K. Teramura and T. Tanaka, *J. Phys. Chem. C*, 2011, **115**, 19320-19327.

167. T. Shishido, T. Miyatake, K. Teramura, Y. Hitomi, H. Yamashita and T. Tanaka, *J. Phys. Chem. C*, 2009, **113**, 18713-18718.

168. S. Furukawa, Y. Ohno, T. Shishido, K. Teramura and T. Tanaka, *ChemPhysChem*, 2011, **12**, 2823-2830.

169. D. A. Aranda, A. D. Ramos, F. B. Passos and M. Schmal, *Catal. Today*, 1996, **28**, 119-125.

170. R. Brown and C. Kemball, *J. Chem. Soc. Faraday Trans.*, 1996, **92**, 281-288.

171. S. Furukawa, A. Tamura, T. Shishido, K. Teramura and T. Tanaka, *Appl. Catal. B: Environ.*, 2011, **110**, 216-220.

172. M. Ziolek, P. Decyk, I. Sobczak, M. Trejda, J. Florek, H. G. W. Klimas and A. Wojtaszek, *Appl. Catal. A: Gen.*, 2011, **391**, 194-204.

173. S. Martínez-Méndez, Y. Henríquez, O. Domínguez, L. D'Ornelas and H. Krentzien, *J. Mol. Catal. A Chem.*, 2006, **252**, 226-234.

174. N. Ballarini, F. Cavani, C. Cortelli, C. Giunchi, P. Nobili, F. Trifirò, R. Catani and U. Cornaro, *Catal. Today*, 2003, **78**, 353-364.

175. M. O. Guerrero-Pérez and M. A. Banares, *Catal. Today*, 2009, **142**, 245-251.

176. P. Korovchenko, N. Shiju, A. Dozier, U. Graham, M. Guerrero-Pérez and V. Guliants, *Top. Catal.*, 2008, **50**, 43.

177. V. V. Guliants, R. Bhandari, A. R. Hughett, S. Bhatt, B. D. Schuler, H. H. Brongersma, A. Knoester, A. M. Gaffney and S. Han, *J. Phys. Chem. B*, 2006, **110**, 6129-6140.

178. J. M. Campelo, D. Luna, R. Luque, J. M. Marinas and A. A. Romero, *ChemSusChem*, 2009, **2**, 18-45.

179. H. Zhao, J. Zhou, H. Luo, C. Zeng, D. Li and Y. Liu, *Catal. Lett.*, 2006, **108**, 49-54.

180. J. M. Campelo, T. D. Conesa, M. J. Gracia, M. J. Jurado, R. Luque, J. M. Marinas and A. A. Romero, *Green Chem.*, 2008, **10**, 853-858.

181. F. W. Zemichael, A. Palermo, M. S. Tikhov and R. M. Lambert, *Catal. Lett.*, 2002, **80**, 93-98.

182. M. Lamoth, M. Plodinec, L. Scharfenberg, S. Wrabetz, F. Girgsdies, T. Jones, F. Rosowski, R. Horn, R. Schlögl and E. Frei, *ACS Appl. Nano Mater.*, 2019, **2**, 2909-2920.

183. L. Lefferts, J. Van Ommen and J. Ross, *Appl. Catal.*, 1986, **23**, 385-402.

184. G. J. Millar and M. Collins, *Ind. Eng. Chem. Res.*, 2017, **56**, 9247-9265.

185. M. Grabchenko, G. Mamontov, V. Zaikovskii and O. Vodyankina, *Kinet. Catal.* , 2017, **58**, 642-648.

186. L. Brugnoli, A. Pedone, M. C. Menziani, C. Adamo and F. d. r. Labat, *J. Phys. Chem. C*, 2020, **124**, 25917-25930.

187. A. R. Almeida, J. A. Moulijn and G. Mul, *J. Phys. Chem. C*, 2011, **115**, 1330-1338.

188. X. Zhang, Z. Qu, X. Li, M. Wen, X. Quan, D. Ma and J. Wu, *Sep. Purif. Technol.*, 2010, **72**, 395-400.

189. V. V. Dutov, G. Mamontov, V. Zaikovskii, L. Liotta and O. Vodyankina, *Appl. Catal. B: Environ.*, 2018, **221**, 598-609.

190. A.-Q. Wang, J.-H. Liu, S. Lin, T.-S. Lin and C.-Y. Mou, *J. Catal.*, 2005, **233**, 186-197.

191. H. Einaga and A. Ogata, *Environ. Sci. Technol.*, 2010, **44**, 2612-2617.

192. V. Raji, M. Chakraborty and P. A. Parikh, *Ind. Eng. Chem. Res.*, 2012, **51**, 5691-5698.

193. R. Chimentao, I. Kirm, F. Medina, X. Rodriguez, Y. Cesteros, P. Salagre and J. Sueiras, *Chem. Commun.*, 2004, 846-847.

194. R. J. Chimentao, F. Medina, J. E. Sueiras, J. L. G. Fierro, Y. Cesteros and P. Salagre, *J. Mater. Sci.*, 2007, **42**, 3307-3314.

195. S. Dhalewadikar, E. Martinez and A. Varma, *Chem. Eng. Sci.*, 1986, **41**, 1743-1746.

196. R. Van Santen and H. Kuipers, *Adv. Catal.*, 1987, **35**, 265-321.

197. W. Menezes, V. Zielasek, K. Thiel, A. Hartwig and M. Bäumer, *J. Catal.*, 2013, **299**, 222-231.

Chapter 2: Experimental methods and techniques

2.1 Materials

A complete list of materials is reported below (table 2.1), materials used for a specific purpose are described under the relevant section headings for elucidation.

Table 2.1 List of reagents used in this thesis experimental work.

Reagents	Formula	Purity/Grade/Form	Supplier
3A	--	3A zeolite	Acros
Acetone	CH_3COCH_3	≥99%	Fisher
Activated charcoal, Darco 4-12 MESH	C	--	Acros
Activated charcoal, Norit 12-40 MESH	C	--	Acros
Activated charcoal, Darco G-60, decolorizing	C	--	Acros
Cerium (IV) oxide	CeO_2	99.9%, trace metal basis	Acros
Cyclohexane	C_6H_{12}	99.5% anhydrous	Sigma
Cyclododecane	$C_{12}H_{24}$	99%	Insight Biotechnology
Cyclooctane	C_8H_{16}	≥99%	Aldrich
Cyclooctanol	$C_8H_{16}O$	97%	Alfa Aesar
Cyclooctanone	$C_8H_{14}O$	98%	Aldrich
Dichloromethane (DCM)	CH_2Cl_2	HPLC grade	Sigma
Deuterated chloroform	$CDCl_3$	99.8%D	VWR
Ethylbenzene	C_8H_{10}	99.8%	Acros
Gold(III) chloride trihydrate	$HAuCl_4{\cdot}3H_2O$	≥99% trace metal basis	Fluka
Hydrochloric acid (aqueous)	HCl	35%	VWR
Iron(III) acetylacetonate	$Fe(C_5H_7O_2)_3$	99+%	Acros
Iron(III) nitrate nonahydrate	$Fe(NO_3)_3{\cdot}9H_2O$	99+%	Acros
Magnesium oxide	MgO	≥97%	Sigma
Magnesium sulfate	$MgSO_4$	99+%	Alfa Aesar
n-decane	$C_{10}H_{22}$	99%	Acros
n-dodecane	$C_{12}H_{26}$	99%	Fischer scientific

Niobium (IV) Oxide	NbO_2	99+%	Alfa Aesar
Niobium (V) Oxide	Nb_2O_5	99.9% trace metals basis	Sigma-Aldrich
Niobium(V) Oxide	Nb_2O_5	99.99% trace metals basis	Aldrich
Nitric acid	HNO_3	68%	VWR
Polyvinylalcohol (PVA)	$(C_2H_4O)_x$	99%+ hydrolysed, MW 8000-10000	Sigma-Aldrich
Silver nitrate	$AgNO_3$	≥99.8%	Sigma
Silver oxide	Ag_2O	99%	Honeywell
Sodium borohydride	$NaBH_4$	Powder, ≥98.0%	Aldrich
Sodium hydroxide	NaOH	≥98%, pellets	VWR
Sodium carbonate	Na_2CO_3	≥99.8%	Honeywell
tert-Butyl hydroperoxide	$C_4H_{10}O_2$	70% solution in water	Merck
Titanium (IV) oxide	TiO_2	99.99% trace metal basis	Acros
Titanium (IV) oxide	TiO_2	Aeroxide ®, p-25	Aldrich
Titanium (IV) oxide	TiO_2	Anatase, 99.8% trace metals basis	Aldrich
Trifluorotoluene	$C_6H_5CF_3$	99%	Alfa Aesar
Zeolite 13X	--	--	Acros

2.2 Catalyst preparation

The aim of designing catalytic materials is to obtain the desired products with high selectivity and yields. As such it is desirable to have catalysts with high activity, and stability which are important characteristics for industrial scale up[1]. Furthermore, in this work we made large use of metal supported nanoparticle catalysts. As the reaction performances of these materials rely on the size of the particles, shape and dispersion of the metal particles[2, 3], and these factors can be controlled, at least up to some extent by the preparation method, the most common synthesis routes for these materials will be briefly described here. Four main preparation methods will be discussed in this part, known as: impregnation (either wetness or incipient)[1, 4], deposition precipitation[1, 5], coprecipitation[1, 6] and sol-immobilization[1, 7, 8].

2.2.1 Principles of supported metal nanoparticle preparation methods

2.2.1.1 Impregnation method

The impregnation method is widely used in the industrial practice as it is a practical and economic process compared to other methods. The wet impregnation process involves the full contact (via absorption) between an excess amount of solution containing a metal dopant precursor of active species and a support. After a drying process to eliminate the solvent containing the precursor, the resultant solid is calcined to convert the metal salt precursor into, most often, a metal oxide or mixed oxide over the support surface, which is displayed in scheme 2.1[4]. It should be mentioned that after the calcination process, a reduction step by H_2 is often followed to chemically convert the metal oxide particles into metallic nanoparticles (in our case, Ag_2O is not always thermally decomposed into Ag^0 after calcination). A variation to this protocol, called 'incipient wetness impregnation' (IWI), is also widely used. In this method the amount of precursor solution is just sufficient to fill the macroscopic pore volume of the support[9]. In industrial application, this method is usually preferred from an economical perspective as the desired amount of solution is equal to the pore volumes. However, undesired gradient effects upon catalyst preparation are created during the process, which is difficult to control. In our research, the wet impregnation method was mainly employed for the preparation of supported Ag or Fe over Nb_2O_5 and other supports like CeO_2, TiO_2, MgO, SiO_2, and then the resultant catalysts were used for the oxidation of cyclooctane and cyclohexane.

The impregnation method is easy to operate, economic especially for noble metals and could be reliably repeated for specific metal loading but it is usually limited by the solubility of

the precursors[1]. This method has been widely used for the preparation of supported metal catalysts for the oxidation of hydrocarbons or to ketones or alcohols or alcohol oxidation. For example, Matthias et al. prepared the silver-based catalysts with different supports for the oxidation of alcohols, which showed the superior performance in the presence of CeO_2 with conversions up to 98% by Ag/SiO_2[10]. Supported Ag over ZrO_2 was prepared for the oxidation of soot in liquid phase, and the hemispherically shaped Ag particles dispersed non-uniformly on ZrO_2 support were obtained[11]. However, it should be mentioned that the metal particle size can be influenced by preparation method (as discussed in section 1.2.2.1), which is an important parameter contributing to the catalytic activity[12, 13]. For example, there is evidence showing that the supported gold particles with the size larger than 30 nm on titania was inactive for the oxidation of CO while the activity of gold particles rises obviously when size is smaller than 4 nm[14], illustrating different nanomaterials may behave differently depending on their size and dispersion[15-17].The size of supported Ag nanoparticles over Al_2O_3 prepared by impregnation method falls in the range of 3.5-25 nm and larger size is found from 12-50 nm in the catalyst prepared by solgel methods[13].

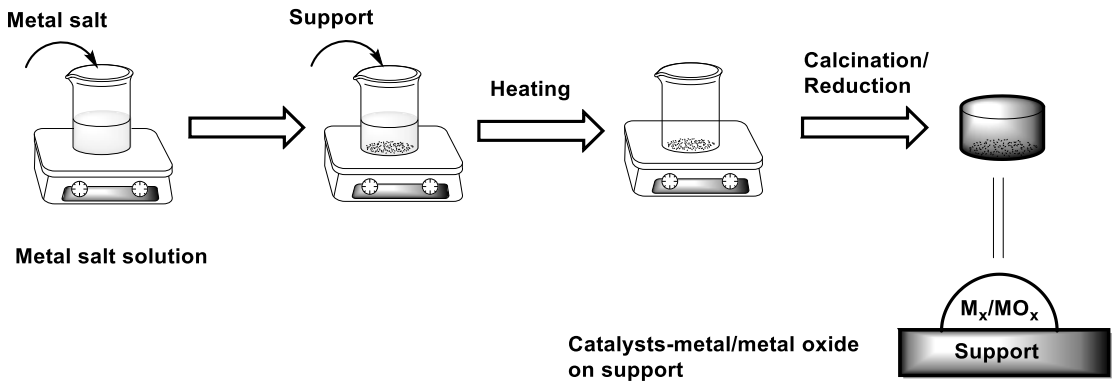

Scheme 2.1 A schematic diagram to illustrate the preparation process of supported metal by wetness impregnation method.[1, 4] The slurry is fully dried at a set temperature (80 °C in our case) and the calcination is operated in the air. A reduction process by H_2 is followed to furtherly induce the formation of single state of metal (Ag^0 in our catalysts).

2.2.1.2 Deposition-precipitation method

Haruta et al. developed the deposition precipitation (DP) method for the preparation of supported gold nanoparticles on metal oxides and smaller gold nanocrystals were found to be deposited on the surface[18] in comparison with that prepared by impregnation method. This procedure (scheme 2.2) involves the addition of a precursor containing solution to a support under stirring. The key step is to adjust the pH of the solution during the synthesis process, by the addition of an alkaline solution (most commonly: NaOH, Na_2CO_3, or urea)[5, 19]. This induces the formation, and the precipitation of $M_xO_y(OH)_z$ clusters, which then deposit over the support surface, with the latter most often a metal oxide. It should be noted that in this procedure, the accurately controlled precipitation which is mainly affected by pH values and deposition time is quite important, as the nucleation of the metal species is generally induced by changing the pH value for the graduating deposition[9]. Classically, deposition precipitation is developed to produce catalysts with metal loadings that exceed those obtained by impregnation which is

limited by solubility of the precursor containing solution[20]. On the other hand, the polyhydroxy metal clusters that will deposit over the catalyst, may not entirely precipitate and as such part of the metal is often lost in solution as it is not deposited on support.

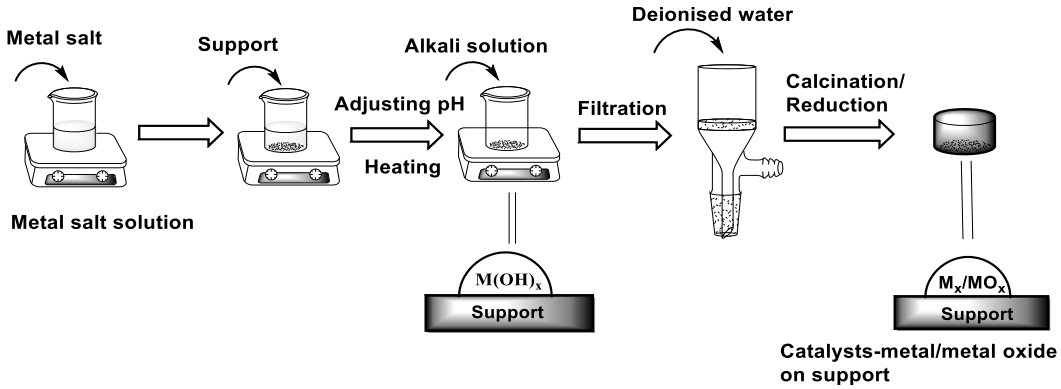

Scheme 2.2 A schematic diagram to illustrate the preparation process of supported metal by deposition precipitation.[5, 19] The pH value is controlled by alkali solution (e.g., NaOH, Na_2CO_3) and Na_2CO_3 with a relatively weak alkalinity is used in preparation process, which should be removed by the washing step with deionised water.

The catalysts prepared by deposition precipitation method exhibits high performances in the oxidation of hydrocarbons. For example, a highly active Au/Al_2O_3 catalyst was prepared for cyclohexane oxidation by molecular oxygen, which indicated that Au/Al_2O_3 catalysts with the gold particles of 3 - 6 nm was selectively reactive (12-13% conversion) for the selective cyclohexane oxidation to cyclohexanone and cyclohexanol under relatively mild conditions[21]. This supported material over TiO_2/SiO_2 was also investigated for the oxidation of cyclohexane, with conversion can be up to 8-9%[22]. In addition, it was found that gold nanoparticles spherical shape prepared by impregnation method were just loaded on the very surface of TiO_2, but the nanoparticles with hemispherical shape from deposition precipitation method were strongly

attached to the support[18, 23, 24]. Hence, different methods could influence the morphology of nanoparticles, which may be related with the catalytic performance.

In our case, we investigated supported Ag nanoparticles over metal oxides applied to the oxidation of cyclooctane and cyclohexane to furtherly extend the application of Ag based catalysts. So the deposition precipitation method was used for the preparation of supported monometallic Ag, Fe or bimetallic Ag and Fe over Nb_2O_5.

2.2.1.3 Coprecipitation method

A metal salt solution is well mixed with a dissolvable precursor that will be converted into the support, which is followed by the addition of basic additive to precipitate for the precipitation of doped metal over support. The slurry is then thoroughly washed by deionised water and the resulting solid will be calcined or reduced for the formation of supported metal oxides or metallic metals on support. This procedure is summarised in scheme 2.3. In this process, a thorough mixing of metal salt solution and support precursor, the order of the addition of various solutions, the coprecipitation temperature and the ageing time of slurry are quite important parameters to be controlled for a uniform distribution of metal particles.[1, 25] Especially the pH value of the mixture should be precisely adjusted to ensure the precipitation of various components in a desired sequence, otherwise the doped metal might hamper the support formation, affecting the structure of catalysts with undesirable properties.[1, 26] In addition, It should be noted in the case of preparing supported metal catalyst with the loading above 10-15%, this method is more favoured[1]. An industrial application of this method is used for the coprecipitation of Cu, Zn, Al to prepare $Cu/ZnO/Al_2O_3$ catalysts which are applied in

the synthesis of methanol.[25, 27] Within our research project, coprecipitation method is not employed as the coprecipitation process of doped metal and support precursor is more difficult to control in comparison with deposition precipitation method, and the metal loading in our research is normally lower than 5 *wt*%. Thus, this method is only discussed here for the completeness as comparison with other methods.

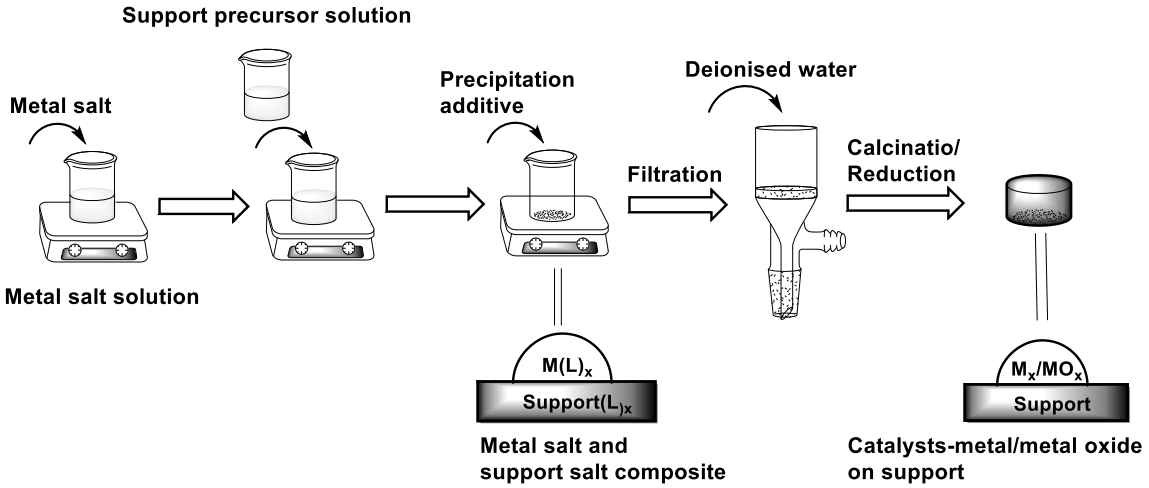

Scheme 2.3 A schematic diagram to display the coprecipitation steps for the preparation of supported metal/metal oxides catalysts. Precipitation additive (e.g., NaOH, Na_2CO_3) is normally added to adjust the pH value.[1, 6, 28, 29]

2.2.1.4 Sol immobilization method

There exists vast literature that this method can control the particle size more precisely with a narrower particle size and obtain high dispersion on the surface[30, 31] compared to the other protocols described above. The preparation process is illustrated in scheme 2.4, in which a reducing agent is added to form the colloids[7], and the metal resultant metal nanoparticles are initially protected from aggregation by the use of ligands (e.g., polyvinyl alcohol)[7, 8], which will then need to be removed afterwards.

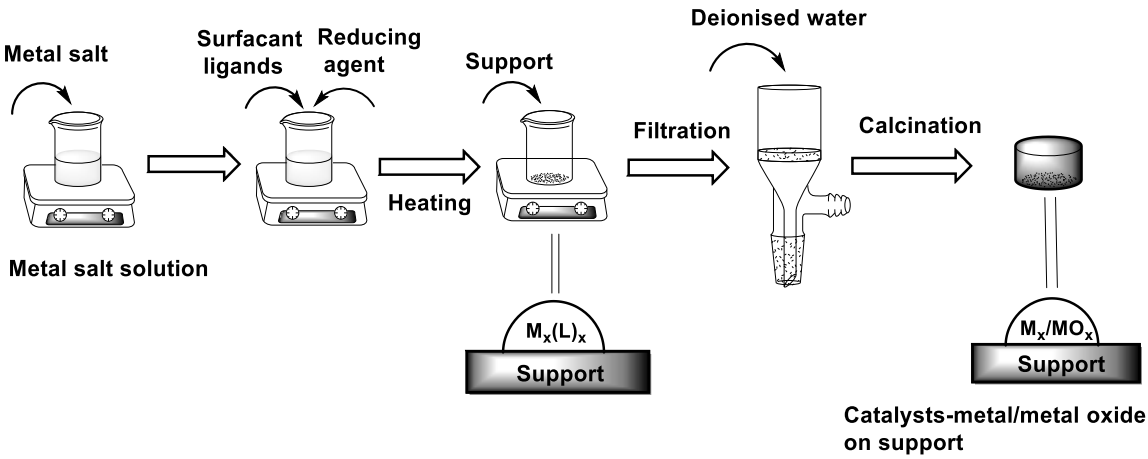

Scheme 2.4 A schematic diagram to illustrate the preparation process of supported metal by sol immobilization method.[7, 8] In this process, a protective ligand is employed to stabilize the particles to against aggregation, which should be removed afterwards.

This method is commonly used for the preparation of supported monometallic and bimetallic catalysts especially for research in academia rather than industry as it is difficult to scale up. Monometallic Ag, Pd and bimetallic Ag-Pd nanoparticles supported on MgO prepared via sol-immobilization method were investigated for the selective oxidation of cyclohexane[8]. It was observed that the supported Ag nanoparticles catalyst prepared by sol-immobilization method showed higher catalytic activity than the catalyst synthesized by impregnation method. And Ag-Pd/MgO catalysts showed enhanced conversion with high selectivity to cyclohexanol compared to the Ag/MgO and PdO/MgO catalysts. Au-Pd bimetallic catalyst was prepared for the oxidation of benzyl alcohol in mild conditions using molecular oxygen as oxidant, which exhibits a conversion > 52% and selectivity of around 100% for benzaldehyde[32]. It has been studied that the catalysts prepared by sol immobilization protocol show superior reaction performances in certain kind of reactions[7, 33, 34], e.g., benzyl alcohol oxidation, cyclohexane oxidation, glycerol oxidation. However, it should be mentioned that

although the smaller particle size may enhance the conversion of reactants, the products distribution may also become complicated, resulting in the decrease of the selectivity for desired products, indicating that the balance between the reactivity and selectivity should be judged. What's more, in case industrial applications are targeted, the sol immobilization method is not a very attractive technique for the preparation of catalysts because of the use of a large volume of water, a costly stabilizing polymer as well as sodium borohydride or a similar reductant[3]. At present, the most convenient method for scaling up would be an impregnation-based method only[1, 3]. From this perspective, our project mainly focused on the application of impregnation method. In our case, sol-immobilization method was mainly used for the preparation of supported Ag/Nb_2O_5, which also served as a comparison or benchmark with the catalysts prepared by impregnation and deposition precipitation method.

In summary: four preparation methods were discussed above: impregnation, deposition-precipitation, coprecipitation and sol-immobilization protocol. The most important features of these methods are: the impregnation method is the easiest to carry out and scale up to industrial production, but the nanoparticles prepared by this method are quite large with a broad particle size distribution. The deposition-precipitation method and sol-immobilization method are more effective in the control of the properties (size, morphology, etc.) of supported metal nanoparticles and there is research demonstrating the difference of particle size and distribution of Pd/ZnO prepared by these three methods and their reaction performances[35]. However, a large number of metals is usually lost in the deposition precipitation method and

sol immobilization involves a lot of synthesis steps including the removal of protective ligand, making it difficult to scale up. A comparison for these methods is illustrated in table 2.2.

Table 2.2 The description of the methods for the preparation of supported metal catalysts[2].

Methods	Advantages	Disadvantages
Impregnation	Simple, low cost; all metal ions in aqueous solution can be supported; suitable for industrial production.	High temperature; large size, poor and inhomogeneously distribution of nanoparticles.
Deposition-precipitation	Small and high distribution of nanoparticles; effective to remove chlorine ions.	Strictly control of pH, temperature and time; poor reproducibility; not suitable for all supports due to isoelectric point; difficult to deposit all metal ions on the supports; an amount of metals is lost in the filtration step.
Coprecipitation	Simple, low cost; small and high distribution of metal nanoparticles.	Strictly control of pH and temperature; poor reproducibility; low metal utilization due to the encapsulation in support.
Sol-immobilization	Small and homogeneously distribution of nanoparticles.	Large number of synthesis steps and reactants; need strict control of the amount of reducing agents; difficult to scale up; stabilizer ligand needs to be removed at the end.

2.2.2 Catalyst preparation process in this research work

2.2.2.1 Wetness impregnation method

Herein, supported Ag/Nb_2O_5 (1 *wt*% of Ag) was prepared by following the procedure (denoted as $WI\text{-}Ag/Nb_2O_5$, others would be specified.) for the preparation of 2 g of catalyst: an appropriate amount of metal salt $AgNO_3$ (0.0315 g) was dissolved into deionized water (20 mL), followed by the addition of Nb_2O_5 (1.9800 g) support to obtain the desired 1 *wt*% metal

weight loading. The slurry was left at 80 °C under vigorous stirring until it was fully dried. Then the solid was heated at 120 °C for 16 h in an oven, followed by calcination at specific time (16 h to 48 h) at temperatures between 180 °C and 300 °C. This procedure was identical across all other dopant metals (Au, Fe) and supports (TiO_2, CeO_2, SiO_2, MgO).

Bimetallic catalysts denoted as WI-Ag-Fe/Nb_2O_5 with various Ag:Fe molar ratios (1:1 and 1:5) were prepared. In principle, the bimetallic catalysts would be expected to display bifunctional catalytic activity, that is: one metal is capable of abstracting H atom of C-H to promote the initiation (possibly by Fe) and another metal could enhance either of C-H abstraction to form the ketone or O-O cleavage to give the alcohol. The procedures for the preparation of bimetallic Ag-Fe/Nb_2O_5 (molar ratio n_{Ag}/n_{Fe}=1) with a specific 1 *wt*% Ag loading followed a sequential addition by doping Fe firstly and then Ag were deposited. This process were as follows: 0.0454 g of $Fe(NO_3)_3$ was dissolved into 20 mL deionised water, followed by the addition of the support Nb_2O_5 (1.9456 g), and then the system was left at 80 °C with vigorous stirring until it was fully dried. The powder was heated at 120 °C for 16 h in oven, followed by calcination at 550 °C for 5 h. After that, 0.0158 g of $AgNO_3$ dissolved into deionised water, with the addition of 0.9900 g of as prepared Fe/Nb_2O_5. The slurry was fully dried at 80 °C. The solid was dried at 120 °C for 16 h in oven, followed by calcination at 180 °C for 16 h, which was the catalyst WI-Ag_1-Fe_1/Nb_2O_5 with the molar ratio between Ag and Fe=1:1. The same protocol was applied for the preparation of the catalysts with a different n_{Ag}:n_{Fe} ratio.

2.2.2.2 Deposition-precipitation method

Supported Ag over Nb_2O_5 catalysts with 1 *wt*% Ag loading was prepared by deposition-

precipitation method as follows (denoted as DP-Ag/Nb_2O_5): 1.98 g of Nb_2O_5 was added to 44 mL of an aqueous solution containing $AgNO_3$ ($4.2 \cdot 10^{-3}$ mol·L^{-1}). The pH value was adjusted to 8-10 by dropwise addition of 0.5 mol·L^{-1} Na_2CO_3, promoting AgOH precipitation on the support Nb_2O_5. The resulting slurry was heated at a constant temperature of 80 °C for 2 h and then washed thoroughly by deionised water. The recovered solid was dried at 120 °C for 16 h, followed by calcination process between 180 °C and 300 °C from 5 to16 h.

Bimetallic catalysts Ag-Fe/Nb_2O_5 (1 *wt*% Ag loading) denoted as DP-Ag-Fe/Nb_2O_5 with two various molar ratios (1:1 and 1:5) between Ag and Fe were prepared by following the sequential addition of Fe and then Ag reactively. As usually the calcination temperature for supported Fe catalysts is above 400 °C for the transformation of $Fe(OH)_x$ to Fe_xO_y[36, 37] while supported Ag is calcined at lower temperature (< 250 °C) in our case, so Fe species is tentatively to be doped firstly. In addition, the structures of bimetallic nanoparticles are more complex than that of monometallic particles, e.g., the two metal components can form the structure like core-shell, chemically ordered or randomly mixed[38-41], which would affect the catalytic performances. Surface segregation in bimetallic nanoparticles have shown effects on many processes like adsorption, corrosion, oxidation, by affecting the composition of two elements than the bulk[42, 43], which is surface dependent that is widely observed on (111) surfaces of Pt[44], Pd[45] and Ir[46]-based catalysts. And it is reported that a controllable segregation of Fe elements is found on the supported Ag nanoparticles over rutile TiO_2.[47] In view of this, Ag and Fe tend to be segregated instead of forming alloys even at nanoscale in the supported bimetallic catalysts. Thus, we tentatively prepared the bimetallic catalysts in a sequential

deposition of Fe then followed by Ag, the process being as follows: 1.9896 g of Nb_2O_5 was added to 44 mL of an aqueous solution containing $Fe(NO_3)_3$ ($4.2 \cdot 10^{-3}$ mol·L^{-1}). The pH value was adjusted to 8-10 by dropwise addition of 0.5 mol·L^{-1} Na_2CO_3, promoting $Fe(OH)_3$ precipitation on the support Nb_2O_5. The resulting slurry was heated at a constant temperature of 80 °C for 2 h and then washed by deionised water. The solid was dried at 120 °C for 16 h, followed by calcination at 550 °C for 5 h. After that, take 1 g of the prepared catalyst Fe/Nb_2O_5 into 22 mL $AgNO_3$ solution ($4.2 \cdot 10^{-3}$ mol·L^{-1}), adjusting the pH value to 9 for the precipitation of AgOH, which was kept at 80 °C for 2 h under stirring. And then the slurry was washed by deionised water thoroughly, followed by the drying at 120 °C for 16 h and calcination at 180 °C for 16 h, which was the catalyst DP-Ag_1-Fe_1/Nb_2O_5 with the molar ratio between Ag and Fe=1:1.

2.2.2.3 Sol immobilization method

The catalyst Ag/Nb_2O_5 with 1 *wt*% Ag loading was prepared by sol-immobilization protocol as follows (SI-Ag/Nb_2O_5). 2.4 g of polyvinyl alcohol (PVA) (1 *wt*% solution) was added with a weight ratio of PVA/Ag (by *wt*%) = 1.2. A 0.1 mol·L^{-1} freshly prepared solution of $NaBH_4$ ($NaBH_4$/Ag by mol = 5) was then added to form a dark-brown sol. After 30 mins stirring at room temperature, the colloid was immobilized by adding Nb_2O_5 under vigorous stirring. After 2 h the slurry was washed thoroughly with deionised water and then dried at 120 °C for 16 h, followed by the calcination at 180 °C for 16 h for the removal of template.

2.2.2.4 Supported metal catalyst reduction with hydrogen

The hydrogen reduction process can further reduce metal species from the oxidation state to sole metal (0 valence) state, this however doesn't preclude the existence of residues small

amounts of metal in high oxidation state at the metal/support interface[8, 48]. In our case, a sample of catalysts prepared by different methods (appropriately 0.50 g) was placed in the centre of a tubular furnace lined with a quartz tube, which was purged with pure nitrogen (1 bar, 100 mL·min^{-1}) for 10 mins, followed by the purge of a gas mixture of 5% H_2/N_2 (2 bar, 20 mL·min^{-1}) and then samples were treated at a selected temperature (180-200 °C) for 30 mins with 10 °C min^{-1} ramp.

2.3 Catalytic tests

In our research, the catalytic tests were carried out by using an array of experimental conditions, including atmospheric air pressure with condenser open to the air, and pressurised O_2 or N_2 atmospheres (0-2 bar in cyclooctane oxidation and 3-5 bar of O_2 in cyclohexane oxidation), aiming for the investigation about the roles of catalysts in the oxidation process. A temperature calibration for reaction devices was carried out to ensure the actual reaction temperature to be identical among different devices.

2.3.1 Temperature calibration of hot plate in reaction set up

During the research, the reaction would be conducted on different reaction set ups (e.g., the one from Asynt company at atmospheric pressure and another one from Radleys that was operated under pressure). Due to the temperature gap between set temperature of hot plate (called ‘set temperature’) and the temperature of reaction mixture inside round bottom flasks (called ‘actual temperature’), there may exist the difference of temperature among the reaction set ups we use even if the set temperature is the same. Thus, in order to keep the temperature identical among different reaction set ups, temperature calibration was carried out to identify

the set temperature and actual temperature, which could enable the reaction occur at the same actual temperature among different set ups, proving the identical results for comparison. In the calibration, *n*-decane (boiling point 174 °C) and cyclooctane (boiling point 151 °C) were used separately. The procedures were as follows: 3 mL of substrates was taken into a round bottom flasks which was placed on the hot plate. A temperature range from 80 °C to 150 °C was considered with measurements every 10 °C. The actual temperature of the substrate in flasks was measured by using a thermistor probe. In this way, the calibration curves were contained accordingly, which is displayed in Fig. 2.1.

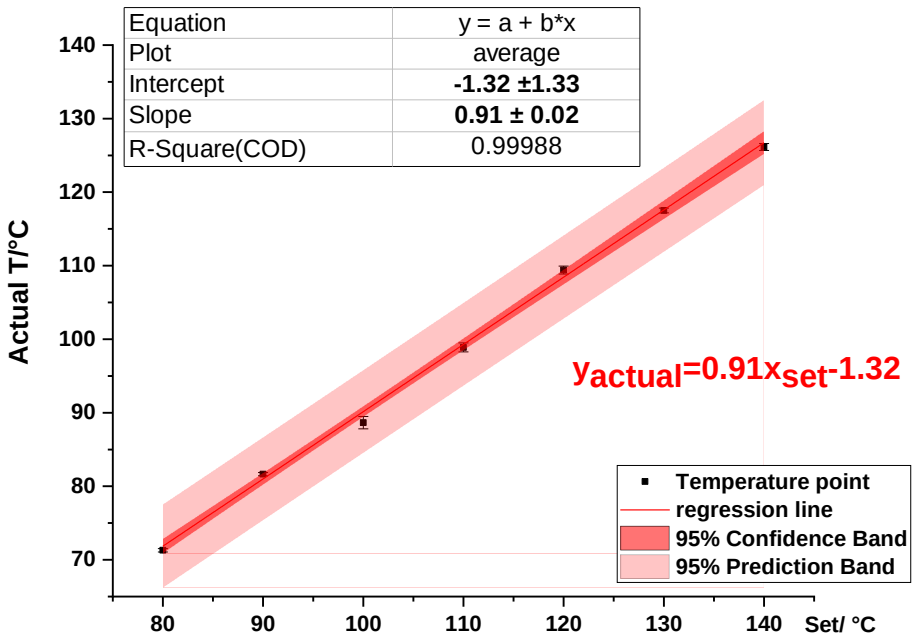

a. Temperature calibration by cyclooctane

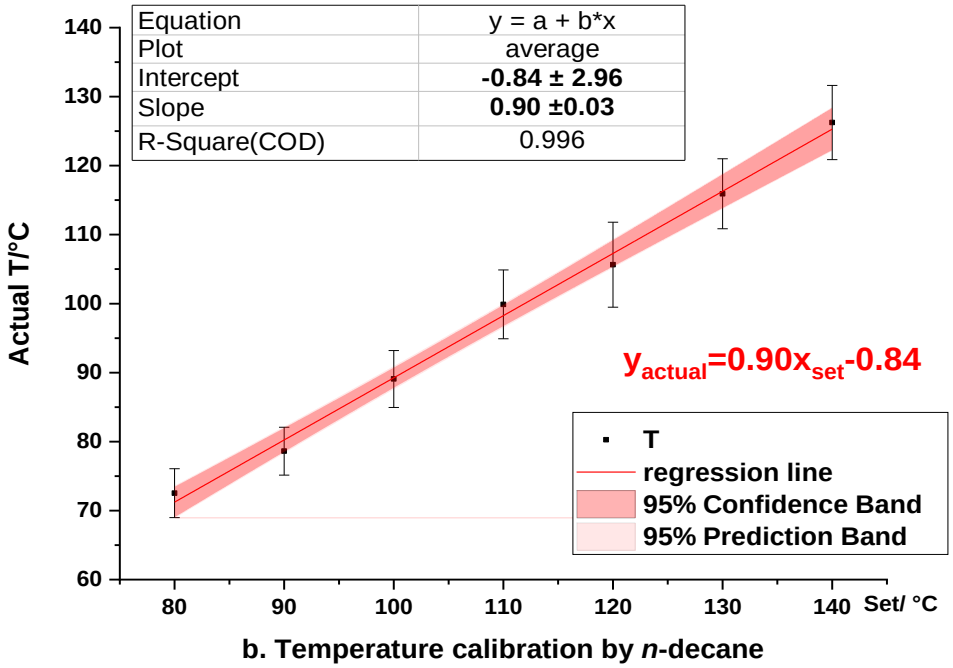

Fig. 2.1 Temperature calibration curves of hot plate by using various media. (a. cyclooctane: y=(0.91±0.02)·x−(1.32±1.33); b. *n*-decane: y=(0.90±0.03)·x−(0.84±2.96).) The process was conducted by setting a specific temperature of hot plate and then test the actual temperature of media inside the round bottom flasks, which were placed on a hot plate by using a thermocouple.

Fig. 2.1 shows that the regression lines when using cyclooctane is T_{actual}=(0.91±0.02)·T_{set}−(1.32±1.33) (as displayed in Fig.2.1-a) and it is T_{actual}=(0.90±0.03)·T_{set}−(0.84±2.96) (Fig.2.1-b) while *n*-decane is used, which are almost identical for both of the curves when taking the errors into account. And it can be observed that both of the intercepts of these regression lines are compatible with 0 (as such no systematic error is present) and all the temperature points spread in the range of confidence bands. In addition, as cyclooctane is used as one of the main reactants in our research, we tend to choose the regression line from cyclooctane for temperature calibration, T_{actual}=(0.91±0.02)·T_{set}−(1.32±1.33) . Moreover, cyclooctane and *n*-decane were employed for

boiling point test based on the regression curve we chose to furtherly confirm the validity of the formula for correction. The boiling point of cyclooctane and *n*-decane are 151 °C and 174 °C respectively at atmospheric pressure, and the corresponding set temperatures should be about 167.4 °C, 192.9 °C from the calibration curves. It was found that all the substrates in flasks were boiled under the set temperatures, and the average actual temperatures measured by a thermometer were 151.2 °C and 174.5 °C separately. Therefore, according to the consideration of cyclooctane as reactant and the boiling temperature test, the regression calibrated by using cyclooctane is reliable to determine the desired actual reaction temperature, that is $T_{actual}=(0.91\pm0.02)\cdot T_{set}-(1.32\pm1.33)$.

2.3.2 Cyclooctane oxidation

2.3.2.1. Test at atmospheric pressure open to air

The catalytic tests were typically carried out by taking 3 mL cyclooctane (0.0223 mol) into a round bottom flask with a water reflux condenser open to the air and under stirring (600 rpm), as shown in Fig. 2.2. In a typical experiment, the catalyst with a specific metal to substrate ratio was added into the reaction system, which was then heated to a desired temperature for a certain of time while stirring, and then allowed it to cool down until below 80 °C (as our tests indicated that there was no observed conversion of cyclooctane when temperature below 80 °C). An aliquot of the final reaction mixture was centrifuged for the separation of catalyst and liquid mixture which was then used for analysis either via ^{1}H-NMR or, if necessary, by using GC-MS.

Fig. 2.2 The reactor apparatus for the test at atmospheric pressure with water reflux condenser open to air.

2.3.2.2. Pressurised tests

The catalytic tests were typically carried out by taking 3 mL cyclooctane (22.3 mmol) into a screw capped pressure resistant round bottom flask (ACE flask) fitted with a glass insert bubbler (ACE tube), with the adding of a certain amount of catalyst under a specific metal to substrate ratio. Before the start of the reaction at a given temperature, the system was tested for the seal ability by purging into oxygen for the sake of safety. The oxygen was then purged into the flask to remove the air by increasing of the pressure of O_2 gradually at 0.5 bar

increments, until the designated pressure was met (usually 2 bar O_2 shown in the pressure gauge). The system was then heated to the desired temperature under stirring for a specific time. The mixture was then centrifuged to separate the solid catalyst and the resulting solution, which was used for analysis either via H-NMR or, if necessary, by using GC-MS.

2.3.3 Oxidation of ethylbenzene and cyclohexane

The procedure for the oxidation of ethylbenzene and cyclohexane was identical to that of cyclooctane. It should be noted that in the oxidation of ethylbenzene, the reaction temperature and initial O_2 pressure were 130 °C and 2 bar respectively with a specific reaction time for 24 h. In addition, the reaction conditions for the oxidation of cyclohexane were optimized by changing the reaction temperature and O_2 pressure (see in chapter 6). Moreover, the oxidation of cyclohexane was also carried out by adding *tert*-butyl hydroperoxide (TBHP) as initiator, with TBHP as 1 mol% with respect to the substrate in reaction mixture. As the TBHP is supplied as a 70% solution in water though, so water should be removed before the tests, 1 mL of TBHP solution was mixed with 5 mL of cyclohexane and left it for 24 h at room temperature. TBHP would be extracted into cyclohexane phase as the higher solubility in comparison with that in water. And then taking 200 μL of the anhydrous TBHP solution in cyclohexane from the cyclohexane phase into 3 mL of cyclohexane for reaction in the presence of catalysts, in which the concentration of TBHP was 1 mol%, verified by ^{1}H-NMR.

2.3.4 Control test for the leaching of Ag^+

It is known that metal species that can leach in solution, besides affecting the catalyst lifetime, can also contribute to the reaction themselves and having catalytic activity, as

discussed in section 1.2.3 of chapter 1. In view of this, preliminary control tests were conducted to assess the role that Ag^+ species that could potentially leached in solution. Identical procedures with that of cyclooctane oxidation were used with $AgNO_3$ as catalyst. It should be noted, that as the amount of metal salt to carry out this control test was usually very minor (even less than 0.5 mg), in order to reduce the experimental error associated to these tests, a concentrated $AgNO_3$ solution in water was prepared, then a volume containing the desired amount of Ag was taken and transferred into a round bottom flask. The flask was dried at 100 ˚C up to dryness, then upon cooling the organic substrate was added.

2.3.5 Oxidation of 1-phenylethyl hydroperoxide

The oxidation of 1-phenylethyl hydroperoxide was carried out in order to collect preliminary data about the stability of this intermediate and the evolution to the corresponding ketone (acetophenone) or alcohol (1-phenyl ethyl alcohol). The tests were conducted by using 100 μL 1-phenylethyl hydroperoxide as reactant dissolved in 2 mL of trifluorotoluene used as solvent into a screw capped pressure resistant round bottom flask (ACE flask) fitted with a glass plunger valve (ACE tube), with the adding of a certain amount of catalyst under a specific metal to substrate ratio. The reaction was carried out under 2 bar N_2 atmosphere at 82 °C and 100 °C respectively. The reaction mixture was centrifuged to separate the solid and solution, and then taking the solution for analysis by H-NMR.

2.3.6 Oxidation of cyclooctane in the presence of filtrates from Nb_2O_5

In order to confirm the reactivity of support Nb_2O_5, different media (HCl, HNO_3, H_2O) were employed to extract possible contaminants or impurities in the parent Nb_2O_5. The procedure

was as follows. 1 g of Nb_2O_5 was mixed with 5 mL of 1 mol·L^{-1} HCl or HNO_3 respectively, followed by stirring at room temperature for 24 h. Then the suspension was filtered and washed using deionised water up to 100 mL. The solution was recovered and analysed via ICP. As a further control test, 2 mL of this filtrate solution was taken into flasks and dried at 100 °C overnight and the residue used to carry out catalytic tests.

In a further control test to assess the effect of leaching[49], the impurities in Nb_2O_5 (1 g) were also filtrated by 80 °C hot water (5 mL) and the filtrated solution was characterized by ICP-MS analysis as well as used, after drying, for catalytic tests.

2.3.7 Oxidation of cyclooctane pre-treated with $MgSO_4$ and zeolite 3A

In order to investigate about the other species in parent cyclooctane, $MgSO_4$ and 3A molecular zeolite were utilised separately to remove the possible alkyl hydroperoxides and water respectively. Autoxidation pathways can be promoted by even trace of peroxides, and the presence of water or alcohols can display effects on the reaction, e.g., peroxides species can act as initiator for C-H cleavage, and the amount of ketone will be higher than that of alcohol with the presence of water in autoxidation process[50, 51] and in some cases water seems to be suppressing the formation of by-byproducts[52]. The scope of these pre-treatments is to eliminate these possible contaminants that could alter the result of the reaction, especially for the initiation step. For this pre-treatment, 0.5 g of fully dried $MgSO_4$ or 3A were mixed with 5 mL of cyclooctane from different suppliers (Sigma-Aldrich and Alfa Aesar), which was kept 72 h at room temperature under stirring, to eliminate the possible traces of peroxides, alcohol and water, followed by the centrifugation to recover cyclooctane. The resulting substrate was then

used for catalytic tests in the presence of Nb_2O_5. The procedure was identical when using 3A zeolites. The results are discussed in chapter 4, section 4.5.

2.4 Analytical methods for reaction mixture and catalysts characterization

In this section characterization methods for the reaction mixture and the catalyst are briefly described and discussed. The identification of molecular species in complex reaction mixture and their quantification, are vital information as they provide the evidence for the performance of a designed catalysts. In this context, the analysis of hydrocarbon containing reaction mixtures, are known to be challenging to characterize[53]. In this work, nuclear magnetic resonance spectroscopy (^{1}H-NMR) was employed for a quick analysis and allowing screening the product distribution at room temperature without the thermal decomposition of alkyl hydroperoxides like in gas chromatography and gas chromatography mass spectrometry (GC-MS) were also used for the qualitative and quantitative analysis of the reaction mixture, as well as inductively coupled plasma mass spectroscopy (ICP-MS) was used for the analysis of metal species in solution. In addition, the characterization techniques used for the catalysts were mainly X-ray powder diffraction (XRPD), X-ray photoelectron spectroscopy (XPS) and transmission electron microscopy (TEM).

2.4.1 ^{1}H Nuclear magnetic resonance spectroscopy (NMR)

Nowadays, nuclear magnetic resonance (NMR) spectroscopy is one of the most important analytical method for the identification of organic compounds. Changes of local magnetic fields around atomic nuclei could be used for qualitative and quantification analysis of compounds in a mixture[54]. ^{1}H NMR concerns the detection of ^{1}H nuclei within the molecules

of a substance to determine the structure of the molecules. This is done by analysing the chemical shift of H, with respect to a reference standard[55, 56]. By the integration of characteristic H-NMR peaks that is correlated with the moles of number of hydrogen and presented substrates, quantitative information will be obtained for the calculation of conversion and selectivity[57].

Conversion and selectivity can be defined by the eq. 2.1a and eq. 2.2 (n_{Pi} is the number of moles of given product, $n_{R,0}$ is the initial number of moles of reactant at the start). In the quantitate analysis by NMR, the conversion can be defined as eq. 2.1b, where $n_{R,0}$ in eq. 2.1a is expressed as the sum of $n_{R,L}$ (the number of moles of reactant left) and the total number of moles of all products, under the circumstances with a closed carbon mass balance[58]. In our case, given that signal areas of peaks are proportional to the moles of number of corresponding H atom (eq. 2.3), ^{1}H-NMR quantification of conversion and selectivity for reaction mixtures can be rearranged in the equations 2.4 and 2.5 and their application is described in section 3.2.1, where A_{Pi} is the area of a given product and m_H is the number of protons of the corresponding signal for a specific compound.

$$\textbf{Conversion \%} = \frac{\sum_i n_{P_i}}{n_{R,0}} \cdot 100\% \qquad \textbf{(eq. 2.1a)}$$

$$\textbf{Conversion \%} = \frac{\sum_i n_{P_i}}{n_{R,L} + \sum_i n_{P_i}} \cdot 100\% \qquad \textbf{(eq. 2.1b)}$$

$$\textbf{Selectivity } (S_i)\% = \frac{n_{P_i}}{\sum_i n_{P_i}} \cdot 100\% \qquad \textbf{(eq. 2.2)}$$

$$n_{P_i} \propto \frac{A_{P_i}}{m_H} \quad \textbf{(eq. 2.3)}$$

$$\textbf{Conversion \%} = \frac{\sum \frac{A_{Pi}}{m_H}}{\frac{A_{left,R}}{m_R} + \sum \frac{A_{Pi}}{m_H}} \cdot 100\% \quad \textbf{(eq. 2.4)}$$

$$\textbf{Selectivity } (S_i)\ \% = \frac{\frac{A_{Pi}}{m_H}}{\sum_i \frac{A_{Pi}}{m_H}} \cdot 100\% \quad \textbf{(eq. 2.5)}$$

It should be noted due to the complexity of the reaction mixture, the selectivity for major products (alcohols, ketones and alkyl hydroperoxides, above 80%) were mainly taken into account in the assessment of the performances of catalysts and other products were grouped as by-products (e.g., esters, acids, usually less than 20%). The conversion and selectivity from ^{1}H NMR analysis are called as 'observed', because the above equations are based on the assumption that all the products present in reaction mixture can be quantitively analysed. In the case of hydrocarbons oxidation, that means the carbon mass balance should be close to 100% within experiment error when applying these equations for the determination of conversion and selectivity. Therefore, in our research carbon mass balance calculation was conducted with internal standard (dichloromethane was used, see section 3.2) to verify the validity of this analysis method, the calculation being done by using eq. 2.6.

$$\textbf{CMB\%} = \frac{\textit{carbon No.}(\textit{products}, C_p) + \textit{carbon No.}(\textit{reactant left}, C_{R,L})}{\textit{initial carbon No.}} \cdot 100\%$$

$$= \frac{\sum_i c_i p_i + c_R n_{R,L}}{c_R n_{R,0}} \cdot 100\% \quad \textbf{(eq. 2.6)}$$

In our research, all the ^{1}H NMR analyses were conducted using a Bruker Advance III 400 spectrometer fitted with a 5 mm PABBO BB/19F-1H/D-GRD probe and a frequency of 400 MHz. $CDCl_3$ was used as solvent in standard NMR tubes. For cyclooctane or cyclohexane, the spectra were referenced to $CHCl_3$ presented in $CDCl_3$ solvent (7.26 ppm) and the characteristic peak of $-CH_3$ (1.22 ppm) or $-CH_2-$ (2.63 ppm) is used as reference for ethylbenzene[59, 60].

2.4.2 Gas chromatography – mass spectrometry (GC-MS)

Today the combination of gas chromatography (GC) and mass spectrometry (MS) is the one of the most important analytical tools for the qualitative and quantitative analysis of organic compounds in complex mixtures[61]. This technique involves the sample preparation, injection and separation of the compounds of a mixture by a specific GC column. The principle of GC relies on the affinity of a compound to a stationary phase, with the analyte that can move through the column on when it is in a mobile phase (in our case helium gas). For an analyte that will be retained more by a column and longer it will be before it is eluted and detected at the end of the column (known as retention time). In this couple technique, the mass spectrometer serves a detector for GC, which is a histogram of the abundance of each ion as a function of m/z (where m is the mass and z is the charge) and serves as the fingerprint to identify the compound represented by a peak on the chromatogram[61-64]. In our research, NMR mainly used as a screening tool and GC-MS is used for an apparently more accurate determination of the reaction mixture and secondary products. It should be noted, however, that in the analysis of hydrocarbon mixtures, due to the analysis condition such as

temperatures above 150 ˚C, these may induce the decomposition of alkyl hydro peroxides during the analysis. Therefore, whether the method case is needed to interpret the experimental results.

GC-MS quantification of conversion and selectivity can be determined with the following equations and the development method is specifically discussed in section 3.3. Herein, the equation is transformed into the following equations 2.7-2.9 based on the definition, where $[R]_{0,intial}$ is the concentration of reactant, and the [Pi] is the concentration of the products calibrated by the internal standard, [IS] and Area(IS) are the concentration and area calibrated by internal standard respectively.

$$\textbf{Conversion \%} = \frac{\sum n(products)}{n_{0,}(initial\ reactant)} = \frac{\sum [p_i]}{[R]_{0,initial}} \cdot 100\% \qquad \textbf{(eq. 2.7)}$$

$$[p_i] = [IS] \cdot \frac{Aera(p_i)}{Aera(IS)} \qquad \textbf{(eq. 2.8)}$$

$$\textbf{Selectivity(}i\textbf{)\%} = \frac{[p_i]}{\sum_i [p_i]} \cdot 100\% \qquad \textbf{(eq. 2.9)}$$

In our case, GC analysis was performed by taking 400 µL of reaction mixture with the addition of 30 µL of *n*-dodecane as the internal standard and then diluting this solution up to 10 mL by using acetone in a volumetric flask. The samples were analysed on an Agilent 7200 accurate mass Q-TOF GC-MS fitted with an Agilent DB-MS-UI 30 m x 0.25 mm x 0.25 µm column or an Agilent DB-WAX-UI 30 m x 0.25 mm x 0.25 µm column. Temperature ramping was conducted as follows: 50 ˚C to 90 ˚C, 40 ˚C·min^{-1}; 90 ˚C to 120 ˚C, 2 ˚C·min^{-1}; 120 ˚C to 250 ˚C, 10 ˚C·min^{-1} then held at 250 ˚C for 2 min.

2.4.3 Inductively coupled plasma mass spectroscopy (ICP-MS)

Inductively coupled plasma mass spectrometry (ICP-MS) is an analytical technique, which in our project has mainly be used as a trace element technique, which can offer extremely low detection limit and make quantifications at ppm level. In this method, a high temperature argon plasma is used to generate positively charged ions, which then produce analyte ground-state atoms from the dried sample aerosol, interacting with the atoms to remove an electron and generate positively charged ions, which are then steered into a mass spectrometer for detection and measurement[65]. ICP-MS has an array of advantages, such as: multielement analysis, short analysis time, detection limits, and isotopic capability, enable it to be widely applied today.

In our research, ICP-MS was employed for the determination of metal ions in the reaction mixture for the leaching analysis of active components in catalysts and the amount of metal in prepared catalysts to determine the metal loading. In addition, it was also used for the analysis of the possible impurities present in Nb_2O_5. For the analysis of metal leaching from a catalyst, the procedure was as follow: 1 mL of reaction mixture was mixed with 10 mL of deionised water thoroughly for 24 h to extract metal ions. The resultant aqueous solution was used for the analysis. Regarding the analysis for metal loading of catalysts, 0.1 g of prepared supported Ag catalysts (Ag/Nb_2O_5) was mixed with 1 mL of concentrated HNO_3 under stirring for 24 h, which was followed by the dilution using deionized water up to 250 mL, and the resulting solution can be analysed for the Ag components in Ag/Nb_2O_5.

2.4.4 X-ray powder diffraction (XRPD)

X-ray diffraction as a non-destructive technique for the determination of the structure of a material. It is widely used for characterizing and probing arrangement of atoms in each unit cell, position of atoms, and atomic spacing angles because of comparative wavelength of X-ray to atomic interplanar distances[66, 67]. X-ray methods are widely used in the field of phase identification, crystal size, crystal structure, residual stress/strain, dislocation density, lattice parameter determination, phase transformation, and crystallographic orientation etc[66, 67]. For the context of our research, the application of XRD mainly involves the investigation about the crystal structure and particle sizes over support. Regarding the determination of crystalline size, it can be estimated by referring to Scherrer equation (eq. 2.10) through XRD[68, 69].

$$t = \frac{0.9\lambda}{\sqrt{B_M{}^2 - B_S{}^2 \cos\theta}} \qquad \textit{(eq. 2.10)}$$

Where t is thickness of the crystallite, λ is incident wavelength of X-ray, θ is the Bragg angle, B_M is the width of the peak and B_S is instrumental broadening at half maximum. In addition, the relative crystallinity was obtained by the integration of full width at half maximum (FWHM) from characteristic peaks for the study about the stability of support and the prepared catalysts.

X-ray analysis was conducted using a Bruker D8 powder Diffractometer using a CuKα X-ray source which was operated at 40 kV and 40 mA on a low-angle flat plate sample holder. Typical routine scanning was in the range of 10-80 ° 2θ for 1h, with the set parameters, 2θ: 15 – 80 °, t (per step): 0.6 s, primary opening: 0.3 °, secondary opening: 9.5 mm, no antiscatter slit.

2.4.5 X-ray photoelectron spectroscopy (XPS)

X-ray photoelectron spectroscopy (XPS) is widely applied in the field of surface characterization and catalysis to provide information on the elemental analysis and the oxidation state of state of elements, which is based on the photoelectric effect that occurs when high energy photons (X-ray as the exciting photon source) hit a material with the consequent emission of electrons (photoelectrons)[70] near the surface. The working principles can be illustrated by Fig. 2.3. As each element has a unique set of binding energies (regarded as different energies between the initial and final states after the emission of electrons from the atom[71]) due to the differences in the chemical potential and polarizability, XPS can be used to identify and determine the concentration and chemical state of the elements in the surface[72, 73]. The photoelectron kinetic energy E_k, can be given by following Einstein's law[73] (eq. 2.11), where *hv* is the energy of the incident radiation, E_b is the binding energy of the emitted electron in a specific level, and Φ_s is the spectrometer work function.

$$E_k = hv - E_b - \Phi_s \qquad \textbf{(eq. 2.11)}$$

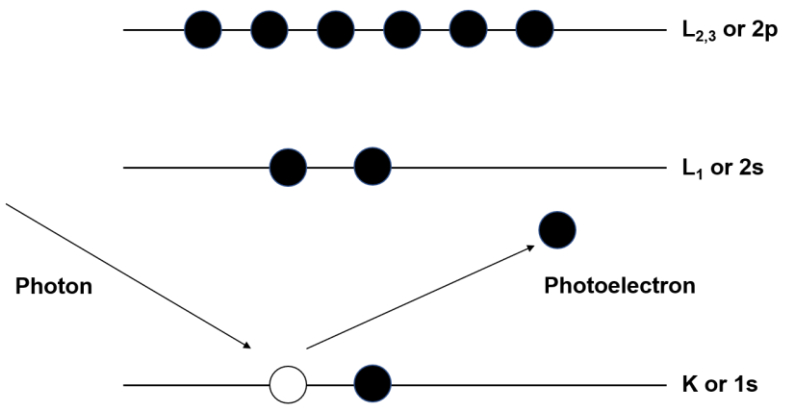

Fig. 2.3 The XPS emission process for a model atom, in which the ejection of photoelectrons is trigged by the X-ray source[73].

In our research, XPS was utilised for the determination of the oxidation states of supported metal/metal oxides (Ag species) over support and the environments around the dopant metals. XPS was performed on a Thermo Fisher Scientific K-alpha^{+} spectrometer and all samples were analysed using a micro-focused monochromatic Al x-ray source (72 W) with the “400-micron spot” mode. All spectra were charge corrected normalising the C 1s component to 284.8 eV[11, 74].

2.4.6 Transmission electron microscopy (TEM)

Transmission electron microscopy can be applied for the analysis of nanostructures such as particles, thin films, fibres as well as the imaging of atoms. A TEM microscope apparatus mainly includes electron gun, electrostatic lenses to focus the electrons before and after the specimen, and a transmitted electron detection system.[75, 76] Electrons from the electron gun can penetrate into a thin specimen and then are observed by the appropriate lenses.[77] And a high vacuum atmosphere is required to prevent the scatting of energetic electrons that is generated from electron gun with gas molecules existed in air. It should be mentioned that the resolution of TEM is controlled by acceleration voltage of electron gun, that is, the acceleration voltages with various values at 40, 100, 200 or 1000 kV will result in the resolutions of around 0.56, 0.35, 0.24 or 0.12 nm.[76] In view of this, it is usually performed with the voltage above 100 kV for a good resolution, and the specimen with high thickness can be observed when the acceleration voltage is higher than 1000 kV, whereas microstructural defects might be caused in specimen.[76, 77]

TEM has been widely used for the screening of properties of supported metal catalyst[77-

[79], e.g., morphology, particle size distribution, for the establishment of structure-activity relationship. In our research, TEM was performed on a Hitachi HF5000 operated at an accelerating voltage 200 kV. Supported Ag particle size distributions was determined from TEM images by accounting least 100 particles in each catalyst.

2.5 References

1. F. Pinna, *Catal. Today*, 1998, **41**, 129-137.
2. L. Di, J. Zhang and X. Zhang, *Plasma Process Polym.*, 2018, **15**, 1700234.
3. P. Paalanen, B. M. Weckhuysen and M. Sankar, *Catal. Sci. Technol.*, 2013, **3**, 2869-2880.
4. L. Sun, L. Jiang, X. Hua, Y. Zheng, X. Sun, M. Zhang, H. Su and C. Qi, *J. Alloys Compd.*, 2019, **811**, 152052.
5. K. P. de Jong, *Synthesis of solid catalysts*, 2009, 111-134.
6. V. Gandhi, R. Ganesan, H. H. Abdulrahman Syedahamed and M. Thaiyan, *J. Phys. Chem. C*, 2014, **118**, 9715-9725.
7. A. Villa, D. Wang, G. M. Veith, F. Vindigni and L. Prati, *Catal. Sci. Technol.*, 2013, **3**, 3036-3041.
8. X. Liu, M. Conte, Q. He, D. Knight, D. Murphy, S. Taylor, K. Whiston, C. Kiely and G. J. Hutchings, *Chem. Eur. J.*, 2017.
9. P. Munnik, P. E. de Jongh and K. P. de Jong, *Chem. Rev.*, 2015, **115**, 6687-6718.
10. M. J. Beier, T. W. Hansen and J.-D. Grunwaldt, *J. Catal.*, 2009, **266**, 320-330.
11. M. Haneda and A. Towata, *Catal. Today*, 2015, **242**, 351-356.

12. C. Della Pina, E. Falletta, L. Prati and M. Rossi, *Chem. Soc. Rev.*, 2008, **37**, 2077-2095.

13. L. Zhang, C. Zhang and H. He, *J. Catal.*, 2009, **261**, 101-109.

14. M. Haruta, S. Tsubota, T. Kobayashi, H. Kageyama, M. J. Genet and B. Delmon, *J. Catal.*, 1993, **144**, 175-192.

15. A. S. K. Hashmi and G. J. Hutchings, *Angew. Chem. Int. Ed.*, 2006, **45**, 7896-7936.

16. S. Tsubota, M. Haruta, T. Kobayashi, A. Ueda and Y. Nakahara, in *Stud. Surf. Sci. Catal.*, Elsevier, 1991, vol. 63, p. 695-704.

17. D. Prieto-Centurion and J. M. Notestein, *J. Catal.*, 2011, **279**, 103-110.

18. M. Haruta, *Cattech*, 2002, **6**, 102-115.

19. R. Zanella, L. Delannoy and C. Louis, *Appl. Catal. A: Gen.*, 2005, **291**, 62-72.

20. J. Bitter, M. Van der Lee, A. Slotboom, A. Van Dillen and K. De Jong, *Catal. Lett.*, 2003, **89**, 139-142.

21. L.-X. Xu, C.-H. He, M.-Q. Zhu and S. Fang, *Catal. Lett.*, 2007, **114**, 202-205.

22. L.-X. Xu, C.-H. He, M.-Q. Zhu, K.-J. Wu and Y.-L. Lai, *Catal. Lett.*, 2007, **118**, 248-253.

23. G. R. Bamwenda, S. Tsubota, T. Nakamura and M. Haruta, *Catal. Lett.*, 1997, **44**, 83-87.

24. T. Hayashi, K. Tanaka and M. Haruta, *J. Catal.*, 1998, **178**, 566-575.

25. M. Behrens, *Catal. Today*, 2015, **246**, 46-54.

26. R. J. White, R. Luque, V. L. Budarin, J. H. Clark and D. J. Macquarrie, *Chem. Soc. Rev.*, 2009, **38**, 481-494.

27. C. Baltes, S. Vukojević and F. Schüth, *J. Catal.*, 2008, **258**, 334-344.

28. A. P. LaGrow, M. O. Besenhard, A. Hodzic, A. Sergides, L. K. Bogart, A. Gavriilidis and N. T. K. Thanh, *Nanoscale*, 2019, **11**, 6620-6628.

29. H. Liang, J. M. Raitano, G. He, A. J. Akey, I. P. Herman, L. Zhang and S.-W. Chan, *J. Mater. Sci.*, 2012, **47**, 299-307.

30. M.-C. Daniel and D. Astruc, *Chem. Rev.*, 2004, **104**, 293-346.

31. C. Baatz, N. Decker and U. Prüße, *J. Catal.*, 2008, **258**, 165-169.

32. G. Zhan, Y. Hong, V. T. Mbah, J. Huang, A.-R. Ibrahim, M. Du and Q. Li, *Appl. Catal. A: Gen.*, 2012, **439**, 179-186.

33. J. Pritchard, L. Kesavan, M. Piccinini, Q. He, R. Tiruvalam, N. Dimitratos, J. A. Lopez-Sanchez, A. F. Carley, J. K. Edwards and C. J. Kiely, *Langmuir*, 2010, **26**, 16568-16577.

34. V. Peneau, G. Shaw, S. J. Freakley, M. M. Forde, N. Dimitratos, R. L. Jenkins, S. H. Taylor and G. J. Hutchings, *Catal. Sci. Technol.*, 2015, **5**, 3953-3959.

35. H. Bahruji, M. Bowker, G. Hutchings, N. Dimitratos, P. Wells, E. Gibson, W. Jones, C. Brookes, D. Morgan and G. Lalev, *J. Catal.*, 2016, **343**, 133-146.

36. A. S. Al-Fatesh, A. H. Fakeeha, A. Ibrahim, W. U. Khan, H. Atia, R. Eckelt, K. Seshan and B. Chowdhury, *J. Saudi Chem. Soc.*, 2018, **22**, 239-247.

37. M. Arsalanfar, A. Mirzaei and H. Bozorgzadeh, *J. Nat. Gas Sci. Eng.*, 2012, **6**, 1-13.

38. L. Peng, E. Ringe, R. P. Van Duyne and L. D. Marks, *Phys. Chem. Chem. Phys.*, 2015, **17**, 27940-27951.

39. C. J. Serpell, J. Cookson, D. Ozkaya and P. D. Beer, *Nat. Chem.*, 2011, **3**, 478-483.

40. Z.-A. Li, M. Spasova, Q. Ramasse, M. Gruner, C. Kisielowski and M. Farle, *Phys. Rev. B*, 2014, **89**, 161406.

41. A. A. Herzing, M. Watanabe, J. K. Edwards, M. Conte, Z.-R. Tang, G. J. Hutchings and C. J. Kiely, *Faraday Discuss.*, 2008, **138**, 337-351.

42. G. Wang, M. A. Van Hove, P. N. Ross and M. I. Baskes, *Prog. Surf. Sci.*, 2005, **79**, 28-45.

43. L. Farsi and N. A. Deskins, *Phys. Chem. Chem. Phys.*, 2019, **21**, 23626-23637.

44. Y. Ma and P. B. Balbuena, *Surf. Sci.*, 2008, **602**, 107-113.

45. H. Guesmi, C. Louis and L. Delannoy, *Chem. Phys. Lett.*, 2011, **503**, 97-100.

46. G. E. Ramirez-Caballero and P. B. Balbuena, *Chem. Phys. Lett.*, 2008, **456**, 64-67.

47. A. Busiakiewicz, A. Kisielewska, I. Piwoński and D. Batory, *Appl. Surf. Sci.*, 2017, **401**, 378-384.

48. S. Tauster, *Acc. Chem. Res.*, 1987, **20**, 389-394.

49. H. Gruber-Wölfler, P. Radaschitz, P. Feenstra, W. Haas and J. Khinast, *J. Catal.*, 2012, **286**, 30-40.

50. J.-R. Chen, H.-H. Yang and C.-H. Wu, *Org. Process Res. Dev.*, 2004, **8**, 252-255.

51. X. Liu, Y. Ryabenkova and M. Conte, *Phys. Chem. Chem. Phys.*, 2015, **17**, 715-731.

52. D. Yang, T. Jiang, T. Wu, P. Zhang, H. Han and B. Han, *Catal. Sci. Technol.*, 2016, **6**, 193-200.

53. S. Blaine and P. E. Savage, *Ind. Eng. Chem. Res.*, 1991, **30**, 2185-2191.

54. F. Malz and H. Jancke, *J. Pharm. Biomed. Anal.*, 2005, **38**, 813-823.

55. J. C. Edwards, *Process NMR Associates LLC, 87A Sand Pit Rd, Danbury CT*, 2009, **6810**.

56. D. P. Hollis, *Anal. Chem.*, 1963, **35**, 1682-1684.

57. G. F. Pauli, T. Godecke, B. U. Jaki and D. C. Lankin, *J. Nat. Prod.*, 2012, **75**, 834-851.

58. F. P. Miknis, D. A. Netzel, S. D. Brandes, R. A. Winschel and F. P. Burke, *Fuel*, 1993, **72**, 217-224.

59. H. E. Gottlieb, V. Kotlyar and A. Nudelman, *J. Org. Chem.*, 1997, **62**, 7512-7515.

60. E. Pretsch, P. Bühlmann, C. Affolter, E. Pretsch, P. Bhuhlmann and C. Affolter, *Structure determination of organic compounds*, Springer, 2000, p 186.

61. T. M. Lovestead and K. Urness, 2019, Materials characterization, 2019, p 235-241.

62. H. M. McNair, J. M. Miller and N. H. Snow, *Basic gas chromatography*, John Wiley & Sons, 2019, p 1-3.

63. F. W. McLafferty, F. Tureček and F. Turecek, *Interpretation of mass spectra*, University science books, 1993, p 1-2.

64. D. L. Pavia, G. M. Lampman, G. S. Kriz and J. A. Vyvyan, *Introduction to spectroscopy*, Nelson Education, 2014, p 120-121.

65. J. R. Dean, L. Ebdon, M. E. Foulkes, H. M. Crews and R. C. Massey, *J. Anal. At. Spectrom.*, 1994, **9**, 615-618.

66. M. J. Cook, N. B. McKeown, J. M. Simmons, A. J. Thomson, M. F. Daniel, K. J. Harrison, R. M. Richardson and S. J. Roser, *J. Mater. Chem.*, 1991, **1**, 121-127.

67. E. Ameh, *Int. J. Adv. Manuf. Syst.*, 2019, **105**, 3289-3302.

68. Y. Zhou and J. A. Switzer, *J. Alloys Compd.*, 1996, **237**, 1-5.

69. Y. Yalçın, M. Kılıç and Z. Çınar, *Appl. Catal. B: Environ.*, 2010, **99**, 469-477.

70. M. Stöcker, *Microporous Mater.*, 1996, **6**, 235-257.

71. J. Chastain and R. C. King Jr, *Perkin-Elmer, USA*, 1992, 261.

72. A. Proctor and P. M. Sherwood, *Anal. Chem.*, 1982, **54**, 13-19.

73. J. Chastain and R. C. King Jr, *Perkin-Elmer Corporation*, 1992, **40**, 221.

74. M. Conte, A. F. Carley and G. J. Hutchings, *Catal. Lett.*, 2008, **124**, 165-167.

75. B. Inkson, in *Materials characterization using nondestructive evaluation (NDE) methods*, Elsevier, 2016, p 17-43.

76. J. i. Kikuchi and K. Yasuhara, *Supramolecular Chemistry: From Molecules to Nanomaterials*, 2012, p 1-13.

77. R. F. Egerton, *Physical principles of electron microscopy*, Springer, 2005, p 10-11.

78. A. Ashcroft, A. K. Cheetham, P. Harris, R. Jones, S. Natarajan, G. Sankar, N. Stedman and J. Thomas, *Catal. Lett.*, 1994, **24**, 47-57.

79. D. J. Smith, M. Yao, L. Allard and A. Datye, *Catal. Lett.*, 1995, **31**, 57-64.

Chapter 3: Method development for the analysis of reaction mixtures

3.1 Overview

Currently approximately 90% of industrial process involves the participation of catalysts, to make these processes more selective by facilitating the production of desired substrates and achieve a more sustainable industrial chemistry[1-3]. In view of this, the research about the evaluation of the performances of catalysts on the reaction is essential. Thus, this part would focus on the discussion about the development of methods for the qualitative and quantitative analysis for the reaction mixtures to assess the effects of catalysts on the model reaction, providing evidence for the design of catalysts. Generally, the identification of a specific molecular species and its quantification in a complex system are two strictly related tasks in chemistry analysis. In our case, in order to assess whether a catalyst is indeed active or selective, an accurate qualitative and quantitative determination method of the composition of the reaction mixture, especially for the intermediates (alkyl hydroperoxides that are thermodynamically unstable[4]) and desired products like alcohols or ketones, is extremely required, which is usually either a spectroscopic or a chromatographic method. A commonly used method for the analysis of reaction mixtures from hydrocarbon oxidation, is gas chromatography (GC) for which is one of the most important analytical methods for the determination of organic substances in a complex mixtures[5]. Moreover, as described in section 2.4.2 of chapter 2, the combination of gas chromatography (GC) and mass spectrometry (MS) (based on the mass spectra matching) can effectively separate and distinguish most of the main products and side products clearly with obviously distinct peaks under proper running

conditions[6]. However, GC-MS analysis is a complex analytical method because it usually requires an accurate calibration for the quantification of components in a reaction mixture, and the samples must be properly pre-treated before analysis, which means that this process is relatively lengthy. In addition, in our case, it involves the analysis of alkyl hydroperoxides, an important intermediate, which can be thermally converted to the corresponding ketones or alcohols once the samples are injected under the analysis conditions of GC-MS[4, 7] (usually operating at a temperature from 180 to 200 °C). From this perspective, it is likely that the samples analysed by GC-MS are not representative of the original samples from a reaction mixture, as the decomposition of alkyl hydroperoxides would result in a higher observed selectivity for alcohol and ketone compounds.

In view of this, the quantitative analysis by nuclear magnetic resonance spectroscopy (NMR) was developed in our research. One of the major advantages of NMR for the scope of our project are: no thermal decomposition of reactive intermediates, as the NMR analysis occurs at room temperature. In comparison, given the possible decomposition of hydroperoxides under the running conditions of GC-MS, a short analysis time is quite important in our case. Therefore, the application of quantitative analysis by ^{1}H NMR and GC-MS and their feasibility referring to carbon mass balance in the oxidation of cyclooctane and cyclohexane are described and discussed in detail.

In addition, and in a wider context of a full characterization of a reaction mixture, and especially in heterogeneous catalysis, a quantitative determination method for the amount of possible metal leaching in solution, and in turn also for the actual amount of metal loaded onto

a support by using inductively coupled plasma mass spectrometry (ICP-MS) will be discussed.

3.2 Quantitative analysis by ^{1}H-NMR

Nowadays, nuclear magnetic resonance spectroscopy (NMR) is one of the most important analytical method for the determination of organic compounds, and it is widely used in the industrial and academic research[8]. The widespread application of the NMR is due to the unique advantages, such as: relatively short analysis time (in a matter of minutes) while chromatographic method is relatively time demanding (up to 1 h for each sample); it is formally a non-destructive technique (although it requires the use of a solvent from which the analyte would need to be recovered) as the probed physical characteristics are not changed in magnetic field, and of high relevance for the detection of compounds we are interested, the analysis is carried out at room temperature. In our context, a room temperature range has to be considered, that is well below the thermal decomposition of alkyl hydroperoxides, as an important intermediate for our reactions. Furthermore, the sample preparation is very convenient and straightforward[8]. Therefore, based on all of these characteristics, H-NMR can be considered as a quick screening tool for the analysis of our reaction samples.

In view of the above discussion and the practical aspects of the analysis for our reaction mixtures involving large number of substrates, avoiding the decomposition of thermally labile intermediates, and quickly gathering data for screening procedures, we decided to quantify the products in reaction mixtures by using ^{1}H-NMR. As described in section 2.4.1 of chapter 2, ^{1}H NMR concerns the detection of hydrogen-1 nuclei, practically protons, within a substance with the aim to determine the structure of organic molecules. This can be achieved by

analysing the chemical shift of H, which depends on the molecular structure of the compound, the solvent and temperature. Meanwhile, it should be noted that the overlap of characteristic H peaks in different substrates may lead to inaccuracies to the experimental values. Based on the all considerations, in our case ^{1}H NMR was employed as a screening tool to quickly assess the activity of a catalyst, and then if necessary, the tests were going to be subjected to GC-MS characterizations and quantification.

3.2.1 Cyclooctane oxidation

Aryl and cyclic hydrocarbons are major feedstocks for the manufacture of precursors or high-value intermediates like acids or ketones, which are among the major building blocks for the polymer industry for the use as fibres, plastics and coatings[9]. In our research, cyclooctane was firstly used as a reactant for the tests (see section 5.2 of chapter 5 for clarification). According to our reaction results, the main products of cyclooctane oxidation are: cyclooctanol, cyclooctanone, cyclooctyl hydroperoxide which account for up to 80% of the reaction mixture, and some by-products, such as cis-9-oxabicyclononane, 1,3-cyclooctadiene, 1,4-cyclooctadiene, 1,5-cyclooctadiene accounting for the remaining less than 20%. By definition, the conversion of cyclooctane (reactant) is defined as the moles of reactant consumed at a fixed time *t*, divided the initial moles of reagent, as expressed in eq. 2.1-a in section 2.4.1 from chapter 2. In the assumption of a carbon mass balance experimentally close to 100 %, that is accounting for experimental error, eq. 3.1 can be used.

$$\textbf{CMB\%} = \frac{\textit{carbon No.(products, } C_p\textit{)} + \textit{carbon No.(reactant left, } C_{R,L}\textit{)}}{\textit{initial carbon No.}} \cdot 100\%$$

$$= \frac{\sum_i c_i p_i + c_R n_{R,L}}{c_R n_{R,0}} \cdot 100\% \qquad \textbf{(eq. 3.1)}$$

3.2.1.1 Quantitative analysis - conversion and selectivity

Given that the signal areas of peaks are proportional to the moles of number of corresponding H atom, the conversion is expressed as the ratio between the sum of the mole amount of all products n_P divided by the initial number of moles of reactant $n_{R,0}$[10]. As from NMR spectra, the amount of reactant left $n_{R,L}$, can be determined by taking the integration areas of characteristic H peaks, by which $n_{R,0} = n_{R,L} + n_P$ is obtained (eq. 3.2). In addition, the selectivity for a product *i*, can be defined as the ratio between the number of moles of specific product n_{pi} divided by the sum of the total number of moles of all products n_P (eq. 3.2).

$$\textbf{Conversion\%} = \frac{\sum_i n_{P_i}}{n_{R,0}} \cdot 100\% = \frac{\sum_i n_{P_i}}{n_{R,L} + \sum_i P_i} \cdot 100\% \qquad \textbf{(eq. 3.2)}$$

$$\textbf{Selectivity}(S_i)\,\% = \frac{n_{P_i}}{\sum_i n_{P_i}} \cdot 100\% \qquad \textbf{(eq. 3.3)}$$

In the quantitative analysis by ^{1}H NMR, the number of moles n_x of a specific species is corresponding to the area of ^{1}H-NMR peak for a given functional group divided by the number of protons for that functional group. In this context, the calculation of conversion can be transformed into the equation 3.4, expressed by the areas. By analysing characteristic H NMR peaks (table 3.1), the major components of the reaction mixture were: cyclooctanol (A_8), cyclooctanone (K_8), cyclooctyl hydroperoxide (P_8) (shown in Fig.3.1). For these compounds, diagnostic peaks at 3.8, 2.4, 4.1 ppm could be directly integrated to obtain areas respectively

as a relative amount for each of them. However, due to the overlap of peaks in the range from 1.0 ppm to 2.3 ppm, it was inaccurate to obtain the area of cyclooctane (1.5 ppm) directly from spectrum. Thus, correction factors were needed and a proper calculation method was established to obtain the relative area of cyclooctane.

$$Conversion\,\% = \frac{\sum \frac{A_{Pi}}{m_H}}{\frac{A_{left,R}}{m_R} + \sum \frac{A_{Pi}}{m_H}} \cdot 100\% \qquad \textit{(eq. 3.4)}$$

Table 3.1 Partial H-NMR signal for the major products in reaction mixtures from cyclooctane oxidation. A_8, K_8, P_8 are major products and X_8 represents all the byproducts. ppm values for assignment are based on the website-Spectral Database for Organic Compounds.[11]

Compound	Characteristic H	No. of H	Peak position (ppm)	Symbol of area
Cyclooctane(C_8)	-C<u>H</u>$_2$-	16H	1.53	A_{C8}
Cyclooctanol (A_8)	-(CH$_2$)$_2$-C<u>H</u>-OH	1H	3.84	A_{A8}
Cyclooctanone (K_8)	-C<u>H</u>$_2$-C=O-C<u>H</u>$_2$-	4H	2.41	A_{K8}
Cyclooctyl hydroperoxide (P_8)	-(CH$_2$)$_2$-C<u>H</u>-OOH	1H	4.10	A_{P8}
Cis-9-oxabicyclononane	-C<u>H</u>-	2H	2.89	A_{ox}
1,4-Cyclooctadiene	=C-C<u>H</u>$_2$-C=	2H	2.70	$A_{1,4ene}$
1,3-Cyclooctadiene	-C<u>H</u>-C=	2H	5.82	$A_{1,3ene}$
1,5-Cyclooctadiene	-C<u>H</u>-C=	4H	5.58	$A_{1,5ene}$

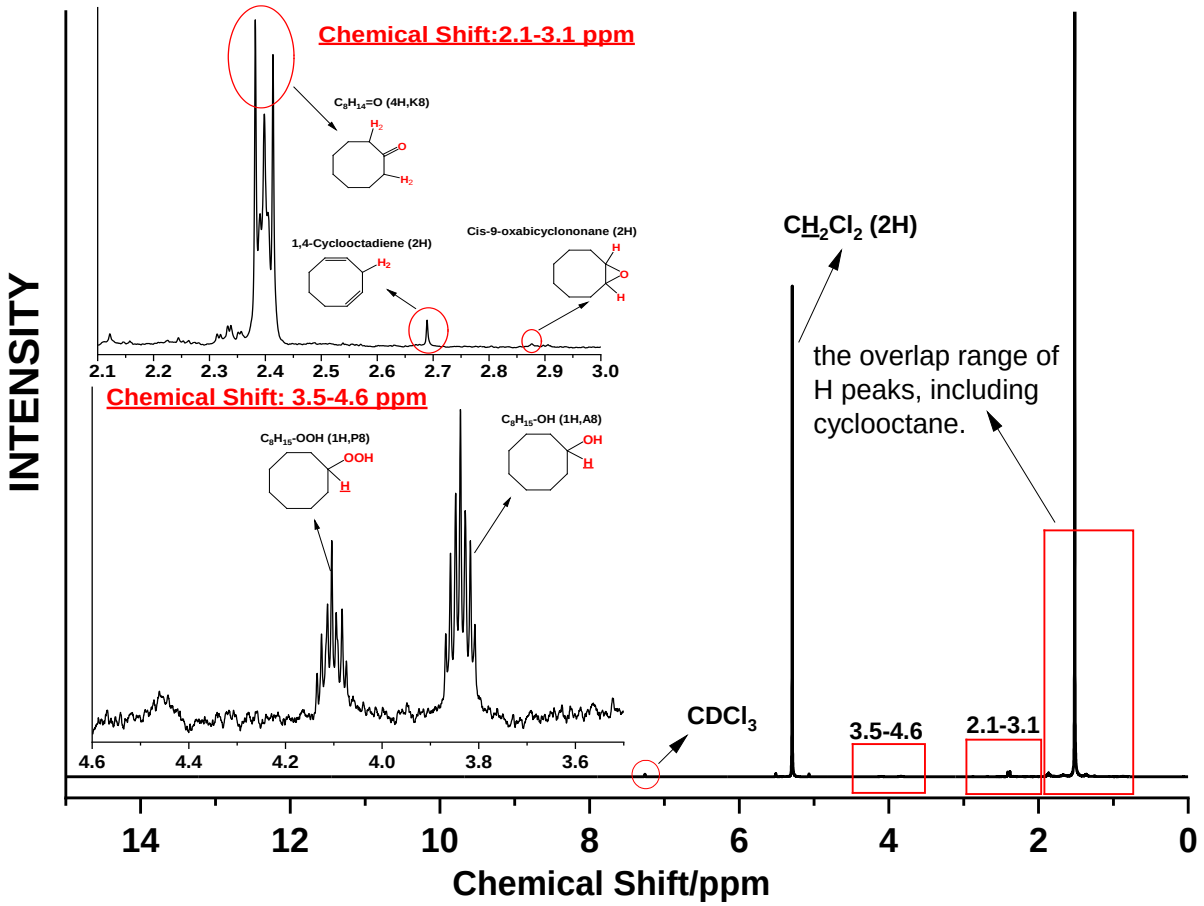

Fig. 3.1 An NMR spectrum of reaction mixture from cyclooctane oxidation. The oxidation was conducted in the presence of Nb_2O_5 (99.9% grade/purity) at 110 °C for 24 h at 1 atmospheric air with condenser open to air.

In this case, the total amount of products can be represented by the integration of area that is divided by the number of protons in ^{1}H-NMR spectra:

$$\textbf{Aera(products)} = \frac{A_{A8}}{1} + \frac{A_{K8}}{4} + \frac{A_{P8}}{1} + A_{X8} \qquad \textbf{(eq. 3.5)}$$

It should be noted that in eq. 3.5, the area of by products (X_8) mainly includes the area of cis-9-oxabicyclononane, 1,4-cyclooctadione, 1,3-cyclooctadiene, etc., herein the A_{x8} can be calculated by equation 3.6.

$$\textbf{Aera}(A_{x8}) = \frac{A_{ox}}{2} + \frac{A_{1,4\text{-ene}}}{2} + \frac{A_{1,3\text{-ene}}}{2} + \frac{A_{1,5\text{-ene}}}{4} \frac{A_{unknown}}{2} \qquad \textbf{(eq. 3.6)}$$

Regarding the relative area of reactant left, as the overlap of peaks in the range from 1.0 ppm to 2.3 ppm among cyclooctane and various products, it was inaccurate to obtain the area of cyclooctane (1.5 ppm) directly from spectrum. Thus, correction factors were introduced to give ep. 3.7. In this way, the area of peaks in the range from 0.5-2.3 ppm was calibrated as 160 (a.u.), and the relative area of H in this range from other components was corrected from characteristic peaks that excludes this range.

$$\textbf{Aera(reactant left)} = \frac{160 - (\frac{A_{A8}}{1} \cdot 15 + \frac{A_{K8}}{4} \cdot 10 + \frac{A_{P8}}{1} \cdot 15 + \frac{A_{X8}}{2} \cdot 12)}{16} \qquad \textbf{(eq. 3.7)}$$

According to the eq. 3.4, the final conversion can be calculated by substituting these values into the formula, expressed as eq. 3.8.

$$\textbf{Conversion\%} = \frac{\frac{A_{A8}}{1} + \frac{A_{K8}}{4} + \frac{A_{P8}}{1} + A_{X8}}{\frac{A_{A8}}{1} + \frac{A_{K8}}{4} + \frac{A_{P8}}{1} + A_{X8} + \frac{160 - (\frac{A_{A8}}{1} \cdot 15 + \frac{A_{K8}}{4} \cdot 10 + \frac{A_{P8}}{1} \cdot 15 + \frac{A_{X8}}{2} \cdot 12)}{16}} x100\% \qquad \textbf{(eq. 3.8)}$$

Furthermore, the selectivity can be obtained by following the similar approach by using the area of specific products divided by the total areas of all products, which is expressed in following eq. 3.9.

$$\textbf{Selectivity } (S_i)\,\% = \frac{\frac{A_{Pi}}{m_H}}{\sum_i \frac{A_{Pi}}{m_H}} \cdot 100\% \qquad \textbf{(eq. 3.9)}$$

3.2.1.2 Carbon mass balance (CMB) by internal standard

In order to develop a quantitative analysis method for the oxidation of hydrocarbons, potential mass loss is a significant factor for consideration as the relatively harsh reaction conditions may lead to formation of gases like CO_2, which is not taken into our analysis method by ^1H NMR. In addition, different criteria for the integration of the NMR peaks, owing to the overlap of characteristic H peaks, or the missing detection for some products in less than 1-2 mol% like acids may also magnify the inaccuracy by the method. In view of this, in order to validate our results it is important that to ascertain a closed carbon mass balance (CMB) by accounting of experimental error, equal to 100%[12, 13].The CMB (in percentage) is be defined as: the ratio between the number of moles of the sum for all the products detected in reaction mixture, including any unreacted reagent, each of them multiplied by its own number of carbon atoms, divided by the number of moles of reagent at the time 0 multiplied by its own number of carbon atoms, as shown in eq. 3.1.

In order to accurately quantify in the components of reaction mixture, we used an internal standard. In our case, dichloromethane (CH_2Cl_2) was selected due to: its high level of purity, and the lack of any overlap with any of the diagnostic peaks of our reaction mixture with a peak at 5.3 ppm (2H). In detail, 100 μL of CH_2Cl_2 was added to a known amount (50 μL) of reaction mixture to calculate the absolute mole amount of the products by referring to the ratios of areas with that of CH_2Cl_2. In this way, we can compare the results obtained by adding internal standard with that from without internal standard to study the feasibility of quantitative analysis by ^{1}H NMR.

The number of moles of 100 μL CH_2Cl_2 is n_{CH2Cl2}=1.56·10^{-3} mol, and the initial value of mole of cyclooctane (50 μL) is $n_{R,0}$=3.72·10^{-4} mol. So the initial mole of carbon is $C_{R,0}$=3.72·10^{-4}·8=2.97·10^{-3} mol. By referring to the area ratio between the products and CH_2Cl_2, the mole of specific product can be calculated respectively by following the equation 3.10. And that total carbon mass number of moles of products ($C_{T\text{-}Pi}$) and the left reactant ($C_{T\text{-}R,L}$) can be obtained by the equation 3.11 and 3.12 respectively.

$$n_{p_i}\textbf{(mol of product } i\textbf{)} = \frac{A_{p_i} / (\text{No. of } H_i)}{A_{CH_2Cl_2} / 2} \cdot n_{CH_2Cl_2} \qquad \textbf{(eq. 3.10)}$$

$$\boldsymbol{C_{T\text{-}P_i}}\textbf{(carbon number of all products, mole)} = \sum_i c_{p_i} n_{p_i}$$

$$= \sum_i \left(c_{p_i} \cdot \frac{A_{p_i} / \text{No. of } H_i}{A_{CH_2Cl_2} / 2} \cdot n_{CH_2Cl_2}\right) \quad \textbf{(eq.3.11)}$$

$$\boldsymbol{C_{T\text{-}R,L}} = n_{R,0} \cdot (1 - C_{conversion}) \cdot 8 \qquad \textbf{(eq. 3.12)}$$

By using the above the calculation, the definition of CMB can be converted into equation 3.13. By adopting the formula in the chosen reaction, the results are shown in table 3.2, which indicates that all the values are in the range of 100±10%, thus proving that the there is no obvious mass loss in the real reaction to an extent, which validates the quantitative analysis by ^{1}H-NMR.

$$\boldsymbol{CMB\%} = \frac{\sum_i \left(c_{p_i} \cdot \frac{A_{p_i} / (No.\ of\ H_i)}{A_{CH_2Cl_2} / 2} \cdot 1.56 \cdot 10^{-3}\right) + 3.72 \cdot 10^{-4} \cdot (1 - Con._{conversion}) \cdot 8}{2.97 \cdot 10^{-3}} \cdot 100\% \qquad \textbf{(eq.3.13)}$$

Table 3.2 Carbon mass balance calculation for cyclooctane oxidation by ^{1}H-NMR. Three set of reactions with different conversion and product distribution were selected for the validation of this calculation method. All reactions were conducted at 110 °C for 24 h at atmospheric air with condenser open to air or 2 bar O_2 (reading from the pressure gauge) respectively. Nb_2O_5 with 9.99% purity was used. 3 mL cyclooctane was used in each test. M(Ag):S=1:1000, M(Nb):S=1:12.

No.	Reaction conditions	Catalyst	Conver-sion%	The number of carbon/mol			CMB/ %
				Initial $C_{T\text{-}R,0}$	Products $C_{T\text{-}p}$	Reactant left, $C_{R,L}$	
1	atmospheric air	Nb_2O_5	16±4		$4.91 \cdot 10^{-4}$	$2.56 \cdot 10^{-3}$	103
2	2 bar O_2	Nb_2O_5	51±9	$2.97 \cdot 10^{-3}$	$1.68 \cdot 10^{-3}$	$1.61 \cdot 10^{-3}$	110
3	2 bar O_2	WI-Ag/Nb_2O_5	81±4		$2.69 \cdot 10^{-3}$	$4.25 \cdot 10^{-4}$	105

3.2.2 Cyclohexane oxidation

The products from cyclohexane oxidation, cyclohexanol and cyclohexanone that are called K/A oil, are crucial intermediates for the synthesis of ε-caprolactam and adipic acid, which are valuable raw materials for the manufacture of nylon-6 and nylon-66.[14-16] Given the great significance of cyclohexane oxidation both in the chemical industry and academic research, the feasibility of quantitative analysis by ^{1}H-NMR was

exploited. Similarly, by following the same approach employed for the analysis of the cyclooctane oxidation in section 3.2.1, a calculation method for the conversion, selectivity and carbon mass balance applied for the oxidation of cyclohexane was developed.

3.2.2.1 Quantitative analysis - conversion and selectivity

From our catalytic tests, it was found that the major products cyclooctanol (A_6), cyclooctanone (K_6), cyclooctyl hydroperoxide (P_6) in the oxidation of cyclohexane had characteristics peaks in an NMR spectrum (table 3.3 and Fig.3.2), which can be directly integrated to obtain areas as relative amount for each of them. Similar to cyclooctane, there was also overlap of peaks in the range of 1.0 ppm to 2.3 ppm, implying the need to account for overlaps, and thus, a calculation process according to the same principles used for cyclooctane oxidation was adopted for cyclohexane.

Table 3.3 Characteristic peak position and identification of major substances in reaction mixtures from cyclohexane oxidation. A_6 (cyclohexanol), K_6 (cyclohexanone), P_6 (cyclohexyl hydroperoxide are major products and by products (X_6) include cyclohexyl ester, hydroxycaproic acid (HA), cyclohexene, adipic acid (AA) and other ring opening products. ppm values for assignment are based on the website-Spectral Database for Organic Compounds[11].

Compound	Characteristic H	No. of H	Peak position (ppm)	Symbol of area
Cyclohexane(C_6)	-C<u>H</u>$_2$-	12H	1.43	A_{C6}
Cyclohexanol (A_6)	-(CH$_2$)$_2$-C<u>H</u>-OH	1H	3.58	A_{A6}
Cyclohexanone (K_6)	-C<u>H</u>$_2$-C=O-C<u>H</u>$_2$-	4H	2.35	A_{K6}
Cyclohexyl hydroperoxide (P_6)	-(CH$_2$)$_2$-C<u>H</u>-OOH	1H	3.79	A_{P6}

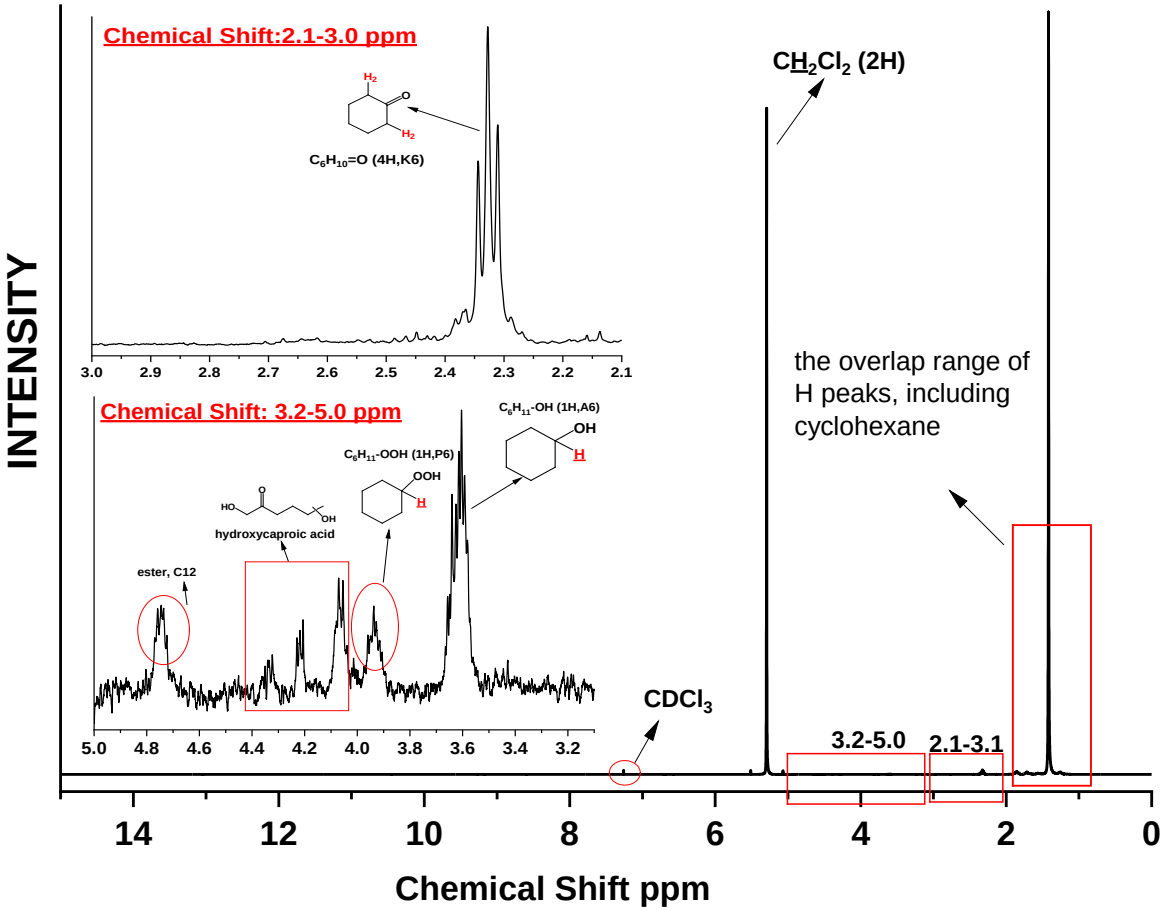

Fig. 3.2 An NMR spectrum of reaction mixture from cyclohexane oxidation. The oxidation was conducted in the presence of WI-Ag/Nb_2O_5 (prepared by wet impregnation method) at 120˚C for 24 h at 4 bar O_2 (reading of the pressure gauge.). M(Ag):S=1:1000.

Furtherly, the formula for conversion can be transformed into equation 3.14, representing by the relative area of corresponding characteristic H peaks. Herein, the side products include cyclohexene, hydroxycaproic acid, cyclohexyl ester, adipic acid, which are expressed as X_6. Similarly, the area of the side products A_{x6} and the area of reactant left can be calculated respectively by the equation 3.15 and 3.16 respectively.

$$\textbf{Conversion\%} = \frac{\frac{A_{A6}}{1} + \frac{A_{K6}}{4} + \frac{A_{P6}}{1} + A_{X6}}{\frac{A_{A6}}{1} + \frac{A_{K6}}{4} + \frac{A_{P6}}{1} + A_{X6} + \sum Area(reactant\ left)} x100\% \quad \textbf{(eq. 3.14)}$$

$$\textbf{Aera}(A_{x6}) = \frac{A_{ester}}{1} + \frac{A_{HA}}{1} + \frac{A_{cyclohexene}}{2} + \frac{A_{ring\ open}}{3} + \frac{A_{AA}}{2} + \frac{A_{unknown}}{2} \quad \textbf{(eq. 3.15)}$$

$$\textbf{Aera(reactant left)} = \frac{120 - (\frac{A_{A6}}{1} \cdot 11 + \frac{A_{K6}}{4} \cdot 8 + \frac{A_{P6}}{1} \cdot 11 + A_{x6} \cdot 9)}{12} \quad \textbf{(eq. 3.16)}$$

3.2.2.2 Carbon mass balance (CMB) by internal standard

Following the same approach used for the carbon mass balance in the oxidation of cyclooctane, 50 µL was taken from 3 mL reaction mixture into 100 µL CH_2Cl_2, using $CDCl_3$ as the solvent for the analysis by NMR. The mole of 100 µL CH_2Cl_2 was n_{CH2Cl2}=1.56·10^{-3} mol, and $n_{R,0}$=4.63·10^{-4} mol. So, the initial amount of carbon by mole was $C_{R,0}$=4.63·10^{-4}·6=2.78·10^{-3} mol. Furthermore, by referring to the area ratio between the regents and CH_2Cl_2, the mole of products can be calculated. By substituting the relevant values into the equation 3.9, the final CMB percentage in the case of cyclohexane is expressed as follows (eq. 3.17).

$$CMB\% = \frac{\sum_i \left(c_{p_i} \cdot \frac{A_{p_i} / (No.\ of\ H_i)}{A_{CH_2Cl_2} / 2} \cdot 1.56 \cdot 10^{-3}\right) + 4.63 \cdot 10^{-4} \cdot (1 - Con._{conversion}) \cdot 6}{2.78 \cdot 10^{-3}} \cdot 100\% \quad \textbf{(eq. 3.17)}$$

In our case, the oxidation of cyclohexane was carried out at 120 °C for 24 h and 4 bar O_2, as an example for the development of our calculation method. By referring to the above equation, the results of chosen tests are shown in table 3.4. All of the CMB are in the range of 95%-105%, indicating that this calculation process is reasonable for the oxidation of cyclohexane. Moreover, the analysis method can show the products distribution for the selectivity for peroxides directly in comparison with GC-MS method. In this context, it is verified that the quantitative analysis by ^{1}H-NMR in cyclohexane oxidation is feasible.

Table 3.4 Carbon mass balance calculation for cyclohexane oxidation by ^{1}H-NMR. A set of tests were selected for the calculation and all the tests were carried out at 120 °C for 24 h.

No.	O_2 pressure	Catalyst	Con. %	The number of carbon/mol			CMB %
				Initial $C_{R,0}$	Products C_p	Reactant left, $C_{R,L}$	
1	5 bar	None	<1	$2.78 \cdot 10^{-3}$	$2.03 \cdot 10^{-5}$	$2.76 \cdot 10^{-3}$	100
2	4 bar	None	<1		$2.10 \cdot 10^{-5}$	$2.76 \cdot 10^{-3}$	99
3	4 bar	Iron acetylacetonate M(Fe):S=1:100	8		$2.28 \cdot 10^{-4}$	$2.60 \cdot 10^{-3}$	102
4	4 bar	WI-Ag/Nb_2O_5 M(Ag):S=1:1000	12		$3.57 \cdot 10^{-4}$	$2.47 \cdot 10^{-3}$	102
5	5 bar	WI-Fe-Ag/Nb_2O_5 M(Ag):S=1:1000	12		$3.33 \cdot 10^{-4}$	$2.50 \cdot 10^{-3}$	102

3.3 GC-MS for the quantitative analysis for cyclooctane oxidation

In view of the above application of ^{1}H NMR in the quantitative analysis of cyclic hydrocarbons oxidation, the method is reliable to assess the performances of different catalysts in our case. However, there may exist some other by-products in the reaction

mixture that cannot be effectively detected by NMR, and the overlap of some characteristic H peaks when there are complex side products that may magnify the error. Our CMB results from ^{1}H-NMR imply that these products only account for a minor percentage that can be negligible. In order to furtherly clarify the validity of the results from ^{1}H-NMR, GC-MS was employed for the analysis of reaction mixtures from cyclooctane oxidation as a comparison, especially for the analysis of by-products, given that the detection limit of GC-MS at ppb level is lower than that of ^{1}H-NMR and a higher resolution of each compounds in GC. Furthermore, in order to ensure for a method to be reliable and statistically robust, it is also important or at least useful that the detection occurs within a linear range. In practice, there are usually two methods for quantification by GC, known as the internal standard method and external standard method. Due to the complex nature of our reaction mixture and the purpose for selectivity of desired products, the internal stand method was adopted in our research.

Quantitative analysis by GC techniques is based on the determination of parameters of the chromatogram related to the amount of the corresponding component, which is internal standard, in the injected sample[17, 18]. Ideally the response of the signal from detector to the concentration of analyte is in a linear way, which means that the area of peaks is proportional to the relative amount of the substances[18], but usually the linearity is in a specific of concentration range depending on the properties of substances, column and running conditions of GC[19]. Thus, it is important to ensure that the concentration of reagents in the samples are in the same or similar linear range of the standards. In view of these considerations, concentrations of

standards and samples were adjusted to be on the same range to ensure the accuracy of our measurements. According to our investigation about the separation of each substance of reaction mixtures in GC chromatograms, shown in Fig. 3.3, *n*-dodecane was selected as the internal standard and the proper analysis conditions were also optimized (injection volume was1 μL with a split ratio at 1:200). It can then be useful to plot the ratio of the analytic signal to the internal standard signal as a function of the compound concentration of the standards, by means of a calibration curve it is then possible to obtain the amount of a certain product.

Table 3.5 Retention time of different substances in reaction mixture. The reaction mixture for analysis is from the oxidation of cyclooctane by WI-Ag/Nb_2O_5 at 110 °C for 24 h at 2 bar O_2. Organic acid was detected while no trace of cyclooctyl hydroperoxide appeared in GC.

No.	Substance	Retention time (min)
1	Ethylcyclohexane	2.82
2	Cyclooctane	3.12
3	Cyclooctene	4.75
4	Cis-9-oxabicyclononane	5.45
5	Cyclooctanone	5.61
6	Cyclooctanol	5.96
7	*n*-Dodecane	6.63
8	1,4-Cyclooctanediene	7.32
9	Caprylic acid	8.20

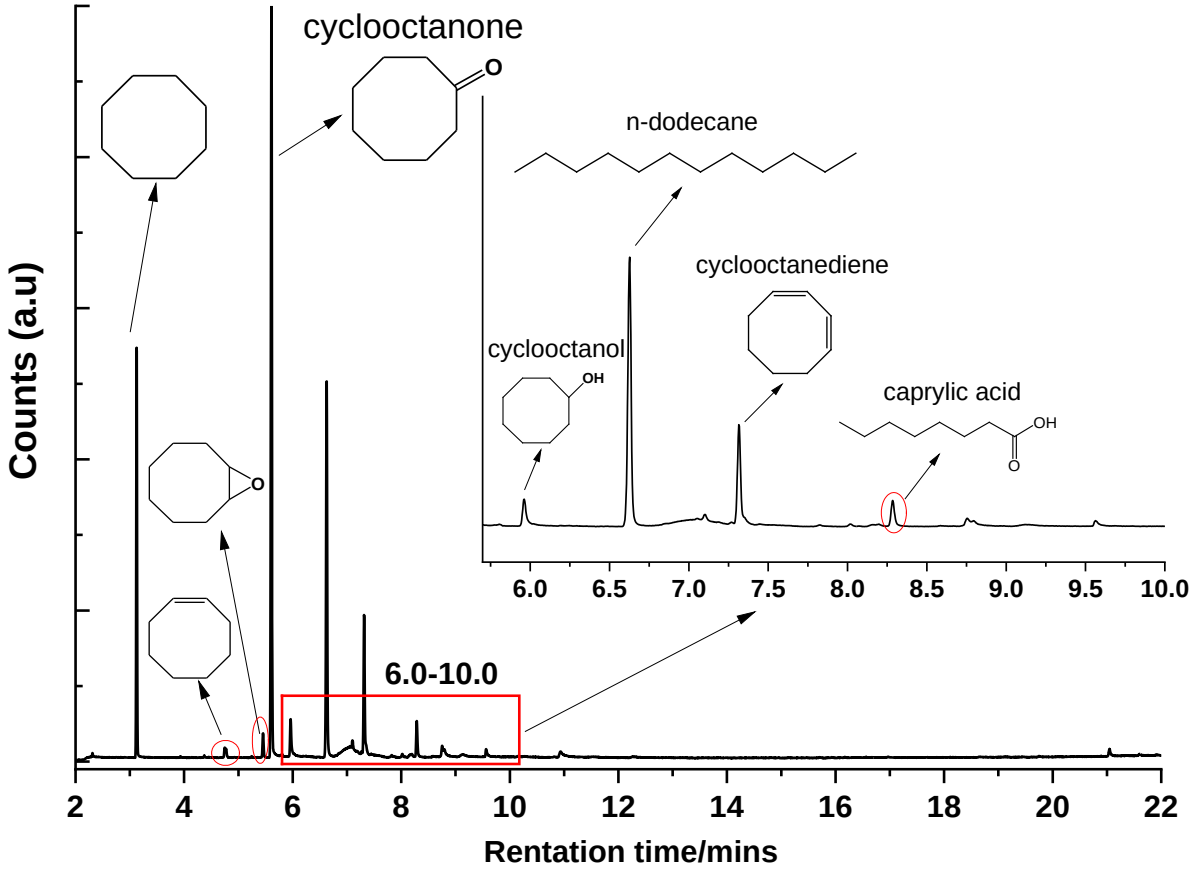

Fig. 3.3 A GC chromatogram of the reaction mixture from cyclooctane oxidation. Reaction was conducted in the presence of WI-Ag/Nb_2O_5 at 110 °C for 24 h at 2 bar O_2. 3 mL cyclooctane was used. M(Ag):S=1:1000. A satisfactory resolution of the compounds was obtained.

The definition of conversion can be expressed as moles consumed of reactant divided by initial moles amount of reactant, herein the equation is transformed into the following equations 3.18, where $[R]_{0,intial}$ is the concentration of reactant (cyclooctane), and [P*i*] is the concentration of the products corrected by the internal standard, as determined by the calibration curve in the linear range. The concentration of products is determined through the internal standard *n*-dodecane, where [IS] and Area(IS) are the concentration and area by integration from GC-MS of the internal standard respectively. Similarly, the selectivity of a given product is defined as equation 3.20, in which all the concentrations of products are calibrated by internal standard by eq. 3.19.

$$\textbf{Conversion\%} = \frac{n_t(\textit{reactant consumed})}{n_{0,}(\textit{initial amount of reactant})} = \frac{\sum[p_i]}{[R]_{0,initial}} \cdot 100\% \qquad \textbf{(eq. 3.18)}$$

$$\textbf{[}p_i\textbf{]} = [IS] \cdot \frac{Aera(p_i)}{Aera(IS)} \qquad \textbf{(eq.3.19)}$$

$$\textbf{Selectivity(}i\textbf{)\%} = \frac{[p_i]}{\sum_i [p_i]} \cdot 100\% \qquad \textbf{(eq. 3.20)}$$

Thus, an appropriate calibration curve by using *n*-dodecane as internal standard and acetone as solvent has been studied to ensure that the analysis is in a linear concentration range. As in our case, cyclooctanol, cyclooctanone and cyclooctyl hydroperoxide were major products in the oxidation of cyclooctane while no cyclooctyl hydroperoxide was observed in chromatograms, thus accordingly regression lines of cyclooctane, cyclooctanol, cyclooctanone were obtained respectively by this means, which are elucidated in Fig 3.4 and 3.5 as follows. The results show that the response of linear signal to the concentration is below 0.075 mol·L^{-1} in Fig. 3.4 for all the three

substances that we analysed here. In this case, the linear concentration is confirmed in our case, which indicates that the quantitative analysis for the concentration of desired major products should lie in this specific range. Therefore, the amount of main components, cyclooctane, cyclooctanol and cyclooctenone in reaction mixture, can be determined by the calibration in the presence of n-dodecane. However, it should be stated that as the hydroperoxides decompose upon GC injection giving approximately equal amounts of corresponding ketones and alcohols[7], the products distribution determined by GC-MS directly is the observed results instead of the actual ones, but the conversion results should not be affected. It is reported that the low temperature injection and reduction with triphenyl phosphine[4, 20, 21] can be employed for the identification of cyclohexyl hydroperoxide in cyclohexane oxidation.

Furthermore, the results we collected by using NMR and GC-MS are compared in table 3.6, indicating the conversion of both is relatively identical (81% by ^{1}H-NMR in comparison with 83% by GC-MS), while the observed products distribution is quite different. As shown, there is no observed cyclohexyl hydroperoxide, and the selectivity for cyclooctanone with 67% is higher in GC-MS method, which may be related with the decomposition of cyclooctyl hydroperoxide. However, it is not expected that K/A ratio determined by GC-MS is exceptionally high (15). To an extent, in our case, this comparison of the data would rather suggest that our analysis results by ^{1}H-NMR is easier and more accurate than the correspondent obtained via GC-MS if we only focus on the major products like alcohol, ketone and alkyl hydroperoxide instead of a

thorough analysis for all the by-products, as the latter contribute only for a small percentage in our tests. Therefore, the analysis for reaction mixture is mainly conducted by ^{1}H-NMR for this research project, especially for the selectivity, but GC-MS can be as an important tool to offer a thorough analysis for the substances which cannot be detected by ^{1}H-NMR. In our case, given that the identical conversion between these two methods and a CMB close to 100% withing experimental error from ^{1}H-NMR, we justify that ^{1}H-NMR can be employed as a quick and reliable screening tool for the quantitative analysis in cyclooctane and cyclohexane oxidation.

Table 3.6 The comparison of reaction results in cyclooctane oxidation obtained by using ^{1}H-NMR and GC-MS respectively. Reaction mixture was from the oxidation conduced at 110 °C for 24 h at 2 bar O_2 with the presence of WI-Ag/Nb_2O_5 (M:S=1:1000).

	^{1}H-NMR	**GC-MS**
Conversion, %	81	83
Cyclooctanol, %	8	5
Cyclooctanone, %	58	67
Cyclooctyl hydroperoxide, %	12	--
By products, %	22	28
K/A ratio	5.5	15.2

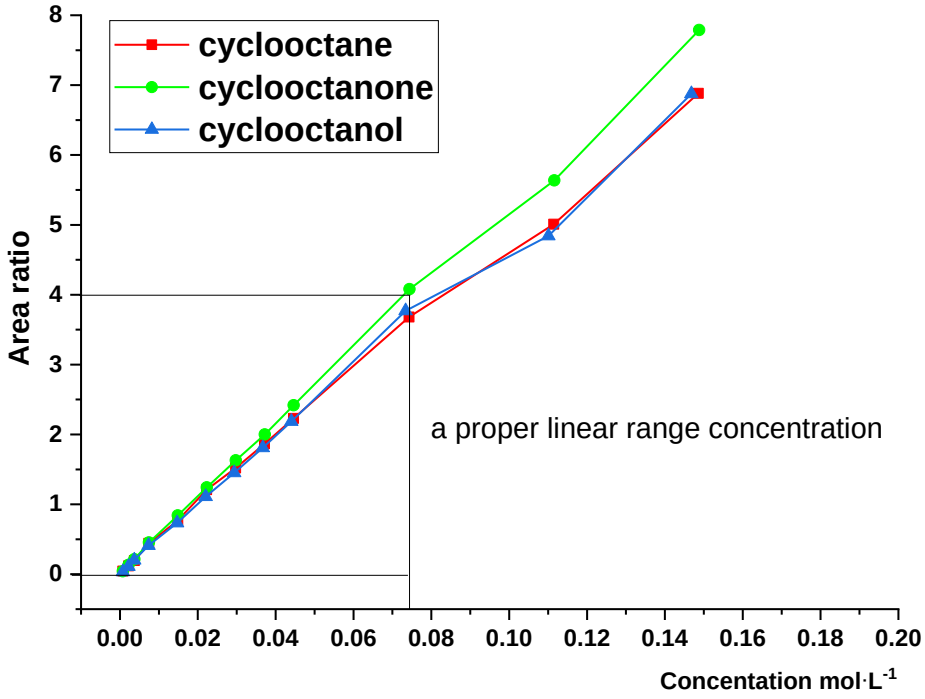

Fig. 3.4 Area ratio between substrates and internal standard (*n*-dodecane) versus the concentration of prepared samples containing cyclooctane, cyclohexanol and cyclohexanone.

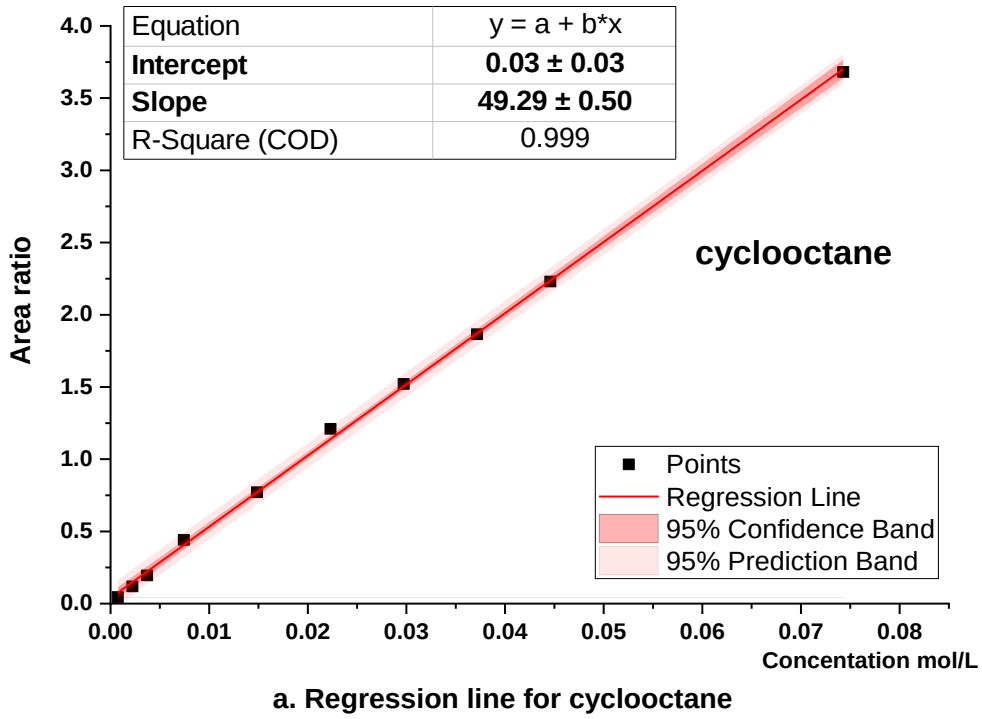

a. Regression line for cyclooctane

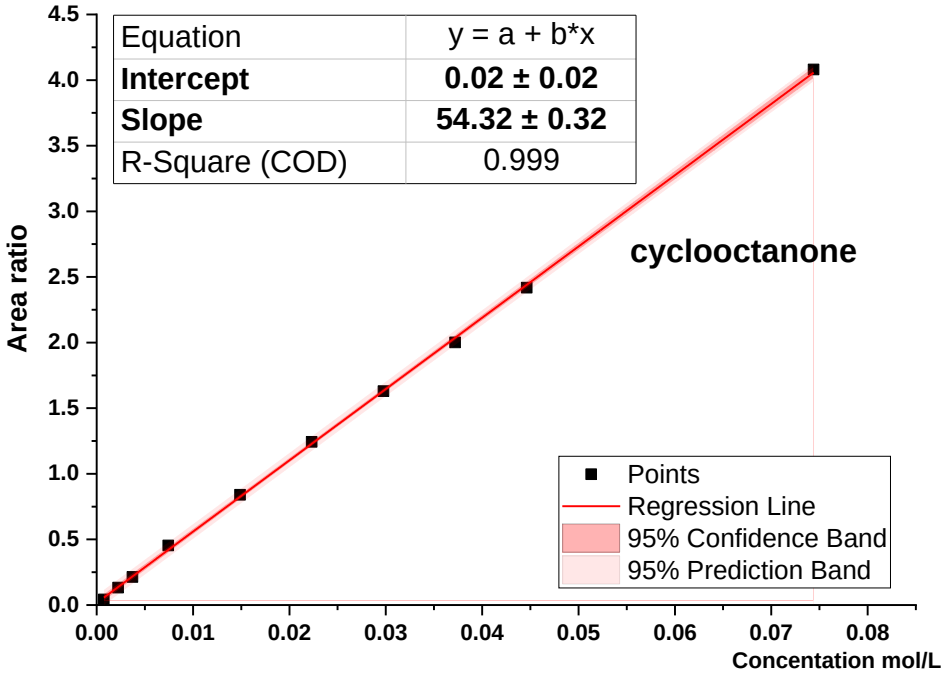

b. Regression line for cyclooctanone

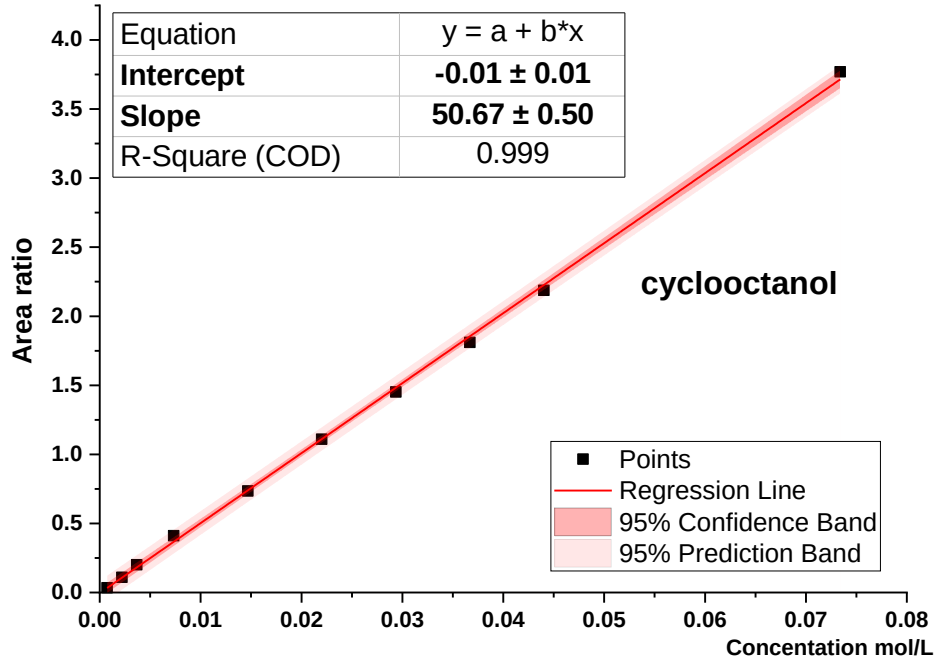

c. Regression line for cyclooctanol

Fig. 3.5 Regression lines of cyclooctane (a), cyclooctenone (b) and cyclooctanol (c) calibrated by using *n*-dodecane as internal standard. The formula for each curve is: a. y = (49.29±0.50)·x + (0.04±0.03); b. y = (54.32±0.0.32)·x + (0.02±0.02); c: y = (50.67±0.50)·x+(-0.01±0.01). All the regression lines are compatible with zero point.

3.4 ICP-MS analysis for metal loading and leaching

As described in chapter 2, inductively coupled plasma mass spectrometry (ICP-MS) in an analytical technique used as a trace element technique, which can offer extremely low detection limit and make the quantification at ppm level[22-24], and the samples are usually in the liquid form. In our research, ICP-MS was mainly used to quantify the metals in the catalysts (mainly Ag species) treated by concentrated HNO_3 to attack catalysts for the release of metals and reaction mixtures which may contain active metal leaching components, as described in 2.4.3 of chapter 2.

3.4.1 Metal loading analysis for supported catalysts

Generally, owing to the sample for ICP-MS analysis being in the liquid phase, the metal components present in a solid catalyst need to be dissolved in solution, and in our case in aqueous media. A given amount of catalyst was dissolved in concentrated HNO_3 at room temperature for 24 h, and then the solution was diluted by using deionized water up to 250 mL, by which the amount of Ag in catalyst attached by HNO_3 can be obtained by ICP-MS. The process is described in chapter 2.4.3. However, it is possibly that there is loss of Ag during preparation process (especially in deposition precipitation process involving the filtration step)[25] and Ag that does not attach to the surface of support, the measured amount of Ag could be lower than the nominal loading. As shown in table 3.7, it is found that the amount of Ag in WI-Ag/Nb_2O_5 is the highest while SI-Ag/Nb_2O_5 lead to the lowest Ag amount. In view of this, a further consideration about the Ag loading observed in TEM images (see section 5.2.6.2 in

chapter 5) and Ag leaching into reaction mixture (section 5.2.5 of chapter 5) could be done. We postulate a higher Ag loading in WI-Ag/Nb_2O_5 as well as the interaction between metal and support (a lower Ag leaching into reaction mixture is observed in DP-Ag/Nb_2O_5 and SI-Ag/Nb_2O_5, suggesting a stronger resistance to acid attack).

Table 3.7 ICP-MS analysis for the metal loading of the prepared supported catalyst. WI-Ag/Nb_2O_5: catalyst prepared by wet incipient impregnation method; DP-Ag/Nb_2O_5: catalyst prepared by deposition precipitation method; SI-Ag/Nb_2O_5: catalyst prepared by sol immobilization protocol.

Catalyst	Nominal metal loading/%	Observed amount of Ag in solution/%
WI-Ag/Nb_2O_5	1 *wt*% Ag	0.63
DP-Ag/Nb_2O_5		0.45
SI-Ag/Nb_2O_5		0.19

3.4.2 Metal leaching analysis in reaction mixtures

As the reaction mixtures are mainly organic solutions, while the samples for the ICP-MS analysis should be in water solution, the detection of possible leached species, was carried out by an extraction procedure form the organic phase in water. In detail: 1 mL of reaction mixture was extracted into 10 mL of deionized water by mixing them thoroughly for 24 h at room temperature, followed by separating the water phase for analysis. The calculation for Ag leaching can be expressed as follows (eq. 3.21), where the total mass amount of Ag added into reaction is usually 2.41 mg in a standard test, that is 3 mL of substrates used in cyclooctane oxidation with a M:S ratio at 1:1000, which is 241 mg of catalysts Ag/Nb_2O_5.

$$\text{Ag leaching\%} = \frac{\text{The mass amount of } Ag^{+} \text{ extracted by water from reaction mixture}}{\text{Total mass amount of Ag species added into reaction}} \cdot 100\%$$

(eq. 3.21)

3.5 Conclusion

An efficient and accurate tool for the quantification analysis of reaction mixtures from the oxidation of cyclooctane and cyclohexane was developed in detail respectively. The results indicated that ^{1}H NMR can work as a reliable and effective method to quickly quantify the major products (ketones, alcohols, alkyl hydroperoxides), especially for the quantification of alkyl hydroperoxides as the analysis process was conducted at room temperature without affecting the thermal stability samples in comparison of GC-MS. Meanwhile, the CMB analysis by using internal standard (dichloromethane) proved the validity of quantitative analysis by ^{1}H NMR method when applied in the oxidation of cyclooctane and cyclohexane.

However, GC-MS with a lower detect limit compared with NMR, is widely used for the quantitative determination to provide a thorough analysis for the substances which cannot be detected by NMR, especially when the sides products are largely produced with higher conversion, but the alkyl hydroperoxides species cannot be directly quantified due to the thermal instability under the analysis conditions, implying that observed product distribution by GC-MS cannot precisely represent the actual sample composition from reaction mixture. Moreover, a comparison of the results quantified by ^{1}H NMR and GC-MS showed that the conversion was consistent while the products distribution was quite different. In this context, ^{1}H NMR can be reliably used for the

quantitative analysis of the cyclooctane and cyclohexane oxidation when we only focused on the study about the major products (ketone, alcohol and alkyl hydroperoxide).

In addition, the ICP-MS analysis method for the determination of actual metal loading of the catalysts and the leaching of metal components in the reaction mixture were established. Determination of metal leaching analysis is of great importance in our research as it is a direct evidence to elucidate the stability and reusability of the prepared supported metal catalysts.

3.6 References

1. F. Cavani, *Catal. Today*, 2010, **157**, 8-15.
2. G. Centi, F. Cavani and F. Trifirò, *Selective oxidation by heterogeneous catalysis*, Springer Science & Business Media, 2012, p 1-2.
3. F. Cavani, G. Centi, S. Perathoner and F. Trifirò, *Sustainable industrial chemistry: Principles, tools and industrial examples*, John Wiley & Sons, 2009, p 1-3.
4. B. P. Hereijgers and B. M. Weckhuysen, *J. Catal.*, 2010, **270**, 16-25.
5. H.-J. Hübschmann, *Handbook of GC-MS: fundamentals and applications*, John Wiley & Sons, 2015, p 1-3.
6. T. M. Lovestead and K. Urness, 2019, p 235-241.
7. G. B. Shulpin, D. Attanasio and L. Súber, *J. Catal.*, 1993, **142**, 147-152.
8. F. Malz and H. Jancke, *J. Pharm. Biomed. Anal.*, 2005, **38**, 813-823.

9. W. Trakarnpruk, A. Wannatem and J. Kongpeth, *J. Serbian Chem. Soc.*, 2012, **77**, 1599-1607.

10. C. A. Wilde, Y. Ryabenkova, I. M. Firth, L. Pratt, J. Railton, M. Bravo-Sanchez, N. Sano, P. J. Cumpson, P. D. Coates and X. Liu, *Appl. Catal. A: Gen.*, 2019, **570**, 271-282.

11. Spectral Database for Organic Compounds, https://sdbs.db.aist.go.jp/sdbs/cgi-bin/direct_frame_top.cgi.

12. K. Kumabe, T. Sato, K. Matsumoto, Y. Ishida and T. Hasegawa, *Fuel*, 2010, **89**, 2088-2095.

13. R. Lloyd, R. L. Jenkins, M. Piccinini, Q. He, C. J. Kiely, A. F. Carley, S. E. Golunski, D. Bethell, J. K. Bartley and G. J. Hutchings, *J. Catal.*, 2011, **283**, 161-167.

14. Y. Wang, J. Zhang, X. Wang, M. Antonietti and H. Li, *Angew. Chem. Int. Ed.*, 2010, **49**, 3356-3359.

15. I. i. a. V. e. Berezin, E. T. Denisov and N. M. Emanuel, *The oxidation of cyclohexane*, Elsevier, 2018, p ix-x.

16. P. Wu, Y. Cao, Y. Wang, W. Xing, Z. Zhong, P. Bai and Z. Yan, *Appl. Surf. Sci.*, 2018, **457**, 580-590.

17. J. W. Diehl and F. P. Di Sanzo, *J. Chromatogr. A*, 2005, **1080**, 157-165.

18. G. Guiochon and C. L. Guillemin, *Quantitative gas chromatography for laboratory analyses and on-line process control*, Elsevier, 1988, p 653-654.

19. S. K. Bhardwaj, K. Dwivedi and D. Agarwal, *Int. J. Anal. Bioanal. Chem.*, 2016, **6**, 1-7.

20. I. Hermans, P. Jacobs and J. Peeters, *Chem. Eur. J.*, 2007, **13**, 754-761.

21. L.-X. Xu, C.-H. He, M.-Q. Zhu and S. Fang, *Catal. Lett.*, 2007, **114**, 202-205.

22. J. W. Olesik, *Anal. Chem.*, 1991, **63**, 12A-21A.

23. R. Thomas, *Practical guide to ICP-MS: a tutorial for beginners*, CRC press, 2013, p 1-3.

24. R. Thomas, *Spectrosc.*, 2001, **16**, 38-42.

25. L. Di, J. Zhang and X. Zhang, *Plasma Process. Polym.*, 2018, **15**, 1700234.

Chapter 4: The unexpected catalytic activity of Nb_2O_5 in the oxidation of cyclic hydrocarbons under mild conditions

4.1 Overview

The selective oxidation of hydrocarbons is a process in which hydrocarbons are transformed to oxygen-containing (oxygenated, oxyfunctionalized) products[1], which involves the cleavage of a C-H bond. However, the high bond dissociation energy of C-H bond (normally in the range of 395-470 $kJ \cdot mol^{-1}$)[2, 3] in hydrocarbons usually requires the presence of a catalyst to make the processes achievable by lowing the energy for the dissociation of C-H bond under relatively mild conditions (e.g., lower temperature below 150 °C and pressure below 10 bar)[4-6]. In this context, another factor to be considered is that the hydrocarbon oxidation if often a low selectivity appears, that is, it often generates large amounts of waste and by-products. In this context a catalyst is beneficial as it can increase the selectivity to specific and desired product (or class of products) thus further contributing to the development of energetically favourable and environmental acceptable chemical processes. As discussed in chapter 1, generally, heterogenous catalysts are made of an active component, most often a transition metal, a support and a promoter, in which support can affect the performances of the catalysts in various ways[7, 8], such as against sintering or aggregation of particles, affecting particles morphology and size[9], inducing metal-support interaction[10], oxygen storage for the promotion of reactions[11]. The specific behaviour of a support depends on the intrinsic properties of used support (e.g., basicity, surface area,

presence of mixed oxidation states)[11-13]. In these perspectives, an array of behaviours can be observed ranging from chemically inert, to a promoter or even as an inhibitor. In this context then, it is important to elucidate the roles of the support for a specific model reaction separately from any metal nanoparticles. A thorough understating about the effects of support on reaction would help to clarity the roles of doped metal in oxidation process as comparison, which is essential for the design of catalysts.

Metal oxides play a very important role in many areas of chemistry, physics and materials sciences[14, 15], and they are widely used as supports for the preparation of supported metal catalysts due to: i) their thermal and mechanical stability for long term use and scale-up production; ii) high surface area is a parameter often assumed to be central to increase the catalytic activity (or the dispersion of deposited metal nanoparticles[16]); iii) the presence of oxygen vacancies might be of importance for partial oxidation reaction as they imply different oxidation states[17]. Meanwhile, the application of metal oxides in the catalysis preparation is the most technologically advanced and economically important, which have been employed for the preparation of catalysts aimed for the selective oxidation (e.g., cyclohexane, ethylbenzene)[18, 19], alkane ammoxidation[20] and selective dehydrogenation[14]. Until now, many metal oxides, such as Al_2O_3, CeO_2, TiO_2, SiO_2, MgO[21-23], have been applied as active components, pure support or as the promoter in the catalyst system. For example, CeO_2 with oxygen storage ability promotes the oxidation of CO[17] or soot[11], while MgO as a support for Au nanoparticles displays inhibiting effect on cyclohexane oxidation which is possibly

correlated with radical trapping by the defects in MgO crystals[24]. Usually a metal oxide to be used as a support is required to be mechanically and thermally stable, and importantly hamper or discourage the sintering of the metal or metal oxide nanoparticles that are deposited on the surface, to provide the surface involving the bonding and reaction of adsorbates.

According to the literature review in section 1.3 of chapter 1, with the aim to introduce innovations in the discovery of materials capable of selective hydrocarbon oxidation, we focused our attention on the use of Nb_2O_5 either as a support for metal nanoparticles or for the use of this material in hydrocarbons oxidation. As a support, our expectations are based on previous research which showed surface niobium oxide-support interaction (SOSI)[25] and strong metal-support interaction (SMSI)[7, 26]. Whereas for the use of bare Nb_2O_5, niobium oxides are presently of great interest in heterogeneous catalysis where they are used as catalyst components or are added in small amounts to catalysts[27], by which the incorporation of Nb^{5+} could induce the formation of active metal-Nb-O_x species (see table 1.4 in chapter 1). In addition, Nb_2O_5 is a metal oxide which may exist in different crystallographic forms[7] which could have a different reactivity, is reportedly resistant to hydrolysis[28] and any partial hydrocarbon oxidation generate water. Nb centres may exists in an array of oxidation states: 2+,4+ and 5+, leading to the correspondent NbO, NbO_2 and Nb_2O_5 oxides. Based on these characteristics, Nb_2O_5 has been explored as a catalyst support in the bulk form and porous form[29, 30] for reaction like esterification, hydrogenation/dehydrogenation,

ammoxidation, the oxidation of alcohols, the photooxidation of hydrocarbons in the presence of solvent[31, 32] and as a support for metal nanoparticles involving Ru[33], Rh[34], Pt[35], Pd[36] species.

However, despite this background and premises there are no actual reports for the use of Nb_2O_5 either as a support or bare metal oxide for the direct oxidation of hydrocarbons by molecule oxygen in the absence of initiator or solvent. This then prompted us to set out to investigate the possible reactivity and or use of this metal oxide for the oxidation of cyclic hydrocarbons based on the following grounds:

i) As we are interested in the development of metal supported nanoparticles and Nb_2O_5 is largely unused for hydrocarbon oxidation, to investigate its characteristic would be a useful control test to discriminate between any reactivity that Ag/Nb_2O_5 systems may have afterwards.

ii) Even if for gas phase reactions, metal oxides like MoO_3[37], V_2O_5[38] and Cr_2O_3[39] are actually active for hydrocarbon oxidation. As Nb belongs to the same group of V and is adjacent to Mo and Cr, this could suggest that Nb maybe is also active for this class of reactions.

iii) Microporous doped Nb_2O_5 with Fe synthesized within the group, showed some activity for *n*-decane oxidation. However, the results were not univocal in terms of origin of the catalytic activity, that is, some conversion (ca. 10% at 1 bar O_2 and 150 °C) was detected but it was unclear if this was due to Fe centers or Nb centers. The study of the activity, if present of Nb_2O_5 for the oxidation of cyclic hydrocarbons, which products

are useful precursor for the fibers sector, could provide a useful background for the development of new materials in this area.

In view of all these considerations, in this chapter, we focus on the potential catalytic properties of Nb_2O_5, and if Nb_2O_5 has any catalytic property, and compare them with most conventional metal oxides like CeO_2, MgO, TiO_2, SiO_2, which are well known as supports in the oxidation of hydrocarbons. In this context, the investigation about the roles of the metal oxide will lay the foundation for the research about the active metal nanoparticles, which will be discussed in next chapter.

4.2 Mechanism for the autoxidation of hydrocarbons

The slow oxidation of hydrocarbons by means of ground state (triplet) molecular oxygen in the liquid phase is termed as autoxidation, which affords organic hydroperoxides as primary intermediates through a radical chain pathway[1]. In this reaction route, the oxidation is initiated by the homolytic cleavage of C-H bond, which can be started by the thermal decomposition in the absence of initiator (eq.4.1), or the initiation triggered by traces of metal in the walls of a reactor/container[40]. This process usually shows a much lower reaction rate since the formation of alkyl radicals is thermodynamically and kinetically unfavourable. And then followed by the equation 4.2-4.5 displaying the propagation process. The formed R· in initiation step is a highly reactive species which can furtherly propagate the chain reaction by reacting with the oxygen species. The addition of radicals to molecular oxygen, usually is a rapid, diffusion-controlled reaction that leads to the formation of hydroperoxyl radicals (eq.

4.2) which can abstract a H atom from a R-H substrate to form a alkyl hydroperoxide, and often considered the rate-determining process[1] (eq.4.3). In both academic and industrial research, initiators like H_2O_2, *tert*-butyl hydroperoxide can be added to facilitate the formation of hydroperoxides, which can obviously shorten the induction time for the reaction. In addition, at elevated temperature, the alkyl hydroperoxides species may undergo thermal decomposition to alcohols, as shown in equation 4.4, and the decomposition process may serve as a major source of free radicals in autoxidation. This process however can be accelerated by a catalyst[18, 40]. Moreover, the side reactions like β-scission of the alkyl hydroperoxyl radicals, make the oxidation process non-selective and based entirely on the statistics of the free-radical chain process.

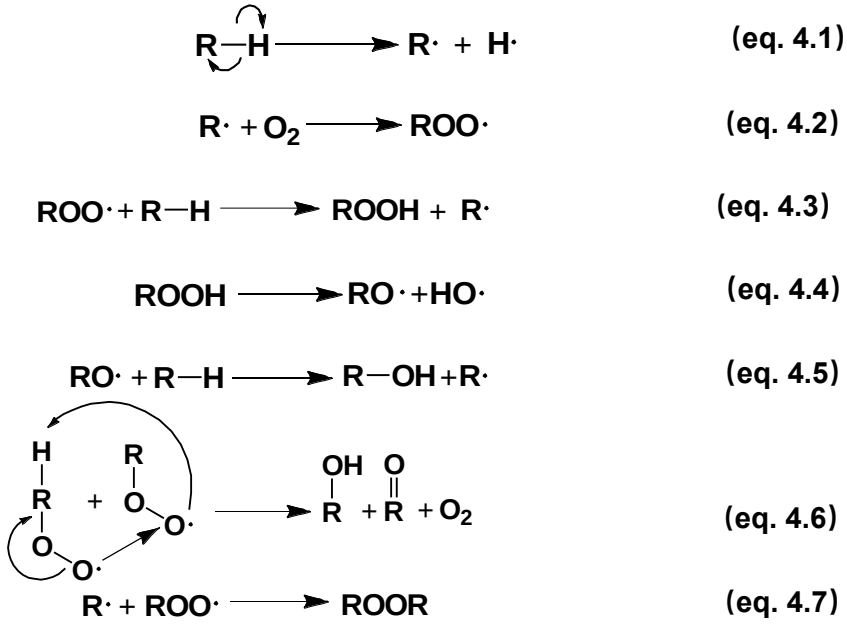

Equation 4.6 and 4.7 illustrate the termination stage, the former, also known as Russell's termination mechanism, exhibiting two alkyl hydroperoxyl radical species

reacts with each other to give a 1:1 molar ratio of ketone and alcohol, which indicates that the K/A ratio in a blank autoxidation process should be close to 1. Also, equation 4.7 reveals that there may be carbo-peroxo by-products, which can be detected via ^{1}H-NMR (see chapter 3). An example of cyclooctane autoxidation is illustrated in scheme 4.1.

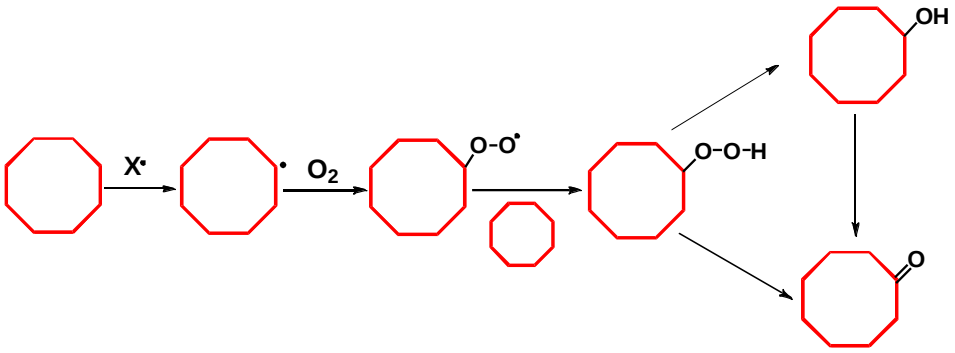

Scheme 4.1 The free-radical pathway for the aerobic autoxidation of cyclooctane in the absence of initiator (X·). A R· radical is formed and it reacts with molecular O_2 to produce hydroperoxide radical, which may involve the diffusion of O_2. Cyclooctyl hydroperoxide is an intermediate which can be furtherly transformed into alcohols and ketones or other side products.

4.3 A study of the reactivity of Nb_2O_5 in the oxidation of cyclooctane: Nb_2O_5 species or impurities

According to the above discussion and literature review in chapter 1, Nb_2O_5 based catalysts are rarely applied for the oxidation of hydrocarbons by molecular O_2 in the absence of solvent. In this section, we will explore the possibility to make use of Nb_2O_5 for the preparation of catalyst aimed for the aerobic oxidation of hydrocarbons instead. To start with, the performances of Nb_2O_5 only in the oxidation process will be investigated, then it will be used afterwards as a support for metal nanoparticles, to

clearly elucidate the roles of metal nanoparticles and the support. In addition, there may exist different polymorphic phases of Nb_2O_5, i.e., TT-, T-, B-, M-, H-, N-, and P-Nb_2O_5[28, 41] (see section 1.3.1 of chapter 1). What should be noted is that the polymorphisms may lead to different reaction performances. In this context, two batches of Nb_2O_5 with two different grades/purities 99.9% and 99.99% will be discussed separately, which are identified as Nb_2O_5-1 and Nb_2O_5-2 respectively.

4.3.1 Catalytic activity of Nb_2O_5-1 for cyclooctane oxidation

This section investigates the behaviours of Nb_2O_5 for the solvent-free aerobic oxidation of cyclooctane. According to our experimental section, catalytic tests were initially carried out at 110 ˚C for 24h at atmospheric air pressure with a condenser open to air or 2 bar O_2 respectively (Fig. 4.1).

The results show that Nb_2O_5-1 strongly promotes the oxidation of cyclooctane under both atmospheric air (16% conversion) and pressurised O_2 (51% conversion) in comparison with the blank tests. This is rather surprising as Nb_2O_5 is generally chemically inert for the oxidation of saturated hydrocarbons, although there are reports it can be activated in the photo oxidation process for the alcohol oxidation in the presence of solvent like acetonitrile[31]. Additionally, the product distribution also changes in the presence of Nb_2O_5: the formation of cyclooctanone (K_8) is facilitated with a higher K/A ratio up to 4.3 under pressurised O_2. As described in section 4.2, the autoxidation of cyclooctane without catalysts follows a free-radical mechanism to form equal amount of ketones and alcohols with K/A ratio around 1 by the decomposition of

intermediate cyclooctyl hydroperoxide. In this perspective, it is possible the product distribution can be optimized to produce more cyclooctanone by using Nb_2O_5. Besides, it should be noted that the conversion of blank tests is very low (0% at 1 atm air and 6% at pressurised O_2), while Nb_2O_5 improve the conversion largely, especially in the presence of pressurized O_2, from 6% of blank test up to 51%. Generally, the cleavage of C-H bond in hydrocarbon is quite challenging as the bond dissociation energy is high (385 $kJ \cdot mol^{-1}$ in cyclooctane[42]). Our results indicate that the presence of Nb_2O_5 can enhance both the transformation of cyclooctane, and the selectivity to cyclooctanone. In order to identify the origin of this unusual behaviour, we set out a systematic series of control tests mainly involving Nb_2O_5-1 to figure out the active species from the Nb_2O_5 and its mechanism in the oxidation, which is discussed in 4.3.2.

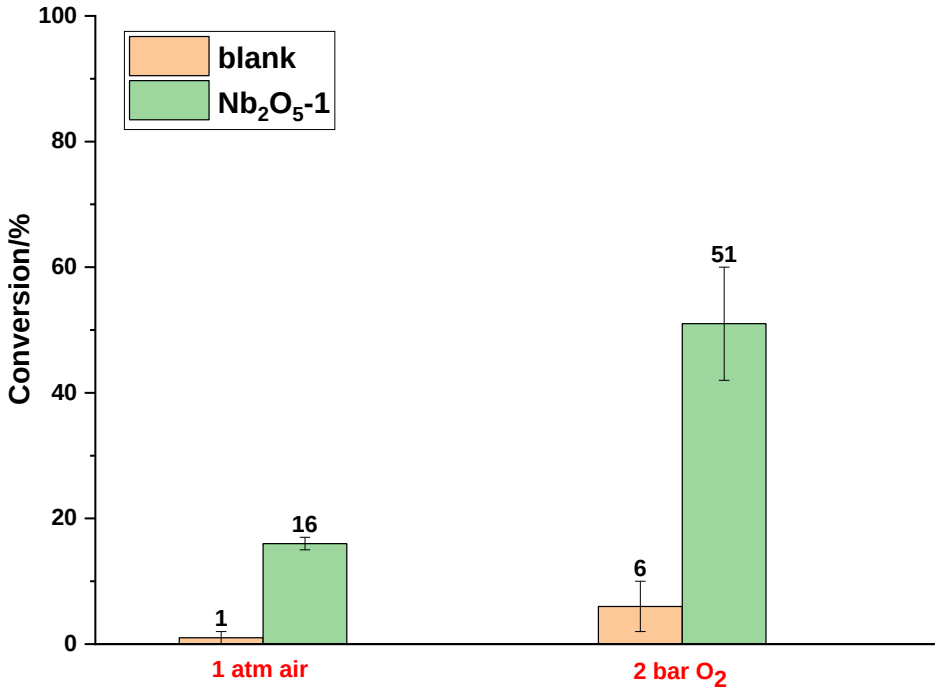

a. The conversion of cyclooctane by Nb_2O_5-1

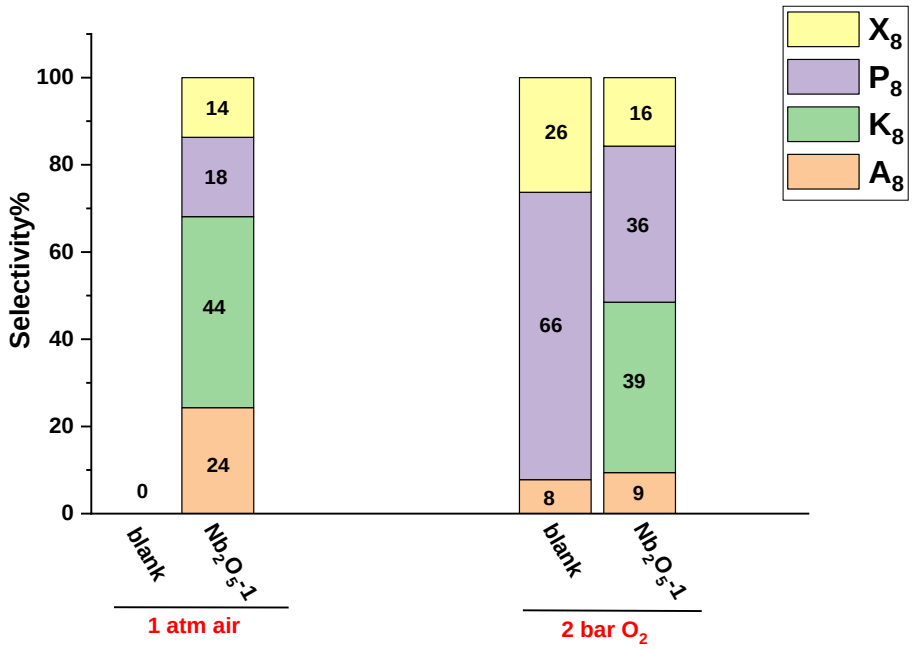

b.The product distribution in cyclooctane oxidation by Nb_2O_5-1

Fig. 4.1 Catalytic activity of Nb_2O_5-1 (99.9% grade/purity) in cyclooctane oxidation. a: Conversion of cyclooctane oxidation by Nb_2O_5-1; b: Product distribution in cyclooctane oxidation. Reaction conditions: 3 mL cyclooctane at 110 ˚C for 24 h at atmospheric pressure using air as oxidant with condenser open to the air and 2 bar pressurised O_2 respectively. Molar ratio between Nb and cyclooctane is 1:12. And all the conversion and selectivity percentage in this chapter are expressed as mol%. A_8: cyclooctanol, K_8: cyclooctanone, P_8: cyclooctyl hydroperoxide, X_8: by products. Where 8 stands for the number of carbon atom.

4.3.2 Catalytic activity of filtrates extracted from Nb_2O_5-1 by various media

From the above section, it was found that bare Nb_2O_5-1 was active itself for the oxidation of cyclooctane by using O_2 as oxidant. Due to the lack of established literature in the use of base Nb_2O_5 for the direct oxidation of hydrocarbons, we considered at first the possibility of 'impurities' in the parent Nb_2O_5, which could enhance the oxidation process. Thus, a systematic study on the nature and the effects of the impurities may exist in Nb_2O_5 has been carried out based on this assumption.

Different extraction protocols were used[43, 44]: filtration of Nb_2O_5 by hot water (80 °C) for the soluble components, washing with HCl (1M) to form chlorinated salts and washing with HNO_3 (1M) that is as an oxidizing agent, processes being described in section 2.3.6 of chapter 2. The filtrate was collected and concentrated up to dryness by treating it at 90 °C for 16 h. Cyclooctane was then added, and the reactivity was tested for the oxidation reaction at 2 bar of O_2 at 110 °C for 24 h.

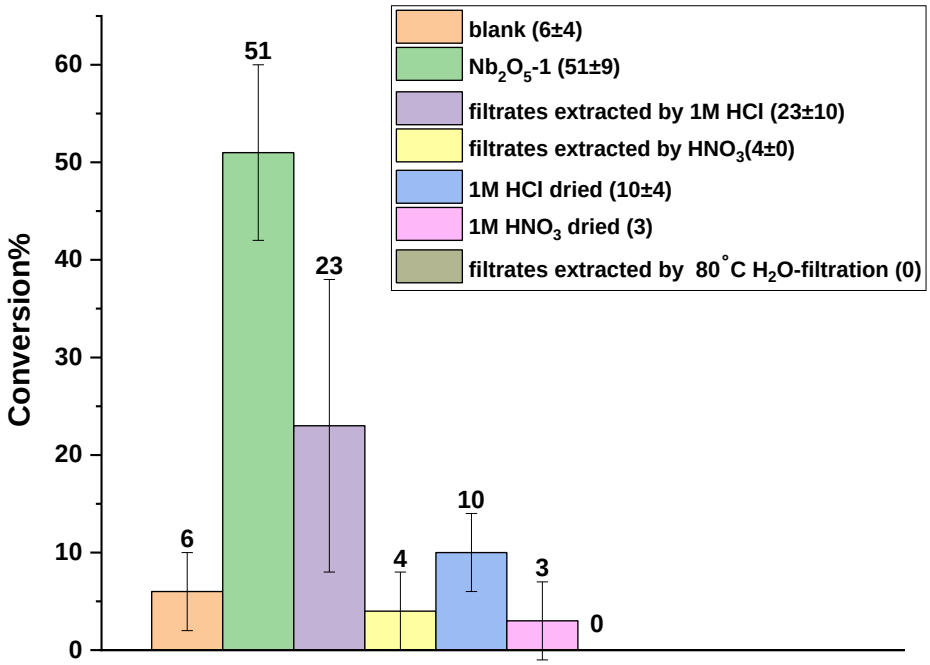

a. Conversion of cyclooctane by extracted filtrates in Nb_2O_5-1

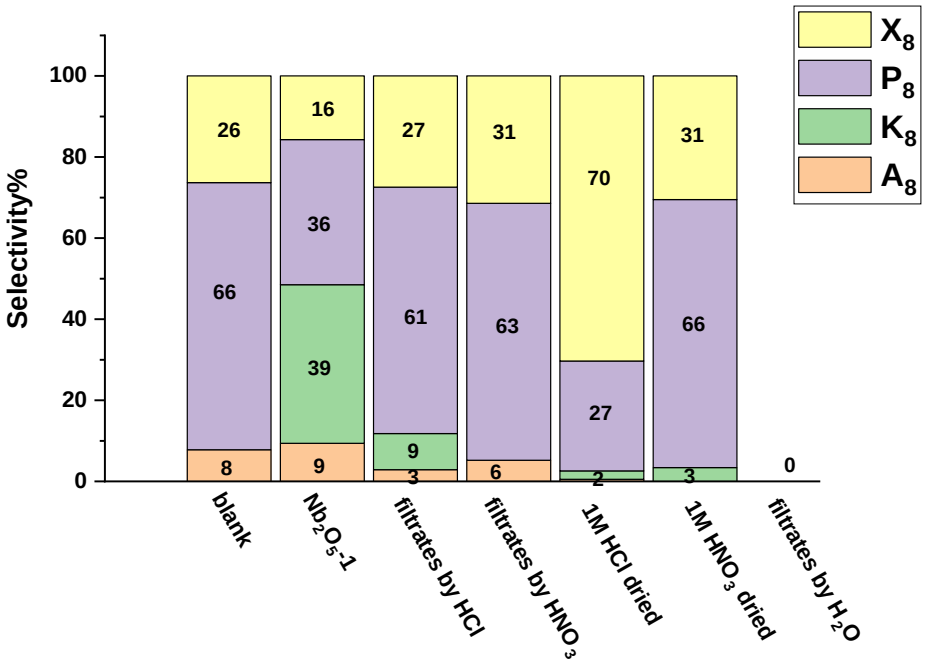

b. Product distribution of cyclooctane oxidation by extracted filtrates in Nb_2O_5-1

Fig. 4.2 Reaction performances of filtrates extracted from Nb_2O_5-1 in the oxidation of cyclooctane. a: Conversion of cyclooctane oxidation by filtrates from Nb_2O_5-1; b: Product distribution of cyclooctane oxidation by filtrates from Nb_2O_5-1. Reaction conditions: at 110 °C for 24 h at 2 bar O_2. The procedures to extract impurities are detailed explained in chapter 2. Filtrates extracted by HCl: 1 g Nb_2O_5 was treated by 5 mL HCl (1M) for 24 h at room temperature and then washed with deionised water up to 100 mL solution. 2 mL of this filtrate solution was taken to be fully dried at 100 °C for the test. The similar procedure for impurities by HNO_3 and H_2O respectively. 1M HCl dried: 2 mL 1 M HCl was dried at 100 °C to test the impurities in HCl as comparison, which was similar with 1M HNO_3 dried.

The results in Fig.4.2-a and b reveal that there is no evident conversion from the dried filtrates obtained from hot water filtration (components analysis by ICP-MS is displayed in table 4.1 and 4.2), and the conversion is 4% when using the filtrate obtained by HNO_3 treatment, which is identical with the conversion of blank test, while the filtrate by treatment with HCl shows an enhanced reactivity for the oxidation with around 23% conversion. As HCl may extract metals that can be present in the Nb_2O_5

matrix, these could be responsible for the catalytic activity that we observe. On the other hand, as from the manufacturing process of HCl and HNO_3 traces of metals can also be present (especially Fe)[45], dried residues from HCl and HNO_3 were also tested. Results indicates that the conversion is identical with the blank test, which rules out the effects of other components from acid. In addition, the products distribution displays that the main product is cyclooctyl hydroperoxide by the filtrate from HCl treatment, indicating that there exist active species for the oxidation.

Thus, there may active species presented in the filtrate extracted by HCl from parent Nb_2O_5 we used based on the discussion. For further research to justify the assumption, ICP-MS is used for the analysis of components in the extraction liquid mixture by different media, which is shown in table 4.1 and table 4.2.

Table 4.1 Full scan analysis of the metal content and impurities present in parent Nb_2O_5-1, expressed in mg of impurity or contaminant per gram of Nb_2O_5-1. Metal extracted with 1 M HCl (HCl-Nb), 1 M HNO_3 (HNO_3-Nb) and 80 ˚C hot water (H_2O-Nb) respectively, and quantification from ICP-MS analysis.

Sample ID, mg	Nb	Al	As	B	Na	Ba	Ca	S	Si
HCl-Nb	0.0528	0.0180	<0.001	0.0359	0.3960	0.0130	0.4055	0.0115	0.0590
HNO_3-Nb	--	0.0725	--	0.1501	0.7290	0.0183	0.4633	0.0173	0.1178
H_2O-Nb	0.0002	--	--	0.0250	0.11	0.0004	0.0025	0.0046	0.0310

Sample ID, mg	Cu	Fe	Sr	I	K	Ti	Mg	Mn	Zn
HCl-Nb	0.0126	0.0056	0.0047	<0.005	0.0508	0.0027	0.0856	0.0007	0.0072
HNO_3-Nb	0.0257	0.0121	0.0049	--	0.0542	--	0.0862	--	0.0111
H_2O-Nb	--	--	--	--	0.0064	--	0.0007	--	--

Table 4.2 Full scan analysis of the metal content and impurities present in parent Nb_2O_5-1, expressed in moles of impurity or contaminant per gram of Nb_2O_5-1. Metal extracted with 1 M HCl (HCl-Nb), 1 M HNO_3 (HNO_3-Nb) and 80 ˚C hot water (H_2O-Nb) respectively, and quantification from ICP-MS analysis.

Sample ID, mol	Nb	Al	As	B	Na	Ba	Ca	S	Si
HCl-Nb	$5.68\cdot10^{-7}$	$6.66\cdot10^{-7}$	$<1.33\cdot10^{-8}$	$3.33\cdot10^{-6}$	$1.72\cdot10^{-5}$	$9.44\cdot10^{-8}$	$1.01\cdot10^{-5}$	$3.58\cdot10^{-7}$	$2.10\cdot10^{-6}$
HNO_3-Nb	--	$2.69\cdot10^{-6}$	--	$1.39\cdot10^{-5}$	$3.17\cdot10^{-5}$	$1.33\cdot10^{-7}$	$1.16\cdot10^{-5}$	$9.00\cdot10^{-8}$	$4.19\cdot10^{-6}$
H_2O-Nb	$2.51\cdot10^{-9}$	--	--	$2.51\cdot10^{-6}$	$4.96\cdot10^{-6}$	$3.16\cdot10^{-9}$	$6.32\cdot10^{-8}$	$1.42\cdot10^{-7}$	$1.10\cdot10^{-6}$

Sample ID, mol	Cu	Fe	Sr	I	K	Ti	Mg	Mn	Zn
HCl	$1.99\cdot10^{-7}$	$1.01\cdot10^{-7}$	$5.37\cdot10^{-8}$	$<3.94\cdot10^{-8}$	$1.30\cdot10^{-8}$	$5.68\cdot10^{-8}$	$3.52\cdot10^{-6}$	$1.33\cdot10^{-8}$	$1.10\cdot10^{-7}$
HNO_3	$4.05\cdot10^{-7}$	$2.17\cdot10^{-7}$	$5.55\cdot10^{-8}$	--	$1.30\cdot10^{-6}$	--	$3.55\cdot10^{-6}$	--	$1.70\cdot10^{-7}$
H_2O-H_2O	--	--	--	--	$1.64\cdot10^{-7}$	--	$3.02\cdot10^{-8}$	--	--

Based on the different results when utilizing impurities extracted by various media for the tests, ICP-MS was used to identify and quantify the metal components of impurities in the filtrate, and the results are shown in table 4.1 and table 4.2. It is observed that the treatment by HCl is not actually extracting impurities but etching the Nb_2O_5 surface by generating a significant amount of Nb species (most likely short chain oligomers of Nb-O-Nb[46, 47], 0.053 mg in per gram of Nb_2O_5), while there is no evident trace of Nb species in other extracted liquid (so the conversion by them is almost none). In this context, we deduce that the Nb species is reactive for the oxidation of cyclooctane, but not the components (like Fe, Cu) in the parent Nb_2O_5. Furthermore, in order to confirm the effects of Fe^{3+} and Cu^{2+} on the oxidation, the dried liquid mixture of $FeCl_3$ and $CuCl_2$ solution with the equal amount of extracted solution by HCl (Table 4.1) was used for the tests, which indicated that there was no obvious conversion (1%).

Thus, we can arrive at the conclusion that the catalytic activity of filtrates extracted by HCl is the leached species of oligomers from Nb_2O_5, and it implies that this material might not be as resistant to hydrolysis as previously thought. In view of this, the stability of Nb_2O_5-1 was tested by the residues after treatment, by which the catalytic activity of Nb_2O_5-1 can be furtherly justified.

4.3.3 Catalytic activity of treated Nb_2O_5 in the oxidation

The last section reveals that there may exist active species only in the impurities extracted by 1 M HCl. In order to furtherly clarify the effects of Nb_2O_5 on the oxidation process, the residues of Nb_2O_5 after treatment were used for the reaction, the results of which shown in Fig. 4.3. The results indicate that the different treated Nb_2O_5 show close conversion with around 50%, which is practically identical with that before treatment (51±9%) when taken the error into account. And the products distribution is quite similar with major products cyclooctanone and hydroperoxides, unveiling that there are no obvious effects of treatment on Nb_2O_5 for the oxidation process. Furthermore, we recycled the Nb_2O_5 after reaction for four times and the material still exhibited a statistically meaningful conversion (35%) and similar products distribution with ketones and hydroperoxides as main products. According to the tests by using treated Nb_2O_5.

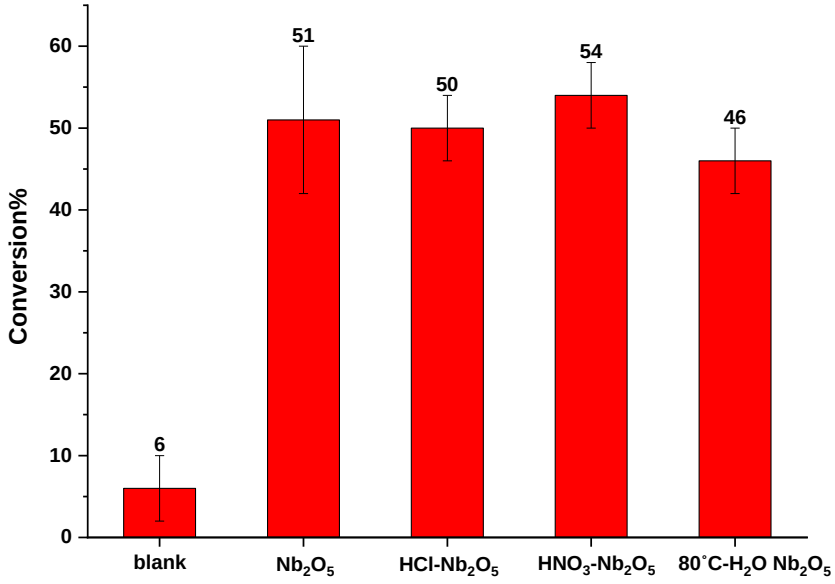

a. The conversion of cyclooctane by treated Nb_2O_5-1 at 2 bar O_2

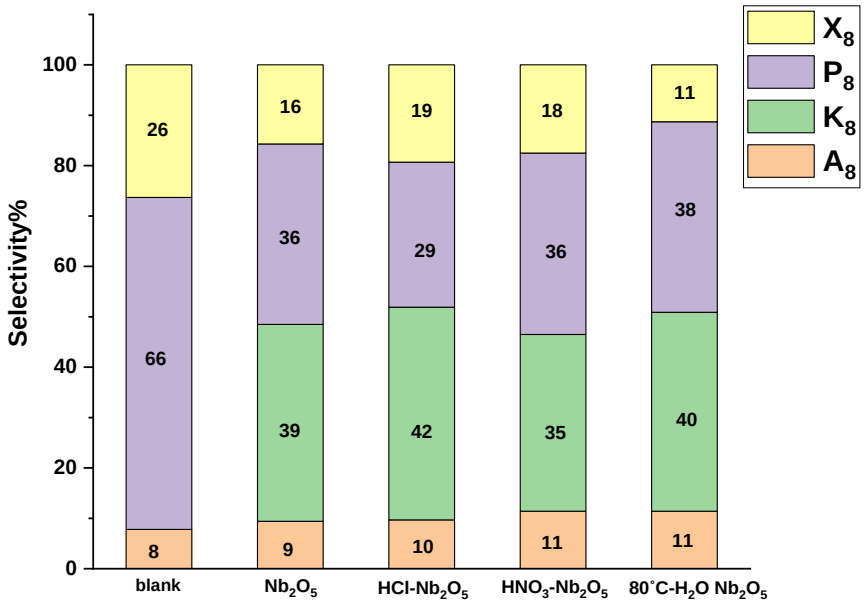

b. Product distribution of cyclooctane oxidation by treated Nb_2O_5-1 at 2 bar O_2

Fig. 4.3 Catalytic activity of Nb_2O_5-1 after treatment with hot filtration and acids in the oxidation of cyclooctane. a: Conversion of cyclooctane oxidation by residues of Nb_2O_5-1; b: Product distribution of cyclooctane oxidation by residues of Nb_2O_5-1. Reaction conditions: at 110 ˚C for 24 h at 2 bar O_2. HCl-Nb_2O_5: 1 g Nb_2O_5-1 was treated by 1 M HCl for 24 h at room temperature and the residue was recycled by H_2O washing. HCl-Nb_2O_5: 1 g Nb_2O_5-1 was treated by 1 M HNO_3 for 24h at room temperature and the residue was recycled by H_2O washing. 80˚C-H_2O Nb_2O_5: 1 g Nb_2O_5-1 was filtered by 80˚C-H_2O and the Nb_2O_5-1 residue was recycled.

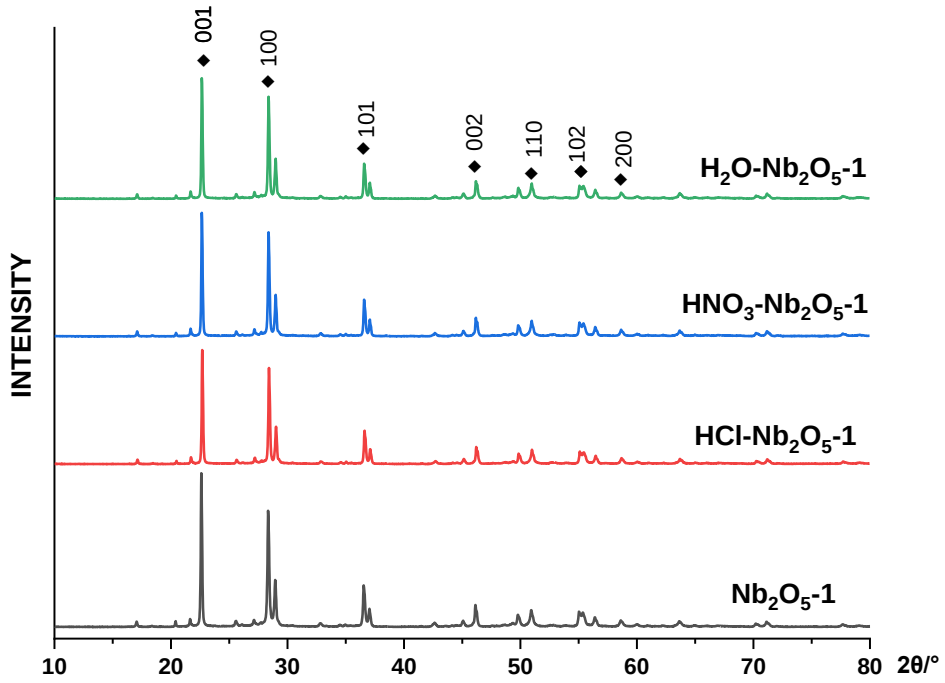

Fig. 4.4 The XRPD patterns[48, 49] of Nb_2O_5-1 residue after treatment by using different media. Nb_2O_5-1: untreated parent Nb_2O_5-1, the relative crystallinity is set as 100% for comparison; HCl-Nb_2O_5-1: Nb_2O_5-1 treated by 1 M HCl for 24 h at room temperature, the calculated relative crystallinity is 100%; HNO_3-Nb_2O_5-1: Nb_2O_5-1 treated by 1 M HNO_3 for 24 h at room temperature, the calculated relative crystallinity is 100%; H_2O-Nb_2O_5-1: Nb_2O_5-1 filtered by 80 ˚C H_2O, the calculated relative crystallinity is 102%. All the samples were dried at 100 ˚C overnight before analysis.

The XRPD patterns in Fig. 4.4 directly display the effects of treatment by different media on the crystal structure of Nb_2O_5-1. The results illustrate that there are no obvious changes of the structure while the intensity of peaks slight decreases after treatment. And the calculated relative crystallinity of the residues after treatment in comparison with untreated Nb_2O_5 indicates that the diluted acids have no observed destruction on the crystal structure of Nb_2O_5, which implies that the acids cannot herein attack the bulk structure of Nb_2O_5 while they may only etch the species on the surface.

Usually Nb_2O_5 is attacked by concentrated HF and dissolves in fused alkali[27]. And the trace of Nb species is observed in the extraction solution by HCl, which indicate that it may be etching of Nb on the surface due to the interaction between Cl^- and Nb, not the Nb species from the bulk structure. In summary, we can conclude that any effect induced by the acid treatments involves only the surfaces of the Nb species, but not their bulk structure and other impurities.

4.3.4 X-ray photoelectron spectroscopy of Nb_2O_5-1

Based on the above discussion, Nb_2O_5-1 is found to be active in the oxidation of cyclooctane. However, it should be noted that there may exist in different polymorphic phases of Nb_2O_5[28] and Nb^{4+} might exist due to the presence of oxygen vacancies in Nb_2O_5[50]. From this perspective, the possibility that Nb species in the oxidation state of NbO_2 is active cannot be ruled out. As XPS is widely used for the study about the oxidation of metal components on the surface[51], we employed this technique for furtherly investigation, results being shown in Fig. 4.5.

In our case, C 1s, O 1s and Nb 3d photoelectron peaks are represented. C 1s signals can be assigned to three components: C-C and C=C bonds at 284.6 eV, C-O groups at 286 eV; C=O and O-C=O groups at 288.2 eV.[43, 52, 53] The peak at ~530.3 eV is corresponding to Nb-O bond[54, 55], while the peak at around 531.5 eV is correlated to the presence of non-lattice oxygen[56], which can be as an implication that the presence of oxygen vacancies[54, 57]. Two observed peaks due to Nb $3d_{3/2}$ and $3d_{5/2}$ in Nb 3d at 210.2 eV and 207.5 eV[58-60] are assigned to the Nb^{5+} in Nb_2O_5, while no peaks assigned

to NbO_2 at 206.2 eV[58, 61] is observed. In this context, we can conclude that Nb species in Nb_2O_5-1 mainly exits in the state of Nb^{5+}, by which it justifies that Nb_2O_5 is active for the oxidation of cyclooctane in our case. In addition, there are two peaks at around 365. 6 eV and 380.9 eV respectively, both of which can be assigned to the Nb 3p 3/2 and 3p ½ in Nb_2O_5[62, 63], while it should be mentioned that these two peaks also can be attribute to the presence of iodine[62] in Nb_2O_5 (shown in table 4). In view of this, these two peaks should be excluded when discussing about the state of Ag species in supported Ag/Nb_2O_5 in the following chapter as Ag 3d is in this region.

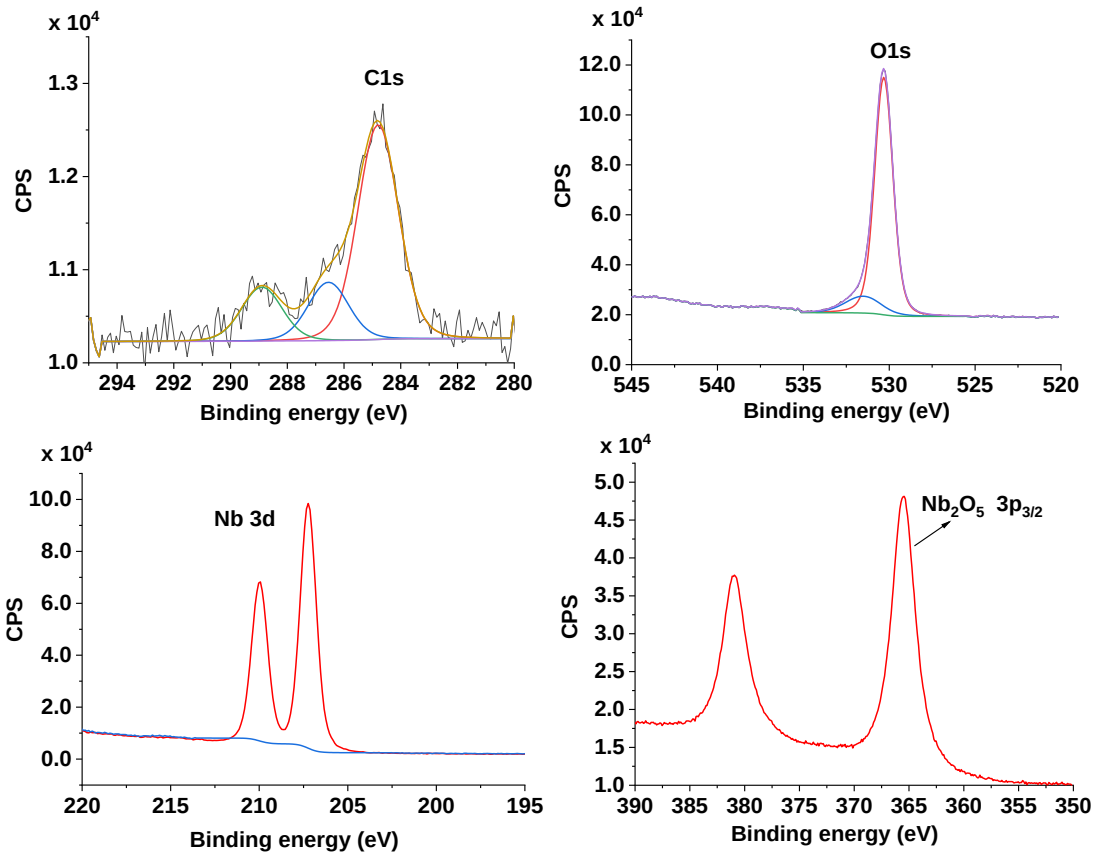

Fig. 4.5 XPS spectra and peak fitting of the C 1s, O 1s and Nb 3d region for Nb_2O_5-1. Two observed peaks in Nb 3d are due to Nb $3d_{3/2}$ and $3d_{5/2}$, both of which are assigned to the presence of Nb^{5+} in Nb_2O_5-1.

4.3.5 XRPD patterns of Nb_2O_5-1 after reaction

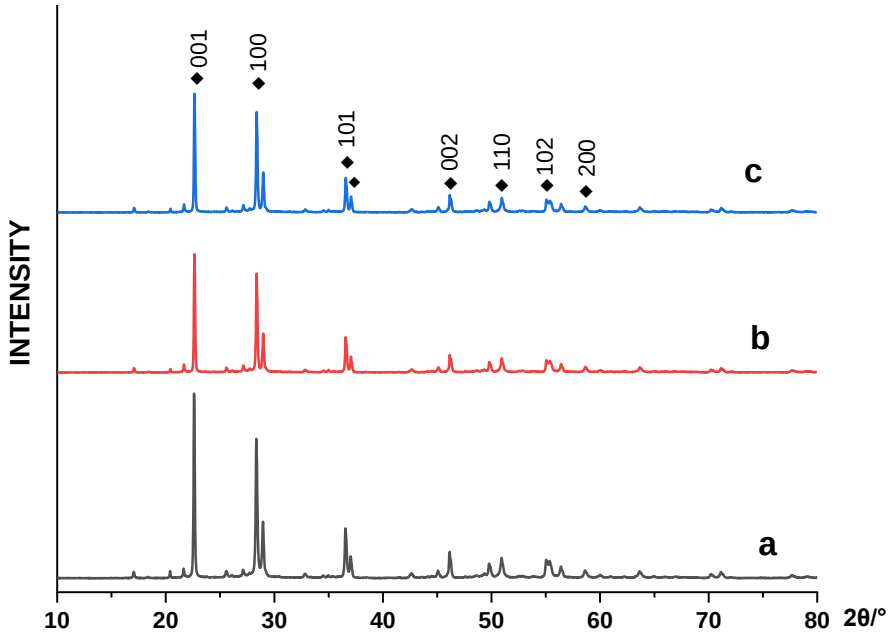

Fig. 4.6 The XRPD patterns of Nb_2O_5-1 after reation under both of 1 atm air and 2 bar O_2:(a) untreated Nb_2O_5-1, the relative crystallinity is set as 100% for comparison; (b) Nb_2O_5-1 after reaction at 1 atm air with condersor open to air, the calculated relative crystallinity is 96%; (c) Nb_2O_5-1 after reaction at 2 bar O_2, the calculated relative crystallinity is 97%. The tests were carried out at 110 ˚C for 24 h and the samples were recycled washed by using actone, followed by drying at 100 ˚C overnight for analysis.

In order to analyse the stability of Nb_2O_5 in the oxidation, XRPD patterns were collected for the analysis of the recyclyed metal oxides washed by using acetone to identify possible changes in the structure. The patterns in Fig.4.6 exhibit that there is no obvious shift of the characteristic peaks and changes of the crystal structure after reaction, while the intensity of peaks slightly decreases in comparison with that of before reaction, which is confirmed by the fact that the calculated relative crystallinity of b and c is 96% and 97% respectively in comparison with untreated Nb_2O_5. In addition,

although the conversin (50%) under 2 bar O_2 is higher comparing with that of under 1 atm air (16%) due to the diffusion effects of O_2, the intensity of peaks of both is identical, indicating that the Nb_2O_5 still keeps the crystal structure after reaction.

4.3.6 Effect of visible light on the catalytic activity of Nb_2O_5 with different crystal structures

It is reported that many metal oxides that exhibits a different reactivity as a function of their crystallographic phase[64-66]. In view of this, we considered the investigation of Nb_2O_5 with different crystallographic forms for the furtherly clarification of catalytic reactivity of Nb_2O_5 in the oxidation. As described in chapter 1, Nb_2O_5 may exist in different polymorphic phases of Nb_2O_5, i.e., TT(pseudohexagonal)-, T(orthorhombic)-, B(monoclinic)-, M(tetragonal)-, H(monoclinic)-Nb_2O_5[28, 41], (see section 1.3.1 of chapter 1). A different crystallographic structure may result in a different atom packing, also for the surface that is delimiting the solid, and in turn exhibiting a different reactivity.

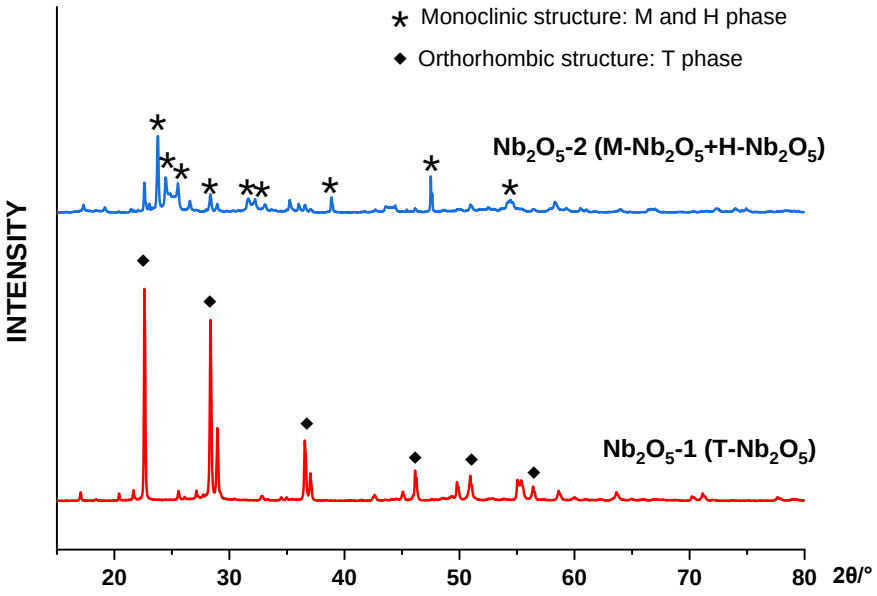

Fig. 4.7 XRPD patterns of Nb_2O_5 with different crystallographic forms. Nb_2O_5-1 with purity of 99.9% and Nb_2O_5-2 with purity of 99.99%. It unveils that these two batch of Nb_2O_5 have different polymorphisms, which may account for the effects of visible light on the oxidation of cyclooctane.

In our case the material so far denoted as Nb_2O_5-1 is an orthorhombic structure T-phase[67], whereas Nb_2O_5-2 is a combination of monoclinic structure (M and H phases) and orthorhombic structure[67], as evidence from XRPD pattens in Fig. 4.7. The presence of mixed phases should not be surprising. In fact, Nb_2O_5 is rather difficult to study as the exact conditions to obtain a specific phase strongly depends on crystallization temperature, impurities of the starting materials, rate and time of heating, and interactions with other components (e.g., supports)[7, 67]. Incidentally it should also be noted that Nb_2O_5-2 has a degree of purity of 99.99% (probably a consequence of the preparation process, and to obtain this phase a temperature higher than 800 °C is needed). However, given the various control tests that we have done for Nb_2O_5-1, we deem the same considerations to apply for Nb_2O_5-2 and therefore the activity to be due to the metal oxide and not to any of the impurities.

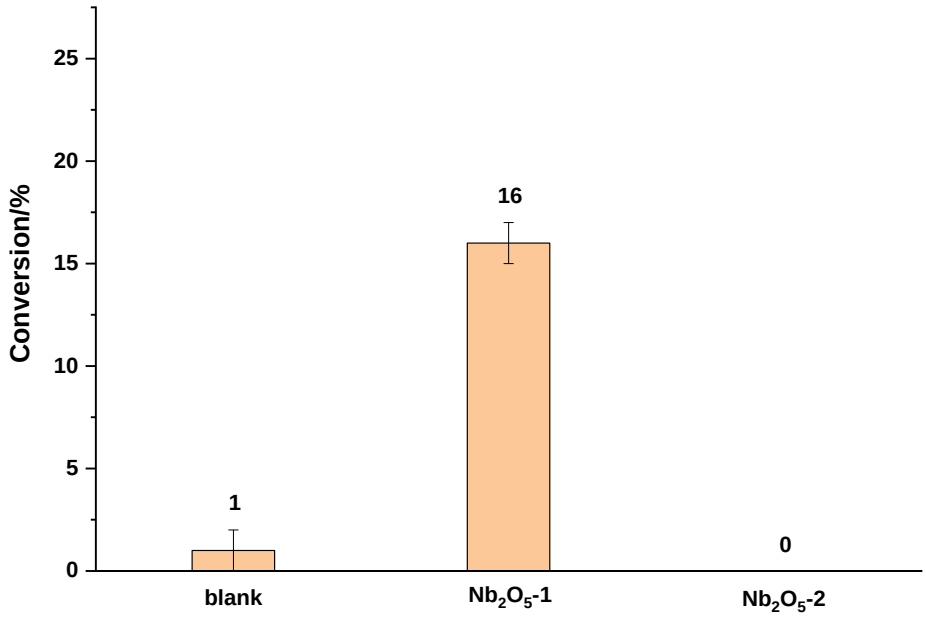

Fig. 4.8 Catalytic reactivity of Nb_2O_5-1 and Nb_2O_5-2 in cyclooctane oxidation. All the tests were carried out at T = 110 ˚C for 24 h at 1 bar atmospheric air with condenser, and M(Nb):S ratio was 1:12. 3 mL of cyclooctane was used.

Very interesting results were obtained, as shown in Fig. 4.8. If a standard test was carried out by using Nb_2O_5-1 (the orthorhombic phase) and the Nb_2O_5-2 (the monoclinic phase), Nb_2O_5-2 doesn't display any catalytic activity, while 16% conversion of cyclooctane is observed with Nb_2O_5-1. This shows then that there is a crystallographic phase dependency for our activity (and further reinforce the activity is not due to Nb-O-Nb species in solution). Similarly, the catalytic activity of MnO_2 in propane oxidation is influenced by the crystal phases of MnO_2[68]. This, however, prompted us to consider experiments by using pressurized O_2 and the effect of a presence and absence of light. Nb_2O_5 is a semiconductor with a band gap of 3.5 eV[50] (for comparison TiO_2 has a band gap of 3.2 eV), and in principle it could be used as a photo catalyst under UV illumination. And there are studies illustrating that Nb_2O_5 is

applied in the oxidation of alcohols under visible light irradiation[69, 70]. Therefore, in view of these aspects, further tests with or without exposure to visible light irradiation at pressurised O_2 were carried out respectively.

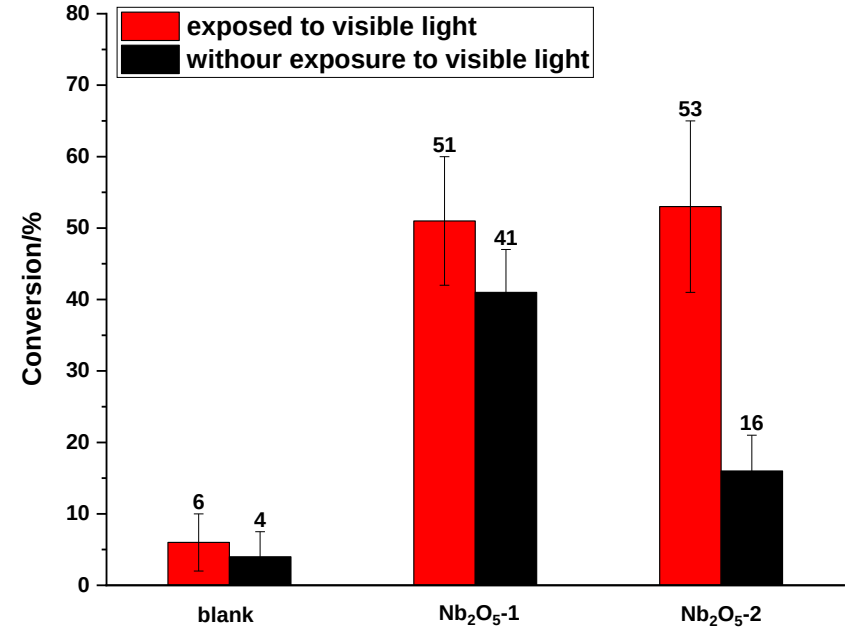

a. Conversion of cyclooctane by Nb_2O_5 with or withoust visible irradiation

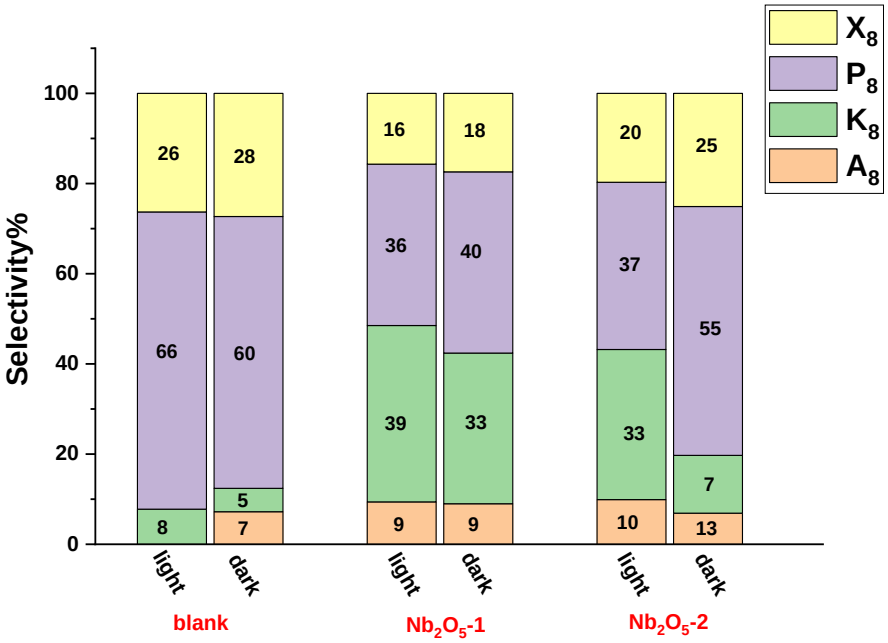

b. Product distribution in cyclooctane oxidation with or without visible light irradation

Fig. 4.9 Catalytic activity of Nb_2O_5 in cyclooctane oxidation under visible light irradiation or without exposure to visible light. Nb_2O_5-1 with purity/grade of 99.9% and Nb_2O_5-2 with

purity/grade of 99.99%. a. Conversion of cyclooctane by two batches of Nb_2O_5 with irradiation of visible light; b. Product distribution of cyclooctane by two batches of Nb_2O_5 with irradiation of visible light. All the tests were carried out at T=110 ˚C for 24 h at 2 bar O_2 with the M(Nb):S ratio was 1:12.

At 2 bar of O_2, both Nb_2O_5-1 and -2 show a similar activity. However, if in the darkness, Nb_2O_5-1 has a decrease in catalytic activity 51% to 41%, although still compatible with the experiment under visible light irradiation if accounting for the experimental error. Whereas Nb_2O_5-2 is strongly dependent on the reaction conditions, with its activity dropping by more than 70% if the oxidation reaction is carried out in darkness. The product distribution by Nb_2O_5-2 is also different, which indicates a trend to produce more cyclooctanone (33%) in the presence of light with a higher K/A ratio of 3.3, compared to a K/A ratio 0.6 in the darkness. Thus, based on the comparison between the performances of these 2 batches of Nb_2O_5, it seems that the crystallographic phase and the irradiation of visible light influence the C-H activation process or the transformation of intermediates as the conversion and selectivity are different, especially the conversion.

To further test this hypothesis, the oxidation of cyclooctane was carried out at 80 °C and 2 bar of O_2. In fact, according to tests carried out in our lab, at this temperature, the oxidation doesn’t take place in the absence of a catalyst which is activated thermally. Under these reaction conditions, nor Nb_2O_5-1 or Nb_2O_5-2 is capable of inducing any activity, which directly implies that none of these materials is able to initiate the reaction (nor thermally nor photochemically). On the other hand, as

these materials are capable to alter both the conversion and the selectivity in a different manner at 110 °C and being light dependent, we speculate they are able to react with the intermediate cyclohexyl hydroperoxide. In fact, a higher consumption of this intermediate would also promote the conversion.

Therefore, based on the present data we have collected, it is postulated that Nb_2O_5 takes part in the decomposition of the intermediate cyclooctyl hydroperoxide to cyclooctanone, and the presence of light enhances this process (and as such this would not be a typical photocatalytic process, in the sense of conversion enhanced by visible light radiation), especially for Nb_2O_5-2, although this may play a role in the selectivity. And this assumption will be studied furtherly by conducting the decomposition of a specific hydroperoxide (1-phenylethyl hydroperoxide) in the presence of Nb_2O_5 directly, which is discussed in chapter 5 in detail.

4.4 Catalytic activity of Nb_2O_5 for other hydrocarbons: cyclohexane, ethylbenzene, *n*-decane

Moreover, in order to furtherly investigate the roles of Nb_2O_5 for the oxidation of hydrocarbons as well as to assess the possibility that it acts as a support for metal nanoparticles, other hydrocarbons have been used as a substrate for catalytic tests as means of comparison. The results are summarised in table 4.3.

Table 4.3 The oxidation of ethylbenzene (EB), *n*-decane, cyclohexane(CyH) by Nb_2O_5 at 1 atm air and pressurised O_2 respectively. Nb_2O_5-1: 99.9% purity, Nb_2O_5-2: 99.99% purity. K-ketones, A-alcohols, P-alkyl hydroperoxides.

Catalyst	Substrates	Reaction conditions	Conversion/%	Selectivity/%			
				K	A	P	by-products
Tests series at an atmospheric air pressure with condenser open to air							
Blank	EB	130 °C for 24h	20	41	21	31	7
Nb_2O_5-1			1	50	27	7	16
Nb_2O_5-2			0	--	--	--	--
Blank	*n*-decane	115 °C for 24h	0	--	--	--	--
Nb_2O_5-1			6	52	42	--	7
Nb_2O_5-2			6	51	42	--	7
Tests series using a pressurized system							
Blank	EB	130 °C for 24h at 2 bar O_2	33	51	20	12	17
Nb_2O_5-1			1	25	0	0	75
Nb_2O_5-2			0	--	--	--	--
Blank	*n*-decane	115 °C for 24h at 1 bar O_2	0	--	--	--	--
Nb_2O_5-1			3	50	42	--	8
Nb_2O_5-2			2	45	46	--	9
Blank	CyH	120 °C for 24h at 4 bar O_2	0.7	0	68	32	0
Nb_2O_5-1			0.9	0	79	5	16
Nb_2O_5-2			0	--	--	--	--

The above results illustrate that both of two types of Nb_2O_5 act as inhibitor, and not just as an inert species, for the oxidation of ethylbenzene in comparison with blank autoxidation. This further reinforces that Nb_2O_5 (regardless the crystal structure) is not able to initiate the reaction, but also to have such an inhibitor role, and it may also quench alkyl peroxide species that would be the chain carrier of the reaction. The latter could be explained by the presence of oxygen vacancies that could trap peroxide

species[24, 71] or a site blocking of the substrate by adsorption to the catalytic surface and as such precluding any catalytic activity[72, 73]. In addition, Nb_2O_5 displays similar behaviours with that in cyclooctane oxidation by enhancing the reaction to an extent. Furtherly, Nb_2O_5 is employed for the oxidation of cyclohexane. There is no obvious conversion of blank autoxidation and in the presences of two species of Nb_2O_5, which implies that in this case Nb_2O_5 is inert or inhibiting this reaction and we assume that the metal oxide might involve in the decomposition of alkyl hydroperoxides according to the above discussion, which will be discussed in detail in chapter 5.

Based on the above results it is evident that it is not possible to provide straightforward 'predictions' for the reactivity of Nb_2O_5 for the reactivity of a substrate with respect to another. It should be noted that the different reaction performances of Nb_2O_5 in the oxidation of cyclooctane, cyclohexane and ethylbenzene is not reasonable, as it seems that Nb_2O_5 enhances the oxidation of cyclooctane directly while inhibits ethylbenzene oxidation. Since that it is confirmed that there is no existence of alkyl hydroperoxides in parent cyclooctane, we deduce that the reactivity of Nb_2O_5 in the oxidation of cyclooctane can be related with the bond dissociation energy (BDE) of C-H bond. As shown in table 4.4, BDE of C-H in cyclohexane is the highest (418 kJl·mol^{-1}) while it is 397 kJ·mol^{-1} in cyclooctane, which may explain the inert performances of Nb_2O_5 in the oxidation of cyclohexane and the enhancement behaviours in the oxidation of cyclooctane. On the other hand, it is postulated that there might already exist trace of other components in the parent cyclooctane, such as

hydroperoxides species or water that could affect the reaction. In view of this, a series of tests to investigate about the effects of possible trace of these species from parent cyclooctane were carried out, as discussed in the next section.

Table 4.4 The bond dissociation energy (BDE) of C-H bond in various hydrocarbons.

Substrates	Formula	BDE of C-H kcal·mol^{-1}	BDE of C-H kJ·mol^{-1}	Reference
Cyclooctane	C_8H_{15}-**H**	92	385	[42]
Cyclohexane	C_6H_{11}-**H**	99	414	[42]
Ethylbenzene	C_6H_5-C**H**$_2$-CH_3	85	356	[42]
n-Decane	$C_{10}H_{21}$-**H**	94	393	[74]

4.5 Tests about the analysis of 'impurities' in parent cyclooctane

According to the above discussion, it is found Nb_2O_5 exhibits different reaction performances in the oxidation of various substrates (cyclooctane, cyclohexane, ethylbenzene, *n*-decane) by enhancing or inhibiting the process. The mechanism of autoxidation in section 4.2 illustrates that the newly formed alkyl hydroperoxides is an essential intermediate to be transferred into alcohols or ketones, which can work as the initiator for the cleavage of C-H of hydrocarbons. In order to confirm that whether there may exist alkyl hydroperoxides or not, the tests about the impurities, mainly trace of alkyl hydro peroxides and water, which are often present in any hydrocarbon were carried out to confirm the effects of other possible species on the reaction. Parent cyclooctane was treated with $MgSO_4$ and 3A molecular sieve to remove alkyl hydroperoxides and water respectively[75-78], and then catalytic tests were conducted in the presence of Nb_2O_5. In addition, as discussed in section 4.1, CeO_2, TiO_2 and MgO

have been widely studied as support for metal nanoparticles in the oxidation of hydrocarbons due to their physical chemistry properties like thermal stability, high surface area and oxygen storage abilities. Herein, these metal oxides were also applied for the oxidation of cyclooctane pretreated by $MgSO_4$ and 3A molecular zeolites.

4.5.1 The reaction performances of various metal oxides in the oxidation of treated cyclooctane

Fig. 4.10 shows that the blank tests in the absence of metal oxides reveals that the conversion of cyclooctane treated by $MgSO_4$ (2 mol%) and 3A (2 mol%) molecular zoolites are identical. In addition, when using TiO_2, MgO and CeO_2 for the oxidation of cyclooctane respectively, the reaction results are also identical before and after the treatment by $MgSO_4$ and 3A zeolite. In comparison, Nb_2O_5 also exerts similar reaction behaviours in the oxidation process. In this context, it is concluded that no trace of alkyl hydroperoxides or water that affect the oxidation process in the parent cyclooctane. Accordingly, we furtherly confirm that the reactivity of Nb_2O_5 in cyclooctane oxidation, and its role is to enhance the decomposition of alkyl hydroperoxides rather than initiate the oxidation by breaking the C-H directly.

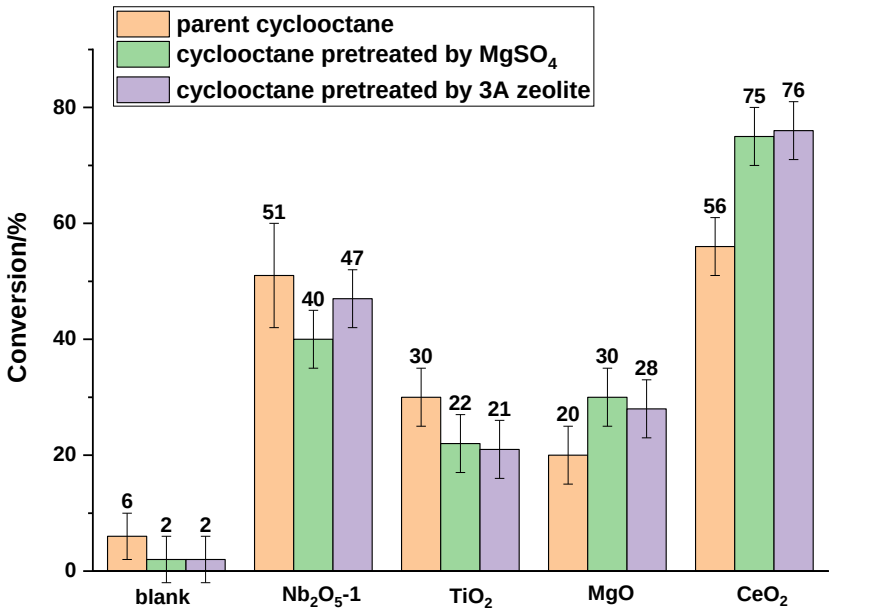

a. Conversion of the pretreated cyclooctane oxidation by metal oxides

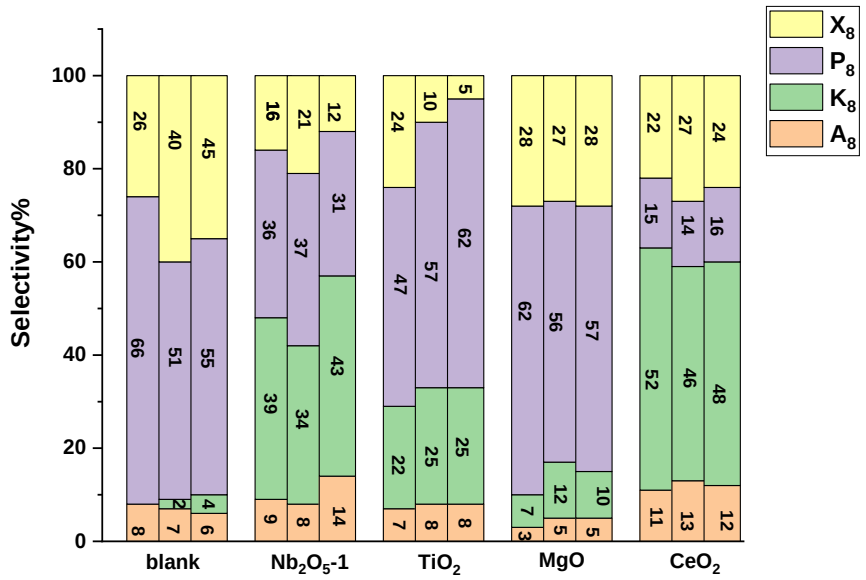

b. Product distribution of pretreated cyclooctane oxidation by metal oxides

Fig. 4.10 Catalytic activity of various metal oxides in cyclooctane oxidation (Sigma Aldrich) pretreated by $MgSO_4$ and 3A molecualr sieve respectivtly. a. Conversion of pretreated cyclooctane by various metal oxides; b. Product distribution of pretreated cyclooctane oxidation by various metal oxides. The tests were conduted at 2 bar O_2 at 110˚C for 24 h and 3mL cyclooctane was used for the reaction with a fixed M:S ratio 1:12. Parent cyclooctane was mixed with dried $MgSO_4$ and 3A molecular sieve and then carried out the oxidation in the presence of metal oxides (process is decribed in section 2.3.7 of chapter 2).

4.5.2 The reaction performances of Nb_2O_5 in the oxidation of ethylbenzene and cyclohexane with the initiator *tert*-butyl hydroperoxide (TBHP)

In view of the inhibiting effects of Nb_2O_5 in the oxidation of ethylbenzene and inert behaviours in the oxidation of cyclohexane, further tests were carried out by adding an initiator *tert*-butyl hydroperoxide (TBHP) for the investigation about mechanism of Nb_2O_5 in the oxidation process. The effect of TBHP on oxidation and its decomposition process are described in section 7.2.2 of chapter 7 in detail.

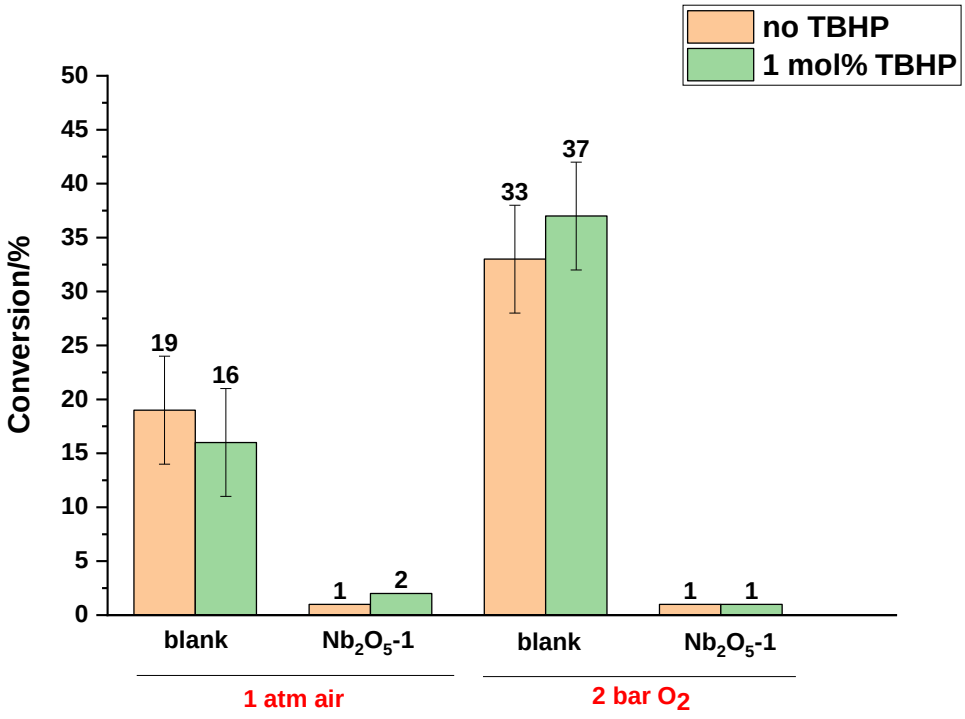

Fig. 4.11 Ethylbenzene oxidation by Nb_2O_5-1 in the presenc of *tert*-butyl hydroperoxide (TBHP). The tests were conduted at 130 ˚C for 24 h under atmospheric air with condenser open to the air and 2 bar pressurised O_2 respectively with a M(Nb):S ratio 1:12. The concentration of TBHP in reaction mixture was 1 mol%.

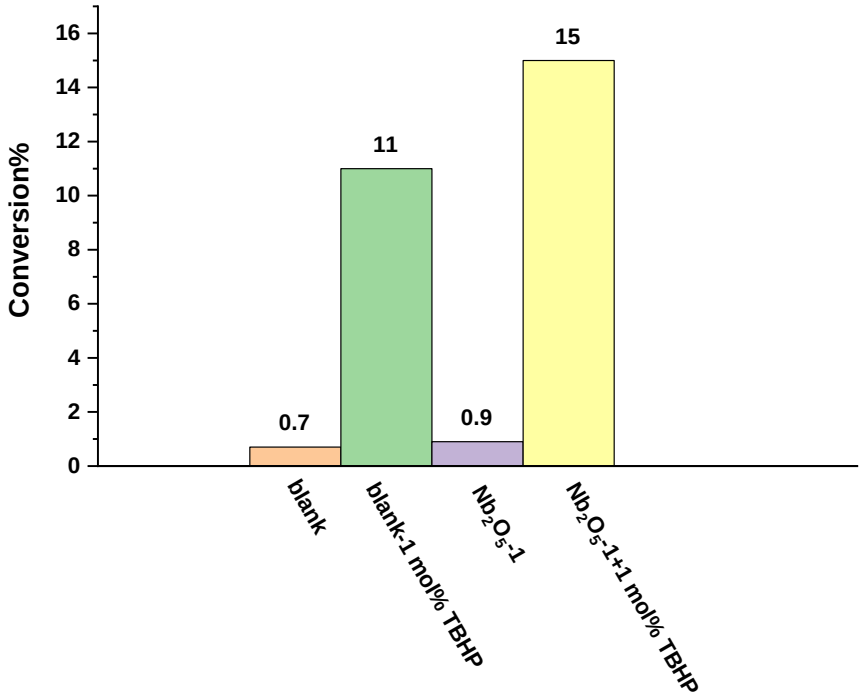

Fig. 4.12 Cyclohexane oxidation by Nb_2O_5-1 in the presenc of tert-butyl hydroperoxide (TBHP). The tests were conduted at 120 ˚C for 24 h at 4 bar pressurised O_2 with M(Nb):S ratio 1:12. The concentration of TBHP in reaction mixture was 1 mol%.

The results indicated that even in the presence of TBHP, Nb_2O_5 still works as the inhibitor (approximately 1% under both 1 atm air and 2 bar O_2) in the oxidation of ethylbenzene in comparison with blank tests (16% at 1 atm air and 37% at 2 bar O_2). In this case, Nb_2O_5 obviously inhibits the oxidation of ethylbenzene even in the presence of TBHP. However, at present it is not clear how it stops the proceeding of this oxidation. It is deduced that the competing absorbance of C-H on the surface of Nb_2O_5, which makes it unrealizable to break under thermal decomposition. In addition, it is found the conversion of cyclohexane is evidently enhanced in the presence of TBHP, which can be up to 10% in the blank tests and 15% by Nb_2O_5, which justifies that trace of hydroperoxides species can initiate the oxidation obviously. As we have

confirmed that there is no trace of alkyl hydroperoxides in parent cyclooctane in section 4.5.1, the results furtherly prove that the observed reactivity of Nb_2O_5 in cyclooctane oxidation is attributed to the lower BDE of C-H bond in cyclooctane.

4.6 Comparison of catalytic activity among various metal oxides (CeO_2, MgO, TiO_2, SiO_2, Nb_2O_5) in cyclooctane and cyclohexane oxidation

According to the discussion carried out so far, and in order to assess if the catalytic behaviours that we observed for Nb_2O_5 is unique for this material or not, we tested an array of metal oxides: CeO_2, MgO, TiO_2 and SiO_2. The above discussion about the performances of Nb_2O_5 in the oxidation of different hydrocarbons implies that Nb_2O_5 can enhance the decomposition of hydroperoxides, especially in the oxidation of cyclooctane. However, it inhibits the oxidation of ethylbenzene, which may be related to a site blocking effect between the substrate molecules and O_2 or radicals quenching effect. The different properties of Nb_2O_5 to the various hydrocarbons cannot be fully elucidated at present, and this prompted us to investigate the effects of CeO_2, MgO, TiO_2 and SiO_2 and restricting them for the oxidation of cyclooctane and cyclohexane as the most relevant substrates for this thesis work.

CeO_2 is a metal oxide known to be used for oxidation reactions (e.g., methane, cyclohexane)[79-81], MgO used for cyclohexane oxidation[82], and TiO_2 is applied in the oxidation of cyclohexane or alcohols[83, 84] as well as SiO_2 is used in the oxidation of cyclohexane and ethylbenzene[19, 85]. All of these are also widely used as support for metal nanoparticles. In view of this we should also anticipate that we don't expect all

of these metal oxides to be active (and if at all) but this is precisely one of the scopes of these control tests, that is to have species like MgO and SiO_2 that are not expected to show activity and as such to validate the activity of Nb_2O_5.

4.6.1 Different metal oxides with various M:S ratios for cyclooctane oxidation

The results are summarised in Fig. 4.13, by investigating different M:S ratios. The conversion of blank autoxidation is around 6% and it can be seen there is no obvious conversion in the presence of MgO and SiO_2, unveiling that both of two metal oxides are inert for the oxidation, but Nb_2O_5, TiO_2 and CeO_2 all exhibit reactivity for the oxidation. Nb_2O_5 and CeO_2 display similar trend with the changes of M:S ratio by sharing high conversion, while Nb_2O_5 shows more stable performances with conversion 38% when the M:S ratio is down to 1:1000 but in comparison it is 13% by CeO_2 under the same M:S ratio. In addition, the products distribution demonstrates that the selectivity for ketone decreases and for hydroperoxides increases with the changes of M:S ratios from 1:10 to 1:1000 in the presence of Nb_2O_5 (Fig. 4.13-b), indicating that Nb_2O_5 can participate in the transformation of hydroperoxides to ketones or alcohols, which also can be observed in the presence of CeO_2. CeO_2 as a covalent oxide, serves as a widely used support material to improve mechanical and thermal stability as well as activity and selectivity of catalysts. This widespread applicability mainly originates from the outstanding oxygen storage capacity which is related with the ease in forming and repairing oxygen vacancies at the surface of solid ceria[23]. And there is research involving about the decomposition hydroperoxides and oxidation of

alkanes over CeO_2 nanoparticles, which unravels that the transformation of hydroperoxides can occur on certain facet (111) surfaces[79]. According to the similar behaviours between Nb_2O_5 and CeO_2, so we propose that Nb_2O_5 may affect the reaction in the same way to an extent. Besides, TiO_2 is usually chemically inert under normal conditions or activated in the photo oxidation process. However, it is found that TiO_2 is reactive in the oxidation with conversion up to 62% when M:S ratio is 1:100. And it should be noted that the products distribution is different from that of Nb_2O_5 and CeO_2 although these three metal oxides all share high conversion, which indicates that the main product is hydroperoxides without changing with M:S ratio. From this perspective, TiO_2 cannot facilitate the decomposition of cyclooctyl hydroperoxide like Nb_2O_5. Incidentally, it should also be noted that the trend broadly follows a kinetic control, in the sense that the lower is the M:S ratio (that is the lower is the amount of catalyst with respect to the amount of substrate) the activity is decreasing. As such these data are not affected by external diffusion or mass transfer limitation.

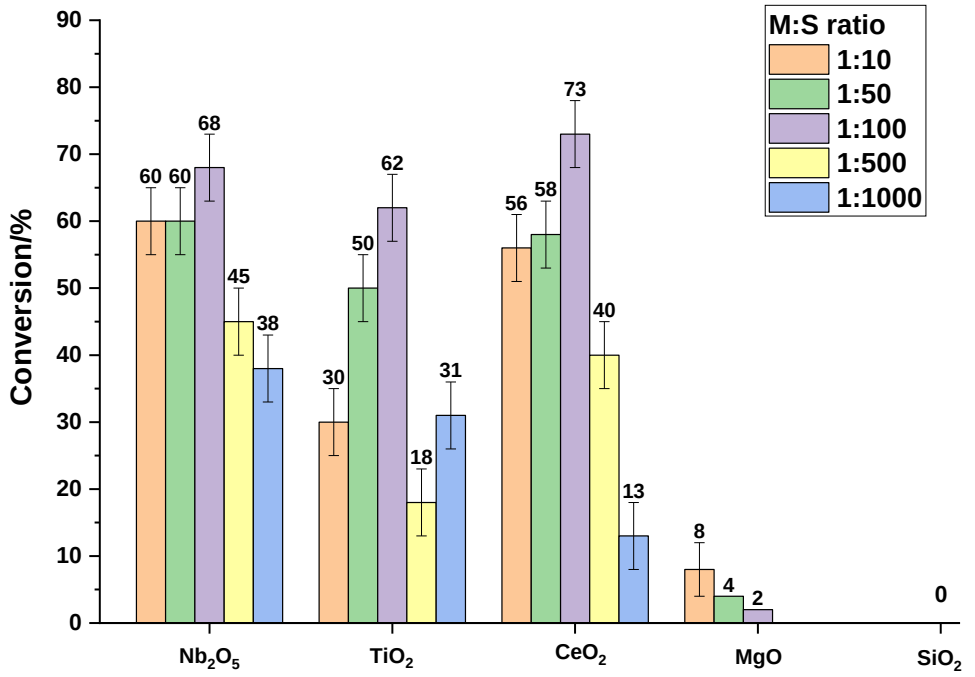

a. Conversion of cyclooctane by different metal oxides

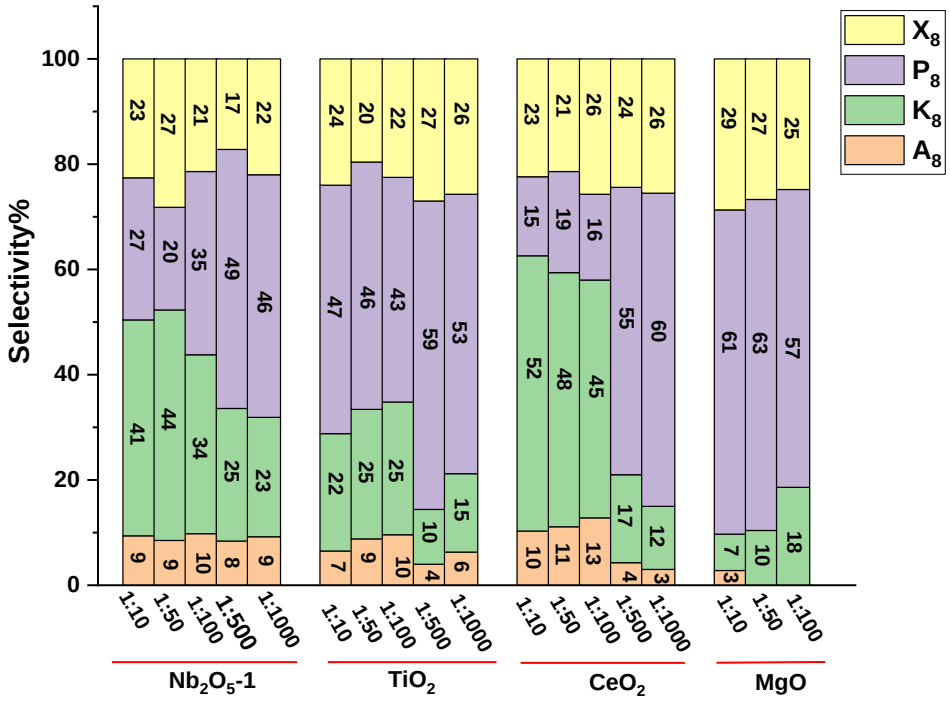

b. Product distribution of cyclooctane oxidation by different metal oxides

Fig. 4.13 Catalytic activity of different metal oxides with various M:S ratios in the oxidarion of cyclooctane. a: Conversion of cyclooctane oxidation with various metal oxides; b. Product distribution of cyclooctane oxidation with various metal oxides. The tests were conduted at 2 bar O_2 at 110˚C for 24 h and 3 mL of cyclooctane was used in each test.

Based on the above discussion, both of Nb_2O_5 and CeO_2 demonstrate similar behaviours for the reaction with the changes of M:S ratios, both of which can enhance the oxidation obviously and the selectivity for hydroperoxides increases when the M:S ratio changes from 1:1000 to 1:10 gradually and the major product is ketones when the ratio is higher than 1:50, indicating that both of them affect the reaction in a similar way to enhance the decomposition of hydroperoxides to produce more ketones. Besides, it is found that TiO_2 also display evident activity, but the dominating product is always hydroperoxides, which is different from the performances of Nb_2O_5. Therefore, according to the discussion about the application of various metal oxides, it seems that Nb_2O_5 and CeO_2 can be appropriate as the support for the oxidation of hydrocarbons because they tend to facilitate the production of ketones, posing a potential as a support for metal nanoparticles (in our case, supported Ag/Nb_2O_5 would be investigated for next chapter). Meanwhile, as Nb_2O_5 is rarely used as a support for the preparation of heterogeneous catalysts that are aimed for hydrocarbons oxidation, thus we will mainly focus on the study about using Nb_2O_5 as the support in our thesis.

4.6.2 The performances in cyclohexane oxidation on fixed M:S ratio

In last section, it is found that there are different performances when using metals oxides for the oxidation of cyclooctane. In comparison, this part uses these metal oxides in the oxidation of cyclohexane at a fixed M:S ratio to furtherly elucidate the roles of them in the oxidation process. The results are shown in table 4.5, which indicates that Nb_2O_5 and CeO_2 are inert in this reaction while they both display high

reactivity in the oxidation of cyclooctane. We deduce that this may be related with the C-H bond dissociation energy as it may be higher in the cyclohexane than that of cyclooctane, causing the initiating process for the formation of hydroperoxides hard to proceed. And at present we postulate that the roles of Nb_2O_5 is to enhance the decomposition of hydroperoxides rather than initiate the reaction. Thus, the propagation process cannot proceed furtherly as there is no formed alkyl radicals.

Table 4.5 Cyclohexane oxidation by various metal oxides. 3 mL cyclohexane was used in the tests and tests were conducted at actual 120°C for 24 h at 4 bar O_2.

Catalyst	M:S	Conversion%	Selectivity%				K/A
			K	A	P	by products	
blank	--	0	0	0	0	0	--
Nb_2O_5-1	1:12	0	0	0	0	0	--
Nb_2O_5-2	1:12	0	0	0	0	0	--
CeO_2	1:12	0	0	0	0	0	--
MgO	1:12	0	0	0	0	0	--
TiO_2	1:12	0	0	0	0	0	--
SiO_2	1:12	0	0	0	0	0	--
Iron (III) acetylacetonate	1:100	8%	45	27	1	27	2

4.7 Conclusion

A study about the reaction performances of various metal oxides on the hydrocarbons was conducted, especially focusing on Nb_2O_5. As it is observed that Nb_2O_5 exhibits unexpected performances in the oxidation of cyclooctane, a systematic study on the nature and the effects of the Nb_2O_5 on the reaction is carried out. Results indicate that the enhanced conversion is observed with the presence of the filtrate extracted by diluted HCl (1 M), and ICP-MS analysis for the components of filtrates

extracted by various media (HCl, HNO_3, hot water) shows that Nb is only observed in the filtrate from HCl treatment. Combing the XRPD patterns that display the crystal structure of Nb_2O_5 is retained after the treatment by different media, this correlation implies that HCl etches the Nb_2O_5 surface by generating a significant amount of Nb species (most likely short chain oligomers of Nb-O-Nb[46, 47]) that is responsible for the reactivity. Furtherly, as the hydroperoxides species can work as the initiator in the reaction, thus the tests about the analysis of impurities in cyclooctane indicates that there is no trace of alkyl hydroperoxide or water species that affect the reaction. Therefore, it is justified that the observed reactivity of Nb_2O_5 in cyclooctane oxidation is not due to the other impurities in substrate, which furtherly justifies the reactivity of Nb_2O_5 in this oxidation process. And the XPS results also confirm that Nb element in Nb_2O_5 exists in the state of Nb^{5+} instead of Nb^{4+}, implying the reactivity is from Nb_2O_5. In addition, based on the comparison between the reaction performances of these 2 batches of Nb_2O_5 (Nb_2O_5-1 with 99.9% purity and Nb_2O_5-2 with 99.99% purity), it seems that the crystallographic phase and the irradiation of visible light could affect the transformation process of intermediates cyclooctyl hydroperoxide. We speculate that the role of Nb_2O_5 is to enhance the decomposition of alkyl hydroperoxides rather than initiate the oxidation by breaking the C-H directly.

In addition, Nb_2O_5 shows different reaction behaviours when using for other hydrocarbons oxidation. It inhibits the oxidation of ethylbenzene in comparison with blank autoxidation while it is inert for cyclohexane oxidation, and the conversion of *n*-

decane is also enhanced. At present, we deduce that this might be related to bond dissociation energy (BDE) of C-H bond, higher activation energy leading to the formation of hydroperoxides hard to proceed. While the inhibiting effect on ethylbenzene oxidation is possibly related with the presence of oxygen vacancies that could trap peroxide species[24, 71] or a site blocking of the substrate by adsorption to the catalytic surface and as such precluding any catalytic activity[72, 73]. Moreover, various metal oxides with different M:S ratios are employed for the oxidation of cyclooctane, indicating that Nb_2O_5 and CeO_2 shares similar behaviours to enhance the oxidation obviously with preferences for the decomposition of hydroperoxides. Based on all the results, it demonstrates a promising prospect for the use of bulk Nb_2O_5 in the oxidation of hydrocarbons for the production of ketones, which will be explored in the next chapter.

4.8 References

1. G. A. Olah, Á. Molnár and G. S. Prakash, *Hydrocarbon Chemistry, 2 Volume Set*, John Wiley & Sons, 2017, p 593-595.
2. S. J. Blanksby and G. B. Ellison, *Acc. Chem. Res.*, 2003, **36**, 255-263.
3. R. H. Crabtree, *Chem. Rev.*, 1995, **95**, 987-1007.
4. F. Cavani, *Catal. Today*, 2010, **157**, 8-15.
5. G. Centi, F. Cavani and F. Trifirò, *Selective oxidation by heterogeneous catalysis*, Springer Science & Business Media, 2012, p 1-4, .

6. R. Liu, H. Huang, H. Li, Y. Liu, J. Zhong, Y. Li, S. Zhang and Z. Kang, *Acs Catal.*, 2014, **4**, 328-336.

7. B. R. Cuenya, *Thin Solid Films*, 2010, **518**, 3127-3150.

8. J. R. Croy, S. Mostafa, H. Heinrich and B. R. Cuenya, *Catal. Lett.*, 2009, **131**, 21-32.

9. J. Zhang, Y. Li, Y. Zhang, M. Chen, L. Wang, C. Zhang and H. He, *Sci. Rep.*, 2015, **5**, 1-10.

10. J.-W. Jun, Y.-W. Suh, D. J. Suh and Y.-K. Lee, *Catal. Today*, 2018, **302**, 108-114.

11. S. Wu, Y. Yang, C. Lu, Y. Ma, S. Yuan and G. Qian, *Eur. J. Inorg. Chem.*, 2018, **2018**, 2944-2951.

12. E. Pakrieva, E. Kolobova, D. German, M. Stucchi, A. Villa, L. Prati, S. Carabineiro, N. Bogdanchikova, V. Cortés Corberán and A. Pestryakov, *Process.* , 2020, **8**, 1016.

13. C. Mateos-Pedrero, H. Silva, D. A. P. Tanaka, S. Liguori, A. Iulianelli, A. Basile and A. Mendes, *Appl. Catal. B: Environ.*, 2015, **174**, 67-76.

14. J. A. Rodríguez and M. Fernández-García, *Synthesis, properties, and applications of oxide nanomaterials*, John Wiley & Sons, 2007, p 1-2.

15. H. H. Kung, *Transition metal oxides: surface chemistry and catalysis*, Elsevier, 1989, p 1-3.

16. A. Gavriilidis, B. Sinno and A. Varma, *J. Catal.*, 1993, **139**, 41-47.

17. S. Chang, M. Li, Q. Hua, L. Zhang, Y. Ma, B. Ye and W. Huang, *J. Catal.*, 2012, **293**, 195-204.

18. B. P. Hereijgers and B. M. Weckhuysen, *J. Catal.*, 2010, **270**, 16-25.

19. V. Raji, M. Chakraborty and P. A. Parikh, *Ind. Eng. Chem. Res.*, 2012, **51**, 5691-5698.

20. R. K. Grasselli, *Catal. Today*, 1999, **49**, 141-153.

21. M. J. Beier, T. W. Hansen and J.-D. Grunwaldt, *J. Catal.*, 2009, **266**, 320-330.

22. X. Liu, M. Conte, Q. He, D. W. Knight, D. M. Murphy, S. H. Taylor, K. Whiston, C. J. Kiely and G. J. Hutchings, *Chem. Eur. J.*, 2017, **23**, 11834-11842.

23. J. Paier, C. Penschke and J. Sauer, *Chem. Rev.*, 2013, **113**, 3949-3985.

24. M. Conte, X. Liu, D. M. Murphy, K. Whiston and G. J. Hutchings, *Phys. Chem. Chem. Phys.*, 2012, **14**, 16279-16285.

25. G. Deo and I. E. Wachs, *J. Catal.*, 1991, **129**.

26. K. Kunimori, Z. Hu, T. Uchijima, K. Asakura, Y. Iwasawa and M. Soma, *Catal. Today*, 1990, **8**, 85-97.

27. I. Nowak and M. Ziolek, *Chem. Rev.*, 1999, **99**, 3603-3624.

28. C. Nico, T. Monteiro and M. P. Graça, *Prog. Mater. Sci.*, 2016, **80**, 1-37.

29. R. Abe, K. Shinohara, A. Tanaka, M. Hara, J. N. Kondo and K. Domen, *J. Mater. Res.*, 1998, **13**, 861-865.

30. M. Gimon-Kinsel and K. Balkus Jr, in *Stud. Surf. Sci. Catal.*, Elsevier, 1998, vol. 117, pp. 111-118.

31. S. Furukawa, T. Shishido, K. Teramura and T. Tanaka, *J. Phys. Chem. C*, 2011, **115**, 19320-19327.

32. T. Shishido, T. Miyatake, K. Teramura, Y. Hitomi, H. Yamashita and T. Tanaka, *J. Phys. Chem. C*, 2009, **113**, 18713-18718.

33. L. Li, L. Dong, X. Liu, Y. Guo and Y. Wang, *Appl. Catal. B: Environ.*, 2020, **260**, 118143.

34. S.-I. Ito, T. Fujimori, K. Nagashima, K. Yuzaki and K. Kunimori, *Catal. Today*, 2000, **57**, 247-254.

35. D. A. Aranda, A. D. Ramos, F. B. Passos and M. Schmal, *Catal. Today*, 1996, **28**, 119-125.

36. R. Brayner, G. Viau, G. M. da Cruz, F. Fiévet-Vincent, F. Fiévet and F. Bozon-Verduraz, *Catal. Today*, 2000, **57**, 187-192.

37. M. Conte, X. Liu, D. M. Murphy, S. H. Taylor, K. Whiston and G. J. Hutchings, *Catal. Lett.*, 2016, **146**, 126-135.

38. H. Ge, G. Chen, Q. Yuan and H. Li, *Chem. Eng. J.*, 2007, **127**, 39-46.

39. Y.-F. Y. Yao, *J. Catal.*, 1973, **28**, 139-149.

40. X. Liu, Y. Ryabenkova and M. Conte, *Phys. Chem. Chem. Phys.*, 2015, **17**, 715-731.

41. H. Schäfer, R. Gruehn and F. Schulte, *Angew. Chem., Int. Ed. Engl.*, 1966, **5**, 40-52.

42. Y.-R. Luo, *Comprehensive handbook of chemical bond energies*, CRC press, 2007.

43. C. A. Wilde, Y. Ryabenkova, I. M. Firth, L. Pratt, J. Railton, M. Bravo-Sanchez, N. Sano, P. J. Cumpson, P. D. Coates and X. Liu, *Appl. Catal. A: Gen.*, 2019, **570**, 271-282.

44. W. D. Xing and M. S. Lee, *Process.*, 2019, **7**, 243.

45. S. S. Pannu, *J. Chem. Educ.*, 1984, **61**, 174.

46. L. J. Burcham, J. Datka and I. E. Wachs, *J. Phys. Chem. B*, 1999, **103**, 6015-6024.

47. M. Ziolek, *Catal. Today*, 2003, **78**, 47-64.

48. Y. Zhou, Z. Qiu, M. Lü, A. Zhang and Q. Ma, *Mater. Res. Bull.*, 2008, **43**, 1363-1368.

49. R. Kodama, Y. Terada, I. Nakai, S. Komaba and N. Kumagai, *J. Electrochem. Soc.*, 2006, **153**, A583.

50. R. A. Rani, A. S. Zoolfakar, A. P. O'Mullane, M. W. Austin and K. Kalantar-Zadeh, *J. Mater. Chem.*, 2014, **2**, 15683-15703.

51. M. Conte, C. J. Davies, D. J. Morgan, T. E. Davies, D. J. Elias, A. F. Carley, P. Johnston and G. J. Hutchings, *J. Catal.*, 2013, **297**, 128-136.

52. S. Akhter, K. Allan, D. Buchanan, J. Cook, A. Campion and J. White, *Appl. Surf. Sci.*, 1988, **35**, 241-258.

53. E. Desimoni and B. Brunetti, *Chemosensors*, 2015, **3**, 70-117.

54. K. Islam, R. Sultana, A. Rakshit, U. Goutam and S. Chakraborty, *SN Appl. Sci.*, 2020, **2**, 1-7.

55. L. Appel, A. Frydman, C. Perez, J. Eon, D. Castner, C. T. Campbell and M. Schmal Schmal, *Phys. Status Solidi B*, 1995, **192**, 477-491.

56. P. He, C. Ye, J. Wu, W. Wei, X. Wei, H. Wang, R. Zhang, L. Zhang, Q. Xia and H. Wang, *Semicond. Sci. Technol.*, 2017, **32**, 055016.

57. Y.-C. Chang, K.-J. Lee, C.-J. Lee, L.-W. Wang and Y.-H. Wang, *IEEE J. Electron Devices Soc.*, 2016, **4**, 321-327.

58. O. Hellwig and H. Zabel, *Phys. B: Condens. Matter.*, 2000, **283**, 228-231.

59. N. Kumagai, K. Tanno, T. Nakajima and N. Watanabe, *Electrochim. Acta*, 1983, **28**, 17-22.

60. R. Romero, J. Ramos-Barrado, F. Martin and D. Leinen, *Surf. Interface Anal.*, 2004, **36**, 888-891.

61. Z. Weibin, W. Weidong, W. Xueming, C. Xinlu, Y. Dawei, S. Changle, P. Liping, W. Yuying and B. Li, *Surf. Interface Anal.*, 2013, **45**, 1206-1210.

62. S. A. Geyer-Lippmann J., Stollmaier F., *Z. Anorg. Allg. Chem.*, 1984, **516**, 55-66.

63. G. McGuire, G. K. Schweitzer and T. A. Carlson, *Inorg. Chem.*, 1973, **12**, 2450-2453.

64. X. Mou, B. Zhang, Y. Li, L. Yao, X. Wei, D. S. Su and W. Shen, *Angew. Chem. Int. Ed.*, 2012, **51**, 2989-2993.

65. X. Liu, J. Liu, Z. Chang, X. Sun and Y. Li, *Catal. Commun.*, 2011, **12**, 530-534.

66. J. Zhang, Y. Li, L. Wang, C. Zhang and H. He, *Catal. Sci. Technol.*, 2015, **5**, 2305-2313.

67. V. S. Braga, J. A. Dias, S. C. Dias and J. L. de Macedo, *Chem. Mater.*, 2005, **17**, 690-695.

68. Y. Xie, Y. Yu, X. Gong, Y. Guo, Y. Guo, Y. Wang and G. Lu, *CrystEngComm*, 2015, **17**, 3005-3014.

69. T. Ohuchi, T. Miyatake, Y. Hitomi and T. Tanaka, *Catal. Today*, 2007, **120**, 233-239.

70. S. Furukawa, T. Shishido, K. Teramura and T. Tanaka, *ChemPhysChem*, 2014, **15**, 2665-2667.

71. M. Conte, H. Miyamura, S. Kobayashi and V. Chechik, *Chem. Commun.*, 2010, **46**, 145-147.

72. J. Li, A. Alsudairi, Z.-F. Ma, S. Mukerjee and Q. Jia, *J. Am. Chem. Soc.*, 2017, **139**, 1384-1387.

73. E. L. Pires, J. C. Magalhães and U. Schuchardt, *Appl. Catal. A: Gen.*, 2000, **203**, 231-237.

74. C. Cullis, M. Hirschler and R. Rogers, *Proc. R. Soc. A*, 1981, **375**, 543-563.

75. F. J. Schenck, P. Callery, P. M. Gannett, J. R. Daft and S. J. Lehotay, *J. AOAC Int.*, 2002, **85**, 1177-1180.

76. K. I. Eller and S. J. Lehotay, *Analyst*, 1997, **122**, 429-435.

77. D. B. G. Williams and M. Lawton, *J. Org. Chem.*, 2010, **75**, 8351-8354.

78. A. Valverde-García, A. R. Fernández-Alba, A. Agüera and M. Contreras, *J. AOAC Int.*, 1995, **78**, 867-873.

79. T. López-Ausens, M. Boronat, P. Concepción, S. Chouzier, S. Mastroianni and A. Corma, *J. Catal.*, 2016, **344**, 334-345.

80. L. Brugnoli, A. Pedone, M. C. Menziani, C. Adamo and F. d. r. Labat, *J. Phys. Chem. C*, 2020, **124**, 25917-25930.

81. S. Colussi, P. Fornasiero and A. Trovarelli, *Chin. J. Catal.*, 2020, **41**, 938-950.

82. X. Liu, M. Conte, M. Sankar, Q. He, D. M. Murphy, D. Morgan, R. L. Jenkins, D. Knight, K. Whiston and C. J. Kiely, *Appl. Catal. A: Gen.*, 2015, **504**, 373-380.

83. J. T. Carneiro, T. J. Savenije, J. A. Moulijn and G. Mul, *J. Photochem. Photobiol. A: Chem.*, 2011, **217**, 326-332.

84. X. Yang, X. Wang, C. Liang, W. Su, C. Wang, Z. Feng, C. Li and J. Qiu, *Catal. Commun.*, 2008, **9**, 2278-2281.

85. J. Xie, Y. Wang, Y. Li and Y. Wei, *React. Kinet. Mech. Catal.*, 2011, **102**, 143-154.

Chapter 5: Supported Ag catalysts over Nb_2O_5 for the oxidation of cyclic hydrocarbons

5.1 Overview

The selective oxidation of hydrocarbons is an important area in petroleum chemistry industry due to the formation of oxygen containing chemicals that are raw materials to produce fibres, coatings, plastics[1]. Among these, one of the most notable examples is the partial oxidation of cyclohexane to cyclohexanol and cyclohexanone which are essential precursors for the manufacture of nylon-6 and nylon 6,6[1, 2]. The use of supported metal nanoparticle catalysts, comprising metals like Au[3-5], Pt[6, 7], Pd[7], Ru[8] have attracted much attention over the past decades for these kinds of reactions, due to their unique properties as compared with bulk metals. Among the metals investigated so far, Ag, however, has received limited attention so far for the partial oxidation of saturated hydrocarbons like cyclohexane or ethylbenzene in liquid phase, and the understanding for its effects during the reaction is insufficient. At present Ag is industrially employed for ethylene epoxidation to produce ethylene oxide (up to 80% selectivity) and dehydrogenation of methanol to formaldehyde[9], which poses an industrial prospect of supported Ag catalysts. Especially for oxidation reactions, in fact Ag can activate oxygen to form superoxide species (O_2^-) due to the adsorbing of oxygen over Ag species[10, 11]; a mechanism often encountered in partial oxidation of organic compounds including hydrocarbons. Furthermore, literature data show that synergetic interactions between Ag and a support could affect the distribution of

oxygen vacancies in bulk and surface of metal oxide (e.g., CeO_2)[12] and the oxygen vacancies generated due to the addition of Ag in metal oxide (CeO_2, TiO_2) is capable of promoting the reductive adsorption of O_2[13]. Besides, if compared with other noble metals like Au, Pt, Pd, and Ru; Ag serves as a promising industrial prospect being less expensive than these metals.

Herein we aim to assess the potential application of supported silver over metal oxides, mainly Nb_2O_5 (see Chapter 4) as well as other metal oxides: CeO_2, TiO_2, MgO, SiO_2 for comparison, as a catalyst for the selective oxidation of cyclic hydrocarbons namely cyclooctane, cyclohexane, as well as ethylbenzene which although not cyclic can provide useful mechanistic information. This with the further aim to provide data useful for structure/activity correlations, and in turn promote the synthesis of catalysts by design.

5.2 Cyclooctane oxidation

In our study, cyclooctane oxidation by molecular O_2 is selected as a model reaction firstly to assess the catalytic performances of prepared catalysts based on following reasons: i) the major products of cyclooctane oxidation (cyclooctanone, cyclooctanol, and in some case cyclooctadiene) are valuable intermediates for industrial organic synthesis; ii) the oxidation process could be easily achieved by using an experimental set-up open to air, and as such also using molecular oxygen from air, without the initial need to use pressurized systems,; iii) from literature research catalysts used in the oxidation of cyclooctane are mainly polyoxometalates[14, 15] and

cobalt based materials[16], and there are not many publications reporting about oxidation of cyclooctane to produce ketones or alcohols utilising supported metal catalysts by using molecular O_2; and iv) as cyclooctane and cyclohexane shares similar physical chemistry properties, it is assumed that the catalytic results from cyclooctane oxidation could provide useful data for the study about cyclohexane oxidation by using the designed supported metal catalysts, which enables us to extend the applications of catalysts for other hydrocarbons oxidation if possible. Therefore, the oxidation of cyclooctane was firstly employed to investigate about catalytic reactivity of supported Ag catalysts. In this section, reaction parameters like temperature, O_2 pressure, metal to substrate ratio, stirring speed are varied to study their effect to changes of catalytic performances (namely conversion and selectivity).

5.2.1 Test at atmospheric pressure using an open system

As discussed in section 1.1 of chapter 1 and 4.2 of chapter 4, autoxidation in the absence of any catalyst is investigated as a background reaction for the comparison with the activity of catalysts. Parameters are varied to achieve a balance between the conversion and selectivity by observing the effects of these parameters on the selectivity to alcohols or ketones (the desired product of our work). Temperature is possibly one of the most significant parameters in catalysis process affecting the equilibrium constant, the initiation step in hydrocarbons oxidation being affected by temperature. Additionally, the effect of time is investigated to observe the kinetics of cyclooctane oxidation in the absence of blank autoxidation. The reaction must be under

a kinetic regime for the comparison among various catalysts otherwise mass transfer could be a dominating factor to affect reaction[17, 18]. Thus, stirring speed and metal to substrate (M:S) ratio are varied for the tests at pressurised O_2 in section 5.2.2.

5.2.1.1 Effect of reaction temperature on cyclooctane oxidation

Supported Ag/Nb_2O_5 with a nominal 1 *wt*% metal loading was used for the oxidation of cyclooctane respectively. As shown in Fig. 5.1, the catalyst WI-Ag/Nb_2O_5 promotes the oxidation of cyclooctane compared with blank autoxidation process. However, when Ag/Nb_2O_5 is used this shows some similarities with autoxidation in the sense the conversion increases with temperature up to a maximum and then decreases. This maximum is observed at about 110 °C for Ag/Nb_2O_5 and 130 °C in the case of autoxidation without catalyst. Meanwhile, when the temperature is below 100 °C, it is apparent that Ag/Nb_2O_5 catalyst provides an obvious enhancement (~14% at 100 °C) of the oxidation of cyclooctane compared with blank autoxidation (~1% at °C). This means Ag/Nb_2O_5 takes part in the reaction and lower the essential energy for the activation of C-H bond. From these data, WI-Ag/Nb_2O_5 catalyst could facilitate the conversion of cyclooctane at lower temperature, whose conversion arrives at about 21% at 110 °C, which is higher than the highest conversion of autoxidation, 13% at 130 °C. However, the conversion decreases at relatively higher temperature. In principle there could be due to several possible reasons: (a) metal leaching; (c) a change of oxidation state and changes of structure of catalyst, (c) diffusion limitation (and solubility) of oxygen in the reaction media (as the experimental set-up is a reflux

condenser open to air). The metal leaching was tested by ICP-MS analysis of the reaction mixture from the tests with the presence of catalysts, whereas to assess oxygen diffusion limitation effects, tests at pressurised O_2 were carried. The oxidation state of Ag could be determined by XPS analysis or XRPD patterns. Moreover, it should be noted that the presence of WI-Ag/Nb_2O_5 can enhance the production of ketones by the transformation of alkyl hydroperoxides, which is consistent of our project goal. Based on the consideration to achieve a reasonably steady conversion and minimize the effects of autoxidation, 110 °C is chosen as the reaction conversion temperature.

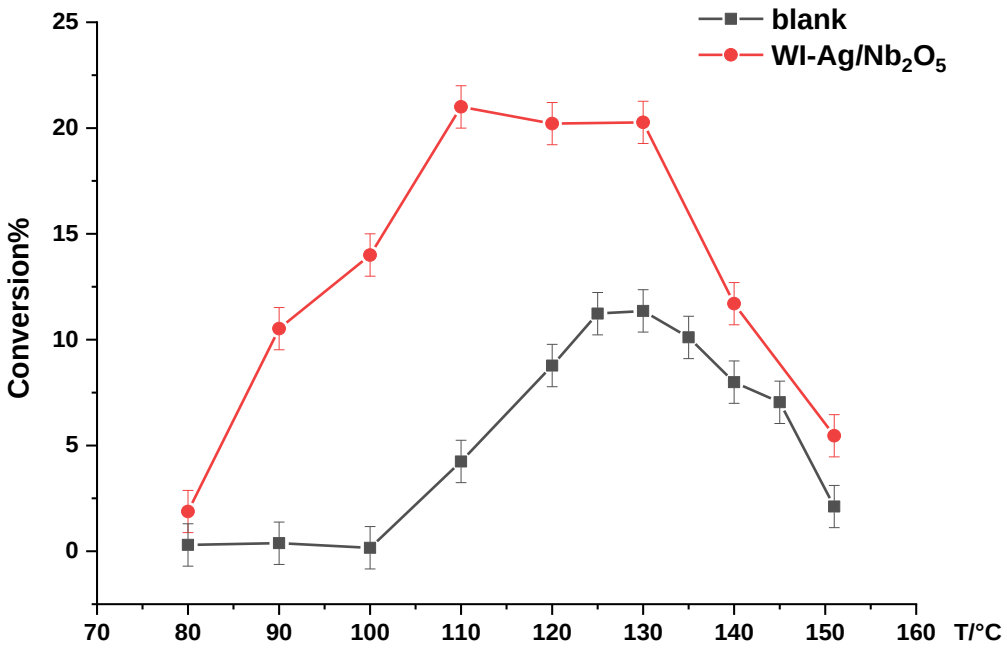

a. Conversion of cyclooctane at different reaction temperatures

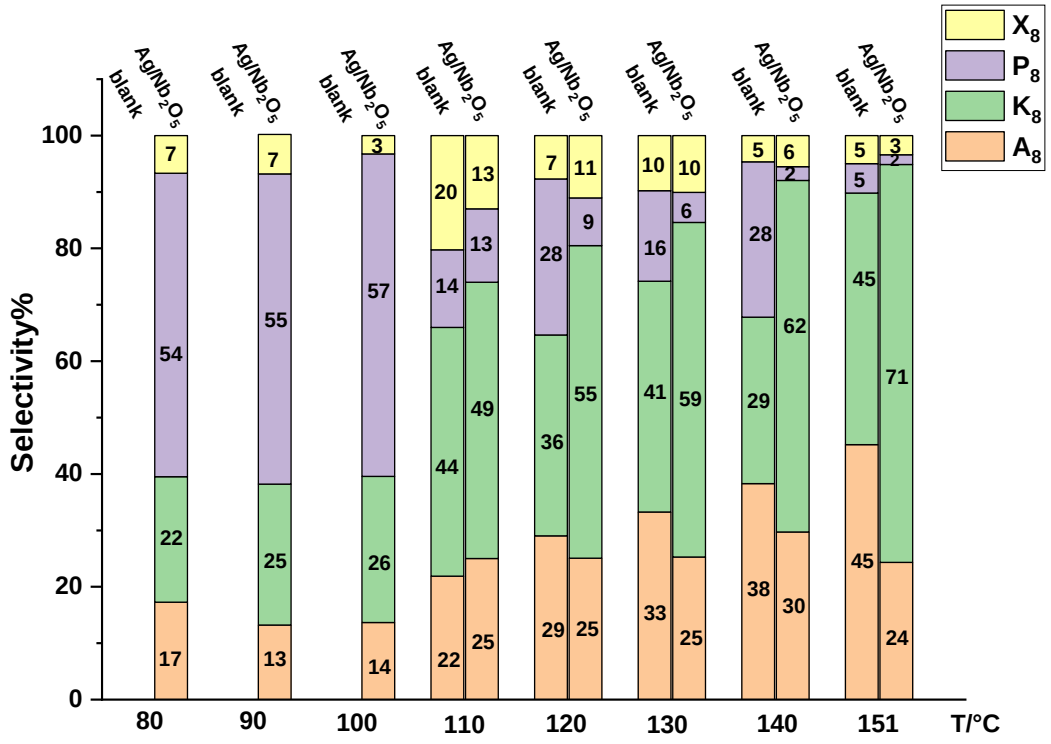

b. Product distribution at different reaction temperatures

Fig. 5.1 Conversion of cyclooctane oxidation at different temperatures. Reaction carried out with M:S ratio of 1:1000, under 1 atm static air with condenser, for 24 h. a: Conversion of cyclooctane; b: Product distribution for cyclooctane oxidation. Catalysts WI-Ag/Nb_2O_5 with theoretical 1 *wt*% metal loading were prepared by wet impregnation method using Nb_2O_5 with grade of 99.9% that was also used for all the catalysts in this chapter. And all the conversion and selectivity percentage in this chapter are expressed as mol%. A_8: cyclooctanol, K_8: cyclooctanone, P_8: cyclooctyl hydroperoxide, X_8: by-products, and represents the same meaning in this chapter.

In comparison with the reaction results from the tests by using Nb_2O_5 (see section 4.3), the conversion of cyclooctane is slightly enhanced (from 16% of Nb_2O_5 to 21% with catalyst) by WI-Ag/Nb_2O_5. The difference is also observed in the selectivity for cyclooctanone and alkyl hydroperoxide, implying that the addition of Ag promotes the transformation of alkyl hydroperoxide to cyclooctanone. From this perspective, it

appears that the abstraction of α-H in alkyl hydroperoxide is enhanced to give ketone due to the existence of Ag species in catalysts. In view of this, Further tests for the investigation about the effects of Ag(0) and Ag^+ in cyclooctane oxidation in pressurized O_2 and the decomposition of alkyl hydroperoxides (1-phenylethyl hydroperoxide) by Nb_2O_5 or Ag/Nb_2O_5 catalysts (section 5.3) were conducted.

5.2.1.2 Effect of reaction time on cyclooctane oxidation

Due to the high conversion of cyclooctane autoxidation without catalyst at 130 °C, and in order to enhance differences between autoxidation and WI-Ag/Nb_2O_5 catalysed process, a temperature of 100 °C is chosen to study the effects of time on reaction performances of Ag/Nb_2O_5 (Fig.5.2). It is observed that conversion with catalyst increases largely before 24 h and reaches nearly a plateau after 72 h (17%), visually like it would be for an equilibrium reaction. On the other hand, our reaction system is open to air, and as such a constant supply of oxygen the reactant should be completely consumed after enough time. In order to explain this effect, which could also be due to a change in catalyst structure, the equilibrium constant K_{eq}, was estimated, based on the assumption (in a simplified scheme) that the ketone was the only product (as this is the one in excess). By using the formula $\Delta G = -nRT\ln K_{eq}$ (eq. 5.1), an estimate of K_{eq} at standard temperature and pressure is obtained, which is around $3 \cdot 10^{59}$. That means the oxidation of cyclooctane should be a complete reaction, as long as oxygen is not a limiting reagent and constantly supplied to the reaction. Therefore, the limitation for the improvement of conversion is probably caused by the property

changes of catalyst during reaction or the diffusion rate (or solubility in liquid phase) of O_2. In addition, there is no obvious reaction activity observed for autoxidation process without catalyst before 48 h at 100 °C. The products of blank autoxidation at a 72 h reaction time are mainly cyclooctyl hydroperoxide (94%), which indicates that higher temperature shortens induction period and the hydroperoxides is a primary product in the oxidation of cyclooctane at lower temperature. Moreover, it is found that there are no obvious changes of conversion and selectivity after 24 h reaction. In addition, although the initiate rates determine, while at the initial rate the conversion is low, leading to a large experimental error (small peaks) in NMR, and the reaction occurring at 24 h are able to gather data with a relatively small experimental error and to allow a comparison of data. In this case, 24 h is used in our tests for catalysts to achieve a balance between conversion and reaction time.

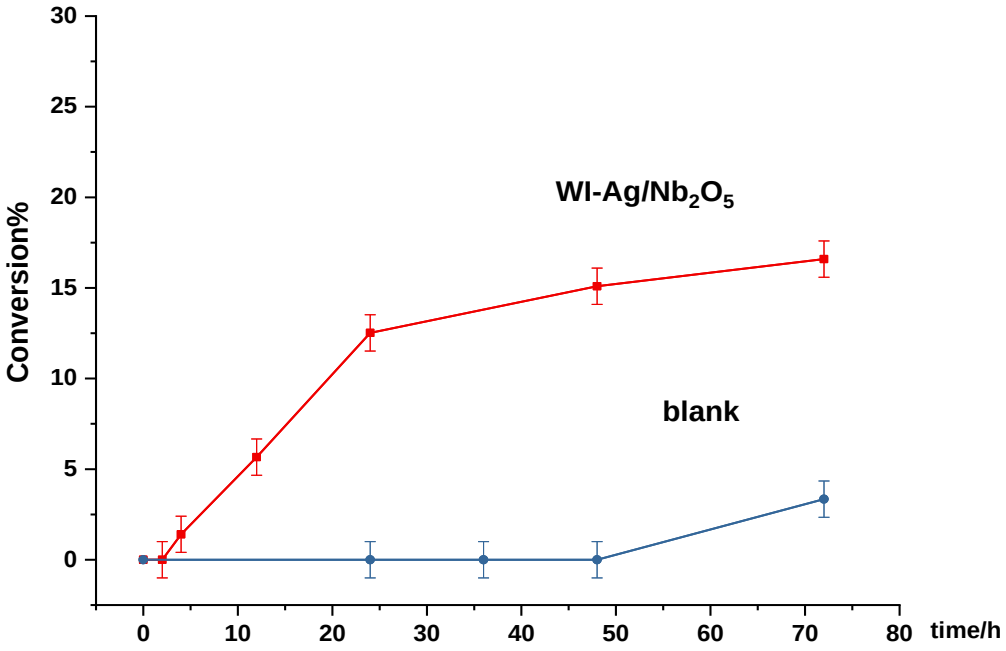

a. Conversion of cyclooctane veruses reaction time

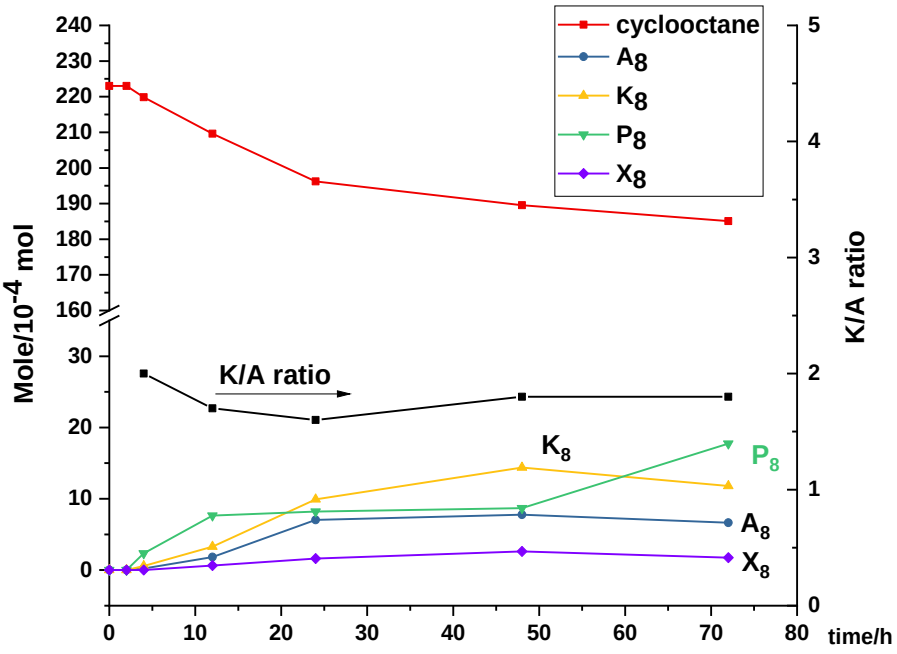

b. Product distribution of cylooctane oxidation versues time

Fig. 5.2 Absolute number of mole and K/A ratio to represent conversion and selectivity of cyclooctane oxidation catalysed by WI-Ag/Nb_2O_5 at 100 °C from 0 to 72 h. a: Conversion of cyclooctane; b: Product distribution for cyclooctane oxidation. 3 mL cyclooctane, M: S=1:1000. The right vertical coordinate represents the K/A ratio.

5.2.2 Test for the oxidation of cyclooctane using pressurized O_2

The diffusion of oxygen might play a significant role in the oxidation process[19]. In fact, after the occurrence of initiation, O_2 will react with a R· radical in a diffusion limited step, to form alkyl hydroperoxides. The reaction carried out in the presence of catalyst at atmospheric pressure seems to show some limitations (the conversion reached a plateau at around 17% even after 72 h at 100 °C), which is possibly related with the improvement of O_2 solubility in liquid phase. Although the O_2 diffusion cannot be ruled out, as comparison the solubility of gases tends to be affected by increasing gases pressure in liquid or solid phase. In this case, cyclooctane oxidation was conducted at

pressurised O_2 in a sealed reactor by constantly suppling gaseous O_2 from cylinder at a fixed pressure.

Furthermore, an increase of pressure would also promote an increase of O_2 solubility in liquid phase. In view of these considerations, tests under pressurised O_2 should increase the conversion per time. This expectation is, in fact, experimentally verified (Fig. 5.3). Reaction results indicate that the conversion of blank autoxidation increases up to 6% until the pressure of O_2 reaches 2 bar, while there is an obvious enhancement in the presence of Nb_2O_5 and WI-Ag/Nb_2O_5, which can be up to 81% by employing WI-Ag/Nb_2O_5. Meanwhile, it should be noted that changes of O_2 pressure from 1 bar to 2 bar enhances the conversion of cyclooctane when Nb_2O_5 and WI-Ag/Nb_2O_5 are presented, especially for Ag/Nb_2O_5 from 67% to 81%. Furthermore, it is apparent that the selectivity to cyclooctanone increases and K/A ratio rises from 3.8 to 7.2 when O_2 pressure rises from 1 bar to 2 bar in the presence of WI-Ag/Nb_2O_5. Therefore, from the perspective of conversion and higher selectivity for ketones, 2 bar O_2 is chosen for an optimum pressure in our tests. Moreover, the studies about photo reactivity of Nb_2O_5 in the oxidation of alcohols and hydrocarbons reveals that both of O_2 and reactant molecules can be adsorbed over the surface to be activated[20,21](as discussed in chapter 4.3) and a competitive adsorption may exist between O_2 and reactants to limit the conversion of substrates[22]. In addition, based on consideration about health and safety for highest working pressure for the reactor, that was used for these studies, we limited the maximum working pressure at 3 bar, and to ensure a

higher safety of reactor for long periods of time, the pressure of O_2 is set at 2 bar for most of our tests with this substrate cyclooctane.

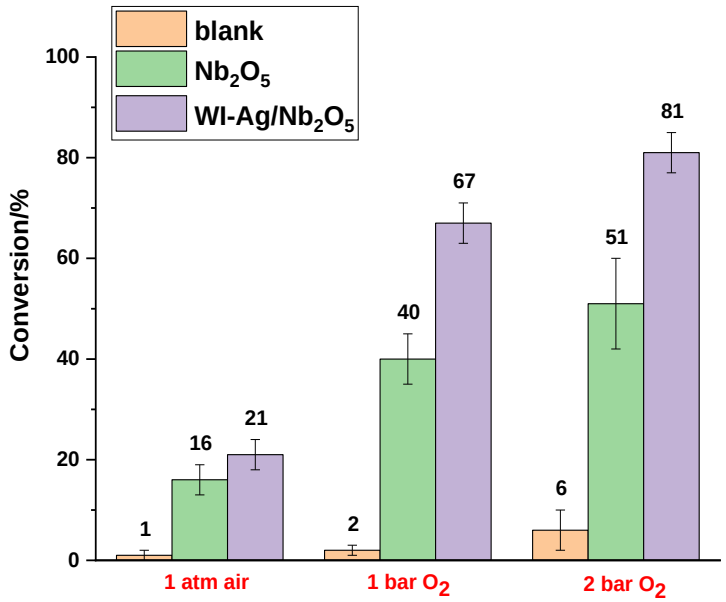

a. Conversion of cyclooctane by Nb_2O_5 or WI-Ag/Nb_2O_5

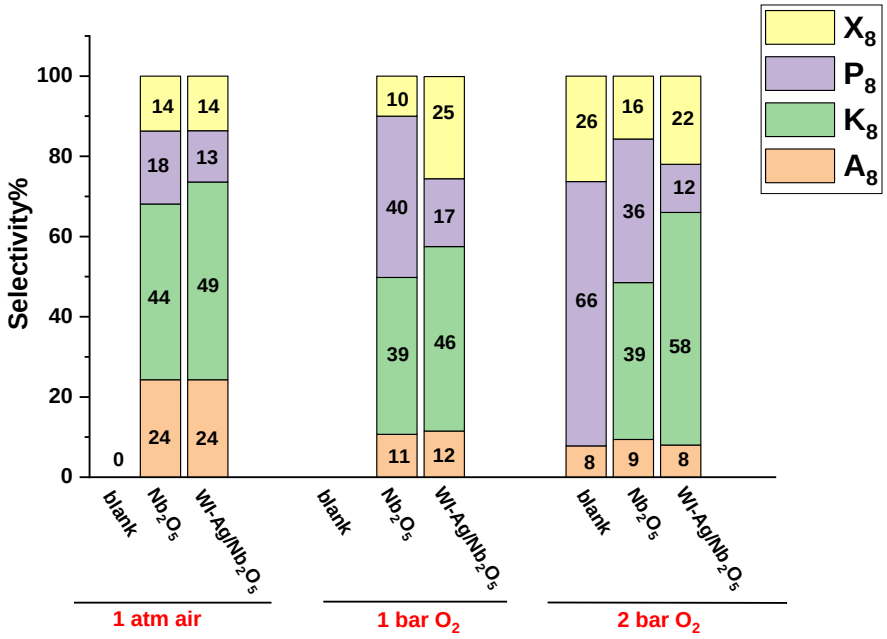

b. Product distribution of cyclooctane oxidation by Nb_2O_5 and WI-Ag/Nb_2O_5

Fig. 5.3 Reaction performances of Nb_2O_5 and WI-Ag/Nb_2O_5 in cyclooctane oxidation. Reaction conditions: 3 mL cyclooctane, 110 ˚C for 24 h at atmospheric air with condenser open to air, 1 bar and pressurised 2 bar O_2 respectively. a: Conversion of cyclooctane; b: Product distribution

for cyclooctane oxidation. Nb_2O_5 used was with grade/purity 99.9%. WI-Ag/Nb_2O_5 was prepared by impregnation method using 99.9% of Nb_2O_5. Molar ratio between Ag and cyclooctane was 1:1000, Nb and cyclooctane was 1:12 and corresponding to the same amount of Nb_2O_5 in Ag/Nb_2O_5 but without the presence of Ag.

5.2.2.1 Effect of metal to substrate (M:S) ratios on cyclooctane oxidation

It is well known that amount of catalyst (M:S ratio) can affect both the conversion and products distribution of a reaction.[18, 23, 24] While it should be noted that in some cases an increase of M:S ratio does not necessarily improve the conversion with the amount of catalysts (specifically the amount of active sites), which can be influenced by parameters like mass transfer[24, 25] and side products[24]. In our case, in order to optimize the amount of catalyst used during reaction for a reasonable balance between conversion and selectivity for desired products from the economic and practical perspective, as well as to assess the presence of diffusion limitation effects on a set of reactions with various M:S ratio under a fixed reaction conditions (110 °C at 2 bar O_2 for 24 h with stirring speed 600 rpm) were conducted (Figure 5.4.a)

The results indicate that with an increase of M:S ratio, conversion of cyclooctane initially increases, until reaches a plateau from M:S ratio 1:2000, with a mol% conversion at around 81%. The increase of conversion in the range from 0 to 1:2000 implies that the dominating factor is the increase of catalyst active sites, while no obvious or only slight rise is observed when M:S ratio increases from 1:2000 to 1:1000, indicating that there might exist mass transport limitations in the range of 1:2000 and 1:1000 when taking the error into account, although at the very edge with a kinetic

regime. In view of this, it would have been probably more appropriate to select a different ratio, eg. M:S ratio lower than 1:2000. But a M:S ratio of 1:1000 can be selected as the highest amount of substrate (or lowest amount of catalyst) at the edge of diffusion or kinetic regime. In addition, product distribution show that the existence of catalyst facilitates the transformation of cyclooctyl hydroperoxide to cyclooctanone when the rate of the reaction is a function of the amount of active sites (M:S < 1:1000), and observed K/A ratio reaches the highest at 7.5 with M:S ratio is 1:1000, which is related with the diffusion of substrates and products in the reaction system[26]. In this case, this furtherly confirms that M:S ratio at 1:1000 is the best compromise for our studies. Moreover, it is observed that the more the reaction proceeds (higher conversion in this case), the larger is the amount of alkyl hydroperoxide that is consumed to form ketone when M:S ratio is below 1:1000, which can be as a point to furtherly illustrate that α-H in alkyl hydroperoxide is abstracted due to the presence Ag species to generate cyclooctanone.

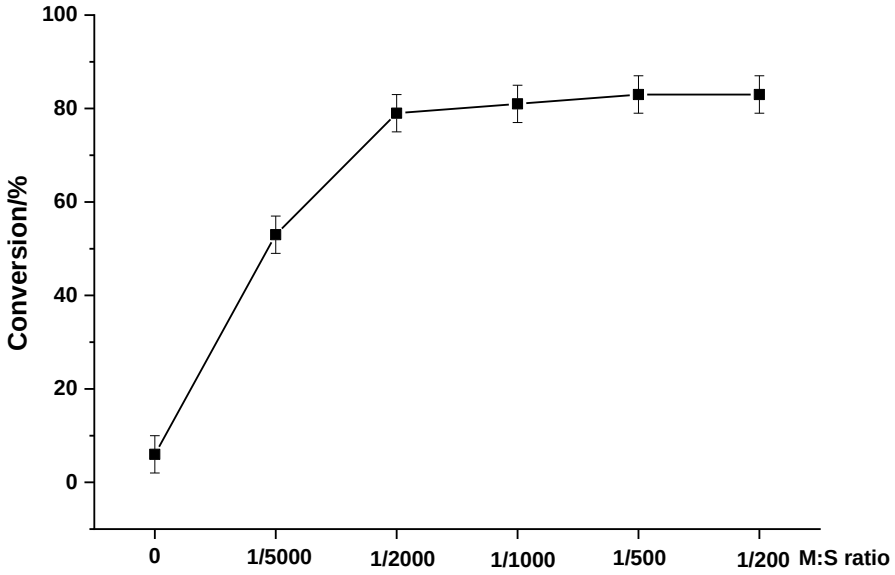

a. Conversion of cyclooctane by WI-Ag/Nb_2O_5 with various M/S ratios

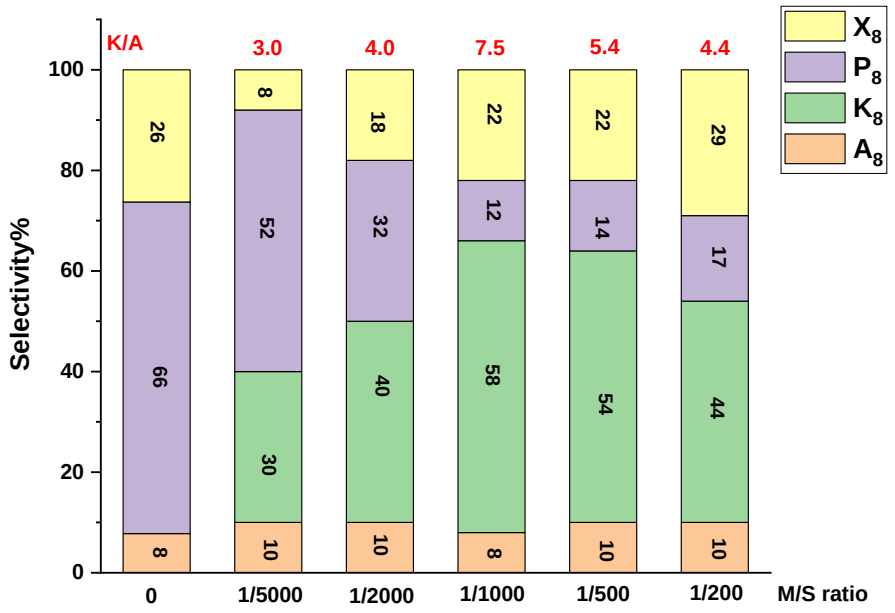

b. Product distribution by WI-Ag/Nb_2O_5 at various M/S ratios

Fig. 5.4 Reaction results of cyclooctane with WI-Ag/Nb_2O_5 (1 *wt*%) prepared by wet impregnation method, at varying M:S ratios. a: Conversion of cyclooctane; b: Product distribution for cyclooctane oxidation. cyclooctane (3 mL), stirring speed = 600 rpm, T = 110 °C, *P*(O_2) = 2 bar, t = 24 h.

5.2.2.2 Effect of stirring speed on cyclooctane oxidation

In a heterogeneous catalysis process, the thoroughly mixing of reactants with catalysts is quite important, which could be achieved by stirring vigorously to enhance mass transfer[17, 23, 26]. Therefore, the stirring speed, is an important parameter which can influence mass transfer, the effect of which was evaluated in a range from 200 rpm to 800 rpm. This limit was selected as a too high or too low stirring speed would make reaction slurry to stir insufficiently or cause splash on the walls the round bottom flasks respectively.

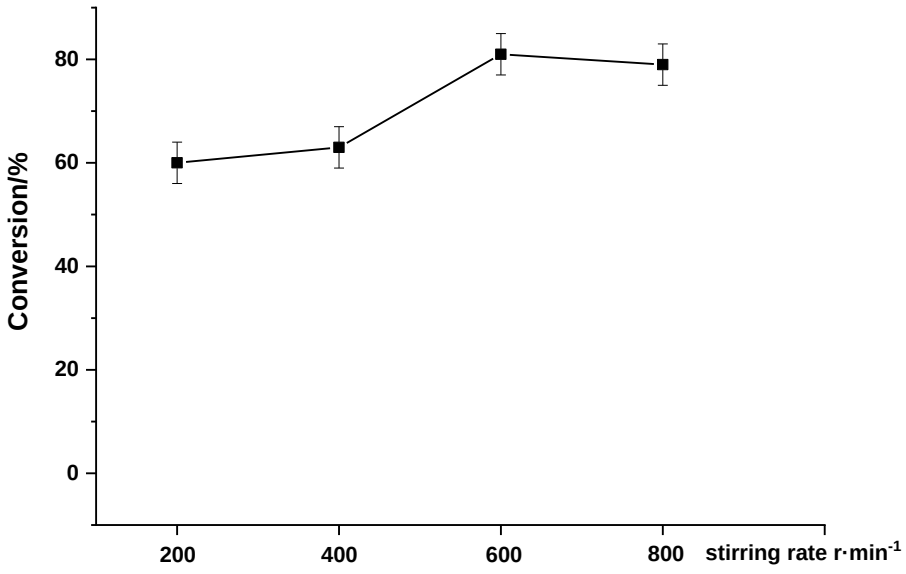

a.The conversion of cyclooctane by WI-Ag/Nb_2O_5 at various stirring rates

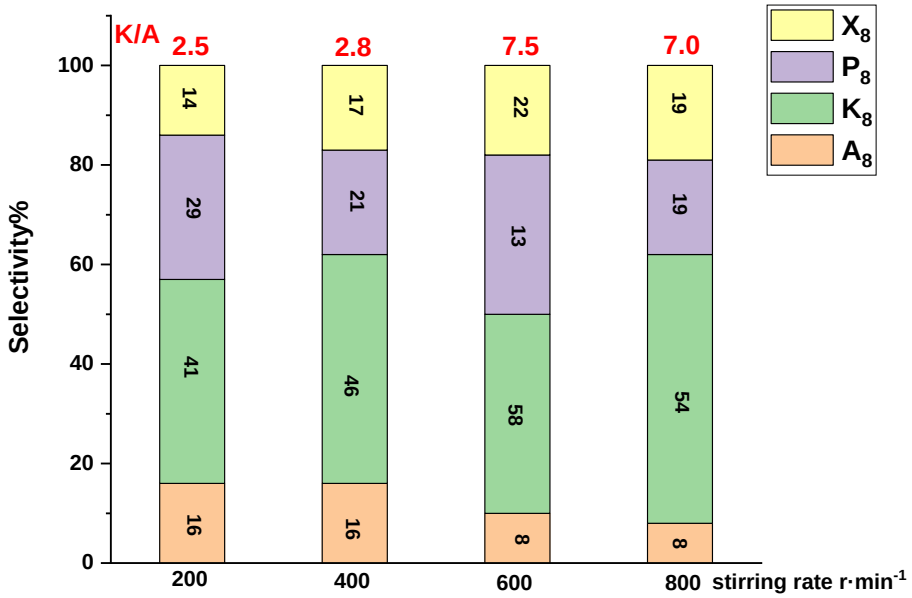

b. Product distribution of cyclooctane by WI-Ag/Nb_2O_5 at various stirring rate

Fig. 5.5 Reaction results of cyclooctane with WI-Ag/Nb_2O_5 (1 *wt*%) prepared by wet impregnation method, at varying stirrer speed. a. Conversion of cyclooctane oxidation; b. Selectivity of cyclooctane oxidation. Cyclooctane (3 mL), M:S = 1:1000, T = 110 °C, $P(O_2)$ = 2 bar, t = 24 h.

As can be seen from the Fig. 5.5-a, no appreciable change in conversion is detected as the stirring speed increases from 200 rpm to 400 rpm; there is a slightly increase of conversion from the speed at 400 rpm to 600 rpm, and it remains identical at around 80% between 600 rpm and 800 rpm. And it is observed that there is no evident difference of conversion and product distribution at 600 rpm and 800 rpm, revealing that the reaction is not limited by O_2 diffusion when stirring rate is above 600 rpm, and the existence of a threshold value suggests in which the resistance due to mass transfer to catalysts particles has been eliminated[17]. By considering these behaviours and in order to ensure the reaction mixture thoroughly mixed without

splashing and the research equipment works at a safe state, an optimized stirring speed is 600 rpm in our case.

5.2.3 Stability of WI-Ag/Nb_2O_5 in cyclooctane oxidation

In the assessment of catalysts properties, beside the catalytic activity (conversion) and selectivity, another very important property of a catalyst is its stability, especially for long term operations under industrial conditions[27, 28]. However, for a heterogeneously catalysed reaction, it is practically inevitable that a catalyst loses reactivity during a reaction. Reasons for the deactivation of a catalyst can be attributed to three main factors, which can be broadly classed as mechanical, chemical and thermal deactivation[28, 29]. Among the chemical deactivation, leaching of active metal is one of the most critical issues for the stability of supported metal catalysts in liquid-phase reactions, which is the loss of metal sites by undesirable extraction into the fluid phase. This phenomenon causes the decrease of catalytic activity and a contamination of reaction products. Generally, the leaching occurs via the formation of free metal ions[30, 31]. In view of these considerations, the stability of the supported Ag catalysts was studied by testing the reactivity of recycled catalyst four times and leaching of Ag was investigated thoroughly.

It can be observed (Fig.5.6) that there are no obvious changes of conversion in the presence of solely Nb_2O_5 with the proceeding of each running test (conversion can be retained at around 40%), indicating that Nb_2O_5 can be reactive, and it is highly stable as reaction proceeds, as proved by XRPD patterns before and after reaction in

section 4.3.6. And product distribution with Nb_2O_5 demonstrates a similar trend in each test, indicating that Nb_2O_5 takes part in reaction. In this case we can conclude that Nb_2O_5 remains active with the proceeding of oxidation.

In comparison with the reaction performances of Nb_2O_5, conversion by WI-Ag/Nb_2O_5 is always higher during every test, implying the presence of active Ag species enhances the oxidation. But it should be noted that the gap of conversion between support and catalyst is getting narrower with the proceeding of each running test, exhibiting that promotion effect of Ag on the oxidation diminished which may be related with influencing factors such as, the leaching of Ag leading to the loss of active metals, sintering of metal nanoparticles[29, 32], poisoning of active sites[29, 33]. In our case, leaching of Ag was investigated in detail. On the other hand, as per repetition of catalytic tests, the activity of both WI-Ag/Nb_2O_5 and Nb_2O_5 is decreasing, and poisoning, or deposition of carbonaceous products cannot be entirely ruled out. Additionally, the product distribution shows that the selectivity for cyclooctane is always higher than that for cyclooctyl hydroperoxide, proving that Ag/Nb_2O_5 can efficiently promote the transformation of the alkyl hydroperoxide to the ketone in comparison with Nb_2O_5. Whilst this effect declines with the proceeding of recycled catalysts, so it states that the selectivity for ketones or alkyl peroxides is probably influenced by presented active Ag sites.

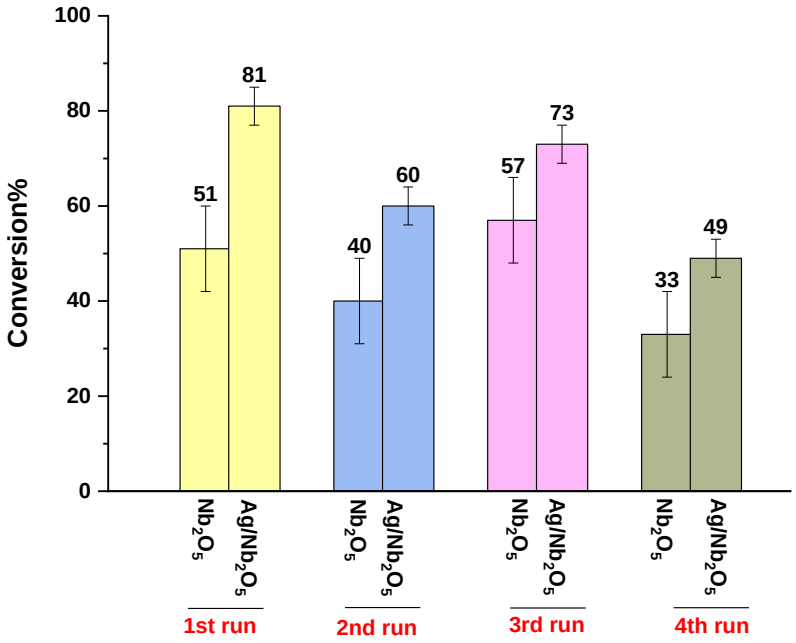

a. Conversion of cyclooctane by recycled catalyst

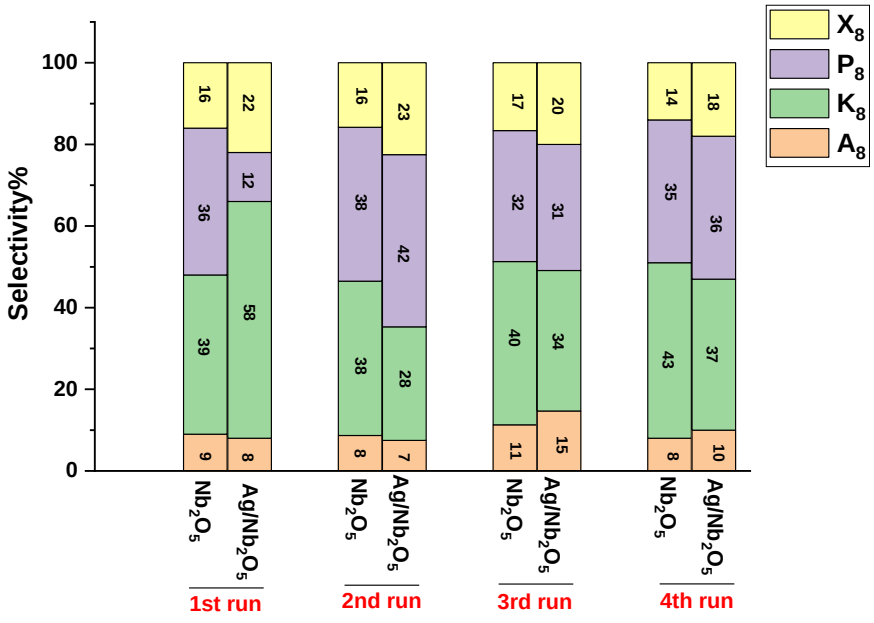

b. Product distribution by recycled catalyst

Fig. 5.6 Reaction results of cyclooctane with recycled Nb_2O_5 (99.9% purity) and WI-Ag/Nb_2O_5 (1 *wt*%) prepared by wet impregnation method respectively. a. Conversion of cyclooctane oxidation; b. Selectivity of cyclooctane oxidation in each running test. M(Ag):S = 1:1000, T = 110 °C, $P(O_2)$ = 2 bar, t = 24 h. After each test, catalyst was recycled by washing and filtrated with acetone and dried at 80 °C overnight. The amount of Nb_2O_5 used in each around of test is the total mass of WI-Ag/Nb_2O_5 minus by the mass of theoretical mass of loaded Ag.

Control tests on leaching of Ag in solution, by using ICP-MS methods, showed that that Ag leaching is the highest in the first-run test with a relative Ag loss of 24%, which is too high to be acceptable in the heterogeneous catalysis process (generally < 5%). The leaching of Ag decreases in the second and third-time test, but there is still 3% loss, indicating that there is possibly of a 'continuous' Ag leaching with the proceeding of the reaction until the fourth time test displaying that there is only 0.5% Ag leaching. It should be the noted that the conversion of Ag/Nb_2O_5 is higher than that of Nb_2O_5 in the fourth time test while the selectivity is similar, indicating the presence of Ag nanoparticles deposited on Nb_2O_5 which is not easy to be attacked from the surface into liquid phase, but the amount of active Ag sites is probably too low to affect the oxidation significantly. Meanwhile, combing the analysis about the decrease of reactivity of Ag/Nb_2O_5 and smaller gap of conversion between Ag/Nb_2O_5 and Nb_2O_5 with the process of test, we can confidently say that the loss of catalytic reactivity is caused by Ag leaching, especially in the first-time reaction with a high leaching. In addition, it should be mentioned the cooperating effects of Ag nanoparticles and Nb_2O_5 can facilitate of alkyl hydroperoxides transformation to ketones to an extent comparing with Nb_2O_5. Also, Ag/Nb_2O_5 still remains high reactivity in the second and third test with a reasonable leaching Ag, indicating a potential development for this catalyst to achieve a high reactivity with low loss of active metals.

Based on above discussion and the results in chapter 4 about the reactivity of Nb_2O_5 for cyclooctane oxidation, Nb_2O_5 shows superior stability in the oxidation of

cyclooctane and the catalyst Ag/Nb_2O_5 prepared by wet impregnation method reveals higher reactivity in comparison with Nb_2O_5, which implies the presence of Ag factually enhances the oxidation process. On the other hand, the leaching of Ag is too high to be neglected and it may also have effects on the oxidation process, and these are both important factor in the design of a catalyst with high reactivity and stability. As a consequence, in order to tackle how to minimize the loss of Ag in solution, it was important to identify the reasons for this leaching and whether leaching Ag can affect the oxidation in the ion state Ag^+, as discussed in the following section 5.2.4.

Table 5.1 ICP analysis for Ag leaching in each reaction. 1 mL reaction mixture was mixed with 10 mL deionised water thorough for 24 h, and the resulting solution from water phase was taken for the analysis by ICP-MS.

No. of test	Ag:R-H	Leaching of Ag /%
1st	1:1000	24.2
2nd	1:1000	3.3
3rd	1:1000	3.1
4th	1:1000	0.5

5.2.4 ICP-MS analysis for Ag leaching in reaction mixtures and its effects on cyclooctane oxidation

Leaching is a significant factor to evaluate the reaction performances of supported metal catalysts applied in the reaction, as the leaching of active metals may result in: i) the loss of reactivity of catalysts as the proceeding of reaction; ii) contamination of products[33, 34]; and iii) occurrence of the homogeneous reaction pathway if the leaching species is active. The most famous cases for the latter was to recognize the reaction

mechanism like the C-C Suzuki cross-coupling reaction by palladium catalysts.[35-37] According to our discussion in section 5.2.3, leaching of Ag from WI-Ag/Nb_2O_5 prepared by wet impregnation method in the oxidation of cyclooctane, was present.

5.2.4.1 Reactivity of leached Ag^+ ($AgNO_3$) in cyclooctane oxidation

To investigate the effects of leached Ag in solution for the oxidation of cyclooctane in the state of Ag^+, $AgNO_3$ was directedly employed for the reaction with various M(Ag):S ratios, shown in Fig. 5.7. The results indicate that Ag^+ species can promote the oxidation to an extent at pressurised O_2 in comparison with autoxidation, which can be up to 32% when the leaching is 24% (corresponding to a mass loss of 2.41 mg of Ag from the parent catalyst), implying that the effects of leached Ag^+ into reaction solution should be considered in our standard catalytic tests by using WI-Ag/Nb_2O_5. An analysis of the selectivity shows that the main product is the alkyl peroxide, ca. 60%, which shares similar products distribution with blank autoxidation, while ketone is the major product when using WI-Ag/Nb_2O_5 with a value at 58%. There are studies about supported Ag nanoparticles applied in the oxidation revealing that oxygen species participating in the oxidation can be effectively activated on Ag^+ sites that are dispersed on the surface of Ag nanoparticles[38-40], which is correlated to the formation of superoxide species. Our experimental observations would support these previous studies. And even more, as the presence of Ag^+ changes the conversion but not the selectivity it is most likely that Ag^+ is involved in the initiation step rather than in the decomposition of the alkyl hydroperoxide intermediate. In view of this, and according

to radical mechanism for hydrocarbons oxidation that the formation of hydroperoxyl radicals (ROO·) is from the reaction between R· and O_2 species, it infers that the presence of Ag^+ accelerates this process to give R· species and in turn (by diffusion) produce ROO· and then ROOH comparing with blank test. In addition, it should be noted that the enhancement of conversion is limited even with increase of the amount of Ag^+, which may possibly be caused by saturated adsorption of O_2 over Ag^+ sites. Ultimately, according to the observed reactivity of Ag^+, the effects of leached Ag species cannot be ignored, and we should reduce leaching of supported Ag from catalysts to minimize the effects. In order to furtherly clarity the source of reactivity by using WI-Ag/Nb_2O_5 (Ag^0, Ag_2O, Ag^+ sites and Nb_2O_5), a number of control tests were conducted, results of which are displayed in the following section.

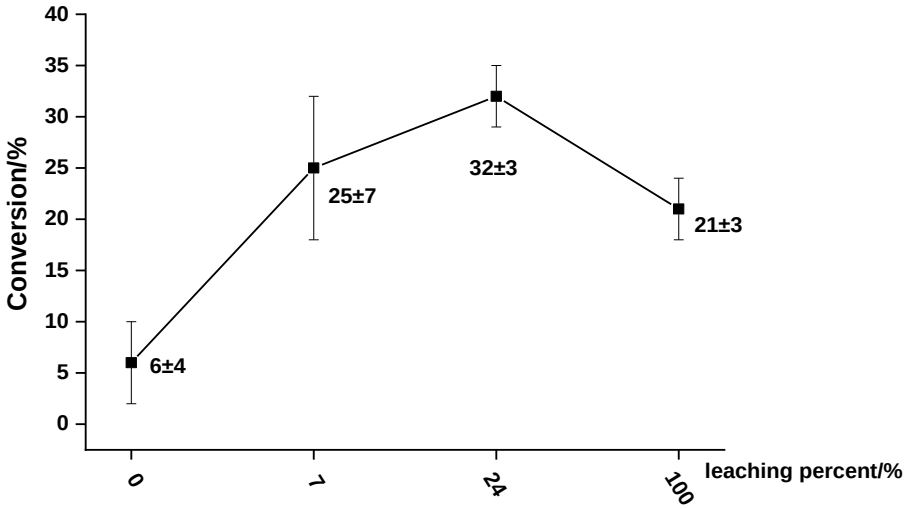

a. The oxidation of cyclooctane in the presence of Ag^+

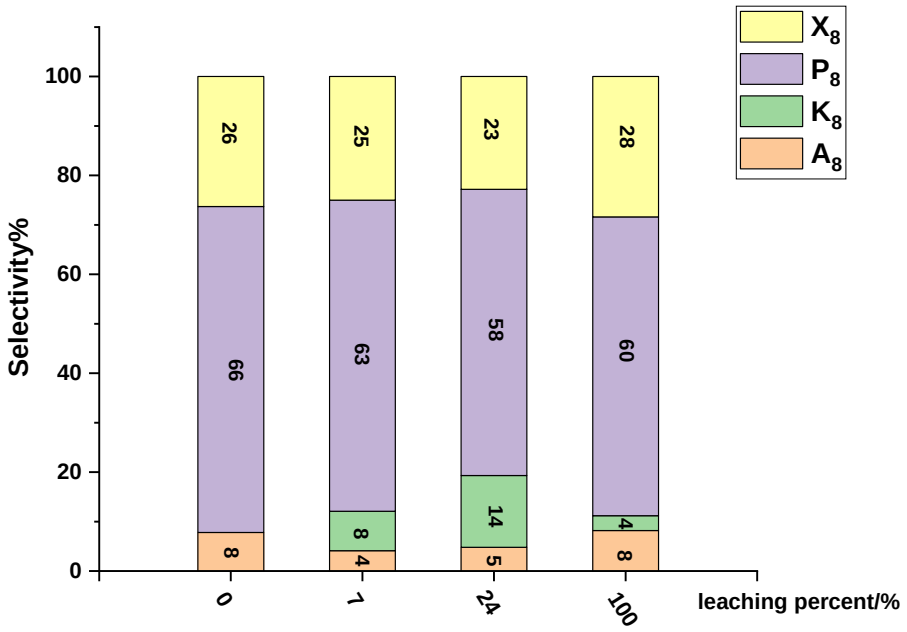

b. The products distribution of cyclooctane oxidation in the presence of Ag^+

Fig. 5.7 Reaction results of leaching tests in the presence of $AgNO_3$. a. Conversion of cyclooctane oxidation by Ag^+; b. Selectivity of cyclooctane oxidation by Ag^+. The leaching percent was based on the tests with M(Ag):S=1:1000 when using 1 *wt*% Ag/Nb_2O_5 (241 mg used), where nominal 2.41 mg Ag was presented in the reaction mixture as 100%. 7% leaching represented the leaching amount of Ag^+ from catalysts was $2.41 \cdot 0.07 = 0.17$ mg; 24% represented the leaching amount of Ag^+ was $2.41 \cdot 0.24 = 0.58$ mg. And the corresponding amount of Ag^+ from $AgNO_3$ was added for reaction. cyclooctane (3 mL), T = 110 °C, $P(O_2)$ = 2 bar, t = 24 h.

5.2.4.2 Reactivity of different Ag species in cyclooctane oxidation

Nb_2O_5 shows catalytic reactivity in the oxidation of cyclooctane and WI-Ag/Nb_2O_5 exhibits higher reactivity with enhanced conversion and selectivity to cyclooctane with an improved K/A ratio in comparison with Nb_2O_5. However, it was observed that the leaching Ag from WI-Ag/Nb_2O_5 could affect the oxidation by activating O_2 to form alkyl hydroperoxides. Therefore, in order to investigate the effects of Ag species (Ag^0, Ag_2O)

from WI-Ag/Nb_2O_5 on reaction, a series of control tests were conducted. In the preparation of Ag/Nb_2O_5 by impregnation method, $AgNO_3$ decomposes to metallic Ag by following the step[40]:

$$2AgNO_3 \longrightarrow Ag_2O + 2NO_2 + 0.5O_2$$

$$Ag_2O \longrightarrow 2Ag + 0.5O_2$$

In this case, it is possible that there may exist both of Ag_2O and metallic Ag at the same time after calcination at 180 °C for 16 h. So pure Ag_2O powder is directly used for the oxidation as comparison.

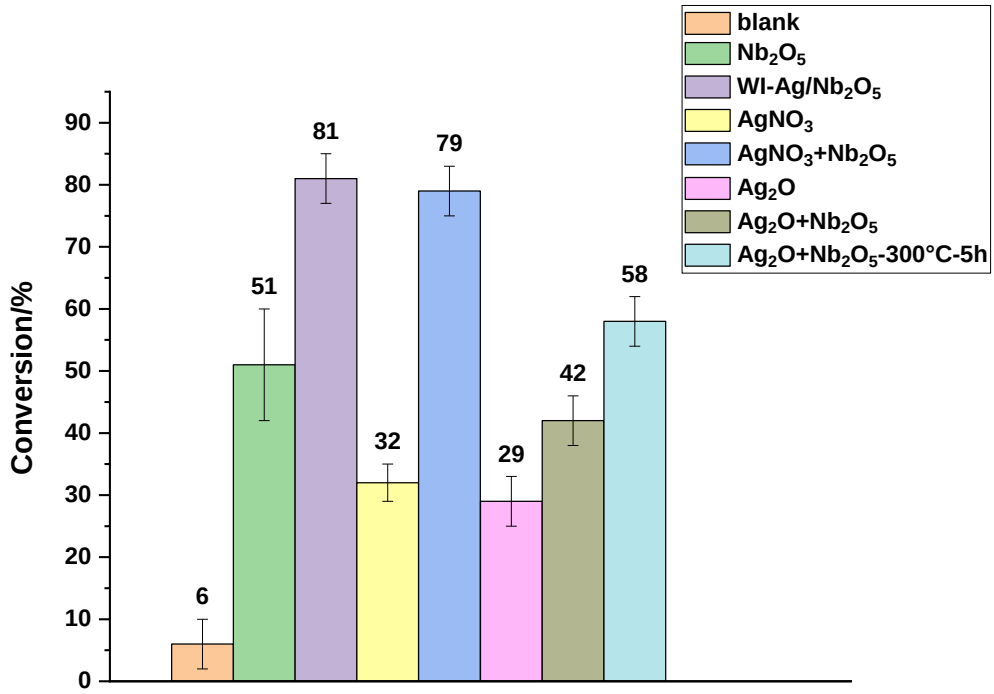

a. Conversion of cyclooctane from control tests for Ag species

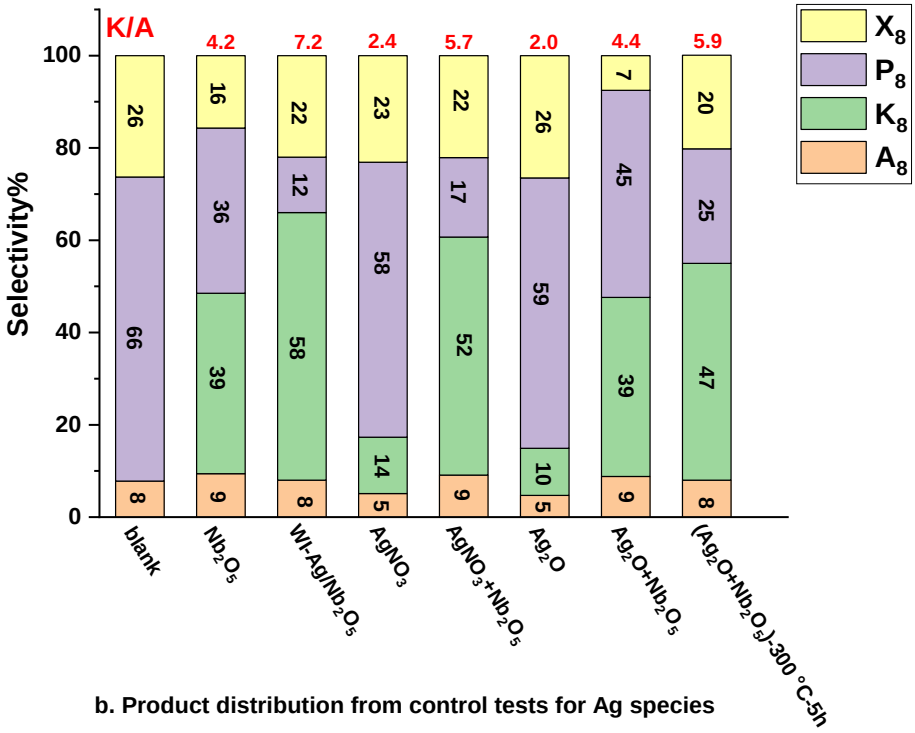

b. Product distribution from control tests for Ag species

Fig. 5.8 Reaction results from the control tests by various Ag species. a. Conversion of cyclooctane oxidation on the top; b. Selectivity of cyclooctane oxidation below. i) Nb_2O_5 with 99.9% grade; ii) WI-Ag/Nb_2O_5 prepared by wet impregnation method with 1 *wt*% Ag; iii) leached Ag tests by using $AgNO_3$-0.0010 g, leaching percent is 24% correspondingly; iv) $AgNO_3$+Nb_2O_5 was prepared by physical grinding with nominal 1 *wt*% Ag loading; v)Ag_2O with M(Ag):S ratio = 1:1000; vi) Ag_2O+Nb_2O_5 was prepared by was prepared by physical grinding of $AgNO_3$ and Nb_2O_5 with nominal 1 *wt*% Ag loading; vii) Ag_2O+Nb_2O_5-300 °C-5 h, mixture vi) was calcined furtherly at 300 °C for 5 h. Cyclooctane (3 mL), T = 110 °C, *P*(O_2) = 2 bar, t = 24 h.

It is possible to observe that the pure Ag_2O powder with M:S ratio = 1:1000 (Fig.5.8) is also reactive with a conversion of 29%, and it shows a high selectivity for cyclooctyl hydroperoxide (~ 60%). It also appears that the reactivity of Ag_2O is similar with that of $AgNO_3$, both of which display a higher selectivity for alkyl hydroperoxides with close conversion. Herein, it is worth noting that the dissociation of C-H bond in methane can be achieved by Ag^+ in Ag-Y[41] and Ag/ZSM-5[42], while this process cannot be activated

by metallic Ag cluster. The main Ag species exists in isolated Ag^+ state at a low metal loading in Ag/ZSM-5, which is capable of reacting with CH_4 to give a CH_3-zeolite complex and silver hydride species, as shown in scheme 5.1[42]. In view of this, one assumption is proposed that Ag^+ ion plays the roles of initiator for the dissociation of C-H bond in cyclooctane, which posing a promising application of Ag^+ in the oxidation of hydrocarbons. In addition, normally it is found that the activation of C-H via abstraction of H atoms can be achieved by an unsaturated metal centre in homogeneous catalysis[43], peroxide species like peroxyl or alkoxy radicals, superoxide species bound to metal centres or metal oxides[1, 44-46]. Based on the discussion about the activation of O_2 by supported Ag particles in chapter 1, thus we arrive at a conclusion that newly formed superoxide species from the activation of adsorbed oxygen species by Ag^+ sites can abstract C-H to initiate the reaction. And there are studies indicating inability of Ag-O to activate C-H bond in ethylene oxidation[44], which supports the explanation that the initiation of cyclooctane oxidation is due to superoxide species.

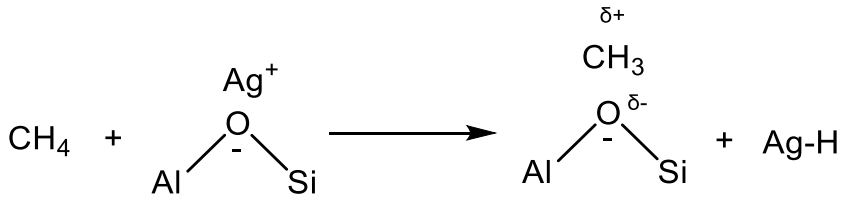

Scheme 5.1 An illustration for the activation of CH_4 by Ag^+ ions in Ag/ZSM-5. Reprinted with permission from 42. Copyright 2004 American Chemical Society.

Besides, we prepared sold mixtures of $AgNO_3$ and Ag_2O with Nb_2O_5 (sample iv. represents $AgNO_3$ + Nb_2O_5, sample *vi*. represents Ag_2O + Nb_2O_5) respectively by

physically grinding them together with a theoretical loading 1*wt*% Ag and tested the reactivity for cyclooctane oxidation. Results display that the conversion (79%) by catalyst sample iv is close to that of the simple adding of Nb_2O_5 (51%) plus leached Ag (32%), and this conversion is nearly identical with that of WI-Ag/Nb_2O_5. And sample *iv* shares a similar product distribution trend with WI-Ag/Nb_2O_5. In this case, it seems that the effects of WI-Ag/Nb_2O_5 on reaction process are from single activity of Nb_2O_5 and $AgNO_3$ respectively, where Ag^+ (free metal ion and Ag_2O) takes parts in the activation of oxygen to form superoxide oxygen species which is responsible for the formation of alkyl hydroperoxides and then Nb_2O_5 enhances the transformation of alkyl hydroperoxides to alcohols or ketones. However, it should be noted that WI-Ag/Nb_2O_5 has a higher K/A ratio and a lower selectivity for the alkyl hydroperoxide, indicating there exists synergy effects between Ag sites and Nb_2O_5 to affect selectivity, which is possibly correlated with supported Ag nanoparticles over the surface of Nb_2O_5. Therefore, supported Ag/Ag_2O nanoparticles in WI-Ag/Nb_2O_5 can affect the selectivity obviously in comparison of $AgNO_3$+Nb_2O_5 where there is no Ag nanoparticles present, as evidenced that the reactivity of Ag nanoparticle is dependent of the size[47, 48]. It is furtherly confirmed that the presence of Ag nanoparticles is important for a desirable generation of ketone.

Additionally, results from the tests by using Ag_2O and Ag_2O + Nb_2O_5 illustrates that the latter exhibits higher conversion and selectivity to alkyl cyclooctyl hydroperoxide, sharing similar changes between $AgNO_3$ and $AgNO_3$ + Nb_2O_5, implying the existence

of Nb_2O_5 could enhance the transformation of alkyl hydroperoxides to alcohols and ketones, which is consistent with our discussion in Chapter 4. Also, it is noted that there is improved conversion, and the selectivity for ketones increases with the decrease for alkyl hydroperoxides after calcination of Ag_2O + Nb_2O_5. As calcination process at 300 °C can facilitate the transformation from Ag_2O to Ag[49, 50], the finding proves that Ag^0 affects the oxidation. Meanwhile, calcined pure Nb_2O_5 exerts no obvious changes in comparison with that parent Nb_2O_5, which eliminates the effects of Nb_2O_5 due to the calcination. The conclusion correlates with the discussion about the presence of Ag nanoparticles (Ag^0) presented in WI-Ag/Nb_2O_5 has impact on reaction. Ultimately, we tend to believe that the presence of Ag^+ sites in WI-Ag/Nb_2O_5 could activate oxygen to form superoxide oxygen species to initiate the oxidation, or promote this process via a direct hydrogen abstraction, and deposited Ag(0) particle would affect the selectivity instead by selectively decomposing the alkyl hydroperoxide intermediate to preferentially form the ketone.

5.2.5 Catalytic performances of supported Ag/Nb_2O_5 prepared by different methods

As previously mentioned, there exists high Ag leaching (24%) into reaction mixture when employing WI-Ag/Nb_2O_5 prepared by wet impregnation method, which is a value too high to be acceptable (generally < 5%). According to leaching tests by using $AgNO_3$, Ag^+ exhibits reactivity for cyclooctane oxidation with a preference to produce alkyl hydroperoxides, and although the loss of active metal into the reaction mixture is

undesirable, the specific reactivity of Ag^+ can provide clues about the reaction mechanism as the data collected so far would suggest Ag^+ is capable to initiate the reaction, whereas Ag(0) particles is capable to selectively decompose the alkyl hydroperoxide (see section 5.3). That said, for the purposes to have a heterogeneous catalyst, the leaching phenomenon should be minimized, and in order to tackle this, we are briefly describing the possible sources here. Generally, the leaching of metal from the surface of support can be caused by attack from organic acids formed in the oxidation due to weak interactions between metal nanoparticles and support, or diffusion of free metal ions into solution phase during catalysis process[30]. For this reason, different preparation methods are adopted to control interactions between metal nanoparticles and support, as evidenced that the catalytic reactivity of supported Ag catalysts can be impacted by preparation method[51, 52].

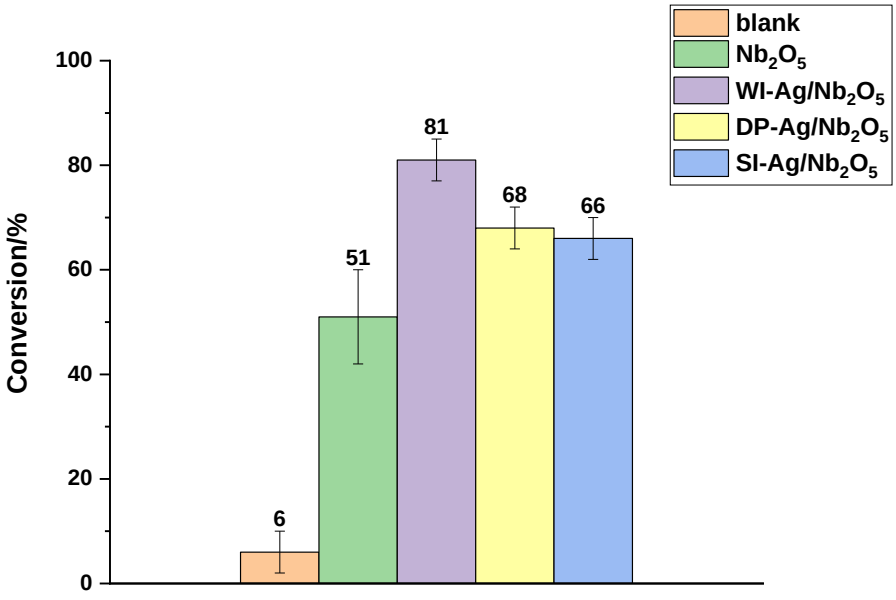

a. Conversion of cyclooctane by Ag/Nb_2O_5 prepared by different methods

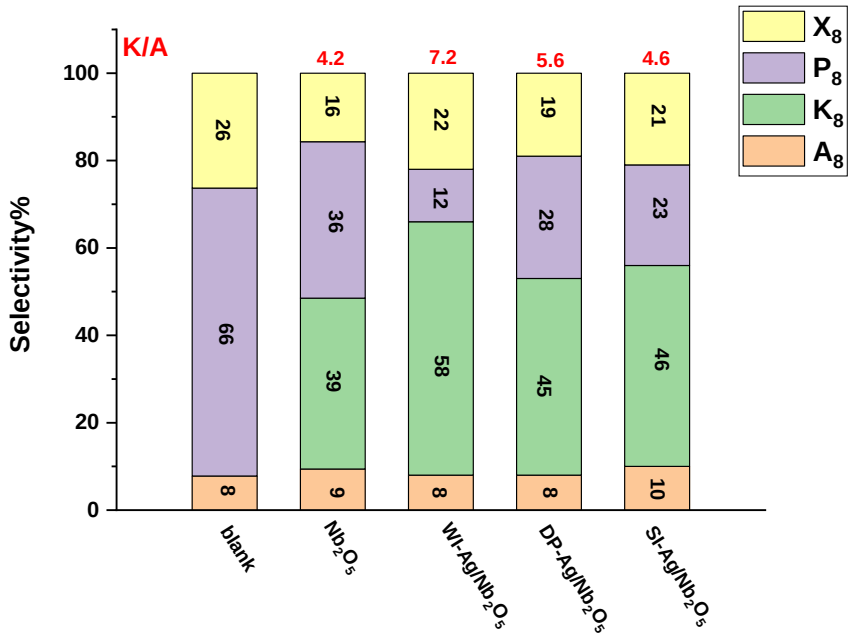

b. Product distribution of Ag/Nb_2O_5 prepared by different methods

Fig. 5.9 Reaction results of Ag/Nb_2O_5 prepared by different methods with nominal 1 *wt*% loading. a. Conversion of cyclooctane oxidation on the top; b. Selectivity of cyclooctane oxidation below. i) Nb_2O_5 with 99.9% grade/purity; ii) WI-Ag/Nb_2O_5 prepared by wet impregnation method; iii) DP-Ag/Nb_2O_5 prepared by deposition precipitation method; iv) SI-Ag/Nb_2O_5 prepared by sol immobilization protocol. cyclooctane (3 mL), M(Ag):S = 1:1000, T = 110 °C, $P(O_2)$ = 2 bar, t = 24 h.

The preparation method wet impregnation (WI), deposition precipitation (DP) and sol immobilization (SI) were separately employed to prepare supported Ag/Nb_2O_5 with 1 *wt*% loading. In the application of these catalysts for cyclooctane oxidation, the results (Fig. 5.9) illustrate that the conversions of DP-Ag/Nb_2O_5 (68%) and SI-Ag/Nb_2O_5 (66%) are similar (and practically identical within experimental error), both of which are slightly lower than that of WI-Ag/Nb_2O_5 (81%). In addition, the product distribution shows that the highest relative selectivity for cyclooctanone with K/A ratio up to 7.0 is obtained by WI-Ag/Nb_2O_5, while DP-Ag/Nb_2O_5 and SI-Ag/Nb_2O_5 have a similar K/A

ratio at ~5.0. Generally, particle size and morphologies of metal nanoparticles can be influenced by preparation method[38, 53], by which the order of the particles is usually WI (10 nm or even larger)> DP >SI (< 5 nm)[54]. However, in our case, the expected smaller size of Ag nanoparticles does not exhibit a higher reactivity, indicating that the size of nanoparticles is not a dominating factor in the oxidation, or this can be carried out by a wide range of particle size distributions. On the other hand, morphologies could exert effects on the reaction[55, 56]. In this case, the reaction performances are possibly influenced by morphologies of Ag nanoparticles. However, based on our conclusion that Ag^+ sites that are dispersed either on the support, or at the interphase in between support and nanoparticles, and these could play a role in activating the oxygen[38, 40, 57]; it is very likely that the already existed Ag in the oxidation state (Ag_2O or Ag^+) in WI-Ag/Nb_2O_5 and the leached amount of Ag^+ into reaction solution enhance oxidation in return, which explains the higher reactivity by WI-Ag/Nb_2O_5. The same behaviour is observed in Ag/CeO_2 prepared by impregnation and deposition precipitation method applied for the oxidation of propylene and carbon monoxide, but the promotion effects are due to the presence of Ag^{2+} which leads to the formation of three different redox couples (Ag^{2+}/Ag^+, Ag^{2+} / Ag^0, and Ag^+/Ag^0), which makes the impregnated solid more efficient with only one pair (we postulate Ag^+/Ag^0) for the sample prepared by DP[57-59]. Usually the amount of Ag^{2+} would be less because Ag^{2+} species are unstable and often requiring a high calcination temperature (> 400 °C) and the presence of Ag^{2+} is usually in minor concentrations[57, 60]. In addition, it is expected that a higher Ag loading of WI-Ag/Nb_2O_5 also contributes to the improved conversion, as an amount of metal is lost

in the filtration step when employing DP or SI protocol (see section 2.2.1 in chapter 2), which is confirmed by TEM (see section 5.2.6.2).

Analysis for Ag leaching by ICP-MS shows that it decreases dramatically by using DP method and SI protocol (table 5.2), especially for SI-Ag/Nb_2O_5 with only 0.2% leaching Ag. This infers that the preparation method could evidently enhance the interaction between Ag nanoparticles and Nb_2O_5 to avoid the release from surface mainly due to the attack of organic acids. Tests by using concentrated HNO_3 to dissolve Ag/Nb_2O_5 also confirms this (section 3.4.1), which indicates that there is only 0.2% observed Ag into the solution for SI-Ag/Nb_2O_5, which is lower than that of WI-Ag/Nb_2O_5 (0.7%) and DP-Ag/Nb_2O_5 (0.5%), exhibiting a strong resistance from acid erosion. From this perspective, we can conclude that the deposition precipitation and sol immobilization protocol could diminish leaching issues obviously, especially by using the latter. However, it should be stressed that WI-Ag/Nb_2O_5 exhibits the 'highest' reactivity and better selectivity for ketone production, experimental evidence that our data suggest being attributed to be the presence of Ag^+ sites (Ag_2O). From this perspective, the promotion effects of Ag^+ should be considered in catalysis process, maybe by considering by-functional catalyst, that is with an oxidation state promoting the initiation, and another oxidation state promoting the selective decomposition of the alkyl hydro peroxide intermediate.

Table 5.2 ICP-MS analysis for Ag leaching in reaction mixture for cyclooctane oxidation. Ag^+ was extracted by extracting 1 mL of reaction mixture into 10 mL deionised water and then analysed the amount of Ag using ICP-MS.

Catalysts	Ag:S	Leaching of Ag /%
WI-Ag/Nb_2O_5	1:1000	24.2
DP-Ag/Nb_2O_5	1:1000	3.2
SI-Ag/Nb_2O_5	1:1000	0.2

5.2.6 Characterization of Ag/Nb_2O_5 catalysts

According to above discussion, supported Ag/Nb_2O_5 exhibits obviously enhanced conversion of cyclooctane with a higher selectivity for cyclooctane, which exerts potential promising prospects for the oxidation of hydrocarbons. In addition, the supported Ag/Nb_2O_5 prepared by different methods demonstrates the differences of reaction behaviours and leached Ag could be decreased by adopting deposition precipitation method and sol immobilization protocol. Therefore, in order to furtherly clarify the reason for changes of catalytic reactivity related with the properties of catalysts, the characterization techniques powder X-ray diffraction (XRPD), transmission electron microscopy (TEM), and X-ray photoelectron spectroscopy (XPS) were employed.

5.2.6.1 XRPD patterns of WI-, DP- and SI-Ag/Nb_2O_5

The standard XRD pattern of Ag (JCPDS file: 65-2871) displays the characteristic peaks of Ag located at 2θ= 38.1°(plane 111), 44.2°(200), 64.4°(220), 77.6°(311), 81.6°(222)[61-64]. The XRPD patterns show that no additional peaks are observed in all the Ag/Nb_2O_5 in comparison with that of undoped Nb_2O_5. It is reported that the intensity

of characteristic Ag peaks (2θ =38.14° and 44.33°) increases with the increase of Ag loading[65, 66] and particle size. And no characteristic peaks of Ag_2O (2θ =27.9°(110), 32.2°(111), 46.3°(211))[67] are observed. In our case the metal loading is probably too low to observe any reflections from doped Ag. And the high dispersion of the silver particle could also make it non-detectable with the XRPD technique[68-70]. Previous research shows that metal loading is an important parameter to affect the reaction, but the excessive amount of loaded metal may cause the bulk monolayer due to the aggregation of nanoparticles, which may cause the loss of reactivity even inactivity of the catalysts.[71-73] Based on this perspective and the economic factors, lower loading of metal is preferred if the reactivity of catalyst can be achieved. Thus, in our case, 1 *wt*% loading was selected.

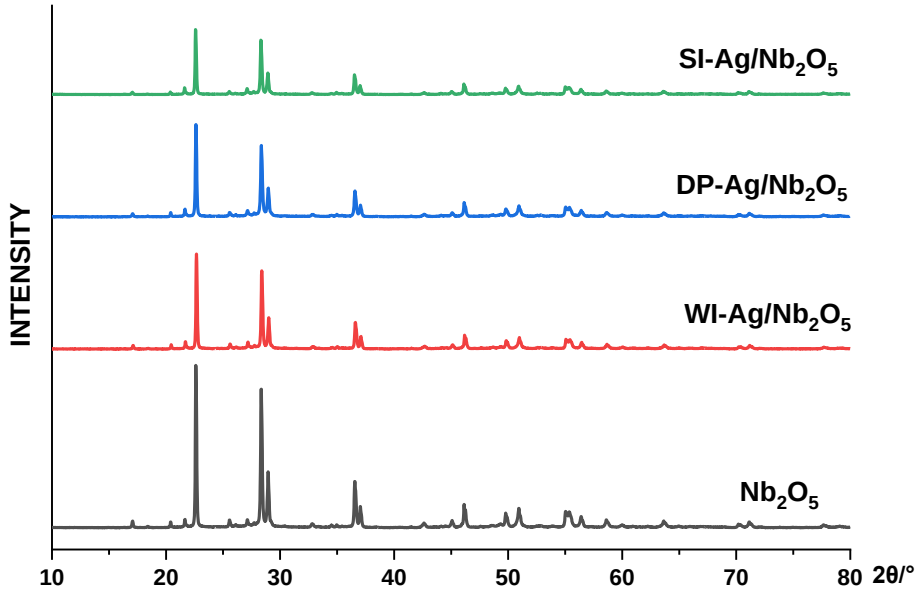

Fig. 5.10 XRPD patterns of Ag/Nb_2O_5 with nominal 1 *wt*% loading prepared by different preparation methods. Nb_2O_5 (99.9% grade) was used. All Ag/Nb_2O_5 catalysts were calcined at 180 °C for 16 h.

5.2.6.2 Transmission electron microscopy (TEM) images of Ag/Nb_2O_5

In order to further correlate the catalytic activity of Ag/Nb_2O_5 prepared by different methods (WI-, DP- and SI-) in cyclooctane oxidation to the catalyst properties (e.g., the amount of supported Ag, particle size), TEM analysis for the catalysts were carried out, as shown in Fig. 5.11. A relatively uniform dispersion of supported Ag/Ag_2O nanoparticles with the size from 2-5 nm is observed in the impregnated catalyst, with a large portion that accounts for around 85% (shown in a6). There exist larger nanoparticles in the size range from 10 to 20 nm, however imaging also illustrates the aggregation of Ag/Ag_2O nanoparticles (a3 and a4). As comparison, a higher and denser metal loading is observed in WI-Ag/Nb_2O_5 comparing with DP- and SI-Ag/Nb_2O_5 (a2, b2 and c2), and the result is also corresponding with the ICP-MS analysis for Ag content in Ag/Nb_2O_5 attacked by concentrated HNO_3 (see chapter 3.4.1), which can contribute to a higher conversion by WI-Ag/Nb_2O_5 as observed in Fig. 5.9. A more uniformly distribution of particles is found in DP- and SI-Ag/Nb_2O_5 compared with WI-Ag/Nb_2O_5. Most of the particles uniformly fall within a size range of below 2 nm in DP-Ag/Nb_2O_5 while larger particles appear in the size range of 2.5-5.0 nm and several particles bigger than 8 nm are found to be deposited separately, which is displayed by Ag imaging (b3). Whereas in SI-Ag/Nb_2O_5, almost all the particles are uniformly dispersed within the narrow range of 2-3 nm, justifying that this protocol can generate small and homogeneously distribution of nanoparticles[74].

In addition, the interface between Ag/Ag_2O particles and Nb_2O_5 seems to be planar and clean in WI-Ag/Nb_2O_5 (a5), while an epitaxial orientation relationship with Nb_2O_5 is shown in DP-Ag/Nb_2O_5 (b5 and b6), by which we assume that the lower Ag leaching (table 5.2) from DP catalyst in oxidation can be attributed to this metal support interaction. Moreover, it is found that the reduction treatment for WI-Ag/Nb_2O_5 leads to the size decrease of particles, most of which fall in the range of 1.5-3 nm. We believe this involves the reduction of Ag_2O to Ag with a smaller size, which in return can be as an evidence for the existence of Ag_2O in impregned catalyst.

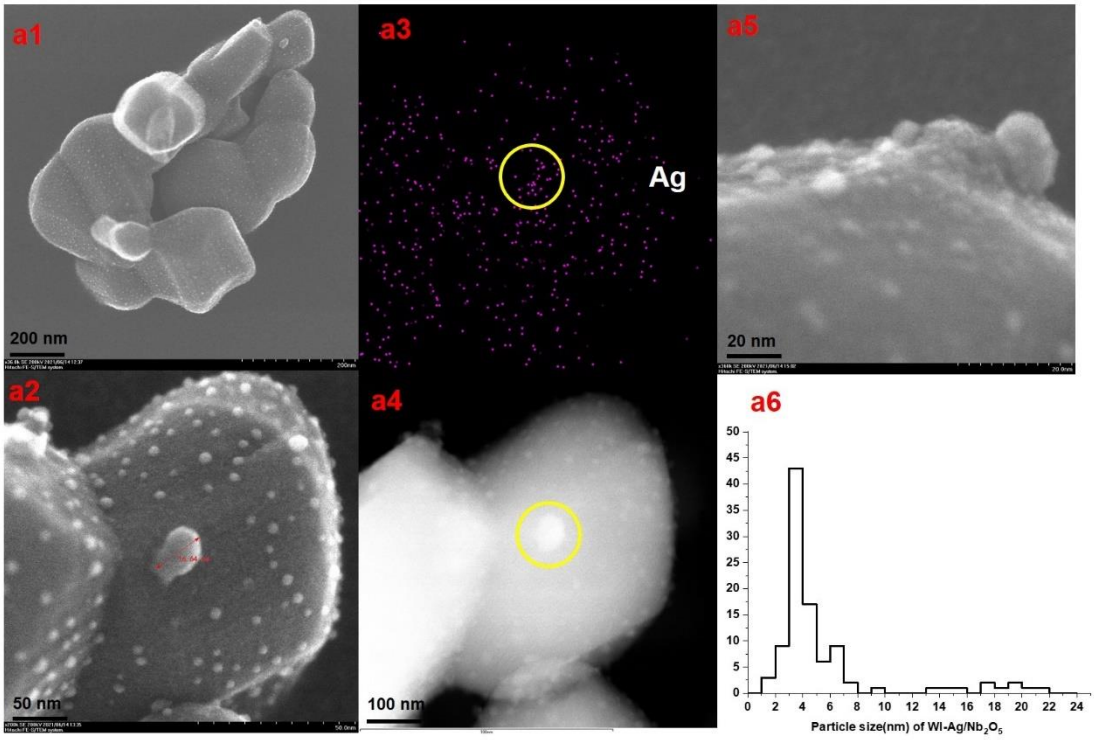

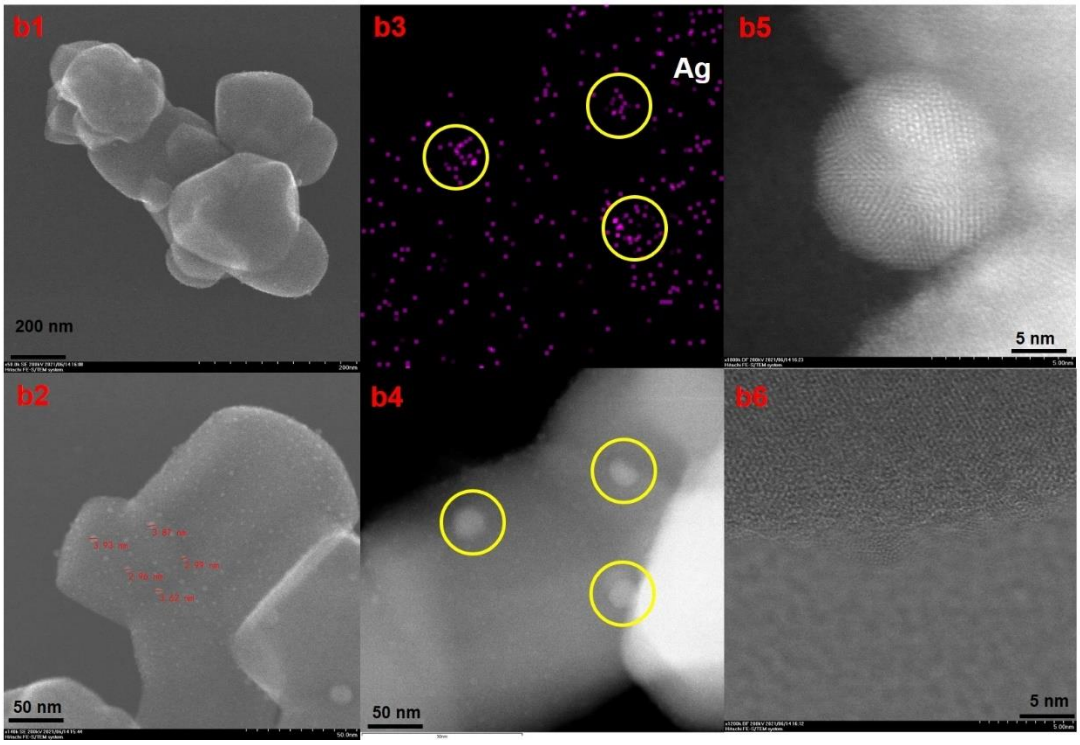
b1
200 nm
b3
Ag
b5
5 nm
b2
50 nm
b4
50 nm
b6
5 nm

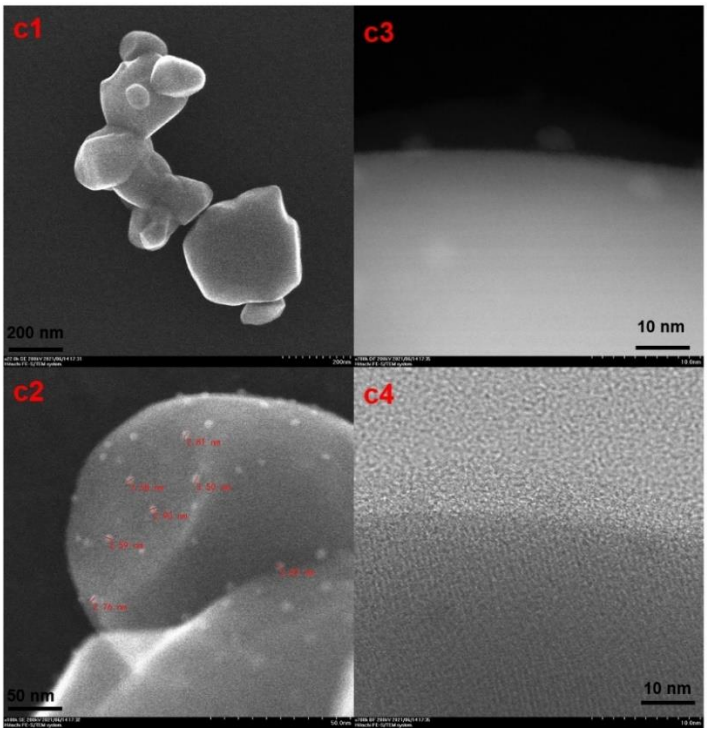
c1
200 nm
c3
10 nm
c2
50 nm
c4
10 nm

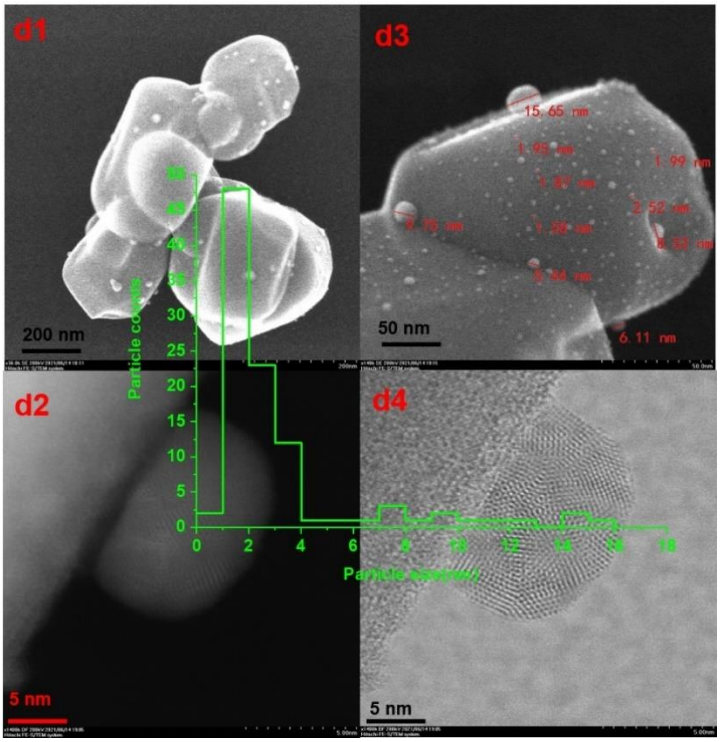

Fig. 5.11 Representative TEM images of Ag/Nb_2O_5 (1 *wt*% loading) prepared by different protocols and EDX mapping for Ag nanoparticles (a3 and b3). a1-a6: $WI\text{-}Ag/Nb_2O_5$; b1-b6: $DP\text{-}Ag/Nb_2O_5$; c1-c4: $SI\text{-}Ag/Nb_2O_5$; d1-d4: the reduction of $WI\text{-}Ag/Nb_2O_5$ by H_2. The count for the distribution of particle size was obtained from a set of 100 particles in each catalyst.

5.2.6.3 X-ray photoelectron spectroscopy of $WI\text{-}Ag/Nb_2O_5$

As we assume that a higher activity by $WI\text{-}Ag/Nb_2O_5$ can be attributed to the presence of Ag_2O particles and TEM analysis implies the presence of Ag_2O particles in $WI\text{-}Ag/Nb_2O_5$, XPS was employed for the study about the oxidation state of Ag species in this catalyst, which is displayed in Fig. 5.12. Both catalysts exhibit peaks diagnostic of Ag 3d 5/2 and 3d 3/2 components with binding energy at 368.4 eV and 374.2 eV respectively [75, 76] (Fig. 5.12-a1 and b1). In contrast there are no observed peaks for Ag_2O even with a higher loading 5 *wt*%, which is usually displayed at 367.7 eV (3d 5/2) and 373.7 eV (3d 5/2)[77, 78], indicating that the supported Ag mainly exists

in the state of Ag(0) in WI-Ag/Nb_2O_5. It is likely that there is no trace of Ag_2O or possibly caused by a low signal for Ag_2O with a very low exposed metal fraction[79], as the case in XRPD analysis (Fig. 5.10). It is possible to observe a small decrease in atomic concentration of O 1s at 530. 3 eV and Nb 3d at 207.2 eV in WI-Ag/Nb_2O_5 with 5 *wt*% Ag loading, that could be attributed to the formation of oxygen vacancies in Nb_2O_5, as evidenced that the addition of Ag into CeO_2/TiO_2 could lead to the formation of oxygen vacancies[13].

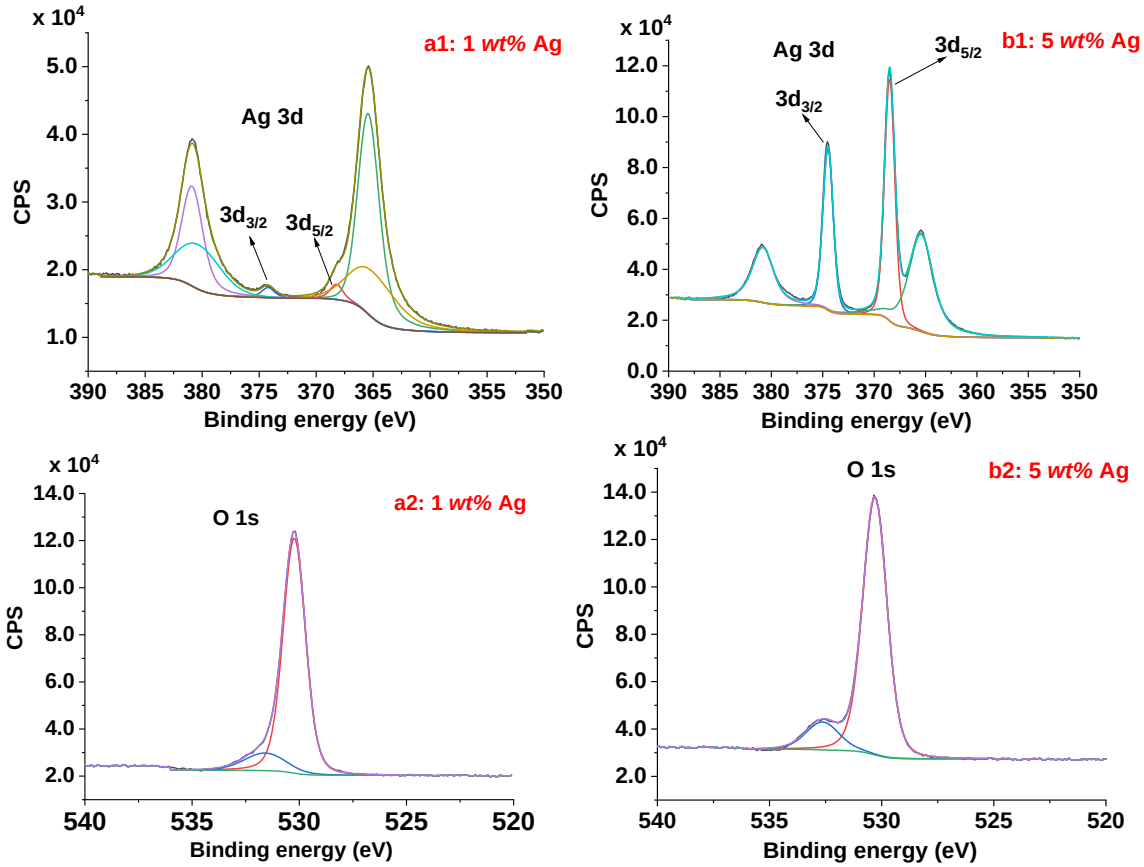

Fig. 5.12 XPS spectra and peak fitting of the O 1s and Ag 3d region for WI-Ag/Nb_2O_5 with 1 *wt*% (a1 and a2) and 5 *wt*% (b1 and b2) loading respectively. 5 *wt*% WI-Ag/Nb_2O_5 was used to magnify the signal of corresponding Ag peaks for the explanation of the possible state of Ag, especially for Ag^+.

Table 5.3 XPS analysis of composition ratio for Nb_2O_5, WI-Ag/Nb_2O_5 with 1 *wt*% and 5 *wt*% Ag loading respectively, by deconvolution Ag 3d and O 1s signals.

Sample	Elements	Position, binding energy, eV	Atomic Concontration%
Nb_2O_5	C 1s	284.8	5.3
	C 1s	286.6	1.4
	C 1s	288.9	1.3
	O 1s	530.3	55.7
	O 1s	531.5	7.8
	Nb 3d	207.2	28.5
WI-Ag/Nb_2O_5 1 *wt*% Ag	C 1s	284.8	5.6
	C 1s	286.5	1.5
	C 1s	288.9	1.2
	O 1s	530.2	55.5
	O 1s	531.6	7.6
	Nb $3d_{5/2}$	207.2	28.1
	Ag $3d_{5/2}$	368.2	0.3
	Ag $3d_{3/2}$	374.2	0.2
WI-Ag/Nb_2O_5 5 *wt*% Ag	C 1s	284.8	3.6
	C 1s	286.4	1.1
	C 1s	288.7	0.8
	O 1s	530.3	51.6
	O 1s	532.6	7.7
	Nb $3d_{5/2}$	207.1	23.7
	Ag $3d_{5/2}$	368.5	6.9
	Ag $3d_{3/2}$	374.5	4.6

5.2.7 Reactivity of supported Ag over different metal oxides prepared by wet impregnation method

As previously described, a support can exert various effects, for example, improving the stability of metal nanoparticles against sintering and aggregation; or providing oxygen vacancies that could play a role in oxidation reaction; affecting physical properties of metal nanoparticles[56]. In heterogeneous catalyst for supported metal nanoparticles, and especially for oxidation reactions, common supports are TiO_2[3,

[80], CeO_2[57, 81], MgO[54], SiO_2[39, 65]. As such, and in order to assess if is there any metal support interaction effect (see section 4.6), the various metal TiO_2, CeO_2, MgO, SiO_2 were also tested for our oxidation reaction and different M:S ratios are applied in the oxidation of cyclooctane and cyclohexane respectively. We anticipate that a promising prospect for the use of Nb_2O_5 in the oxidation to produce ketones or alcohols. This is relevant, as there is not much evidence veiling the performances of Nb_2O_5 as support in the oxidation of hydrocarbons with molecular oxygen directly without the presence of additives, and as such with implications beyond the current studies. For our comparisons the catalysts were mainly prepared by wet impregnation method as it is the most straightforward (see chapter 2, section 2.2.1 and 2.2.2).

5.2.7.1 Comparison of catalytic performances for supported Ag over different metal oxides

The results for the oxidation of cyclooctane (Figure 5.13) indicate that all of prepared catalysts can obviously enhance the conversion of cyclooctane, among which supported Ag over Nb_2O_5, MgO and CeO_2 have similar values (approximately 80%) and Ag/SiO_2 shows lowest conversion in comparison with others, while it is observed that Ag/Nb_2O_5 and Ag/CeO_2 also share similar products distribution with alcohols and ketones as major products (Fig. 5.13-b). Together with the reaction data of pure support with various M:S ratios in cyclooctane oxidation from section 4.6.1, it is possible to conclude that Nb_2O_5 can participate in the oxidation process like CeO_2, which indicates that the active oxygen species can be generated from surface

chemisorbed molecular oxygen, as demonstrated in the studies about CeO_2 as support[12]. Additionally, the existence of Ag particles can improve the selectivity to a ketone with higher K/A ratio, especially for calcined Ag/Nb_2O_5, by which K/A ratio can be up to 7.2. Whereas supports like MgO and SiO_2 appears to be both as inert in the oxidation, thus the observed changes in the catalytic performances in the presence of Ag/MgO and Ag/SiO_2 can be attributed to the existence of silver particles, but product distribution demonstrates that the major product is alkyl hydroperoxide intermediate when using Ag/MgO, which although it can provide some mechanistic information, it does not promote high yields of ketones or alcohols.

However, as the support can affect the properties of nanoparticles, and despite our calcination temperature does promote the decomposition of any Ag_2O to Ag, we nevertheless considered the experimental procedure to carry out a reduction of catalysts by H_2 can furtherly facilitate the transformation of Ag from oxidation state (Ag_2O) to metallic Ag^0 state[40, 82]. It also should be noted that the reduction process (200 °C for 0.5 h) may also lead to the sintering of supported metal nanoparticles at the same time. By comparing the reaction performances before and after reduction by H_2/N_2 in Fig. 5.13, the conversions are identical within the experimental error, for Ag/Nb_2O_5, Ag/TiO_2, Ag/MgO and Ag/CeO_2 while it decreases in the presence of Ag/SiO_2, and there are obvious differences of product distribution. It is observed that the selectivity to cyclooctane decreases and the one for cyclooctyl hydroperoxide increases at the same time for Ag/MO_x(M=Nb, Ce, Ti, Si), which tentatively ascribed

to the changes of the oxidation state of Ag species from Ag_2O to metal Ag (this is speculated by changes in catalyst's colour from lightly grey to light purple for Ag/Nb_2O_5, which would correspond to the plasmon resonance of Ag(0)[83, 84]. Another option could be a change of particle size. Therefore, the results confirm that the presence of Ag^+ species (Ag_2O) in Ag/Nb_2O_5 prepared by wet impregnation method could affect selectivity in comparison with that of SI-Ag/Nb_2O_5 prepared by sol immobilization protocol as there may exist only reduced Ag for the latter method[54]. Besides, very similar catalytic performances between Ag/Nb_2O_5 and Ag/CeO_2 were detected before and after reduction which could also implies that the metal oxides behave similar in the oxidation process due to the presence of oxygen vacancies.

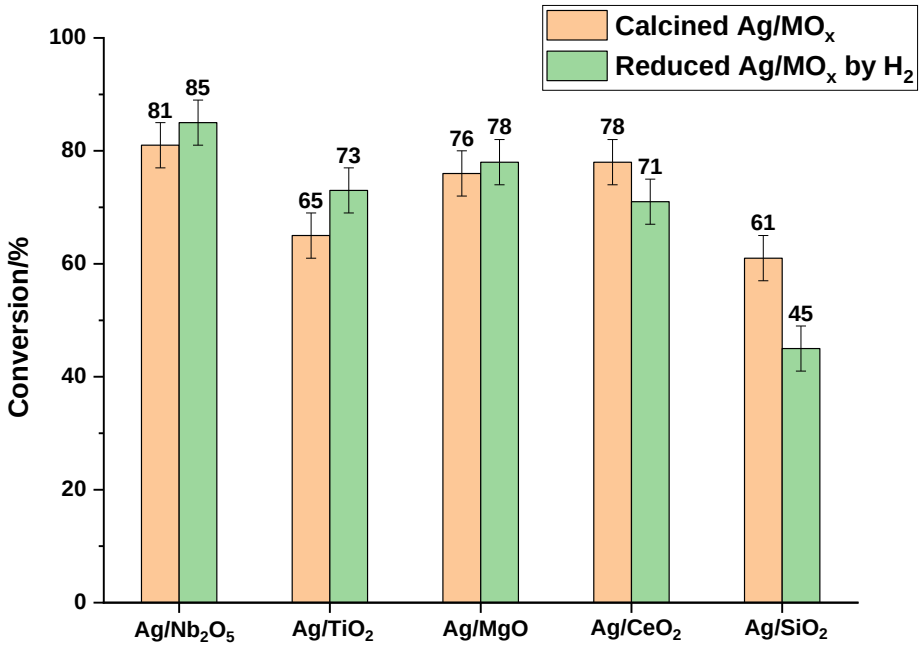

a. Conversion of cyclooctane by supported Ag over supports

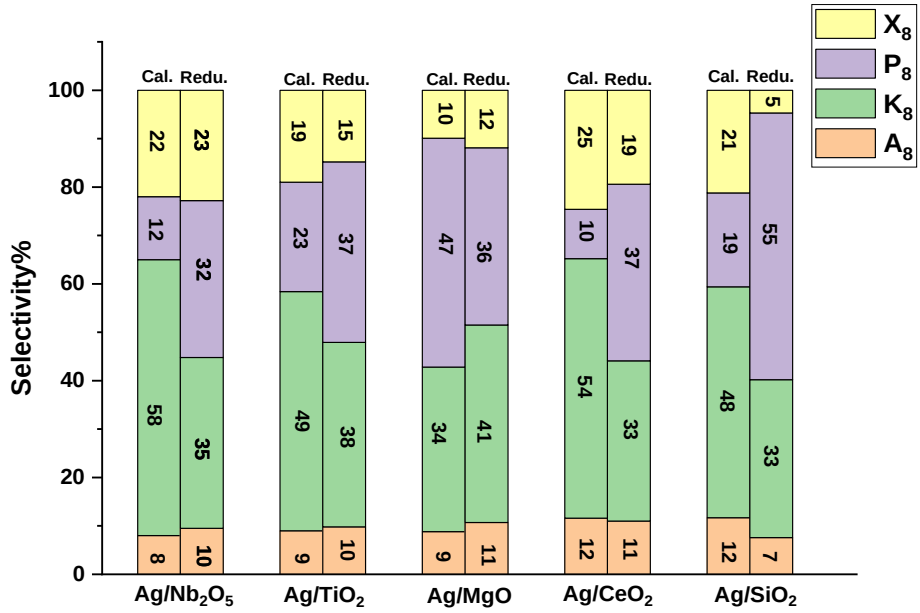

b. Product distribution by supported Ag over supports

Fig. 5.13 Reactivity of supported Ag with 1 *wt*% Ag loading over various metal oxides (Nb_2O_5, TiO_2-P25, MgO, CeO_2, SiO_2) prepared by wet impregnation method. a. Conversion of cyclooctane oxidation by Ag/MeO_x on the top; b. Selectivity of cyclooctane oxidation by Ag/MeO_x. Tests were conducted at 110 ˚C at 2 bar O_2 for 24 h with M:S ratio=1:1000, 3 mL cyclooctane used. Calcined Ag/MO_x (Cal.) was prepared at 180 ˚C for 16 h and reduced Ag/MO_x (Redu.) was reduced at 200 ˚C for 0.5 h in 5 % H_2/N_2 atmosphere.

5.2.7.2 ICP-MS analysis for determination of Ag leaching

An analysis for leaching including both the supported metal and the support was carried out (table 5.4 and Fig.5.14). With the only exception of Ag/MgO, the reduction treatment significantly reduced the leaching of Ag by a factor of 2 or 3. This effect can tentatively be explained by that Ag may be less prone to leaching than Ag_2O, especially when organic acids are formed during the reaction. Also, the difference of selectivity could be correlated with the leached Ag into reaction resolution, which has been discussed that presence of Ag^+ can activate O_2 to facilitate the formation of alkyl

hydroperoxides or activate C-H bond. With respect to the metal oxide support, instead, all the supports that we tested are suitable for this scope but MgO. This oxide is very basic compared to the others that we have used, and it may be attacked by organic acids in solution, even in small amount.

Table 5.4 ICP-MS data from cyclooctane oxidation with Ag/MOx with nominal 1 *wt*% loading prepared by wet impregnation method. Sample collected via solvent exchange with denoised water. Reaction conditions: M:S = 1:1000, T =110 ˚C, $P(O_2)$ = 2 bar, t = 24 h.

Catalyst	Conversion %	Leaching-Ag %	Leaching-support metal %
Cal.-WI-Ag/Nb_2O_5	81	24.0	--
Cal.-WI-Ag/TiO_2	65	10.6	$2.1 \cdot 10^{-4}$
Cal.-WI-Ag/CeO_2	78	12.7	$1.4 \cdot 10^{-3}$
Cal.-WI-Ag/MgO	76	0.6	$4.6 \cdot 10^{-1}$
Cal.-WI-Ag/SiO_2	61	3.1	$3.8 \cdot 10^{-2}$
Redu.-WI-Ag/Nb_2O_5	85	5.0	$3.2 \cdot 10^{-4}$
Redu.-WI-Ag/TiO_2	73	9.3	$1.7 \cdot 10^{-4}$
Redu.-WI-Ag/MgO	78	4.4	1.4
Redu.-WI-Ag/CeO_2	71	1.6	$1.8 \cdot 10^{-4}$
Redu.-WI-Ag/SiO_2	45	0.3	$2.4 \cdot 10^{-2}$

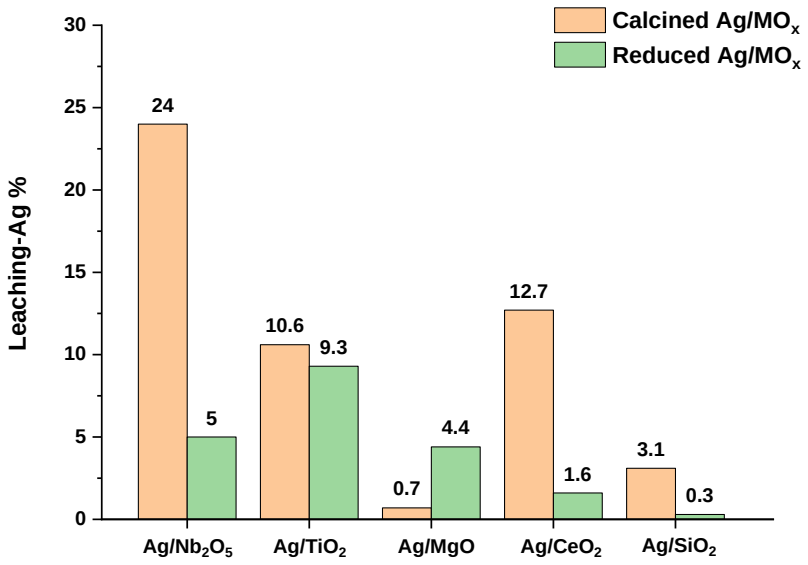

Fig. 5.14 Comparison of leaching Ag in reaction mixture from catalysts Ag/MO_x before and after reduction by 5% H_2 in H_2/N_2.

5.2.7.2 XRPD pattern of Ag/Nb_2O_5 reduced by H_2

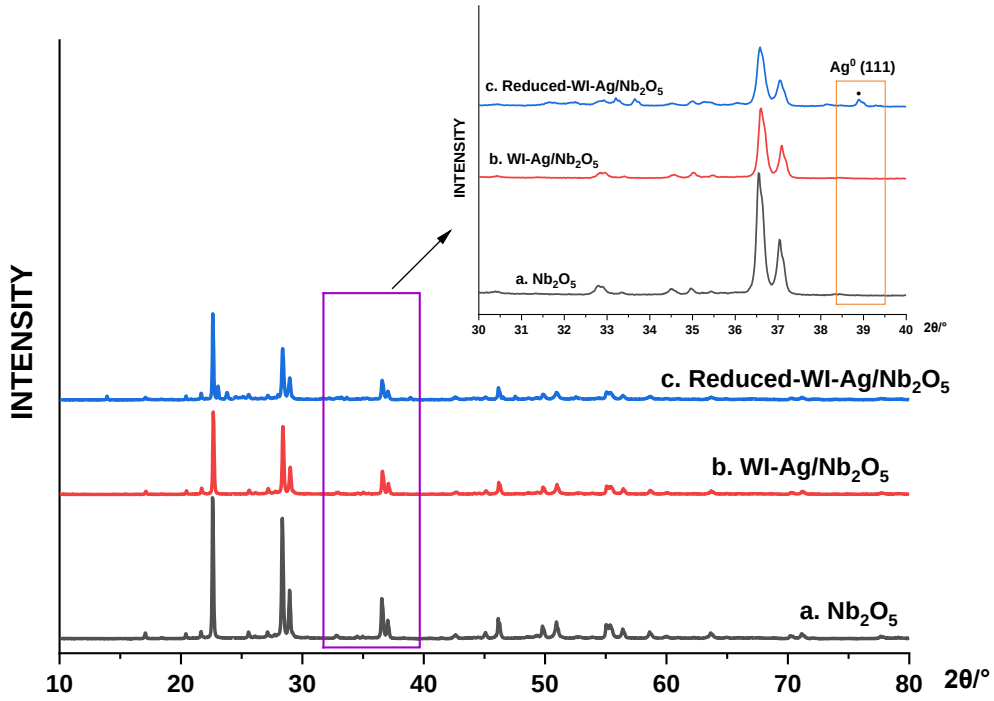

Fig. 5.15 XRPD patterns of Ag/Nb_2O_5 with nominal 1 *wt*% loading prepared by wet impregnation method. a. Nb_2O_5 with 99.9% purity/grade was used; b. WI-Ag/Nb_2O_5 catalyst was calcined at 180 °C for 16 h; c. Reduced-WI-Ag/Nb_2O_5 was prepared by 5% H_2 in H_2/N_2 reduction of WI-Ag/Nb_2O_5 at 200 °C for 0.5 h.

Fig. 5.15 shows XRPD patterns obtained for WI-Ag/Nb_2O_5 before and after reduction, which illustrates that the sample reduced by H_2 displays a peak at $2\theta = 38.5°$ corresponding to the (111) plane on which intact O_2 can exist in both physiosorbed and chemisorbed states[13], which is a characteristic peak of Ag^0 reflection. Thus, it is very likely that the reduction process facilitates the transformation from Ag_2O to Ag^0, and the presence of relatively higher amount of Ag^0 enables it to be detected with the XRPD technique. In addition, the high dispersion of silver particles could make it non-detectable by XRPD[68] and it is possible that the reduction process leads to the

aggregation of Ag particles[68], which is possibly evidenced by the colour changes from light grey to purple that also can be an indicative of the changes of particle size, causing the identification of Ag^0 in XRPD patterns.

In addition, the XRPD (Fig.5.16) patterns of DP-Ag/Nb_2O_5 synthesized by deposition precipitation method illustrates that no diffraction peaks of Ag are observed after reduction. Perhaps there are no oxidation state changes in the reduction process by H_2, and the low loading of Ag leads to be unidentified in the collected XRPD patterns. The results furtherly justify the difference of catalytic reaction performances between WI-Ag/Nb_2O_5 and DP-Ag/Nb_2O_5 due to the dispersion of Ag species with different valances.

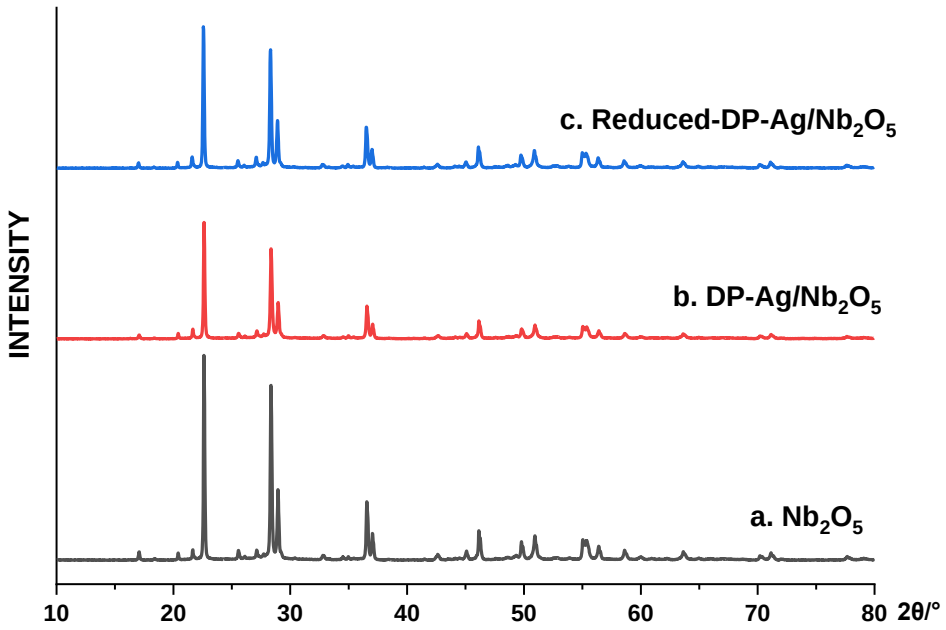

Fig. 5.16 XRPD patterns of Ag/Nb_2O_5 with nominal 1 *wt*% loading prepared by different preparation method. a. Nb_2O_5 with 99.9% purity/grade was used; b. DP-Ag/Nb_2O_5 catalyst was calcined at 180 °C for 16 h; c. Reduced-DP-Ag/Nb_2O_5 was prepared by 5% H_2/N_2 reduction of DP-Ag/Nb_2O_5 at 200 °C for 0.5 h.

5.3 Decomposition of 1-phenylethyl hydroperoxide

As discussed in chapters 1 and 3, alkyl hydroperoxides (R-OOH) are important intermediate in the oxidation of hydrocarbons, especially when this occur via a free-radical pathway and they are formed by the reaction between alkyl radicals (R·) and O_2 to form peroxyl radical species (ROO·) with hydrocarbons (R-H) in autoxidation, which is thermodynamically and kinetically unstable to be decomposed to alcohols and ketones as well as by-products like esters, organic acids[85]. At present, studies are mainly focused on the reaction pathway and mechanism of the various catalysts in the direct oxidation of hydrocarbons, while the decomposition of alkyl hydroperoxide has received limited attention as this species with the presence of α-H on near C-OOH is easily to be autoxidised under normal conditions. A combined theoretical and experimental study about the transformation of cyclohexyl hydroperoxide is conducted in the presence of CeO_2 nanoparticles, revealing the decomposition process can proceed over a low-coordinated Ce^{4+} centre to give cyclohexanone[86]. It would therefore be useful to study the decomposition pathway either catalysed or not of an alkyl hydroperoxide, and to use this as a substrate rather than to obtain this as intermediate. As the synthesis of cyclooctyl hydroperoxide is challenging, but there are instead, protocols[87] for the synthesis of phenyl ethyl hydroperoxide, which is also of relevance for the current thesis work, we then synthetized and used as a substrate ethyl hydroperoxide in the presence and absence of a catalyst to assess its evolution to a ketone or an alcohol.

As we wanted to investigate of the reactivity of both Nb_2O_5 and Ag towards the decomposition of phenyl ethyl hydroperoxide, we preliminary carried out blank autoxidation tests in the absence of any catalyst. For this scope, a reaction temperature of 82 °C was selected according to previous research within our group about the oxidation of ethylbenzene by niobium oxide based catalysts[88], which indicates that 1-phenylethyl hydroperoxide is the major product from ethylbenzene oxidation at this temperature. Tests were firstly conducted at 82 °C under 2 bar N_2 or O_2 by adding 100 µL 1-phenylethyl hydroperoxide and 2 mL benzotrifluoride as solvent (inert for the reaction). The use of a solvent was introduced to mitigate the lengthy process of the synthesis of 1-phenylethyl hydroperoxide with only very minor amount produced. Under our experimental conditions and given the molecular structure of 1-phenylethyl hydroperoxide, we expect a reaction mixture containing this substrate and the corresponding ketone (acetophenone) and alcohol (1-phenyl ethyl alcohol). An NMR spectrum is displayed in Fig. 5.17, which reveals the corresponding characteristic peaks of 1-phenylethyl hydroperoxide (5.1 ppm 1H, 1.5ppm 3H), acetophenone (8.0 ppm 2H, 2.6 ppm 3H), 1-phenylethanol (4.9 ppm 1H), as shown in the spectrum.

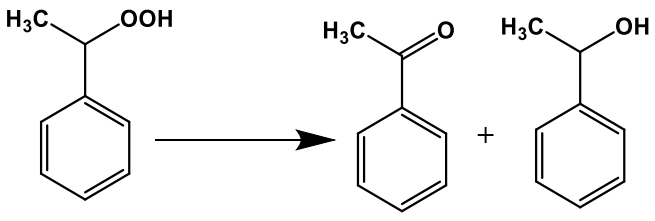

Scheme 5.2 A simplified pathway of 1-phenylethyl hydroperoxide decomposition.

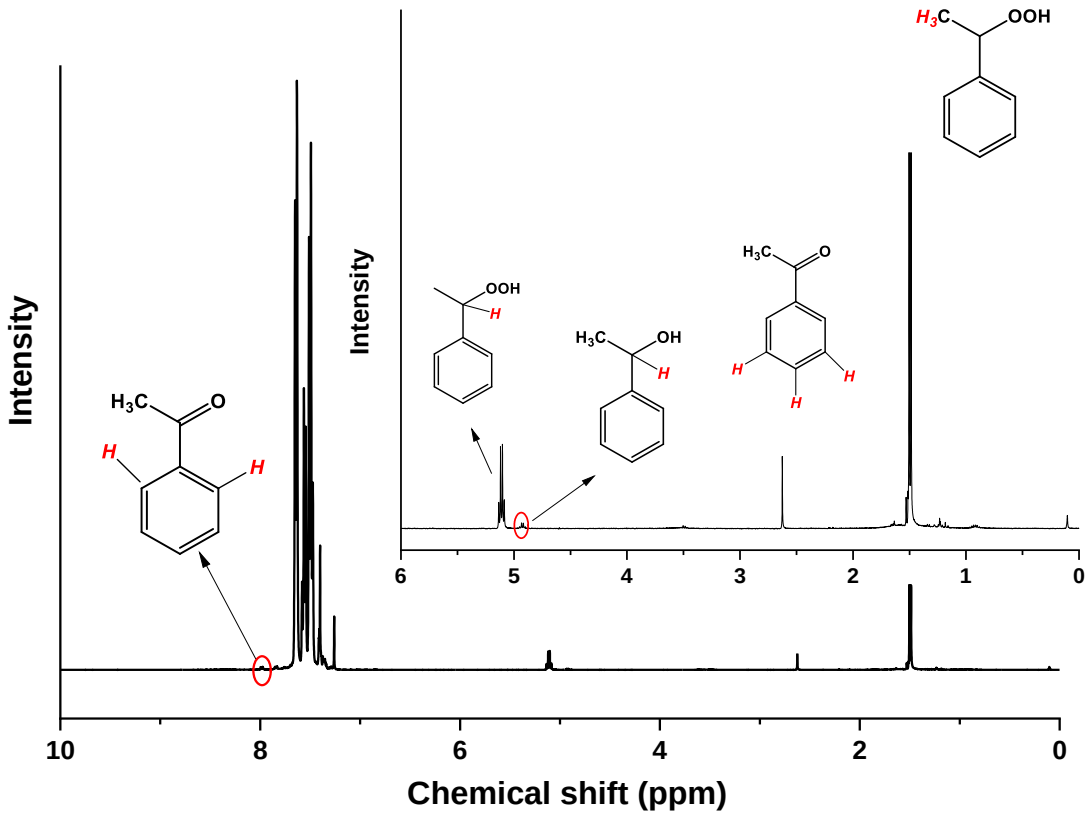

Fig. 5.17 NMR spectrum for the reaction mixture obtained from decomposition of 1-phenylethyl hydroperoxide in the presence of WI-Ag/Nb_2O_5 at 2 bar N_2 at 82 ˚C for 36 h. M(Ag):S=1:100.

5.3.1 Decomposition of 1-phenylethyl hydroperoxide in N_2

Before the tests, the purity of 1-phenylethyl hydroperoxide was verified by NMR, which is around 93% due to presence of acetophenone, 1-phenylethanol (assuming the ketone and alcohol as products). Thus, we set the conversion at the first start (t=0 h) at 7% and reaction results are displayed in Fig. 5.18. It is observed that there are no evident changes of blank tests in the absence of catalysts even after 60 h of reaction time, while if in presence of Nb_2O_5 this metal oxide enhances the alkyl peroxide decomposition largely. It is reported that cyclohexyl hydroperoxide can be deprotonated by interacting with oxygen atoms in CeO_2 and formed peroxo fragment

is attached on a low coordinated Ce^{4+} sites[86]. By following this process, the dissociation of O-O bond occurs to give cyclohexanol. In view of this, and based on the comments about that solely Nb_2O_5 and CeO_2 or Ag/Nb_2O_5 and Ag/CeO_2 show an identical catalytic performance in the oxidation of cyclooctane (see chapter 4 and section 5.2.7 in this chapter). We speculate that the decomposition of 1-phenylethyl hydroperoxide over Nb_2O_5 proceeds in the similar way with CeO_2, as evidenced by the decrease of K/A ratio in the presence of Nb_2O_5 in Fig. 5.18-b. Moreover, we have proved that Nb_2O_5 is truly active in the direct oxidation of cyclooctane in the absence of initiator (chapter 4), indicating that the initiation process can be achieved by the presence of Nb_2O_5. It is proposed that there are active oxygen species generated from surface chemisorbed molecular oxygen as in the case of CeO_2[12, 89]. The formed superoxide oxygen bound to metal centre is capable of abstracting H atom of R-H to give R• radicals[1, 45], by which the radical chain reaction proceeds. In addition, we have tested that cyclooctanol can be transformed into cyclooctanone under the reaction conditions for cyclooctane oxidation with the conversion up to 90%, which can be one of the reasons that K/A ratio is above 1 by Nb_2O_5 in cyclooctane oxidation by molecular O_2.

In addition, it is found that Ag^+ from $AgNO_3$ does not take part in the decomposition of alkyl hydroperoxides. However, it should be noted that the conversion by WI-Ag/Nb_2O_5 is obviously lower than that in the presence of Nb_2O_5, which indicates that the presence of Ag species inhibits the decomposition of 1-phenylethyl hydroperoxide by blocking the interactions between substrates molecules and Nb_2O_5. Wu et al. reported that the addition of Ag decreases the amount of surface ($V_{O\text{-}s}$) vacancies with

a rise of the bulk oxygen vacancies in CeO_2 at the same time, proving that the role of silver is correlated to the redistribution between the surface and bulk oxygen vacancies[12]. Thus, we assume that this process might occur in Nb_2O_5.

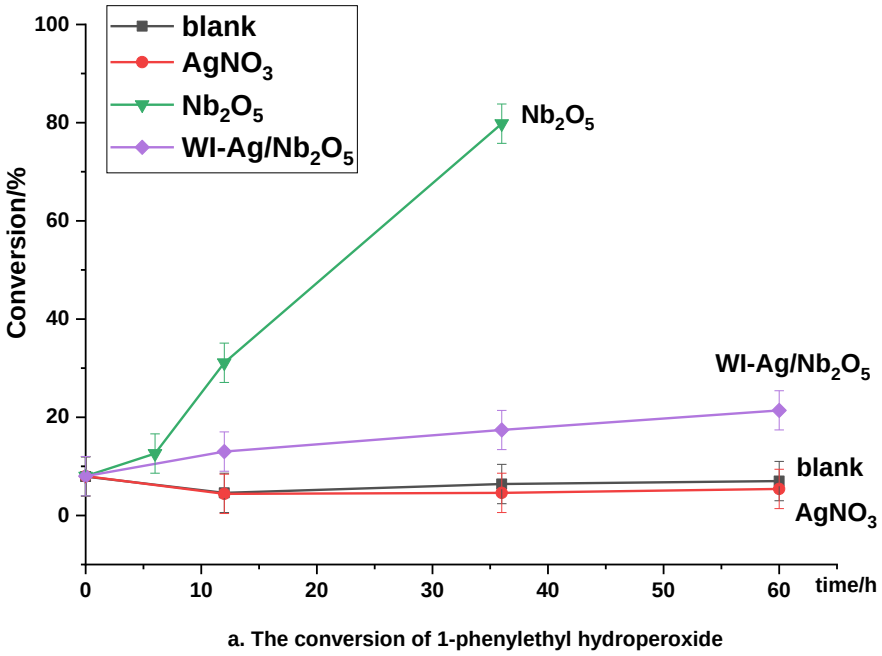

a. The conversion of 1-phenylethyl hydroperoxide

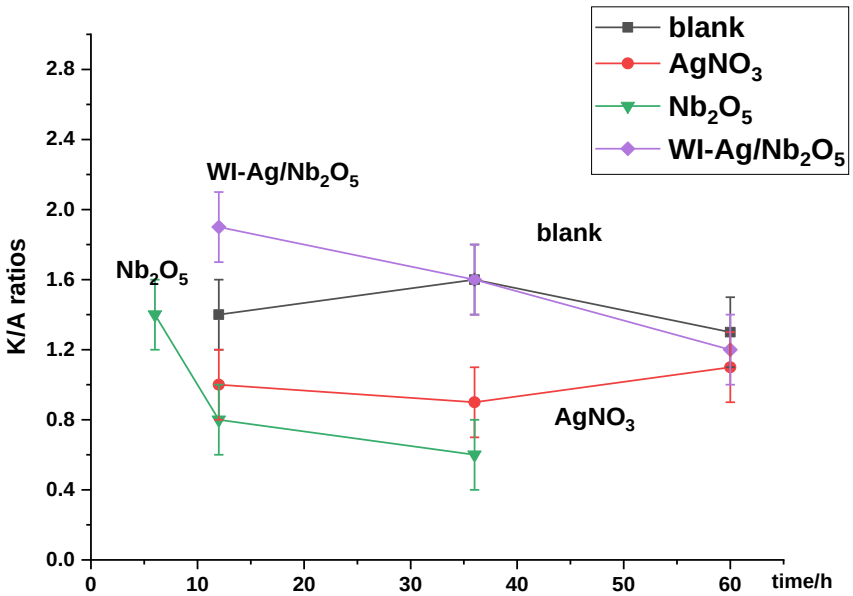

b. The K/A ratios of 1-phenylethyl hydroperoxide decomposition

Fig. 5.18 Decomposition of 1-phenylethyl hydroperoxide under 2 bar N_2 at 82 ˚C. 0.0854 g Nb_2O_5 with 99.9% purity used; WI-Ag/Nb_2O_5 prepared by wet impregnation method with 1 *wt*%

loading. The tests were conducted at 82 ˚C with M(Ag):S ratio=1:100. 100 µL 1-phenylethyl hydroperoxide was taken and 2 mL benzotrifluoride was used as inert solvent.

5.3.2 Decomposition of 1-phenylethyl hydroperoxide in the presence of O_2

Furthermore, tests at 2 bar O_2 were conducted to investigate about effect of O species on the decomposition of 1-phenylethyl hydroperoxide in comparison with tests at 2 bar N_2. It is found that reaction results (Fig.5.19-c) by Nb_2O_5 are identical between the tests at pressurised N_2 and O_2, which directly implies that O_2 does not participate in the decomposition process of 1-phenylethyl hydroperoxide. And although the conversion by WI-Ag/Nb_2O_5 is close, K/A ratio increase in comparison with that of Nb_2O_5 and blank test, from which it is proposed that the existence of Ag species (Ag_2O and Ag^0) can be responsible for the activation of oxygen that reacts with alcohol (1-phenyl ethyl alcohol) to produce acetophenone. The results are corresponding with that WI-Ag/Nb_2O_5 can lead to higher selectivity for ketones and K/A ratio in the oxidation of cyclooctane. Meanwhile, the newly formed oxygen species (possibly O_2^-)[1, 44] by Ag species or Ag particles is capable of abstracting α-H atoms from 1-phenylethyl hydroperoxide leading to formation of peroxyl radicals (C_6H_5-(C·)OOH-CH_3) which evolves into acetophenone and hydroxyl radical species, leading to the rise of K/A ratio.

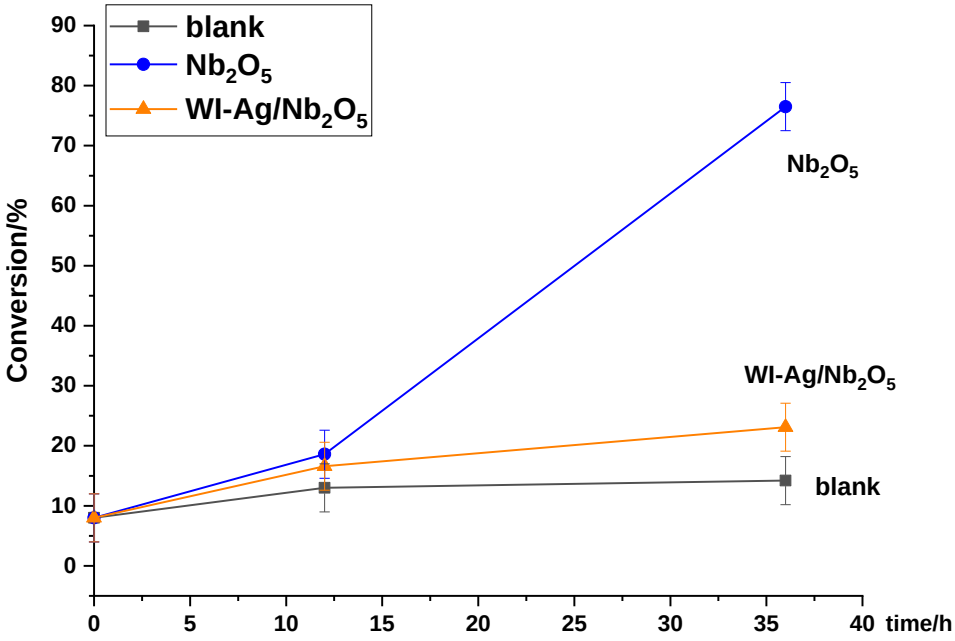

a. Conversion of 1-phenylethyl hydroperoxide under pressurised O_2

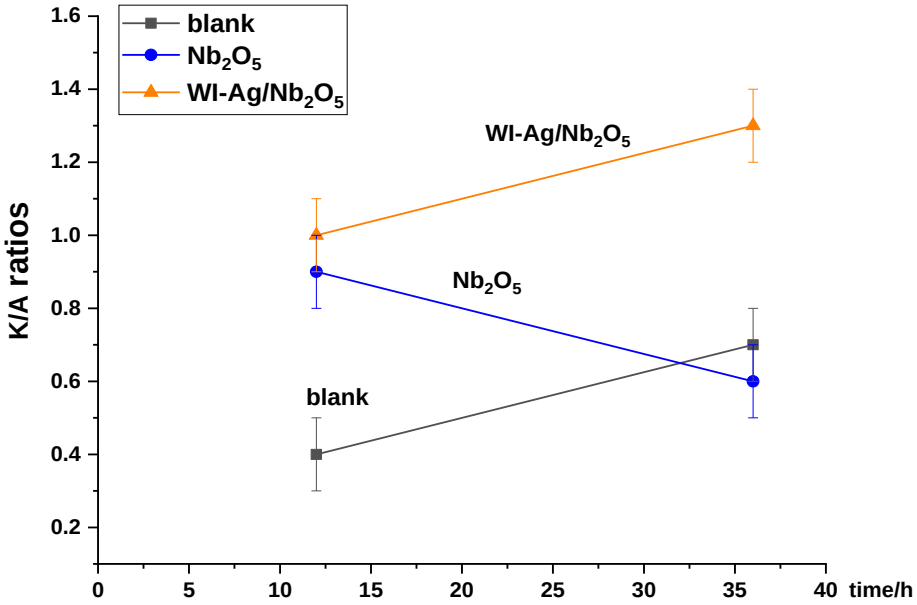

b. The K/A ratios of 1-phenylethyl hydroperoxide decomposition

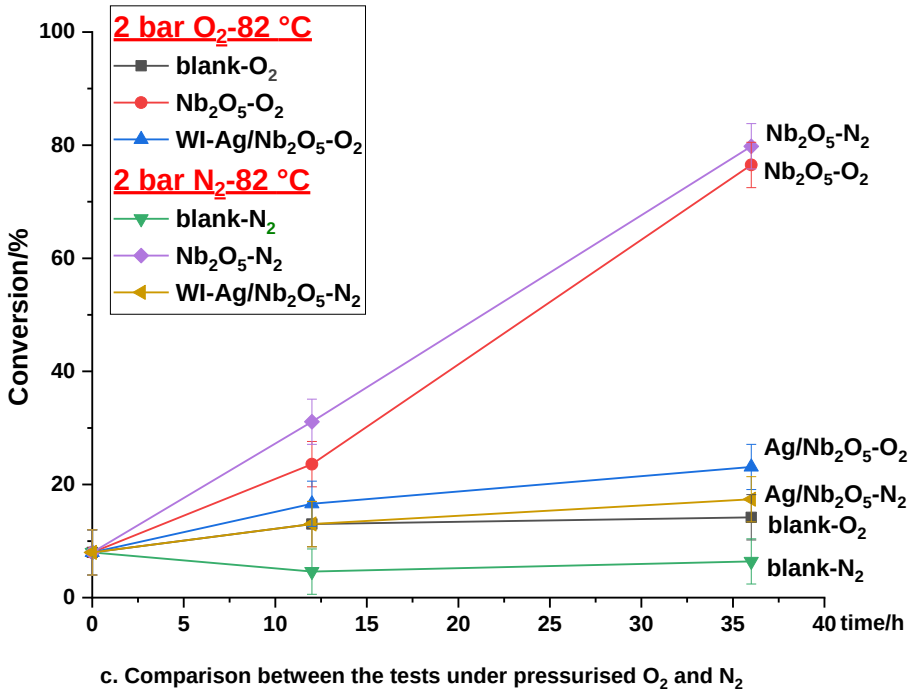

c. Comparison between the tests under pressurised O_2 and N_2

Fig. 5.19 Decomposition of 1-phenylethyl hydroperoxide at pressurised 2 bar O_2 at 82 ˚C. a. Conversion of 1-phenylethyl hydroperoxide in O_2 on the top; b. K/A ratio of 1-phenylethyl hydroperoxide decomposition; c. Comparison of conversion between the tests in N_2 and O_2 respectively. 0.0854 g Nb_2O_5 with 99.9% purity/grade used; WI-Ag/Nb_2O_5 prepared by wet impregnation method with 1 *wt*% loading. The tests were conducted at 82 ˚C with M(Ag):S ratio=1:100. 100 µL 1-phenylethyl hydroperoxide was taken and 2 mL benzotrifluoride was used as solvent.

Ultimately, we conclude that Nb_2O_5 participates in the decomposition of alkyl hydroperoxides directly and the presence of Ag species (Ag_2O and Ag) in catalyst could activate oxygen effectively and improve selectivity for ketones with higher K/A ratio.

5.4 A proposed reaction mechanism by Ag/Nb_2O_5 in cyclooctane oxidation

According to the results and discussion carried out so far, a simplified scheme to explain the reaction mechanism of cyclooctane oxidation by Nb_2O_5 and Ag/Nb_2O_5 is proposed separately, as shown in scheme 5.3 and 5.4 respectively.

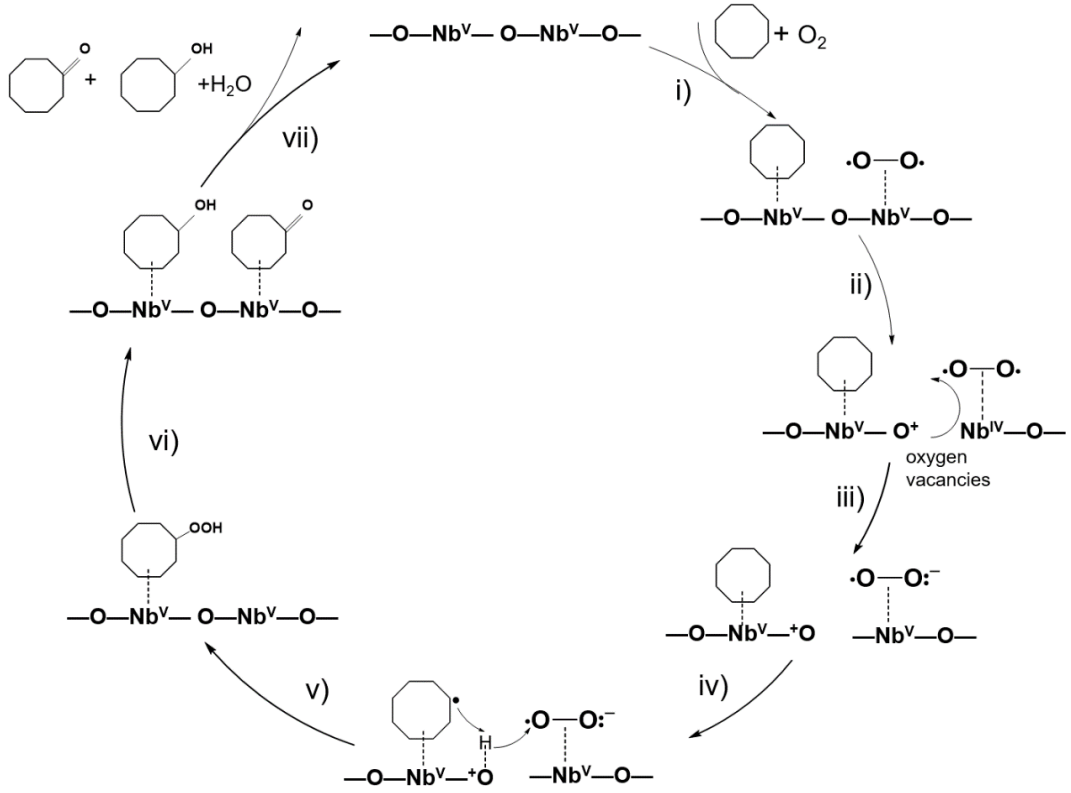

Scheme 5.3 A simplified proposed scheme for the reaction mechanism of Nb_2O_5 in cyclooctane oxidation by molecular oxygen. Active oxygen species can be generated from surface chemisorbed molecular oxygen that is related to the oxygen vacancies, as in the case of CeO_2[12, 89].

Scheme 5.3 proposes that O_2 could be activated to form superoxide species by the vacant oxygen sites[90], accompanied by the changes of valance of Nb from Nb^V to Nb^{IV}. The formed alkyl hydroperoxide is decomposed on the surface of Nb_2O_5 to

produce both of ketone and alcohol, which can occur at different sites and facets[86]. However, it should be mentioned that this scheme is only applied for the oxidation where Nb_2O_5 is active, as it has been discussed in section 4.4 that Nb_2O_5 exhibits different reaction performances in the oxidation of cyclohexane and ethylbenzene, which is possibly related with bond dissociation energy[91, 92] or site blocking[93] (like MoO_3[94]) for the substrate adsorption.

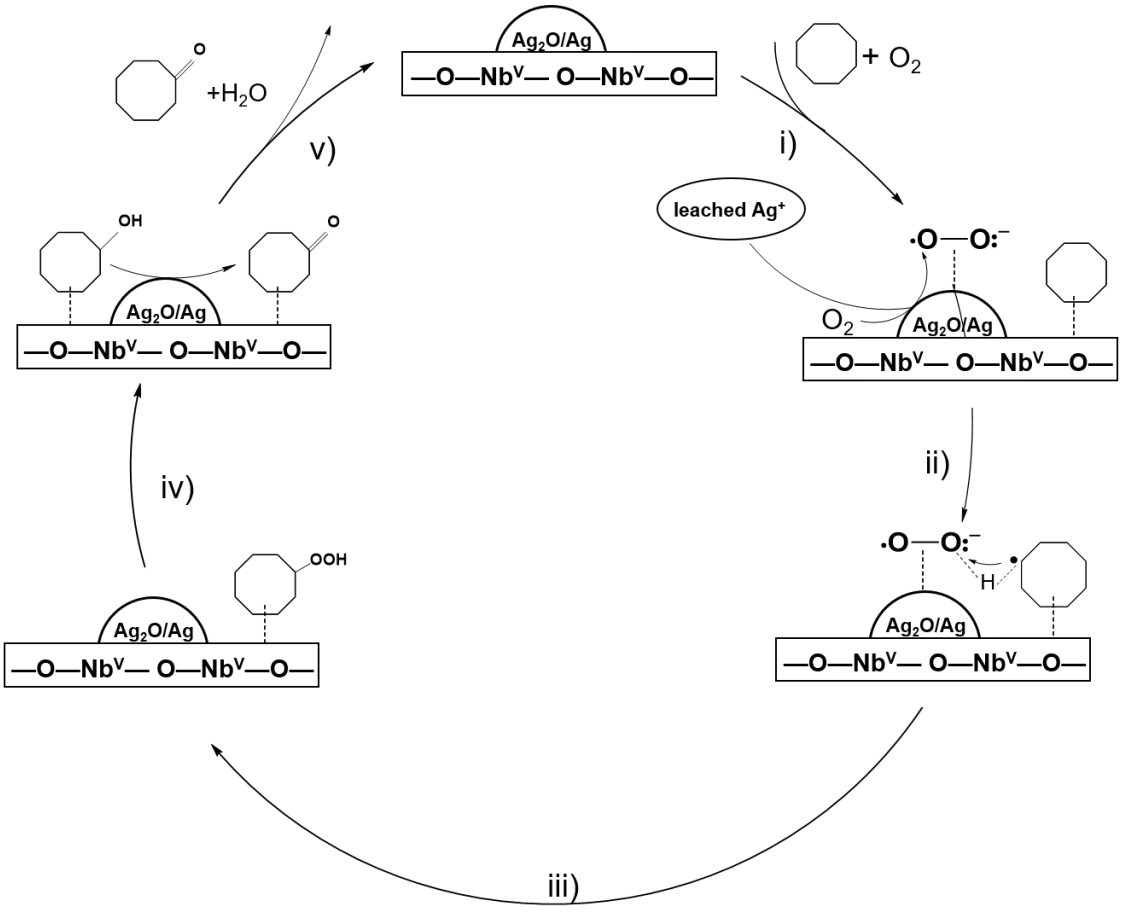

Scheme 5.4 A simplified proposed scheme for the reaction mechanism of Ag/Nb_2O_5 in cyclooctane oxidation by molecular oxygen.

We also propose a reaction mechanism by Ag/Nb_2O_5 to be a bit different from that of Nb_2O_5, as shown in scheme 5.4. In this case, O_2 is mainly activated by Ag species

(Ag_2O, Ag^+) on the Nb_2O_5 surface as the Ag-O interaction is more efficient[13], and the newly formed superoxide species is adsorbed on the surface of Ag particles, which abstracts H atoms from cyclooctane to initiate the reaction. Besides, the leaching Ag^+ is probably bounding to the surface of Ag particles to adsorb oxygen. The presence of Ag particles can enhance the oxidation of cylooctanol to yield cyclooctanone, which can be as a reason to explain a higher selectivity for ketone in comparison with that of Nb_2O_5.

5.5 Conclusion

A series of supported Ag over Nb_2O_5 catalysts were prepared for the oxidation of cyclooctane and the optimum reaction conditions were identified including parameters like M:S ratio, stirring speed, temperature. The optimum conditions were developed: 110 ˚C under 2 bar O_2 for 24 h with a M:S ratio 1:1000 at a stirring speed 600 rpm. By using these reaction conditions, WI-Ag/Nb_2O_5 prepared by wet impregnation method exhibits an enhanced conversion (81%) and a high selectivity (~60%) to cyclooctanone, and a promoting effect than that of Nb_2O_5, indicating that the existence of Ag species (most likely Ag_2O and Ag) facilitates the oxidation and optimized product distribution furtherly. However, it should be noted that there exists evident Ag leaching into reaction resolution from WI-Ag/Nb_2O_5 and the leached Ag^+ can also contribute to the reaction in homogeneous phase. The reactivity is possibly correlated with activation of O_2 by Ag^+ to form superoxide species that bound to metal centres or metal oxide, which reacts with hydrocarbons to produce peroxyl radicals.

Different methods, such as wet impregnation (WI), deposition precipitation (DP) and sol immobilization (SI) method were employed for the preparation of supported Ag/Nb_2O_5. The reaction data from cyclooctane oxidation reveal that WI-Ag/Nb_2O_5 shows a higher conversion and K/A ratio in comparison with that of DP-Ag/Nb_2O_5 and SI-Ag/Nb_2O_5, and DP-Ag/Nb_2O_5 and SI-Ag/Nb_2O_5 share a similar reactivity. The differences instead, are possibly attributed to the parameters like nanoparticle size[95, 96], morphologies[38], the oxidation state of Ag[57, 97], and the interaction between silver and support[68, 98, 99]. In our case, it is very likely related with the oxidation state of Ag species as Ag^+ exhibits the ability to enhance the generation of alkyl hydroperoxides by activating O_2 and the distribution of Ag species with various valances over Nb_2O_5 could affect oxidation process. Meanwhile, it is observed that leaching of Ag into reaction mixtures is obviously decreasing without losing much activity when utilising DP and SI method, especially the latter, posing a promising prospect to dimmish the effects of leaching species by strengthening the interactions between metal nanoparticles and support. In addition, a set of control tests by using physical mixing of ($AgNO_3$ + Nb_2O_5) and (Ag_2O + Nb_2O_5) further justify our suggestions about the roles of Ag^+ and Ag^0 in the oxidation process. Furthermore, the supported Ag over various metal oxides (Nb_2O_5, CeO_2, TiO_2, MgO, SiO_2) prepared by wet impregnation method were applied for the oxidation of cyclooctane, the results of which hint that the Ag/Nb_2O_5 and Ag/CeO_2 display higher conversion and selectivity for ketones before reduction by H_2. Although there is loss of selectivity for ketones after the reduction of Ag/Nb_2O_5 and Ag/CeO_2, the leaching of Ag is obviously decreased and they still pose an optimized

product distribution with the maintaining of conversion in comparison with other catalysts, indicating that Ag/Nb_2O_5 and Ag/CeO_2 is more appropriate for our reaction.

In order to investigate about the synergistic effect of Ag species and Nb_2O_5 in the oxidation of hydrocarbons, 1-phenylethyl hydroperoxide was used as a substrate over Nb_2O_5, WI-Ag/Nb_2O_5 both in anaerobic (N_2) and aerobic (sole O_2) conditions respectively. The results show that Nb_2O_5 participates in the decomposition of alkyl hydroperoxides directly and Ag species (Ag_2O and Ag) in catalyst could activate oxygen effectively and improve selectivity for ketones with relatively higher K/A ratio. According to these evidences, a simplified reaction scheme is proposed to provide an insight into the oxidation process based on our understanding, which is essential for the design of catalyst.

5.6 References

1. M. Conte, X. Liu, D. M. Murphy, K. Whiston and G. J. Hutchings, *Phys. Chem. Chem. Phys.*, 2012, **14**, 16279-16285.
2. I. Hermans, T. L. Nguyen, P. A. Jacobs and J. Peeters, *ChemPhysChem*, 2005, **6**, 637-645.
3. D. I. Enache, J. K. Edwards, P. Landon, B. Solsona-Espriu, A. F. Carley, A. A. Herzing, M. Watanabe, C. J. Kiely, D. W. Knight and G. J. Hutchings, *Science*, 2006, **311**, 362-365.
4. H. Miyamura, R. Matsubara, Y. Miyazaki and S. Kobayashi, *Angew. Chem. Int. Ed.*, 2007, **46**, 4151-4154.

5. S. Rojluechai, S. Chavadej, J. W. Schwank and V. Meeyoo, *Catal. Commun.*, 2007, **8**, 57-64.

6. T. Mallat, Z. Bodnar, A. Baiker, O. Greis, H. Strubig and A. Reller, *J. Catal.*, 1993, **142**, 237-253.

7. S. Carrettin, P. McMorn, P. Johnston, K. Griffin, C. J. Kiely and G. J. Hutchings, *Phys. Chem. Chem. Phys.*, 2003, **5**, 1329-1336.

8. Z. Opre, J.-D. Grunwaldt, M. Maciejewski, D. Ferri, T. Mallat and A. Baiker, *J. Catal.*, 2005, **230**, 406-419.

9. L. Kundakovic and M. Flytzani-Stephanopoulos, *Appl. Catal. A: Gen.*, 1999, **183**, 35-51.

10. A.-Q. Wang, C.-M. Chang and C.-Y. Mou, *J. Phys. Chem. B*, 2005, **109**, 18860-18867.

11. L. Y. Margolis and V. N. Korchak, *Russ. Chem. Rev.*, 1998, **67**, 1073-1082.

12. S. Wu, Y. Yang, C. Lu, Y. Ma, S. Yuan and G. Qian, *Eur. J. Inorg. Chem.*, 2018, **2018**, 2944-2951.

13. L. Brugnoli, A. Pedone, M. C. Menziani, C. Adamo and F. d. r. Labat, *J. Phys. Chem. C*, 2020, **124**, 25917-25930.

14. R. Karcz, P. Niemiec, K. Pamin, J. Połtowicz, J. Kryściak-Czerwenka, B. D. Napruszewska, A. Michalik-Zym, M. Witko, R. Tokarz-Sobieraj and E. M. Serwicka, *Appl. Catal. A: Gen.*, 2017, **542**, 317-326.

15. W. Trakarnpruk, A. Wannatem and J. Kongpeth, *J. Serbian Chem. Soc.*, 2012, **77**, 1599-1607.

16. X. Wang, B. Lei, L. Ma, L. Zhu, X. Zhang, H. Zuo, D. Zhuang and Z. Li, *Chem. Asian J.*, 2017, **12**, 2799-2803.

17. C. Resini, F. Catania, S. Berardinelli, O. Paladino and G. Busca, *Appl. Catal. B: Environ.*, 2008, **84**, 678-683.

18. A. Villa, N. Janjic, P. Spontoni, D. Wang, D. S. Su and L. Prati, *Appl. Catal. A: Gen.*, 2009, **364**, 221-228.

19. R. Hartunian, W. Thompson and S. Safron, *J. Chem. Phys.*, 1965, **43**, 4003-4006.

20. S. Furukawa, T. Shishido, K. Teramura and T. Tanaka, *J. Phys. Chem. C*, 2011, **115**, 19320-19327.

21. T. Shishido, T. Miyatake, K. Teramura, Y. Hitomi, H. Yamashita and T. Tanaka, *J. Phys. Chem. C*, 2009, **113**, 18713-18718.

22. F. H. Ribeiro, M. Boudart, R. A. Dalla Betta and E. Iglesia, *J. Catal.*, 1991, **130**, 498-513.

23. S. Demirel-Gülen, M. Lucas and P. Claus, *Catal. Today*, 2005, **102**, 166-172.

24. A. Dubey, V. Rives and S. Kannan, *J. Mol. Catal. A Chem.*, 2002, **181**, 151-160.

25. M. Allian, A. Germain, T. Cseri and F. Figueras, in *Stud. Surf. Sci. Catal.*, Elsevier, 1993, vol. 78, pp. 455-462.

26. J. R. Bourne, *Org. Process Res. Dev.*, 2003, **7**, 471-508.

27. G. C. de Araújo and M. do Carmo Rangel, *Catal. Today*, 2000, **62**, 201-207.

28. S. Kim, Y. F. Tsang, E. E. Kwon, K.-Y. A. Lin and J. Lee, *Korean J. Chem. Eng.*, 2019, **36**, 1-11.

29. C. H. Bartholomew, *Appl. Catal. A: Gen.*, 2001, **212**, 17-60.

30. M. Hartmann and S. Ernst, *Angew. Chem. Int. Ed.*, 2000, **39**, 888-890.

31. J. J. Dijkstra, J. C. Meeussen and R. N. Comans, *Environ. Sci. Technol.*, 2004, **38**, 4390-4395.

32. S. C. Parker and C. T. Campbell, *Phys. Rev. B* 2007, **75**, 035430.

33. S. Schauermann, J. Hoffmann, V. Johánek, J. Hartmann, J. Libuda and H. J. Freund, *Angew. Chem. Int. Ed.*, 2002, **41**, 2532-2535.

34. L. D. Pachon and G. Rothenberg, *Appl. Organomet. Chem.*, 2008, **22**, 288-299.

35. A. V. Gaikwad, A. Holuigue, M. B. Thathagar, J. E. ten Elshof and G. Rothenberg, *Chem. Eur. J.*, 2007, **13**, 6908-6913.

36. Z. Niu, Q. Peng, Z. Zhuang, W. He and Y. Li, *Eur. J. Chem.*, 2012, **18**, 9813-9817.

37. J.-S. Chen, A. N. Vasiliev, A. P. Panarello and J. G. Khinast, *Appl. Catal. A: Gen.*, 2007, **325**, 76-86.

38. M. Haneda and A. Towata, *Catal. Today*, 2015, **242**, 351-356.

39. G. Corro, U. Pal, E. Ayala and E. Vidal, *Catal. Today*, 2013, **212**, 63-69.

40. E. Aneggi, J. Llorca, C. de Leitenburg, G. Dolcetti and A. Trovarelli, *Appl. Catal. B: Environ.*, 2009, **91**, 489-498.

41. T. Baba, H. Sawada, T. Takahashi and M. Abe, *Appl. Catal. A: Gen.*, 2002, **231**, 55-63.

42. S. Miao, Y. Wang, D. Ma, Q. Zhu, S. Zhou, L. Su, D. Tan and X. Bao, *J. Phys. Chem. B*, 2004, **108**, 17866-17871.

43. S. Bhaduri and D. Mukesh, *Homogeneous Catalysis*, Wiley Online Library, 2014.

44. T. Pu, H. Tian, M. E. Ford, S. Rangarajan and I. E. Wachs, *ACS Catal.*, 2019, **9**, 10727-10750.

45. D. Mandon, H. Jaafar and A. Thibon, *New J. Chem.*, 2011, **35**, 1986-2000.

46. R. E. Kenson and M. Lapkin, *J. Phys. Chem.*, 1970, **74**, 1493-1502.

47. J. Guo, A. Hsu, D. Chu and R. Chen, *J. Phys. Chem. C*, 2010, **114**, 4324-4330.

48. Y. Lei, F. Mehmood, S. Lee, J. Greeley, B. Lee, S. Seifert, R. E. Winans, J. W. Elam, R. J. Meyer and P. C. Redfern, *Science*, 2010, **328**, 224-228.

49. J. F. Weaver and G. B. Hoflund, *Chem. Mater.*, 1994, **6**, 1693-1699.

50. Q. Wu, M. Si, B. Zhang, K. Zhang, H. Li, L. Mi, Y. Jiang, Y. Rong, J. Chen and Y. Fang, *Nanotechnology*, 2018, **29**, 295702.

51. M. Grabchenko, G. Mamontov, V. Zaikovskii, V. La Parola, L. Liotta and O. Vodyankina, *Appl. Catal. B: Environ.*, 2020, **260**, 118148.

52. M. Grabchenko, G. Mamontov, V. Zaikovskii and O. Vodyankina, *Kinet. Catal.*, 2017, **58**, 642-648.

53. A. S. K. Hashmi and G. J. Hutchings, *Angew. Chem. Int. Ed.*, 2006, **45**, 7896-7936.

54. X. Liu, M. Conte, Q. He, D. Knight, D. Murphy, S. Taylor, K. Whiston, C. Kiely and G. J. Hutchings, *Eur. J. Chem.*, 2017.

55. T. Nanba, S. Masukawa, A. Abe, J. Uchisawa and A. Obuchi, *Catal. Sci. Technol.*, 2012, **2**, 1961-1966.

56. B. R. Cuenya, *Thin Solid Films*, 2010, **518**, 3127-3150.

57. M. Skaf, S. Aouad, S. Hany, R. Cousin, E. Abi-Aad and A. Aboukaïs, *J. Catal.*, 2014, **320**, 137-146.

58. X.-Y. Gao, S.-Y. Wang, J. Li, Y.-X. Zheng, R.-J. Zhang, P. Zhou, Y.-M. Yang and L.-Y. Chen, *Thin Solid Films*, 2004, **455**, 438-442.

59. A. Samokhvalov, E. C. Duin, S. Nair and B. J. Tatarchuk, *Appl. Surf. Sci.* , 2011, **257**, 3226-3232.

60. A. Samokhvalov, S. Nair, E. C. Duin and B. J. Tatarchuk, *Appl. Surf. Sci.* , 2010, **256**, 3647-3652.

61. K. Faseela, S. Singh and S. Baik, *Sci. Rep.*, 2016, **6**, 1-9.

62. P. Zhenyan, H. Li, Q. Yunxiang, Y. Hanmin, Z. Xiuge, F. Bo, Z. Wenwen and H. Zhenshan, *Chinese J. Catal.* , 2011, **32**, 428-435.

63. P. Hu and Y. Cao, *Dalton Trans.* , 2012, **41**, 8908-8912.

64. P. Khanna, N. Singh, S. Charan, V. Subbarao, R. Gokhale and U. Mulik, *Mater. Chem. Phys.*, 2005, **93**, 117-121.

65. V. Raji, M. Chakraborty and P. A. Parikh, *Ind. Eng. Chem. Res.*, 2012, **51**, 5691-5698.

66. R. Mohamed and E. S. Aazam, *Int. J. Photoenergy*, 2011, **2011**.

67. Z. H. Dhoondia and H. Chakraborty, *Nanomater. Nanotechnol.*, 2012, **2**, 15.

68. D. Chen, Z. Qu, S. Shen, X. Li, Y. Shi, Y. Wang, Q. Fu and J. Wu, *Catal. Today*, 2011, **175**, 338-345.

69. C. A. Castro, P. Osorio, A. Sienkiewicz, C. Pulgarin, A. Centeno and S. A. Giraldo, *J. Hazard. Mater.*, 2012, **211**, 172-181.

70. R. Mohamed and I. A. Mkhalid, *J. Alloys Compd.*, 2010, **501**, 301-306.

71. J. Speder, L. Altmann, M. Bäumer, J. J. Kirkensgaard, K. Mortensen and M. Arenz, *RSC Adv.*, 2014, **4**, 14971-14978.

72. L. Salvati Jr, L. E. Makovsky, J. Stencel, F. Brown and D. M. Hercules, *J. Phys. Chem.*, 1981, **85**, 3700-3707.

73. S. Ma, Y. Lan, G. M. Perez, S. Moniri and P. J. Kenis, *ChemSusChem*, 2014, **7**, 866-874.

74. L. Di, J. Zhang and X. Zhang, *Plasma Processes and Polymers*, 2018, **15**, 1700234.

75. S. W. Han, Y. Kim and K. Kim, *J. Colloid Interface Sci.*, 1998, **208**, 272-278.

76. S. Chang, M. Li, Q. Hua, L. Zhang, Y. Ma, B. Ye and W. Huang, *J. Catal.*, 2012, **293**, 195-204.

77. G. B. Hoflund, J. F. Weaver and W. S. Epling, *Surf. Sci. Spectra*, 1994, **3**, 157-162.

78. N. Wei, H. Cui, Q. Song, L. Zhang, X. Song, K. Wang, Y. Zhang, J. Li, J. Wen and J. Tian, *Appl. Catal. B: Environ.*, 2016, **198**, 83-90.

79. C. A. Wilde, Y. Ryabenkova, I. M. Firth, L. Pratt, J. Railton, M. Bravo-Sanchez, N. Sano, P. J. Cumpson, P. D. Coates and X. Liu, *Appl. Catal. A: Gen.*, 2019, **570**, 271-282.

80. J. T. Carneiro, T. J. Savenije, J. A. Moulijn and G. Mul, *J. Photochem. Photobiol. A*, 2011, **217**, 326-332.

81. A. S. Reddy, C.-Y. Chen, C.-C. Chen, S.-H. Chien, C.-J. Lin, K.-H. Lin, C.-L. Chen and S.-C. Chang, *J. Mol. Catal. A Chem.*, 2010, **318**, 60-67.

82. M.-f. Luo, X.-x. Yuan and X.-m. Zheng, *Appl. Catal. A: Gen.*, 1998, **175**, 121-129.

83. K.-C. Lee, S.-J. Lin, C.-H. Lin, C.-S. Tsai and Y.-J. Lu, *Surf. Coat. Technol.*, 2008, **202**, 5339-5342.

84. K. H. Leong, B. L. Gan, S. Ibrahim and P. Saravanan, *Appl. Surf. Sci.*, 2014, **319**, 128-135.

85. I. Hermans, J. Peeters and P. A. Jacobs, *J. Phys. Chem. A*, 2008, **112**, 1747-1753.

86. T. López-Ausens, M. Boronat, P. Concepción, S. Chouzier, S. Mastroianni and A. Corma, *J. Catal.*, 2016, **344**, 334-345.

87. T. G. Driver, J. R. Harris and K. Woerpel, *J. Am. Chem. Soc.*, 2007, **129**, 3836-3837.

88. P. K. Singh, University of Sheffield, 2017, p 65-68.

89. M. Machida, Y. Murata, K. Kishikawa, D. Zhang and K. Ikeue, *Chem. Mater.*, 2008, **20**, 4489-4494.

90. T. Nanba, S. Masukawa, A. Abe, J. Uchisawa and A. Obuchi, *Appl. Catal. B: Environ.*, 2012, **123**, 351-356.

91. R. D. Bach and O. Dmitrenko, *J. Am. Chem. Soc.*, 2004, **126**, 4444-4452.

92. Y.-R. Luo, *Comprehensive handbook of chemical bond energies*, CRC press, 2007.

93. J. T. Goldstein and G. Ehrlich, *Surf. Sci.*, 1999, **420**, 1-5.

94. Z. Jiang, W. Huang, H. Zhao, Z. Zhang, D. Tan and X. Bao, *J. Mol. Catal. A Chem.*, 2007, **268**, 213-220.

95. L. Zhang, C. Zhang and H. He, *J. Catal.*, 2009, **261**, 101-109.

96. W. Menezes, V. Zielasek, K. Thiel, A. Hartwig and M. Bäumer, *J. Catal.*, 2013, **299**, 222-231.

97. L. Jin, K. Qian, Z. Jiang and W. Huang, *J. Mol. Catal. A Chem.*, 2007, **274**, 95-100.

98. Z. Qu, F. Yu, X. Zhang, Y. Wang and J. Gao, *Chem. Eng. J.*, 2013, **229**, 522-532.

99. C. E. Volckmar, M. Bron, U. Bentrup, A. Martin and P. Claus, *J. Catal.*, 2009, **261**, 1-8.

Chapter 6: Application of supported Ag over Nb_2O_5 catalysts for the oxidation of cyclohexane under mild conditions

6.1 Overview

Among the oxidation of hydrocarbons, cyclohexane oxidation is of very large significance, as it is industrially used to produce cyclohexanol and cyclohexanone (in a reaction mixture known as 'K/A oil') which are precursors for caprolactam and adipic acid, which are important building blocks for the manufacture of nylon-6 and nylon-6,6.[1-3] Industrially the oxidation process is carried out at 140-160 °C and 10-15 bar, in the presence of cobalt-based homogeneous catalysts like cobalt naphthenate promoting a free-radical mechanism[4, 5]. However, the conversion is normally kept below 5% to avoid the formation of large amount of by-products (e.g., ring-opened derivatives, 6-hydroxyhexanoic acid) by preventing the reaction proceeding in an unselective way for the maintaining of a good selectivity for K/A oil at around 70-85%[6, 7]. The route of cyclohexane oxidation for the production of K/A oil that are furtherly converted to adipic acid in the presence of HNO_3 is illustrated in scheme 6.1 and a free radical pathway involving the formation of intermediates (cyclohexyl hydroperoxide) as well as a main chain carrier role it plays to give major products, alcohol and ketone, is demonstrated in scheme 6.2 (section 6.2.1). Although the one step oxidation of cyclohexane to adipic acid is in fancy, it usually requires the addition of initiator (e.g., tert-Butyl hydroperoxide) and the presence of solvent at the same time, as well as the demands for the reactor design, which limits the industrial production[8, 9]. Also the long

chain reaction from cyclohexane to adipic acid will result in a more complicated product distribution, e.g., the formation of by-products like glutaric acid or succinic acid [10]. In view of this, it is quite challenging and important to overcome this limitation to improve the conversion while still preserving a reasonable selectivity for K/A oil both from academic and industrial perspective, which is proved by the fact that numerous of efforts have been put into for the design of efficient catalysts applied in cyclohexane oxidation to achieve this purpose[6, 11-13].

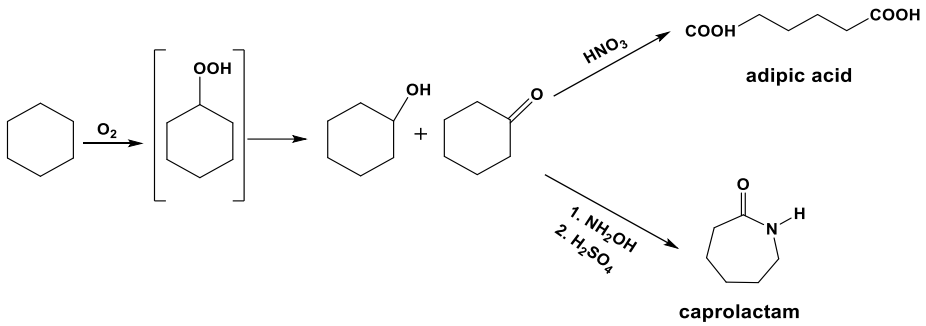

Scheme 6.1 An oxidation process for the conversion of cyclohexane cyclooctane and cyclohexanone (K/A oil), that are furtherly converted to adipic acid or ε-caprolactam.[14] Reprinted from ref. 14 with permission from Elsevier.

Moreover, according to the discussion in chapter 5, supported Ag/Nb_2O_5 exhibits superior reaction performances in cyclooctane oxidation by O_2 in the absence of solvent or initiator with a high conversion (around 80% at 2 bar O_2 by WI-Ag/Nb_2O_5) and preferred selectivity for ketone and alcohol, especially for ketone (~ 60% by WI-Ag/Nb_2O_5). Among various mechanistic options, we proposed that the activation of O_2 can be achieved by Ag^+ sites[15, 16] to form superoxide species, which then abstracts H atom from cyclohexane to initiate the reaction. According to this hypothesis, it would be possible to carry out the oxidation of cyclohexane under mild reaction conditions

even without any external organic initiator or solvent. The mild reaction conditions can minimize the formation of by-products and save energy from an economic point of view, and the absence of solvent or initiators tentatively causes less contamination for products and lower separation cost. Therefore, in this chapter we will explore the feasibility of supported Ag nanoparticles for cyclohexane oxidation, which is an application that received limited attention so far. Supported bimetallic Ag-Fe/Nb_2O_5 is investigated for this reaction, and compare our catalytic results to those of iron (III) acetylacetonate.[16, 17]

6.2 Determination and optimization of reaction conditions for cyclohexane oxidation

The oxidation of cyclohexane is conducted industrially by means of Co(II) naphthenate or Co(II)$(acac)_2$, which promotes a catalyst cycle known as Haber-Weiss cycle[11, 17, 18] (as shown in scheme 1.2 from chapter 1). Since that our aim is to design a more effective catalytic system and that catalysts do require their own activation temperature, it is important to determine an appropriate set of reaction conditions by accounting for both temperature and pressure. In view of this, and given the autoxidation nature of cyclohexane oxidation, preliminary catalytic tests were carried out without any catalysts and with the presence of iron(III) acetylacetonate ($Fe(acac)_3$) exploring temperature ranges in between 120 and 140 °C and O_2 pressure in the range from 3 to 5 bar. Similar to what was done for the study of cyclooctane oxidation: the collected results from blank autoxidation could provide a background for the

comparison with catalytic process to eliminate the effect of blank autoxidation under the same reaction conditions. Furthermore, if there is no obvious autoxidation occurring in the absence of catalyst, this can be an implication that the conversion of cyclohexane is triggered by catalyst during catalytic tests. In addition, the oxidation by $Fe(acac)_3$ gives the results that can be used to elucidate the roles of Fe species in cyclohexane oxidation, offering the evidence for the preparation of supported bimetallic Ag-Fe/Nb_2O_5 catalysts. It should also be noted that, like in the case of cyclooctane, quantitative analysis for cyclohexanol, cyclohexanone, cyclohexyl hydroperoxide and the possibly formed side products is needed, and this was mainly carried out by using ^{1}H-NMR.

6.2.1 Cyclohexane autoxidation

It is well known that the autoxidation of cyclohexane proceeds through a free-radical chain mechanism, as shown in scheme 6.2.[1, 5, 19] Generally, the autoxidation process occurs without any catalyst or in the presence of transition metal ion catalyst[20] (i.e. soluble cobalt (II) salts). During the autoxidation process, the formed reactive carbon centred parent radical (C_6H_{11}·) reacts with O_2 that are from oxygen dissolved into reaction solution or adsorbed oxygen species on metal centre[21, 22], to yield alkyl peroxyl radicals (C_6H_{11}-OO·), which is a diffusion-controlled step. C_6H_{11}-OO· as a main radical chain carrier, can react further with C_6H_{12} to give cyclohexyl hydroperoxide (CHHP), which interacts with C_6H_{11}-OO · to yield to cyclohexane. Two C_6H_{11}-OO· radicals undergo a chain-termination step to give cyclohexanol and

cyclohexanone (eq. 6.8). Generally in industrial scale, the conversion of cyclohexane autoxidation is generally limited to be lower than 5% to maintain a good selectivity for cyclohexanol and cyclohexanone (K/A ratio=1-1.5), as a higher conversion would lead to the formation of ring-opened by products like adipic acid, glutaric acid, which in turn by a set of dehydration and condensation reaction could lead to reaction mixtures accounting for 30-40 products with clear selectivity loss, and waste.[20, 23, 24]

Autoxidation process in the absence of any catalyst is studied firstly to provide a benchmark as comparison to elucidate the catalytic performances of supported catalysts. Temperature plays an important role in the oxidation process as the initiation can be occurred by thermal decomposition[25] or the walls of the reactor to abstract a H atom to give radicals[26, 27]. And given the solubility of O_2 in liquid phase affected by O_2 pressure, in our case, impact factors, reaction temperature and O_2 pressure are mainly investigated.

Initiation:

$C_6H_{12} \longrightarrow C_6H_{11}\cdot$ (**eq. 6.1**)

Propagation:

$C_6H_{12} + O_2 \longrightarrow C_6H_{11}\text{-}OO\cdot$ (**eq. 6.2**)

$C_6H_{11}\text{-}OO\cdot + C_6H_{12} \longrightarrow C_6H_{11}\text{-}OOH + C_6H_{11}\cdot$ (**eq. 6.3**)

Cyclohexanone formation:

$C_6H_{11}\text{-}OO\cdot + C_6H_{11}\text{-}OOH \longrightarrow C_6H_{11}\text{-}OOH + C_6H_{11}\text{-}(C\cdot)OOH$ (**eq. 6.4**)

$C_6H_{11}\text{-}(C\cdot)OOH \longrightarrow C_6H_{10}{=}O + \cdot OH$ (**eq. 6.5**)

Cyclohexanol formation:

$C_6H_{11}O\cdot + C_6H_{12} \longrightarrow C_6H_{11}\text{-}OH + C_6H_{11}\cdot$ (**eq. 6.6**)

Cleavage of cyclohexyl hydroperoxide (CHHP):

$C_6H_{11}\text{-}OOH \longrightarrow C_6H_{11}\text{-}O\cdot + \cdot OH$ (**eq. 6.7**)

Peroxyl condensation reaction:

$$2C_6H_{11}\text{-}OO\cdot \longrightarrow C_6H_{11}\text{-}OH + C_6H_{10}{=}O + O_2 \qquad \textbf{(eq. 6.8)}$$

Scheme 6.2 Free radical mechanism of cyclohexane oxidation by molecular O_2 for the formation of cyclohexanol and cyclohexanone. [1, 5, 19] C_6H_{11}-OO· is a main radical chain carrier, and the formation of cyclohexanol (e.q. 6.6 and 6.7) or cyclohexanone (e.q. 6.4 and 6.5) involves two reaction paths.

The temperature ranging from 120 °C to 140 °C and O_2 pressure varying from 3 to 5 bar were investigated (Fig. 6.1). As expected, temperature plays a significant role in the autoxidation process. The results show that no obvious conversion is observed when reaction is carried out at 120 °C. At a temperature of 130 °C instead, it appears that the conversion is around 5% and this can be enhanced 15% by an increase of O_2 pressure from 3 bar to 4 bar, remaining unchanged until the pressure of O_2 is 5 bar, and the conversion is improved furtherly at a temperature of 140 °C. It is observed that the conversion decreases when O_2 pressure rises from 4 bar to 5 bar at 140 °C, which is related with the phase changes as the vapour pressure of O_2 is 4.5 bar at 140 °C, leading to the diffusion limitations when cyclohexane is in liquid phase at 5 bar O_2. In addition, it is possible that a competitive adsorption may exist between O_2 and reactants to limit the conversion of substrates[22], an excess of O_2 poisoning the catalyst without leaving the surface to inhibit the transformation of reactants.

Moreover, although higher temperature facilitates the oxidation of cyclohexane, product distribution (Fig. 6.1-b) shows that the selectivity to cyclohexanol and cyclohexanone is lower as a higher amount of generated by-products, and a higher K/A ratio above 1 is probably caused by the formation of water[28]. It should be stressed

that a higher K/A ratio is favoured as a high yield of ketone would be obtained by preserving a reasonable conversion, where yield is equal to that the overall conversion multiplied by selectivity of desired product. Thus, in our case, the selectivity and K/A ratio is taken into account at the same time to assess the selectivity driven by catalysts. At industrial level, the conversion is deliberately limited to 4-5% to preserve a reasonable selectivity to alcohol and ketone and minimize the formation of by-product.[18, 29, 30], and the reaction mixture can be recycled by distillation as well as the unreacted cyclohexane is recycled to the reactor. A possible way to enhance the selectivity could be catalysts capable of non-radical pathways [19]. On the other hand, this approach is in pursuit since the 1970s and not achieved yet. In this thesis work we are rather aiming to identify selective decompositions of the key alkyl hydroperoxide intermediate to drive the reaction to a ketone or an alcohol regardless if the process is free-radical or non-free-radical.

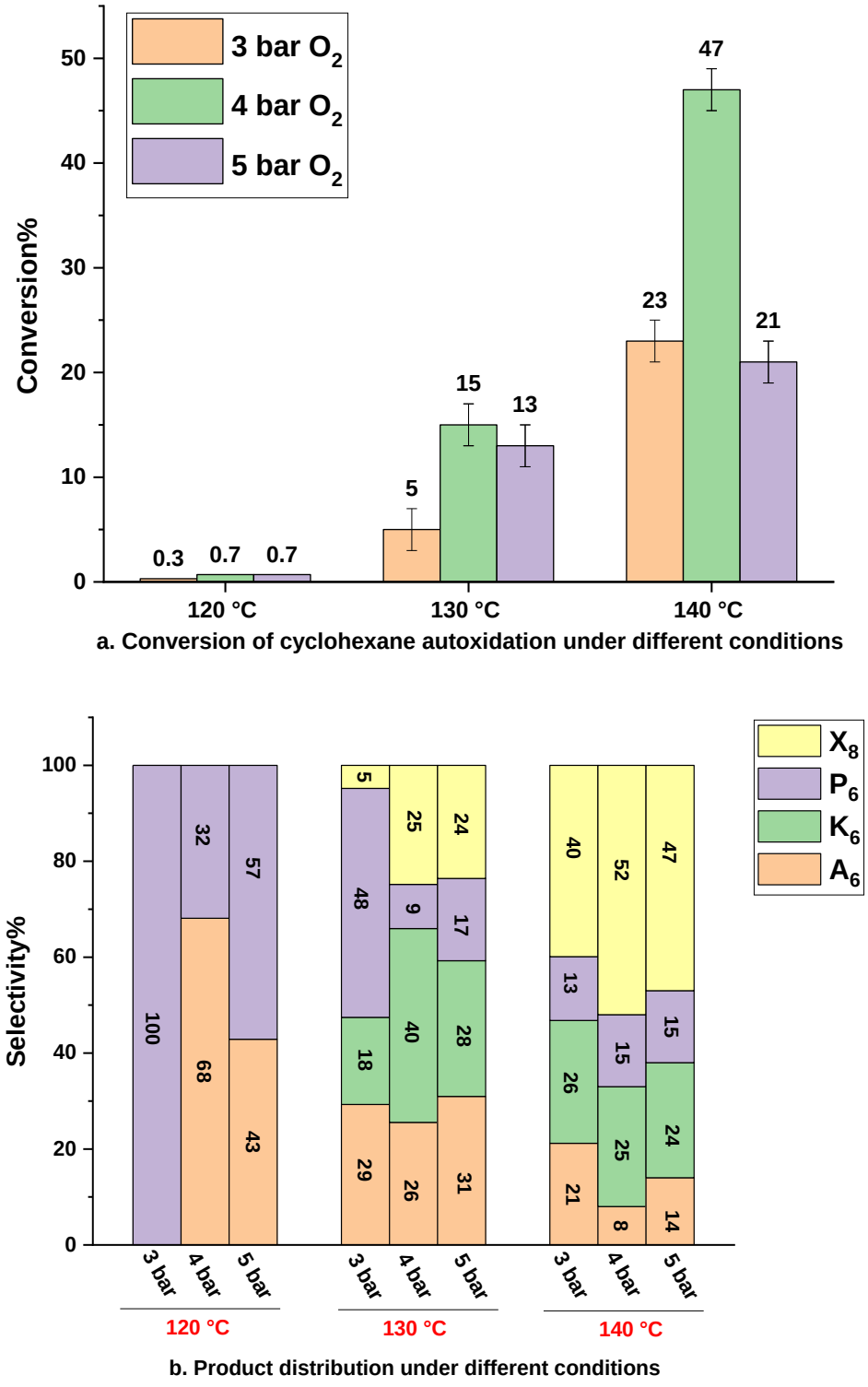

Fig. 6.1 Reaction results of cyclohexane autoxidation at different reaction temperatures and O_2 pressure for 24 h. a: Conversion of cyclohexane; b: Product distribution for cyclohexane oxidation. 3 mL cyclohexane used. And all the conversion and selectivity percentage in this

chapter are expressed as mol%. A_6-cyclohexnol, K_6-cyclohexanone, P_6-cyclohexyl hydroperoxide, X_6-by products, and all represents the same meaning in this chapter.

Furthermore, as the boiling point of cyclohexane is 80 °C, whereas the temperature for either C-H activation or catalyst activation is above 110 °C, a pressurised system is needed to preserve cyclohexane in liquid phase. From literature data, the vapour pressure of cyclohexane is 3 bar at 120 °C, 3.7 bar at 130 °C and 4.5 bar at 140 °C.[31, 32] Therefore, the working pressure should be at least 3 bar at 120 °C and 4 bar is preferred. In view of all of these considerations, and our own data, the proposed reaction conditions for catalytic tests are preliminarily set as 120 °C at 4 bar O_2. At these conditions no obvious autoxidation occurs, providing a benchmark to assess the reactivity of catalysts. Under this circumstance, the observed conversion of cyclohexane should be enhanced due to the presence of supported Ag catalysts in our case, while the catalysis process is active via non-autoxidation or autoxidation mechanism needs to be considered.[18, 33]

6.2.2 Tests by using iron (III) acetylacetonate ($Fe(acac)_3$)

In order to design a more effective catalytic system to dimmish the high energetic demand and improve the yield of K/A oil, there are studies demonstrating that, soluble iron (tris(acetylacetonato) iron(III)) and copper (bis(trimethylacetate) copper(II)) catalysts in the presence of *tert*-butyl hydroperoxide (TBHP), cyclohexane can be selectively oxidised at 70 °C to cyclohexane and cyclohexanone with an optimized selectivity of 90%, but the iron catalyst deactivates due to adipic acid from the

overoxidation of cyclohexanone[34]. In addition, homogeneous GoAgg^{II} system ($FeCl_3$ with H_2O_2 as oxidant) applied in cyclohexane oxidation gives a selectivity for cyclohexanone with 94% after 10 h[35], and soluble Fe (III) chelates like iron trispivalate and iron tris(hexafluoroacetylacetonate) displays a high yield of ketone and alcohol in the presence of TBHP[36]. Iron(III) acetylacetonate is applied into ethylbenzene oxidation with a promising production for acetophenone.[37] It is found that in the oxidation process, Fe(III) species can react with the TBHP or hydrogen peroxide to facilitate the formation of reactive alkyl peroxides[38], and it is assumed that newly formed cyclohexyl hydroperoxide may with Fe species (or Ag particles) to enhance the oxidation. In addition, supported Fe/Fe_xO_y and Ag/Ag_2O particles tends to remain segregated[39] to play the bifunctional catalytic activity, one being as initiator and other component being active for alkyl hydroperoxides decomposition. From this perspective, soluble iron(III) acetylacetonate ($Fe(acac)_3$) is often used as a benchmark instead of cobalt naphthenate, for the oxidation of cyclohexane by O_2 without any initiator (THBP or H_2O_2). And with this role, it was also used in the present study.

And in fact, the conversion of cyclohexane is obviously improved when employing $Fe(acac)_3$ as the catalyst at d120 °C in comparison with the blank autoxidation (Fig. 6.2). In addition, the product distribution (Fig. 6.2-b) exhibits that the lower selectivity for peroxyl hydroperoxide in comparison with blank tests implies the decomposition by $Fe(acac)_3$. The evidently enhanced effect by $Fe(acac)_3$ at 120 °C exerts that it is feasible to realize the conversion of cyclohexane at a relatively milder condition, which

is beneficial to achieve a high selectivity for ketone and alcohol by preserving a reasonable conversion at the same time. But a higher temperature would lead to a large amount of by-products formed. It should be note that an increase of O_2 pressure does not increase the conversion from 120 °C to 130 °C, whereas the amount of by-products increases probably because the formed acids are capable to trigger dehydration and condensation reactions. From this perspective, a higher pressure is not favoured for the selectivity of desired products. Moreover, it is found that the amount of cyclohexanone is usually in excess compared with the that of alcohol in the existence of $Fe(acac)_3$, which is likely to be caused by the presence of water that are produced during the oxidation process[18, 28].

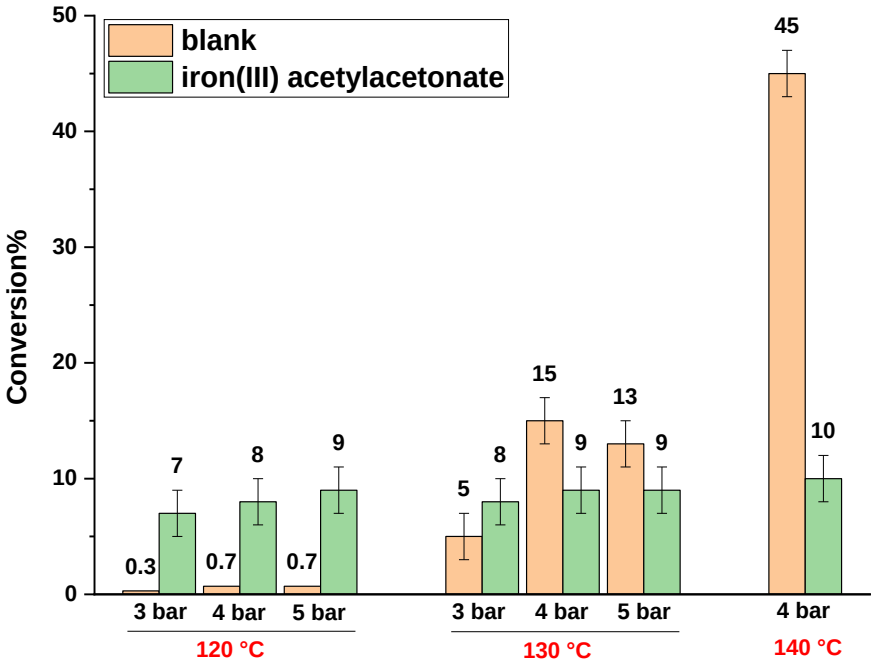

a. Conversion of cyclohexane oxidation by iron acetylacetonate

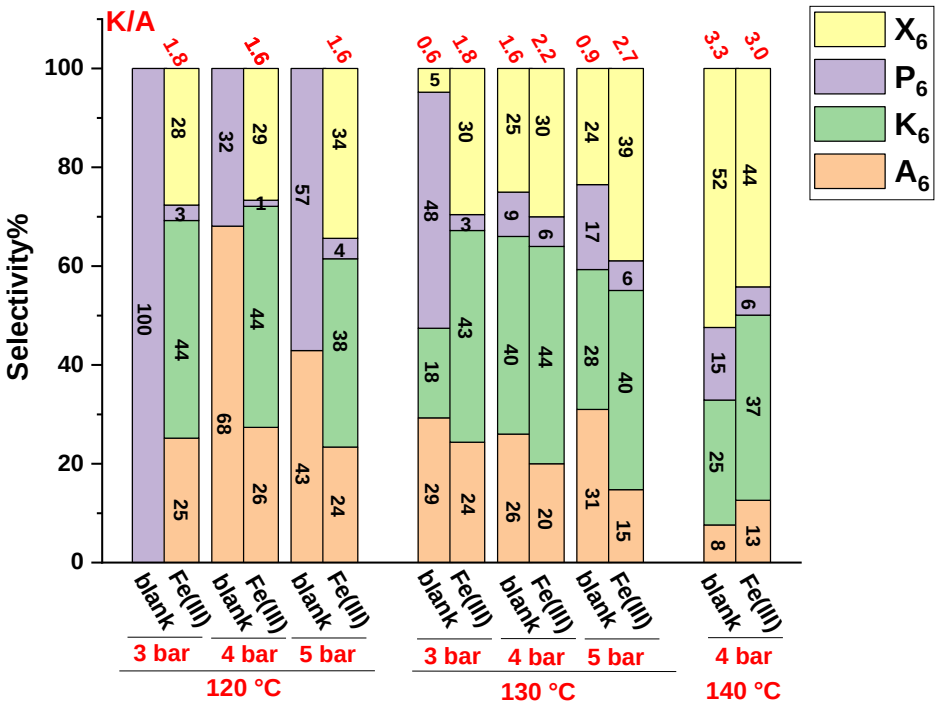

b. Product distribution by iron acetylacetonate

Fig. 6.2 Reaction results of cyclohexane oxidation by iron(III) acetylacetonate at different reaction temperatures and O_2 pressure for 24 h. a: Conversion of cyclohexane; b: Product distribution for cyclohexane oxidation. 3 mL cyclohexane used with M(Fe):S=1:100.

6.3 Catalytic tests and reactivity of supported Ag nanoparticles over Nb_2O_5

Based on the discussion about the application of supported Ag nanoparticles over Nb_2O_5 in the oxidation of cyclooctane, the catalyst exhibits superior reaction performances. Herein, Ag/Nb_2O_5 is directly employed for the oxidation of cyclohexane under the optimized reaction conditions, 120 °C at 4 bar O_2 for 24 h. Furthermore, the stirring speed and metal to substrate (M:S) ratio were varied as a form of control tests for diffusion. As for cyclooctane, the reaction should be under a kinetic regime otherwise the mass transfer may play a significant role in oxidation[40, 41].

6.3.1 Reactivity of Ag/Nb_2O_5 prepared by wet impregnation method

Supported Ag/Nb_2O_5 prepared by wet impregnation method with a nominal 1 *wt*% metal loading was used for the oxidation of cyclohexane without initiator, and as for cyclooctane and ethylbenzene, control tests by using the support only were carried out. As shown in Fig. 6.3, the conversion of cyclohexane by Nb_2O_5 (99.9% purity) is around 0.9%, which is close to that a blank autoxidation test. Therefore, the C-H activation of for cyclohexane cannot be directly achieved by Nb_2O_5 under our reaction conditions. This result is in contrast with those obtained for cyclooctane. We tentatively explain this difference by the fact that cyclohexane is relatively harder to be oxidised due to its higher C-H dissociation energy (ca. 414 $kJ \cdot mol^{-1}$ for cyclohexane and 385 $kJ \cdot mol^{-1}$ forcyclooctane[42, 43]). It follows that when cyclohexane is used as a substrate, the catalytic reactivity of Ag/Nb_2O_5 is then mainly attributed to Ag sites. In our tests of WI-Ag/Nb_2O_5 in the oxidation of cyclohexane compared with blank autoxidation process, with a conversion up to 13%, which is even higher than that of $Fe(acac)_3$ with a lower M:S ratio. Moreover, the product distribution shows that a high selectivity for cyclohexanol and cyclohexanone (~73%), with an excess of ketone (48%) and a lower selectivity for by products in comparison with that from $Fe(acac)_3$. Normally, a K/A ratio of approximately 1-1.5 is obtained in an autoxidation process if no catalyst is present. In our case, a promising higher K/A ratio of around 2.0 (±0.2) is detected when using Ag/Nb_2O_5, which together with a higher conversion makes WI-Ag/Nb_2O_5 a promising catalyst for this reaction and our investigations.

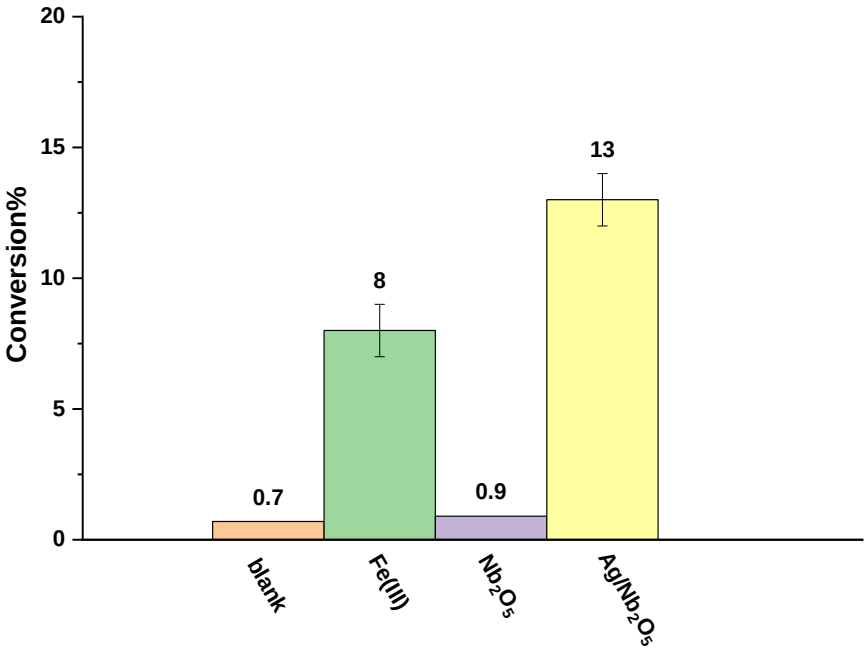

a. Conversion of cyclohexane oxidation by Ag/Nb_2O_5

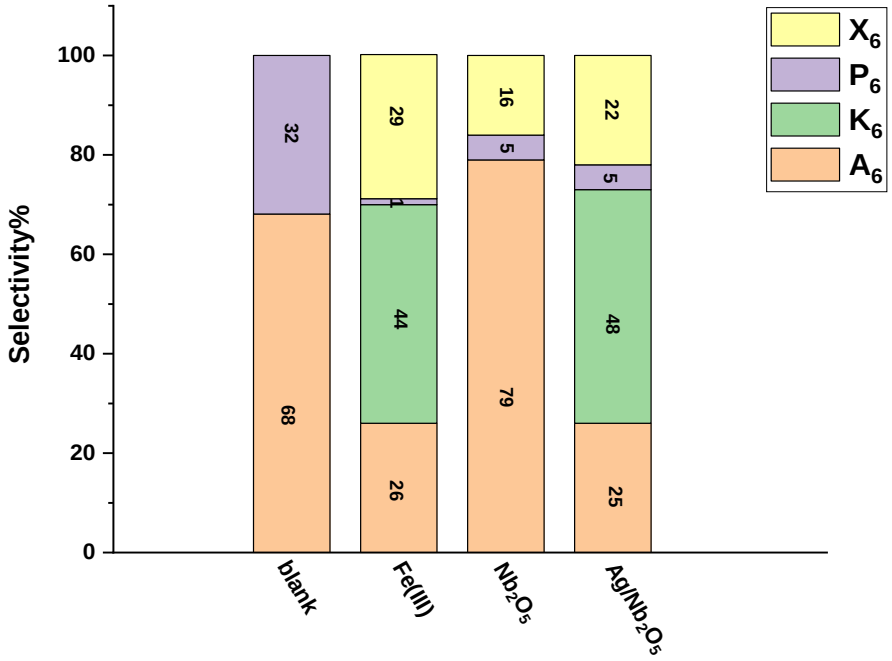

b. Product distribution by Ag/Nb_2O_5

Fig. 6.3 Cyclohexane oxidation in the presence of WI-Ag/Nb_2O_5 with 1 *wt*% loading prepared by wet impregnation method. a: Conversion of cyclohexane; b: Product distribution for cyclohexane oxidation. 3 mL cyclohexane used and M(Ag):S=1:1000. Fe(III) denotes iron(III) acetylacetonate and M(Fe):S=1:100. T = 120 °C, $P(O_2)$ = 4 bar, t = 24 h.

According to our discussion in chapters 5 (section 5.2.4 and 5.2.5) about the roles of Ag sites of WI-Ag/Nb_2O_5 in the oxidation of cyclooctane, that is Ag^+ species (supported Ag_2O) could facilitate the formation of alkyl hydroperoxide, and some literature about the formation of superoxide species (O_2^-)[16, 44]. We assume these same features are in place during cyclohexane oxidation and Ag^+ is `capable of abstracting H atoms. Furthermore, it is reported that in catalysis process, the amount of formed cyclohexanone tends to be in excess of cyclohexane with K/A ratios <1 if the homo-cleavage of the O–O bond in cyclohexyl hydroperoxide is a major path[1, 45], leading to the formation of C_6H_{11}–O· and ·OH (eq. 6.7). C_6H_{11}–O· is capable of reacting with C_6H_{12} to give cyclohexanol and ·OH is more reactive than ROO·[46, 47], accounting for the larger amount of cyclohexanol than that of cyclohexanone. Whereas in our case more cyclohexanone is produced in the presence of Ag/Nb_2O_5, which is possibly ascertained to the effect of Nb_2O_5 on the decomposition of alkyl hydroperoxides that facilitating the convert of cyclohexyl hydroperoxide as discussed in section 5.3, that is by abstracting a H atom in alpha to the C-OOH group of the cyclohexyl hydro peroxide intermediate.

6.3.2 Control tests for diffusion

As commented in chapter 5.2, in any heterogeneous catalytic process, diffusion is an ever-present phenomenon involving the transfer of reactant form a fluid phase to the catalyst surface and of product from the catalyst surface to the fluid phase, and this could be significant important factor to affect the reaction rate or selectivity,

especially in large scale production[40-42]. Herein, the oxidation should be under a kinetic regime for the comparison among different tests. So stirring speed and metal to substrate ration (M:S ratio) were varied to identify the reaction is under a kinetic or a diffusion regime.

6.3.2.1 Effect of changes of metal to substrate (M:S) ratios for the oxidation of cyclohexane

In order to investigate about the effect of M:S ratio on cyclohexane oxidation and ensure the oxidation is conducted in a regime when no observed diffusion limitation, a set of reactions with various M:S ratio under a fixed reaction conditions (120 °C at 4 bar O_2 for 24 h with stirring speed 600 rpm) were conducted.

Reaction results indicate that the conversion of cyclohexane rises obviously at the first start from M:S=0 to 1:5000, and there is slight increase until reaches a plateau from M:S ratio 1:1000, with a conversion at ~ 12% by taking error into account. The increase of conversion in this range illustrates that the oxidation is mainly influenced by the amount of active sites, which is mainly supported Ag/Ag_2O nanoparticles in our case. While no obvious or only slight rise is observed when M:S ratio increases from 1:2000 to 1:1000, indicating that there might exist mass transport limitations in the range of 1:2000 and 1:1000 when taking the error into account. In view of this phenomenon, a M:S ratio at 1:1000 was chosen as the highest amount of substrate (or lowest amount of catalyst) to avoid falling into a diffusion limitation regime. In addition, the product distribution (Fig. 6.4-b) shows that the catalyst facilitates the

transformation of cyclohexyl hydroperoxide to cyclohexanone when the rate of the reaction is a function of the amount of active sites (M:S < 1:1000), implying that the catalysts is capable of abstracting α-H atom for the formation of ketone. While the highest K/A ratio value with 1.8 is obtained when M:S is 1:1000, indicating a larger amount of catalysts does not imply a more suitable product distribution, which is correlated with the diffusion of substrates and products in the reaction system[48]. In this case, this furtherly confirms that M:S ratio at 1:1000 is the best compromise for our studies.

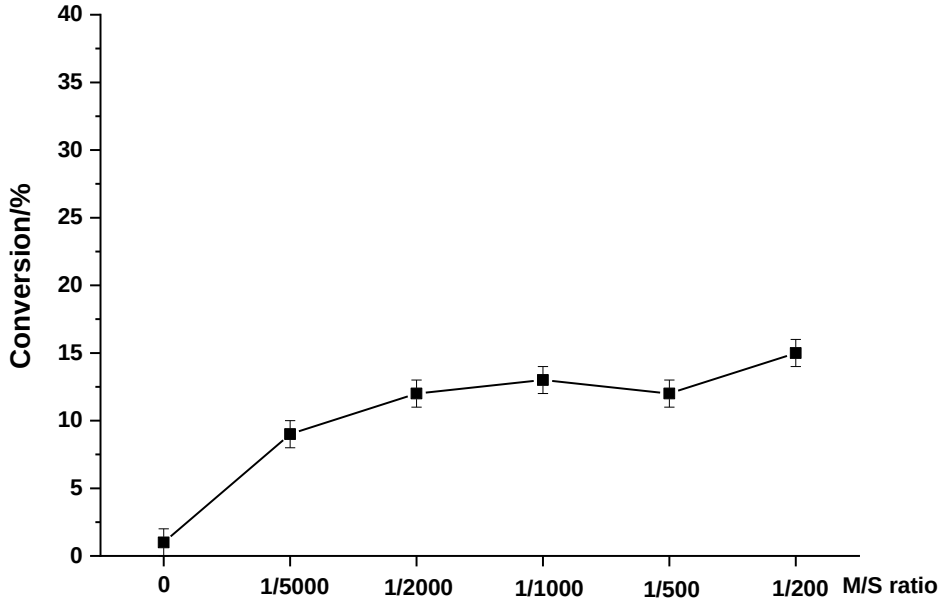

a. Conversion of cyclohexane by WI-Ag/Nb_2O_5 with various M/S ratios

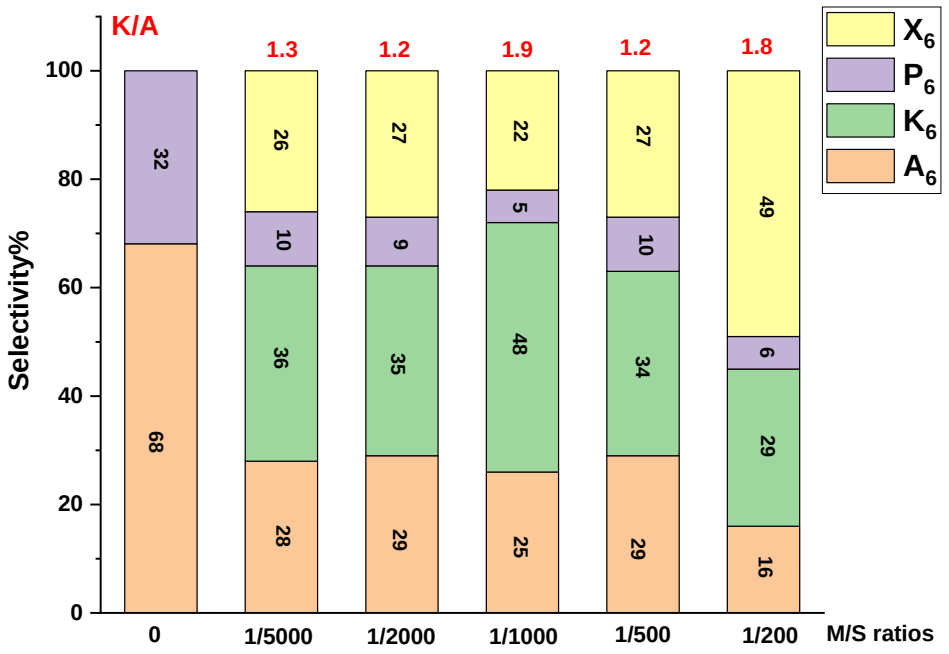

b. Product distribution by WI-Ag/Nb_2O_5 with various M/S ratios

Fig. 6.4 Reaction results of cyclohexane oxidation with WI-Ag/Nb_2O_5 (1 *wt*%) prepared by wet impregnation method, at varying M:S ratios. a: Conversion of cyclohexane; b: Product distribution for cyclohexane oxidation. cyclohexane (3 mL), stirring speed=600 rpm, T = 120 °C, $P(O_2)$ = 4 bar, t = 24 h.

6.3.2.2 Effect of stirring speed to cyclohexane oxidation

It is found that mixing can affect reaction rates and product distribution in some cases[48]. Stirring speed, as a parameter influencing mass transfer during the oxidation process, was investigated in the range from 200 rpm to 800 rpm to observe the effect on cyclohexane oxidation. Too high or too low stirring speed would make reaction slurry insufficiently thorough mixing or cause splash inside the round bottom flasks.

Fig. 6.5 displays that there are no obvious changes of conversion as the speed increases from 200 rpm to 800 rpm, with a constant value at approximately 13% by considering the experimental error, indicating that the oxidation is not limited by O_2

diffusion in this regime. Meanwhile, by examining the selectivity, it appears that the rise of stirring rate from 200 to 600 rpm improves the selectivity for cyclohexanone with a higher K/A ratio to an extent, followed by the decrease of selectivity for cyclohexanone and increase for by products when stirring speed rise up to 800 rpm. The results reveal that although conversion is not limited by the diffusion of O_2 in this regime, the differences of product distribution at various stirring rate is possibly correlated with mass transfer of formed products[40, 41] as the oxidation proceeds. With the purposes to eliminate O_2 diffusion and achieve an optimized product distribution, and in order to ensure the reaction mixture thoroughly mixed without splashing, a stirring speed at 600 rpm is used for our experiments.

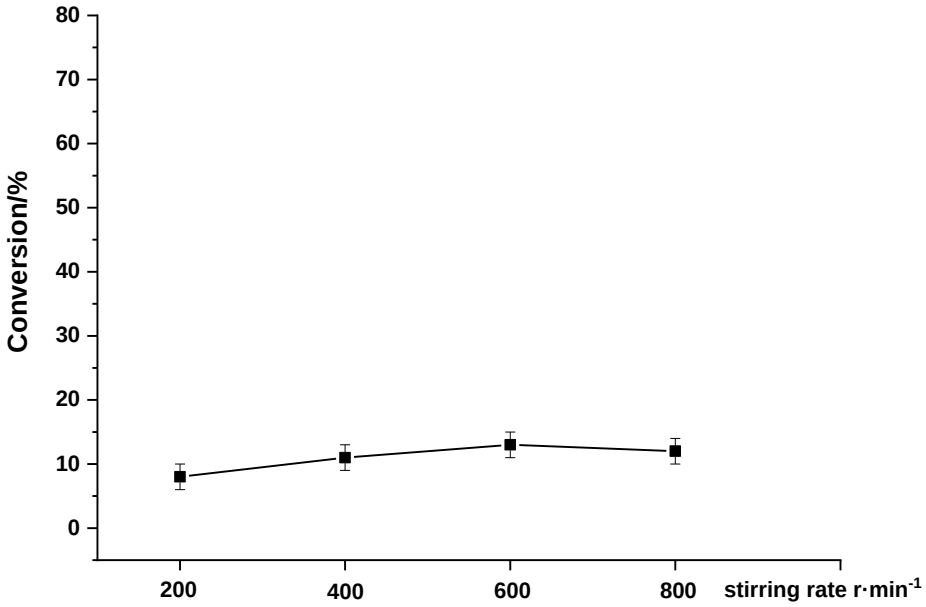

a.Conversion of cyclooctane by WI-Ag/Nb_2O_5 at various stirring rates

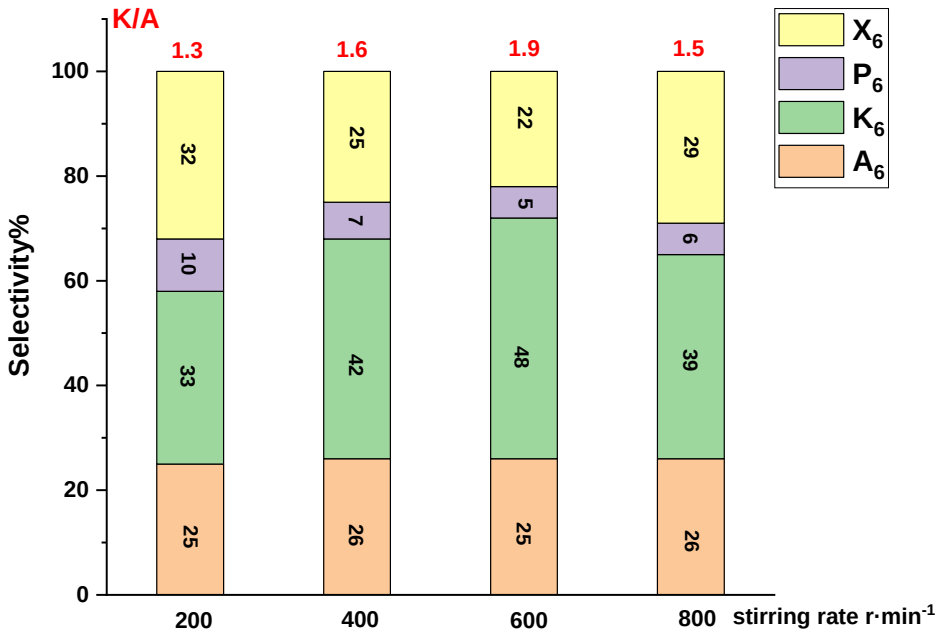

b. Product distribution by WI-Ag/Nb_2O_5 at various stirring rate

Fig. 6.5 Reaction results of cyclohexane oxidation with WI-Ag/Nb_2O_5 (1 *wt*%) prepared by wet impregnation method, at varying stirrer speed. a: Conversion of cyclohexane; b: Product distribution for cyclohexane oxidation. Cyclohexane (3 mL), M:S = 1:1000, T = 120 °C, *P*(O_2) = 4 bar, t = 24 h.

6.3.3 Catalytic reactivity of supported Ag/Nb_2O_5 prepared by different methods

As the physical properties (i.e. size, oxidation state of active metals) of supported metal nanoparticles catalysts can be controlled by the preparation methods, which would affect the catalytic behaviours[49, 50]. So the supported Ag/Nb_2O_5 prepared by different methods, wet impregnation(WI), deposition precipitation(DP) and sol immobilization(SI) method were furtherly applied in the oxidation of cyclohexane respectively.

6.3.3.1 The reaction performances of Ag/Nb_2O_5

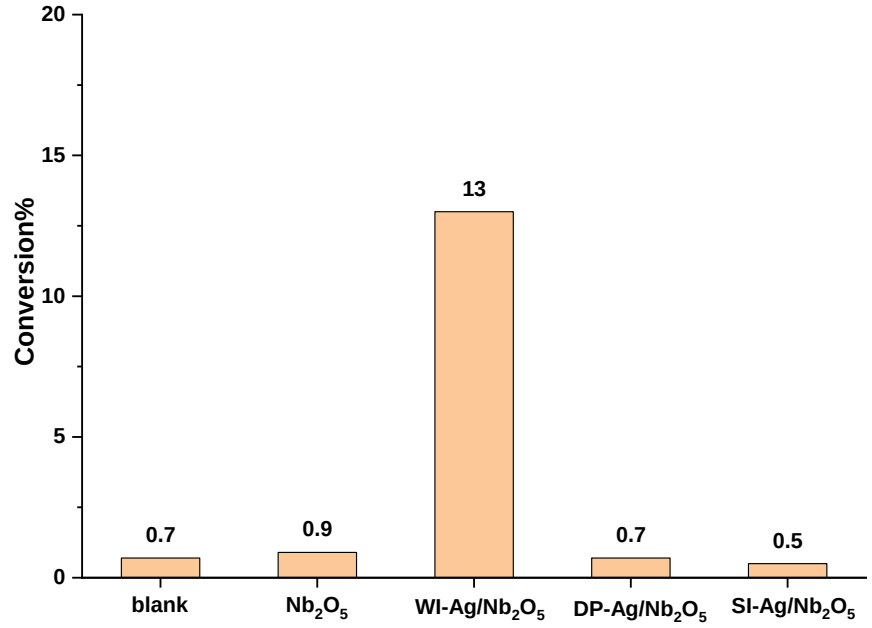

a.Conversion of cyclohexane by Ag/Nb_2O_5 prepared with different methods

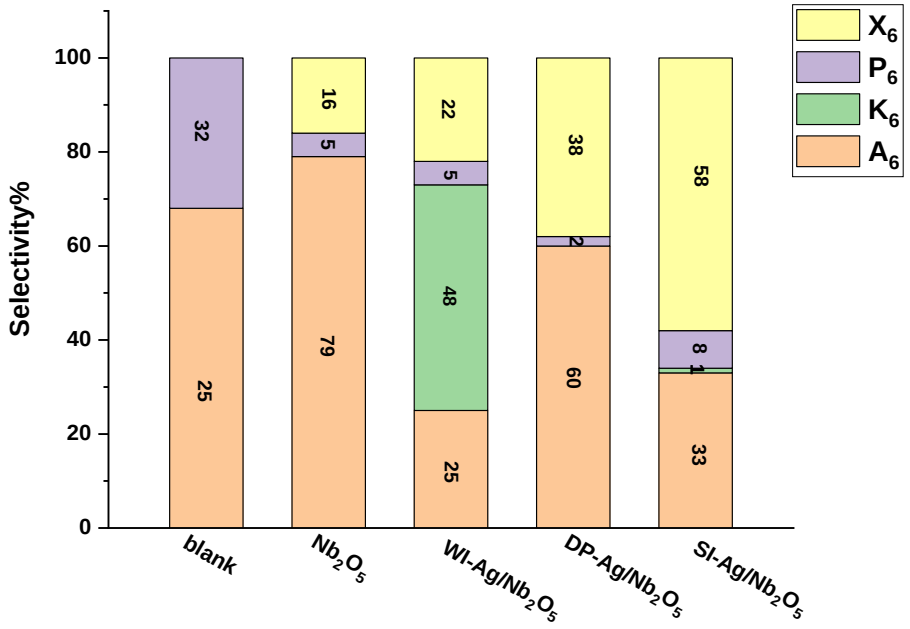

b. Product distribution by Ag/Nb_2O_5 prepared with different methods

Fig. 6.6 Cyclohexane oxidation by Ag/Nb_2O_5 (1 *wt*%) prepared by different methods. WI-Ag/Nb_2O_5 prepared by wet impregnation method; DP-Ag/Nb_2O_5 prepared by deposition precipitation method; SI-Ag/Nb_2O_5 prepared by sol immobilization protocol. a: Conversion of

cyclohexane; b: Product distribution for cyclohexane oxidation. 3 mL cyclohexane was used. M(Ag):S = 1:1000, T = 120 °C, $P(O_2)$ = 4 bar, t = 24 h.

The catalytic activity of supported Ag nanoparticles shows a marked difference on the preparation methods in Fig. 6.6. The reaction results show there is no significant conversion when DP-Ag/Nb_2O_5 or SI-Ag/Nb_2O_5 are used, and both of these materials have a negligible conversion as of Nb_2O_5, whereas WI-Ag/Nb_2O_5 exerts evidently promotion effect on the oxidation with a conversion at around 13%. Additionally, in comparison with WI-Ag/Nb_2O_5, it would appear that both DP-Ag/Nb_2O_5 and SI-Ag/Nb_2O_5 have a lower selectivity to cyclohexanone. However, as the conversion of these materials is compatible with zero, unlike the conversion by WI-Ag/Nb_2O_5, such large difference in conversion doesn't allow for a straightforward like-for-like comparison of the selectivity for these materials. As the size of nanoparticles is often affected by the synthesis method, and usually the smaller nanoparticles the higher the reactivity, we would also expect that a catalyst prepared by sol immobilization protocol, could lead to overoxidation, or in other words oxidation beyond a desired product, and this probably explains the excess amount of by-products in the presence of SI-Ag/Nb_2O_5. At present we also tentatively attribute the difference in reactivity to the presence of Ag^+ species in impregnation catalysts, which is possibly Ag_2O nanoparticles[51]. And normally metallic rich Ag^0 species presents in the catalysts prepared by deposition precipitation and sol immobilization method[27]. In addition, it is reported that the possible existed Ag^{2+} species in impregnation catalyst could make three redox couples (Ag^{2+}/Ag^+, Ag^{2+}/Ag^0, and Ag^+/Ag^0) compared with one (Ag^+/Ag^0) in

catalyst prepared by deposition precipitation method[52-54], which could be an factor leading to the high activity of WI-Ag/Nb_2O_5. In view of these factors and considerations, we consider the higher activity of WI-Ag/Nb_2O_5 if compared with the nearly inert behaviour of DP and SI-Ag/Nb_2O_5, to be more likely to be caused by the different oxidation state of Ag species of catalysts. In addition, it should be mentioned that a higher Ag loading of WI-Ag/Nb_2O_5 is observed in the TEM images in comparison with DP- and SI-Ag/Nb_2O_5 catalysts, which accounts for the high activity in cyclohexane oxidation.

6.3.3.2 ICP-MS analysis for determination of Ag leaching

As for the previous sections, the determination of leached Ag amount into reaction mixture was carried out by ICP-MS. Our results show that the amount of leached Ag is very minor at around 0.01%, this result is excellent and indicates that the WI-Ag/Nb_2O_5 catalyst shows high stability during the oxidation process with low loss of active metals. This is in stark contrast to the high Ag leaching (relative 24%) observed for cyclooctane oxidation. We speculate this is possibly due to a lower yield of by products, especially organic acids formed in reaction. Thus, showing that the leaching of an active metal is not an absolute phenomenon but relative to the kind of catalyst and reaction under study. From this perspective, Ag/Nb_2O_5 prepared by wet impregnation method displays a promising prospect in cyclohexane oxidation by preserving a high stability with minor loss of Ag. Moreover, as depicted that Ag^+ species is capable of activating O_2 to form superoxide species, therefore, the effect of Ag^+ on

cyclohexane oxidation is investigated, as shown in section 6.4.

Table 6.1 Full scan analysis of the metal content and impurities present in reaction mixture, expressed in mg of contaminant in 3 mL reaction mixture. Sample extracted via deionised water. The tests were conducted at 120 °C, 4 bar O_2 for 24 h, with M:S ratio 1:1000. The amount of Ag used in oxidation is 2.99 mg. Amount of trace metals reported in mg unit.

Sample ID	Ag	Al	As	B	Ba	Ca
WI-Ag/Nb_2O_5	0.0002	0.0108	0.0015	0.0489	0.0028	0.0181

Sample ID	Fe	K	Mg	Na	Si	Zn
WI-Ag/Nb_2O_5	0.0001	0.0057	0.0017	0.1251	0.0219	0.00001

6.4 Effect of leaching Ag on cyclohexane oxidation by using $AgNO_3$

As discussed in section 1.2 from chapter 1, the metal leaching phenomenon should be considered in the application of supported metal catalysts. From this perspective, although the leaching of Ag from WI-Ag/Nb_2O_5 is very low in cyclohexane oxidation, the effect of Ag^+ into reaction mixture on cyclohexane oxidation is investigated to provide the evidence for elucidating the reaction mechanism of catalyst.

The catalytic reactivity of free Ag^+ species in solution increases with the increase of M:S ratio, as demonstrated in Fig. 6.7. According to the ICP-MS analysis for Ag leaching from WI-Ag/Nb_2O_5 (3 mg Ag presented in reaction) with a value 0.01%, the conversion by leached species is around 0.5%, which is much lower if compared to the conversion of WI-Ag/Nb_2O_5 (13%), implying that the leaching effect of Ag^+ can be neglected. From this perspective, the effect of leached Ag into reaction mixture on cyclohexane oxidation is practically negligible, further implying that the oxidation

process is catalysed in a heterogeneous way instead of homogeneous one. On the other hand, according to our results, Nb_2O_5 is capable of decomposing alkyl hydroperoxides into alcohols and ketones. Thus, the formed cyclohexyl hydroperoxide can be furtherly transformed due to the presence of Nb_2O_5 to enhance the conversion cyclohexane. Product distribution displays that the K/A ratio remains at approximately 1 with the changes of M:S ratio, which is an implication that this oxidation process follows an autoxidation mechanism. This means that Ag^+ ions as part of the catalyst structure, that is bound to Ag or Nb_2O_5 are likely to only take part in the activation of O_2 to initiate the oxidation without controlling the decomposition step of cyclohexyl hydroperoxide. This is in analogy and as evidenced by a proposed reaction mechanism in cyclooctane oxidation from our research.

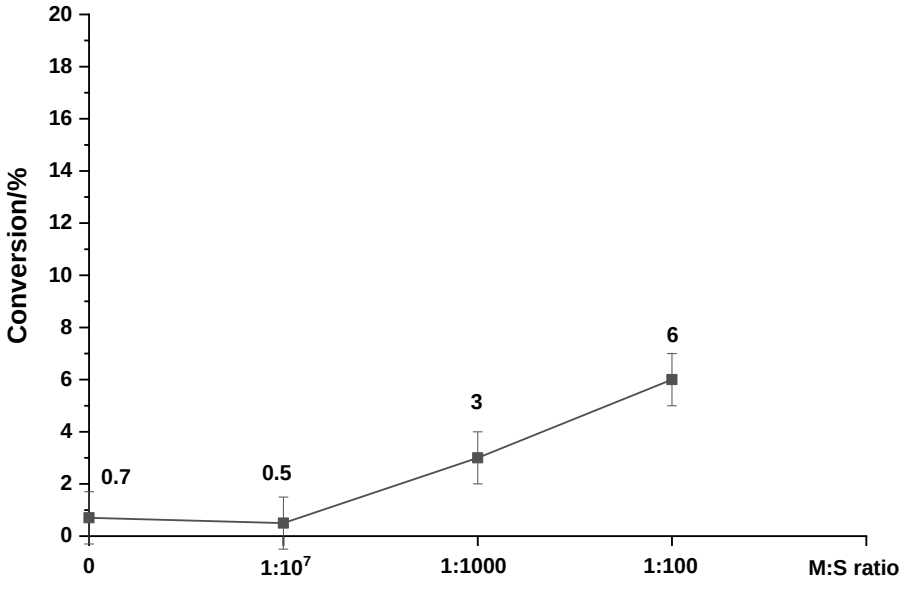

a. Conversion of cyclohexane by leaching Ag in the presence of $AgNO_3$

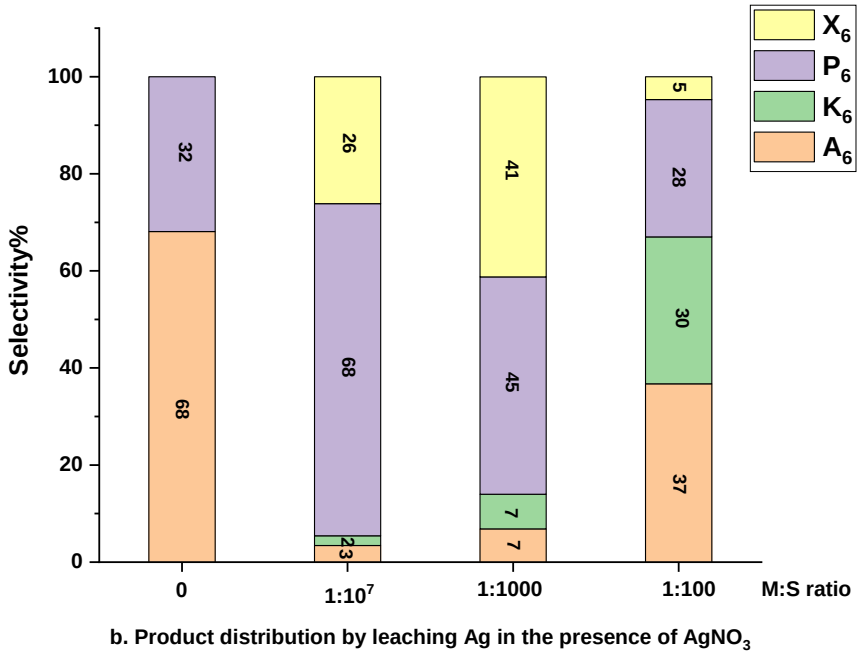

b. Product distribution by leaching Ag in the presence of $AgNO_3$

Fig. 6.7 Reaction results of leaching tests in the presence of $AgNO_3$ with various M:S ratios. a: Conversion of cyclohexane; b: Product distribution for cyclohexane oxidation. Cyclohexane (3 mL), T = 120 °C, $P(O_2)$ = 4 bar, t = 24 h.

6.5 The application of supported bimetallic Ag-Fe/Nb_2O_5 in cyclohexane oxidation

In view of the above discussion, we found that supported Ag/Nb_2O_5 prepared by wet impregnation method was able to enhance the oxidation of cyclohexane by using O_2 as oxidant without the need of organic initiators under mild reaction conditions, while preserving a high selectivity to cyclohexanone and cyclohexanol at the same time, which poses a promising application in the oxidation. It is known, however that soluble iron species, homogenous catalyst like $Fe(acac)_3$, are employed in cyclohexane oxidation in the presence of *tert*-butyl hydroperoxide, where Fe(III) species can react with hydroperoxides species (i.e. TBHP or hydrogen peroxide) to

facilitate the formation of reactive alkoxy (RO·) and hydroxyl radicals (HO·)[34, 38]. In heterogeneous catalysis, supported Fe nanoparticles catalysts have been studied in the field such as, supported Fe over activated carbon or Al_2O_3 with particle size distribution in the range of 3-16 nm are found to be active in Fischer-Tropsch process[55, 56]; supported Fe/MCM-41 are applied in the oxidation of alcohols by using H_2O_2 as oxidant[57]. Furthermore, compared to other transition metals, iron-based catalysts exhibit the advantages that it is inexpensive, environmentally benign, and less toxic. Thus, the addition of Fe as second component in bimetallic catalysts is expected to decrease the amount of more expensive metal while preserving a high catalytic activity meanwhile. It should be noted that all of these useful characteristics are combined with another 'special' one aspect, that is Fe normally does not easily form alloys with Ag, both elements being expected to be surface segregated[58, 59]. Thus, a bimetallic Ag/Fe catalyst is expected to be also bifunctional, with Ag that promotes the reaction and Fe that induces elements of selectivity. In fact, although it is known that the catalytic properties of bimetallic catalysts can be improved in comparison with monometallic catalysts, due to the to the charge transfer playing a prominent role[45, 60-62]. In contrast, our expected bifunctional catalyst would not be bound to activity driven only by the electron density at the surface of the particle.

6.5.1 Catalytic reactivity of Ag-Fe/Nb_2O_5

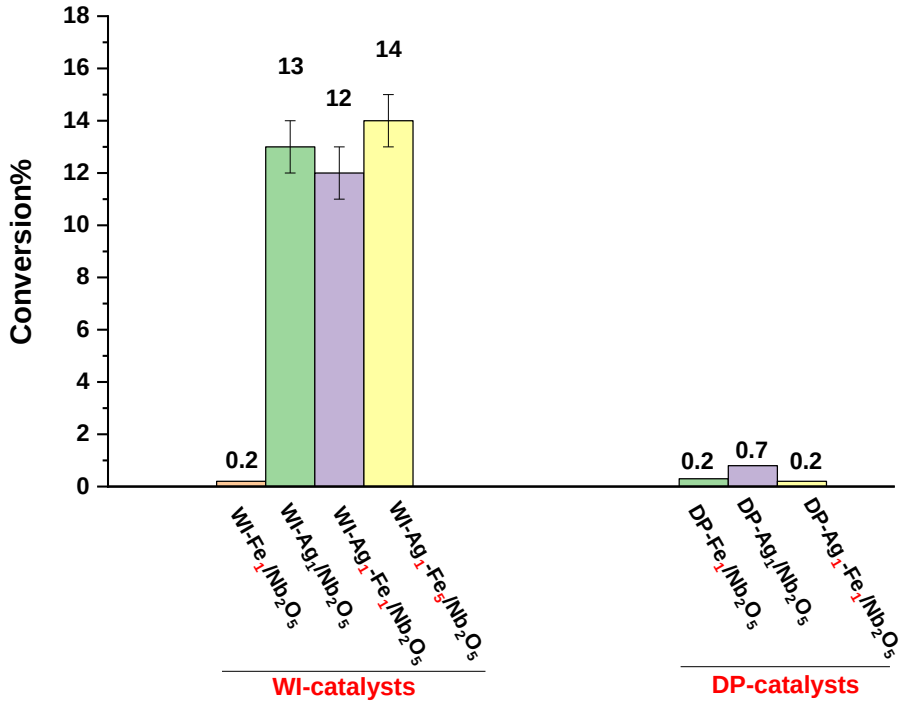

a. Conversion of cyclohexane by Ag-Fe/Nb_2O_5

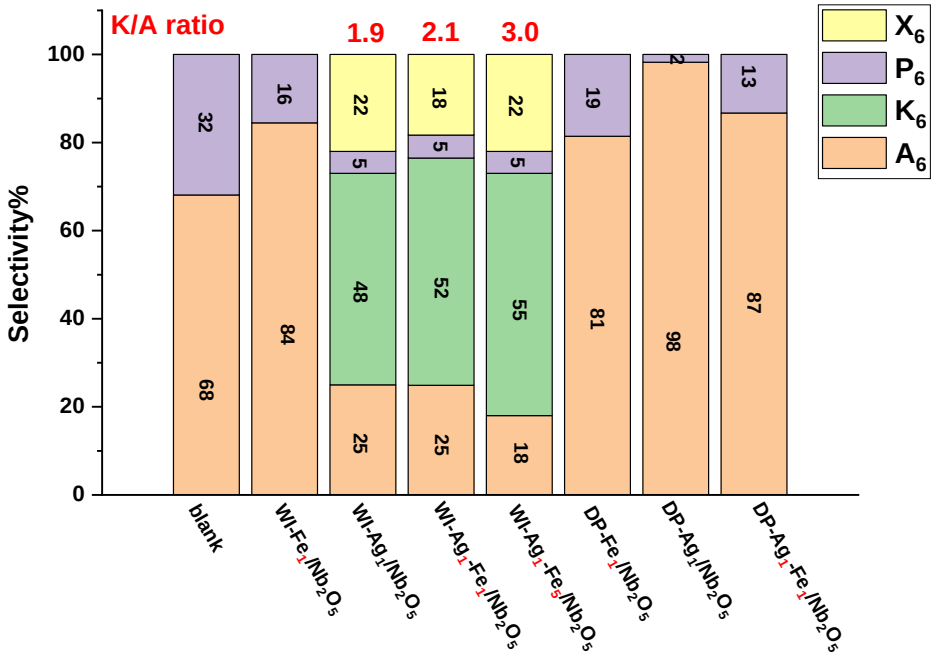

b. Product distribution by Ag-Fe/Nb_2O_5

Fig. 6.8 Cyclohexane oxidation by supported bimetallic Ag-Fe/Nb_2O_5 catalysts. a: Conversion of cyclohexane; b: Product distribution for cyclohexane oxidation. The loading of Ag is 1 *wt*%

in all catalysts. WI(DP)-Ag_1-Fe_1/Nb_2O_5 denotes the catalyst prepared by wet impregnation (deposition precipitation) method with molar ratio n(Ag):n(Fe)=1:1; WI-Ag_1-Fe_5/Nb_2O_5 denotes the catalyst prepared by wet impregnation method with molar ratio n(Ag):n(Fe)=1:5; WI(DP)-Fe_1/Nb_2O_5 denotes the by wet impregnation (deposition precipitation) method with Fe loading 0.52 *wt*%. The pH value in DP method was 9 and calcination temperature was 550 °C for 5 h for Fe/Nb_2O_5. cyclohexane (3 mL), M(Ag):S=1:1000, T = 120 °C, $P(O_2)$ = 4 bar, t = 24 h.

The conversion is obviously enhanced in the presence of supported WI-Ag/Nb_2O_5 and WI-Ag-Fe/Nb_2O_5, whereas the use of only WI-Fe/Nb_2O_5 seems to act as inert for the reaction. However, the nearly identical conversion of WI-Ag/Nb_2O_5 and WI-Ag-Fe/Nb_2O_5 catalysts tentatively proves that the existence of Fe species shows no enhancement effect on the conversion of cyclohexane. There is however a small change in K/A ratio with an increase in Fe:Ag molar ratio presenting the trend to facilitate the formation of cyclohexanone and improve K/A ratio. Thus supporting our working hypothesis of a bimetallic but also bifunctional catalyst with Ag regions promoting the conversion of the reaction and Fe regions promoting an enhanced selectivity. In our study, $Fe(NO_3)_3 \cdot 9H_2O$ was used as a precursor for the preparation of catalysts and the calcination temperature was 550 °C. Studies[63-65] demonstrate that the final decomposition products are mainly α-Fe_2O_3 where the valance of Fe is 3. As WI-Fe/Nb_2O_5 proves no direct effect on cyclohexane oxidation, herein, the supported Fe_2O_3 nanoparticles over Nb_2O_5 in bimetallic Ag-Fe/Nb_2O_5 play a role in the decomposition of cyclohexyl hydroperoxide, a key intermediate that can be transformed to cyclohexanone or cyclohexanol[1, 19]. Following the radical mechanism, the ketone can be obtained via the recombination of two peroxyl radicals to give an

equal amount of cyclohexanol and cyclohexanone or α-H abstraction by the chain carrier $C_6H_{11}O_2$· to give cyclohexanone (as shown in eq. 6.4 and 6.5). From this perspective, it is deduced that the presence of Fe(III) species may facilitate the reaction in a path that with the formation of cyclohexyl peroxyl radicals $C_6H_{11}O_2$·. Thus, it is possible that the Fe(III) species reacts with cyclohexyl hydroperoxide to give $C_6H_{11}O_2$·, as evidenced in the case of oxidation by means of Co(III) salts[5, 20]. Other factors though, can come into place: the formation of $C_6H_{11}O$· radicals that can abstract H atom to give cyclohexanol, a fraction of the $C_6H_{11}O$· radicals can be converted to by-products (6-hydroxyhexanoic acid)[19, 20], as observed that the yield for 6-hydroxyhexanoic acid slightly increases. In addition, cyclohexanol can be converted into cyclohexanone during the oxidation under this reaction conditions. Therefore, these factors may contribute to the excess amount of cyclohexanone than cyclohexanol.

However, no obvious conversion when using the supported monometallic Ag/Nb_2O_5 and bimetallic $Ag\text{-}Fe/Nb_2O_5$ prepared by deposition precipitation method. This, however, can be due to a number of reasons: a lack of segregation for Ag and Fe species, unreactive mixed metal oxides. Furthermore it should also be considered that $Fe(OH)_3$ species, which are the precursor to Fe_2O_3 upon calcination, are amphoteric and a pH of 9 can be too basic and promote the redissolution of the metal. In addition, it should be mentioned that all the catalytic tests were conducted in the absence of initiator (i.e., TBHP) and that supported Ag/Nb_2O_5 and $Ag\text{-}Fe/Nb_2O_5$ prepared by wet impregnation can initiate the reaction without any initiator with a

superior performance and an economical factor is considered meanwhile. Besides, there is research indicating that catalysis system including Ag can perform as good as organic radicals for the initiation of cyclohexane oxidation[27]. Therefore, an initiator is not necessarily needed for a catalytic system.

6.5.2 ICP-MS control tests

ICP-MS analysis results show that the highest leaching of Ag and Fe occurs in the presence of WI-Ag_1-Fe_5/Nb_2O_5, with the value at 0.01% and 0.002% based on the nominal added weight amount of Ag (2.99 mg) and Fe (7.75 mg) from this catalyst. Herein, it is ascertained that the supported bimetallic Ag-Fe/Nb_2O_5 is efficient for cyclohexane oxidation by preserving a high stability with low metal leaching. Ultimately, we can conclude that Ag-Fe/Nb_2O_5 prepared by wet impregnation method followed by a straightforward calcination in air displays a promising application in the oxidation of cyclohexane, favouring to produce ketone and remaining a high stability by stabilizing the nanoparticles to resist metal leaching. In addition, the improved reaction performances in comparison with monometallic Ag/Nb_2O_5 implies a synergetic effect, most likely occurring between supported Ag_2O and Fe_2O_3 nanoparticles in bimetallic catalysts.

Table 6.2 Full scan analysis of the metal content and impurities present in reaction mixture, expressed in mg of contaminant in 3 mL reaction mixture. Sample extracted via deionised water. The tests were conducted at 120 °C, 4 bar O_2 for 24 h, with M(Ag):S ratio=1:1000. 3 mL cyclohexane used.

Sample ID	Ag	Al	As	B	Ba	Ca
WI-Ag/Nb_2O_5	0.00018	0.01080	0.00147	0.0489	0.00279	0.01806
WI-Ag_1-Fe_1/Nb_2O_5	0.00024	0.00891	0.00108	0.0387	0.00282	0.01542
WI-Ag_1-Fe_5/Nb_2O_5	0.00030	0.00963	0.00108	0.0372	0.0024	0.01416

Sample ID	Fe	K	Mg	Na	Si	Zn
WI-Ag/Nb_2O_5	0.00012	0.00570	0.00174	0.1251	0.02187	0.00009
WI-Ag_1-Fe_1/Nb_2O_5	0.00015	0.00591	0.00174	0.1140	0.02325	0.00012
WI-Ag_1-Fe_5/Nb_2O_5	0.00015	0.00501	0.00147	0.1065	0.01767	0.00033

6.5.3 XRPD patterns of WI-Ag-Fe/Nb_2O_5

XRPD patterns in Fig. 6.9 show that no additional peaks are observed in Ag/Nb_2O_5 and Ag-Fe/Nb_2O_5 catalysts compared with that of undoped Nb_2O_5, even in the catalyst WI-Ag_1-Fe_5/Nb_2O_5 with 2.6 *wt*% Fe loading. As discussed in section 5.2.6, the low loading of supported metals could prohibit the observation of reflection from doped nanoparticle[66], and a high dispersion of particles could also make it non-detectable with the XRPD technique[67]. Besides, there may exist the overlap of characteristic peaks between Fe_2O_3 and Nb_2O_5, for example, at 2θ=36-37 °, the facet (110) of Fe_2O_3[68] and Nb_2O_5[69], 2θ=55-57 °, the facet (116) of Fe_2O_3 and (200) of Nb_2O_5. So the high intensity of Nb_2O_5 peaks may hinder the observation for characteristic peaks from the reflection of supported Fe_2O_3.

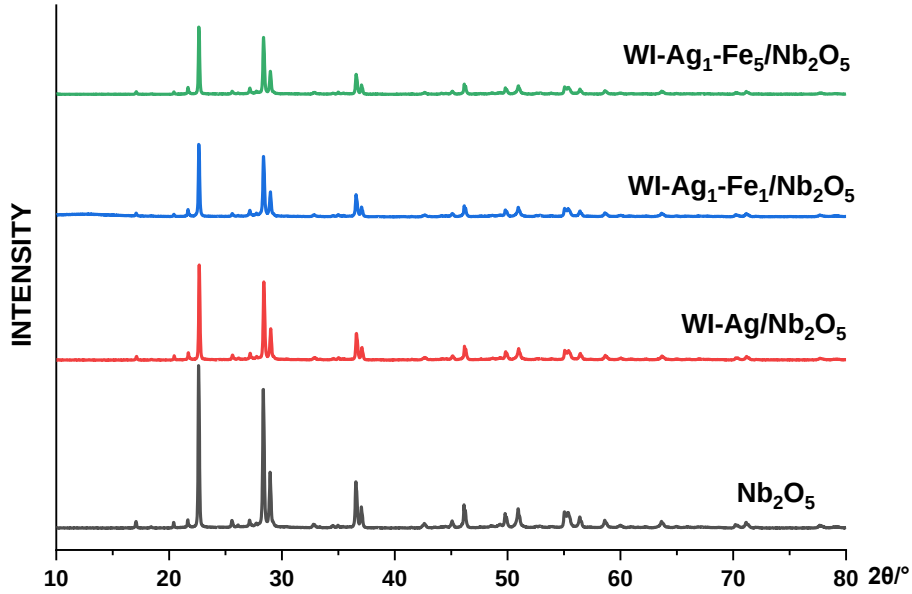

Fig. 6.9 XRPD patterns of Ag/Nb_2O_5 and $Ag\text{-}Fe/Nb_2O_5$ with nominal 1 *wt*% Ag loading prepared by wet impregnation method. WI-Ag_1-Fe_1/Nb_2O_5: the molar ratio is n(Ag):n(Fe)=1:1; WI-Ag_1-Fe_5/Nb_2O_5: the molar ratio is n(Ag):n(Fe)=1:5.

Similarly, XRPD patterns (Fig. 6.10) of supported monometallic Ag/Nb_2O_5, Fe/Nb_2O_5 and bimetallic $Ag\text{-}Fe/Nb_2O_5$ prepared by deposition precipitation method shows that no apparent diffraction peaks of Ag or Fe_2O_3 are directly observed. The reasons for this are the same as those discussed above.

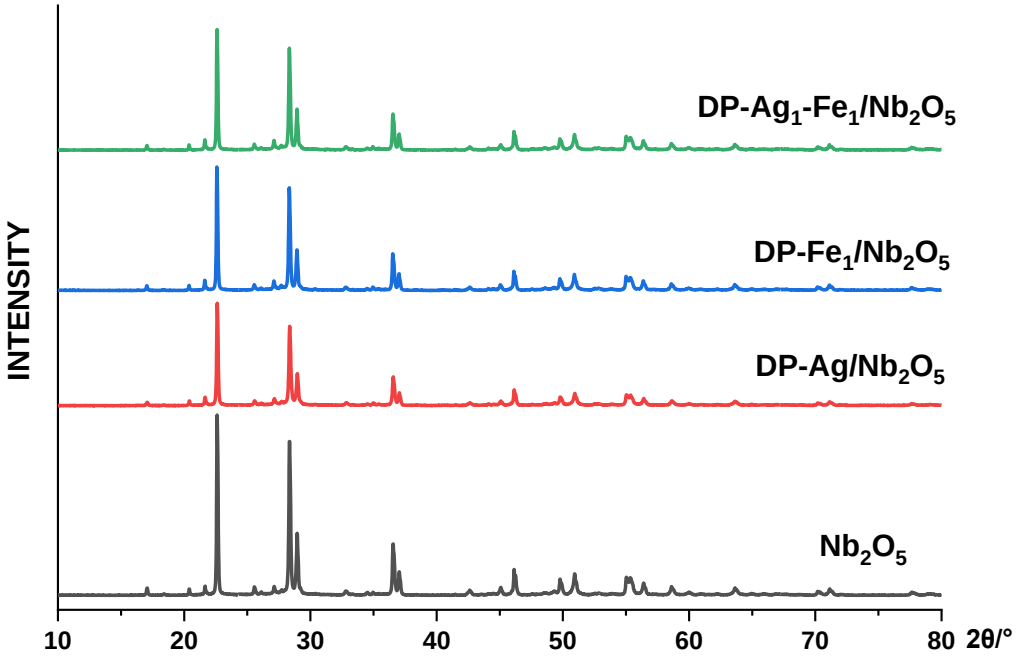

Fig. 6.10 XRPD patterns of Ag/Nb_2O_5 and $Ag\text{-}Fe/Nb_2O_5$ with nominal 1 *wt*% Ag loading prepared by deposition precipitation method. DP-Ag_1-Fe_1/Nb_2O_5: the molar ratio is n(Ag):n(Fe)=1:1; DP-Fe_1/Nb_2O_5: the nominal Fe loading is 0.52 *wt*%.

6.6 Conclusion

Supported monometallic Ag/Nb_2O_5 and bimetallic $Ag\text{-}Fe/Nb_2O_5$ were applied for the oxidation of cyclohexane under mild reaction conditions without initiator or solvent. Our optimized reaction conditions (120 ˚C, 4 bar O_2) are developed for the catalytic tests based on the blank autoxidation process without catalyst and the tests in the presence of $Fe(acac)_3$. In the catalytic tests by using WI-Ag/Nb_2O_5, M:S ratios and stirring speed are varied to ensure the reaction occurs under a kinetic regime at a stirring speed 600 $r{\cdot}min^{-1}$ with a M:S ratio = 1:1000. The results unveil that WI-Ag/Nb_2O_5 has a superior performance with an enhanced conversion maintaining at 13% while still preserving a high selectivity for cyclohexanone and cyclohexanol (>70%),

especially for cyclohexanone with a high K/A ratio (~1.9). A high stability of catalyst was verified by ICP-MS analysis showing only traces amount of Ag into reaction mixture. The activity of the supported Ag/Nb_2O_5 is highly dependent on the preparation method and only the catalysts prepared by wet impregnation method exhibits reactivity in the oxidation process while precipitated or sol-immobilized catalysts shows no catalytic activity, which is tentatively ascertained to the presence of supported Ag_2O nanoparticles in impregnation catalysts, which implies that the activation of O_2 by Ag^+ is more efficient than Ag^0 in our catalysis system. Thus, Ag/Nb_2O_5 prepared by wet impregnation method is a viable catalytic system for cyclohexane oxidation under mild conditions.

Moreover, the incorporation of a second metal Fe in supported bimetallic $Ag\text{-}Fe/Nb_2O_5$ prepared by wet impregnation method induces a synergistic effect towards the oxidation of cyclohexane. It is found that the selectivity for cyclohexanone is improved with a higher K/A ratio up to 3.0 without losing the conversion in comparison with that of monometallic $WI\text{-}Ag/Nb_2O_5$. In view of this, the bimetallic catalyst reveals a better reaction performance by optimizing the product distribution for cyclohexanone, which is an important precursor for the production of adipic acid, a building block for the manufacture of nylon-6 or nylon-66. Therefore, the results illustrate a great potential for the exploitation of supported Ag based catalysts in cyclohexane oxidation under mild reaction conditions with lower temperature (~120 °C) and pressure (~4 bar O_2).

6.7 Reference

1. B. P. Hereijgers and B. M. Weckhuysen, *J. Catal.*, 2010, **270**, 16-25.
2. M. T. Musser, *Ullmann's Encyclopedia of Industrial Chemistry*, 2000, p 49-50.
3. I. i. a. V. e. Berezin, E. T. Denisov and N. M. Emanuel, *The oxidation of cyclohexane*, Elsevier, 2018, p 1-3.
4. A. Ramanathan, M. S. Hamdy, R. Parton, T. Maschmeyer, J. C. Jansen and U. Hanefeld, *Appl. Catal. A: Gen.*, 2009, **355**, 78-82.
5. M. Conte, X. Liu, D. M. Murphy, K. Whiston and G. J. Hutchings, *Phys. Chem. Chem. Phys.*, 2012, **14**, 16279-16285.
6. A. A. Alshaheri, M. I. M. Tahir, M. B. A. Rahman, T. B. Ravoof and T. A. Saleh, *Chem. Eng. Sci.*, 2017, **327**, 423-430.
7. I. Hermans, P. Jacobs and J. Peeters, *Chem. Eur. J.*, 2007, **13**, 754-761.
8. A. Alshammari, A. Koeckritz, V. N. Kalevaru, A. Bagabas and A. Martin, *ChemCatChem*, 2012, **4**, 1330-1336.
9. S. Van de Vyver and Y. Román-Leshkov, *Catal. Sci. Technol.*, 2013, **3**, 1465-1479.
10. M. Hasanzadeh, G. Karim-Nezhad, M. Mahjani, M. Jafarian, N. Shadjou, B. Khalilzadeh and L. Saghatforoush, *Catal. Commun.*, 2008, **10**, 295-299.
11. D. L. Vanoppen, D. E. De Vos, M. J. Genet, P. G. Rouxhet and P. A. Jacobs, *Angew. Chem., Int. Ed. Engl.*, 1995, **34**, 560-563.

12. J. Medina-Valtierra, J. Ramírez-Ortiz, V. M. Arroyo-Rojas and F. Ruiz, *Appl. Catal. A: Gen.*, 2003, **238**, 1-9.

13. M. Conte, X. Liu, D. M. Murphy, S. H. Taylor, K. Whiston and G. J. Hutchings, *Catal. Lett.*, 2016, **146**, 126-135.

14. U. Schuchardt, D. Cardoso, R. Sercheli, R. Pereira, R. S. Da Cruz, M. C. Guerreiro, D. Mandelli, E. V. Spinacé and E. L. Pires, *Appl. Catal. A: Gen.*, 2001, **211**, 1-17.

15. A.-Q. Wang, J.-H. Liu, S. Lin, T.-S. Lin and C.-Y. Mou, *J. Catal.*, 2005, **233**, 186-197.

16. A.-Q. Wang, C.-M. Chang and C.-Y. Mou, *J. Phys. Chem. B*, 2005, **109**, 18860-18867.

17. Y. Wang, *Res. Chem. Intermed.* , 2006, **32**, 235-251.

18. X. Liu, Y. Ryabenkova and M. Conte, *Phys. Chem. Chem. Phys.*, 2015, **17**, 715-731.

19. I. Hermans, P. Jacobs and J. Peeters, *Chem. Eur. J.* , 2007, **13**, 754-761.

20. I. Hermans, J. Peeters and P. A. Jacobs, *The Journal of Physical Chemistry A*, 2008, **112**, 1747-1753.

21. R. Schlögl, A. Knop-Gericke, M. Hävecker, U. Wild, D. Frickel, T. Ressler, R. E. Jentoft, J. Wienold, G. Mestl and A. Blume, *Top. Catal.*, 2001, **15**, 219-228.

22. I. Hermans, J. Peeters and P. A. Jacobs, *Top. Catal.*, 2008, **50**, 124-132.

23. I. Hermans, J. Peeters and P. A. Jacobs, *ChemPhysChem*, 2006, **7**, 1142-1148.

24. I. Hermans, J. Peeters and P. A. Jacobs, *Top. Catal.*, 2008, **48**, 41-48.

25. G. A. Olah, Á. Molnár and G. S. Prakash, *Hydrocarbon Chemistry, 2 Volume Set*, John Wiley & Sons, 2017, p 593-595.

26. M. Conte, H. Miyamura, S. Kobayashi and V. Chechik, *Chem. Commun.*, 2010, **46**, 145-147.

27. X. Liu, M. Conte, Q. He, D. Knight, D. Murphy, S. Taylor, K. Whiston, C. Kiely and G. J. Hutchings, *Chem. Eur. J.* , 2017.

28. J.-R. Chen, H.-H. Yang and C.-H. Wu, *Org. Process Res. Dev.*, 2004, **8**, 252-255.

29. C.-C. Guo, M.-F. Chu, Q. Liu, Y. Liu, D.-C. Guo and X.-Q. Liu, *Appl. Catal. A: Gen.*, 2003, **246**, 303-309.

30. R. Kumar, S. Sithambaram and S. L. Suib, *J. Catal.*, 2009, **262**, 304-313.

31. M. Ewing and J. S. Ochoa, *J. Chem. Thermodyn.* , 2000, **32**, 1157-1167.

32. D. Mackay, W.-Y. Shiu and S. C. Lee, *Handbook of physical-chemical properties and environmental fate for organic chemicals*, CRC press, 2006, p 398-400.

33. M. Hartmann and S. Ernst, *Angew. Chem. Int. Ed.*, 2000, **39**, 888-890.

34. U. Schuchardt, R. Pereira and M. c. Rufo, *J. Mol. Catal. A Chem.*, 1998, **135**, 257-262.

35. U. Schuchardt, E. KRAHEMBUHL and W. Carvalho, *New J. Chem.*, 1991.

36. D. H. Barton, S. D. Bévière and D. R. Hill, *Tetrahedron*, 1994, **50**, 2665-2670.

37. L. Matienko and L. Mosolova, *Pet. Chem.*, 2008, **48**, 371-380.

38. H. Fallmann, T. Krutzler, R. Bauer, S. Malato and J. Blanco, *Catal. Today*, 1999, **54**, 309-319.

39. A. Busiakiewicz, A. Kisielewska, I. Piwoński and D. Batory, *Appl. Surf. Sci.* , 2017, **401**, 378-384.

40. C. Resini, F. Catania, S. Berardinelli, O. Paladino and G. Busca, *Appl. Catal. B: Environ.*, 2008, **84**, 678-683.

41. A. Villa, N. Janjic, P. Spontoni, D. Wang, D. S. Su and L. Prati, *Appl. Catal. A: Gen.*, 2009, **364**, 221-228.

42. Y.-R. Luo, *Comprehensive handbook of chemical bond energies*, CRC press, 2007.

43. S. Furukawa, T. Shishido, K. Teramura and T. Tanaka, *J. Phys. Chem. C*, 2011, **115**, 19320-19327.

44. L. Y. Margolis and V. N. Korchak, *Russ. Chem. Rev.*, 1998, **67**, 1073-1082.

45. X. Liu, M. Conte, M. Sankar, Q. He, D. M. Murphy, D. Morgan, R. L. Jenkins, D. Knight, K. Whiston and C. J. Kiely, *Appl. Catal. A: Gen.*, 2015, **504**, 373-380.

46. M. Conte, K. Wilson and V. Chechik, *Rev. Sci. Instrum.*, 2010, **81**, 104102.

47. M. Conte and V. Chechik, *Chem. Commun.*, 2010, **46**, 3991-3993.

48. J. R. Bourne, *Org. Process Res. Dev.*, 2003, **7**, 471-508.

49. M. Grabchenko, G. Mamontov, V. Zaikovskii, V. La Parola, L. Liotta and O. Vodyankina, *Appl. Catal. B: Environ.*, 2020, **260**, 118148.

50. M. Grabchenko, G. Mamontov, V. Zaikovskii and O. Vodyankina, *Kinet. Catal.*, 2017, **58**, 642-648.

51. M. Conte, J. A. Lopez-Sanchez, Q. He, D. J. Morgan, Y. Ryabenkova, J. K. Bartley, A. F. Carley, S. H. Taylor, C. J. Kiely and K. Khalid, *Catal. Sci. Technol.*, 2012, **2**, 105-112.

52. M. Skaf, S. Aouad, S. Hany, R. Cousin, E. Abi-Aad and A. Aboukaïs, *J. Catal.*, 2014, **320**, 137-146.

53. X.-Y. Gao, S.-Y. Wang, J. Li, Y.-X. Zheng, R.-J. Zhang, P. Zhou, Y.-M. Yang and L.-Y. Chen, *Thin Solid Films*, 2004, **455**, 438-442.

54. A. Samokhvalov, E. C. Duin, S. Nair and B. J. Tatarchuk, *Appl. Surf. Sci.*, 2011, **257**, 3226-3232.

55. D. Barkhuizen, I. Mabaso, E. Viljoen, C. Welker, M. Claeys, E. van Steen and J. C. Fletcher, *Pure Appl. Chem.*, 2006, **78**, 1759-1769.

56. J. M. Campelo, D. Luna, R. Luque, J. M. Marinas and A. A. Romero, *ChemSusChem: Chemistry & Sustainability Energy & Materials*, 2009, **2**, 18-45.

57. C. González-Arellano, J. M. Campelo, D. J. Macquarrie, J. M. Marinas, A. A. Romero and R. Luque, *ChemSusChem*, 2008, **1**, 746-750.

58. A. Busiakiewicz, A. Kisielewska, I. Piwoński and D. Batory, *Appl. Surf. Sci.*, 2017, **401**, 378-384.

59. S. Kunze, P. Grosse, M. Bernal Lopez, I. Sinev, I. Zegkinoglou, H. Mistry, J. Timoshenko, M. Y. Hu, J. Zhao and E. E. Alp, *Angew. Chem.*, 2020, **132**, 22856-22863.

60. G. Sharma, A. Kumar, S. Sharma, M. Naushad, R. P. Dwivedi, Z. A. ALOthman and G. T. Mola, *J. King Saud Univ. Sci.*, 2019, **31**, 257-269.

61. N. Toshima and T. Yonezawa, *New J. Chem.*, 1998, **22**, 1179-1201.

62. Z.-Q. Zhang, J. Huang, L. Zhang, M. Sun, Y.-C. Wang, Y. Lin and J. Zeng, *Nanotechnology*, 2014, **25**, 435602.

63. P. Melnikov, V. Nascimento, I. Arkhangelsky, L. Z. Consolo and L. De Oliveira, *J. Therm. Anal. Calorim.* , 2014, **115**, 145-151.

64. M. Elmasry, A. Gaber and E. Khater, *J. Therm. Anal. Calorim.*, 1998, **52**, 489-495.

65. A. M. Gadalla and H.-F. Yu, *J. Mater. Res*, 1990, **5**.

66. R. Mohamed and I. A. Mkhalid, *J. Alloys Compd.*, 2010, **501**, 301-306.

67. C. A. Castro, P. Osorio, A. Sienkiewicz, C. Pulgarin, A. Centeno and S. A. Giraldo, *J. Hazard. Mater.*, 2012, **211**, 172-181.

68. G. Tong, J. Guan, Z. Xiao, X. Huang and Y. Guan, *J. Nanoparticle Res.*, 2010, **12**, 3025-3037.

69. H. Wen, Z. Liu, J. Wang, Q. Yang, Y. Li and J. Yu, *Appl. Surf. Sci.*, 2011, **257**, 10084-10088.

Chapter 7: A preliminary exploitation of supported Ag over activated carbon applied into cyclic hydrocarbons oxidation under mild conditions

7.1 Overview

Activated carbon materials have been widely applied as catalyst support, especially for fine chemistry applications[1-3]. There are a few studies about the use of supported nanoparticles over activated carbons employed in various oxidation reactions[4-6], such as the oxidation of glycerol, cyclohexane. The modified materials can also act as catalysts on their own[2, 7, 8], e.g., cyclohexanol oxidation, alcoholysis of epoxides. The success of the applications of activated carbon as a support for catalytic materials is attributed to properties like, extended pore structure, high surface area, the feasibility of tailoring of surface chemistry to meet the catalytic demands (e.g., surface properties can be altered by acid treatment and heat treatment in nitrogen is found to eliminate oxygenated groups like carbonyl/quinone groups, which results in the decrease of selectivity for adipic acids in cyclohexane oxidation[1]), as well as the low cost and the stability in both acidic and alkaline environments[1, 9-11]. Meanwhile, as carbon can be burnt, which enables the easy recovery of the active catalytic metals[12]. It is reported that the surface oxygen groups (e.g. hydroxyl, carboxyl, quinone, peroxide, aldehyde[13]) are especially relevant for the catalysts performances: i) the surface oxygen group can decrease the hydrophobicity of the carbon, improving the accessibility of metal precursor in the impregnation process[14]; ii) the pH values of

aqueous carbon slurries can be controlled by surface oxygen groups, which affects the impregnation process[15]; iii) the oxygen groups are responsible for the anchoring sites as nucleation centres for the deposition of metallic particles[12, 16]. In view of these effects, oxygen functional groups play a significant role in controlling the properties of activated carbon-based catalysts. The functional groups can be generated spontaneously by exposure to the atmosphere, or oxidative and thermal treatment can modify the concentration of these groups[9, 17-19]. In addition, the high surface area and pore structure of activated carbon are capable of affecting the dispersion of an active metal and the diffusion of reactants and products, by which the observed reaction performances could be influenced[20, 21]. However, there might exist limitations of mass transfer in the reaction process due to the presence of rich porous structure and the interactions between active sites and substrate molecules can be blocked. The anchoring sites for active phase might be limited, resulting in a nonuniform dispersion of active metals on the surface of activated carbon[17, 22]. Thus, the porosity and surface oxygen groups of activated carbon can be tuned to meet the specific catalytic process.

According to the roles of supported Ag nanoparticles in the oxidation of cyclooctane and cyclohexane for the activation of O_2 to enhance the oxidation without initiator under mild reaction conditions, the application of supported Ag over activated carbon in cyclic hydrocarbons oxidation was firstly exploited. Since activated carbon is reported to be capable of stabilizing the high oxidation state of metals[16] and the presence of Ag^+ species is proved to be effective in the initiation step according to the discussion in chapter 5 and 6, from this perspective it is expected that a higher

abundance of Ag^{+} species promoted by activated carbon will enhance the oxidation process furtherly. Although, activated carbon can reduce the supported metals from metal oxides state to metallic metals (e.g., in the case of supported gold over activated carbon, Au^{3+} is reduced to Au^{0} [23, 24]). In view of these two features, it is possible that there will be coexistence of Ag^{0} and Ag^{+} (Ag_2O) species, which will affect the reaction performance of catalysts, providing insights to furtherly distinguish the roles of Ag or Ag^{+} species in hydrocarbons oxidation process. In our case, three commercial activated carbons (Darco 4-12 mesh(AC-1), Norit GAC 12-40(AC-2) and Darco G-60(AC-3), all supplied by Acros) without pre-treatment were used as supports in supported Ag/AC catalysts. These various kinds of activated carbon are all commercially available and they pose different properties, e.g., surface areas, pore volume or acid/basic properties (AC-1 displays acidity while AC-2 is basic[16, 25]), by which the catalysts properties like particle size can be adjusted. Therefore, given the effects of activated carbon as support, carbon-based catalysts were prepared for the tests in cyclooctane and cyclohexane oxidation.

7.2 Cyclooctane oxidation

In this part, supported Ag/AC with different types of activated carbon prepared by using a wet impregnation protocol was applied in the oxidation of cyclooctane under a fixed optimized reaction condition (110 °C, 2 bar O_2, 24 h, 600 rpm).

7.2.1 Tests in the presence of supported Ag/AC prepared by wet impregnation method

Surprisingly against our working hypothesis (the feasibility of Ag/AC catalysts on the ground of C being able to stabilize Ag^+ but still preserving a Ag(0) component), our catalytic tests (table 7.1) show that there is no obvious conversion in the presence of activated carbon or supported Ag/C catalysts. In comparison with the blank tests, the catalysts even inhibit the reaction to an extent. In the catalyst dried at 120 °C for 16 h before calcination, most of the Ag species probably exists in the status of $AgNO_3$ and the impregnated catalyst after calcination (180 °C for 16 h) is likely to be rich in supported Ag_2O nanoparticles. Whereas both of them show no reactivity for the oxidation, whose performances are different from that of Ag/Nb_2O_5. According to our results, Ag^+ in $AgNO_3$ and supported Ag_2O/Ag in impregned Ag/Nb_2O_5 is capable to enhance the formation of alkyl hydroperoxides in the oxidation of cyclooctane and cyclohexane by activating the O_2[26]. In view of this, it appears that the effect of Ag species is hindered due to the presence of activated carbon in our case. The tests in the presence of ($AgNO_3$+AC) (physically mixed by grinding together) suggest the inactivity for the oxidation, furtherly implying that the enhanced impact of Ag species for the oxidation is blocked. We speculate that these results may be ascribed to the chemical structure of carbon itself, which is rich in conjugated double bonds (Fig. 7.1). On the other hand, double bonds are known to react with radical species[27, 28]. If this is the case, the carbon would then act as a radical quencher, and it would also explain

the inhibition effect that we observe in the presence of activated carbon only, but it would also indirectly prove that the reaction mechanism would be entirely free-radical based, even in the presence of Ag species. Therefore, even in view of this result not fulfilling out working hypothesis it does still provide extremely valuable mechanistic information.

Table 7.1 Reaction results of activated carbon and supported Ag/AC in cyclooctane oxidation. All Ag/AC catalysts was loaded with nominal 1 *wt*% Ag. 3 mL cyclooctane used with M(Ag):S=1:1000. $P(O_2)$ = 2 bar. T = 110 °C, t = 24 h. AC-1 denotes Darco 4- 12 mesh activated carbon; AC-2 denotes Norit 12-40 mesh activated carbon; AC-3 denotes Darco G60 activated carbon. All types of the activated carbon were unmodified. Ag/AC-1 (2, 3) denotes the catalysts prepared by using AC-1 (2, 3) respectively.

Catalysts	Preparation conditions	Conversion/ %	Selectivity/%			
			A_8	K_8	P_8	X_8
blank	--	6±4	0	8	66	26
AC-1	Parent activated carbon	0.2±4	0	6	52	42
AC-2		0.3±4	0	7	55	38
AC-3		0.2±4	0	4	57	39
Ag/AC-1	Dried at 120 °C for 24h	0.2±4	0	4	38	58
Ag/AC-2		0.3±4	0	0	54	46
Ag/AC-3		0.2±4	0	0	49	51
Ag/AC-1	Calcined at 180 °C for 24h	0.2±4	0	6	79	16
Ag/AC-2		0.3±4	0	16	45	39
Ag/AC-3		0.2±4	0	7	59	34
($AgNO_3$+AC-1)	Physical mixing by grinding	0.2±4	0	9	53	38
($AgNO_3$+AC-2)		0.2±4	0	9	41	50
($AgNO_3$+AC-3)		0.2±4	0	7	45	48

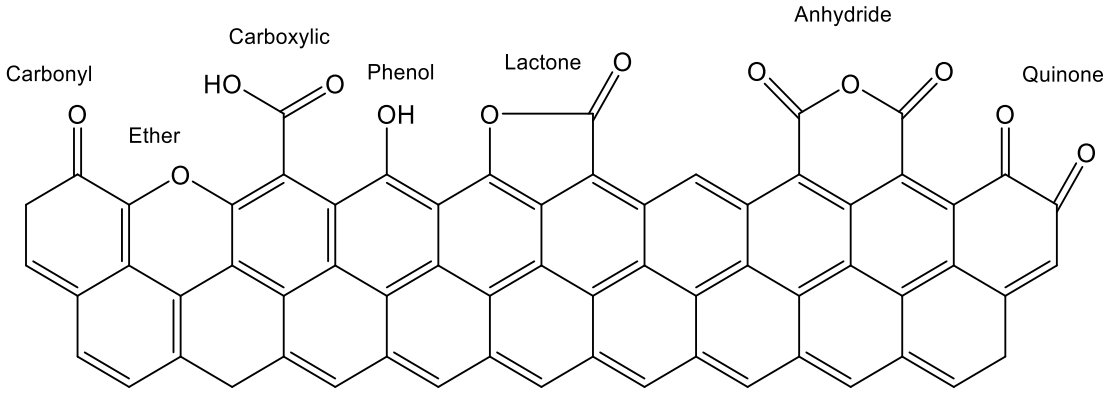

Fig. 7.1 A illustration of surface oxygen groups in carbon materials.[2, 18] Reprinted from Figueiredo, J. L, et al., with permission from Elsevier.

Although we consider this factor to be the major one for the inactivity of our materials, for completeness, we have considered the following other options: i) The deposition of supported Ag/Ag_2O nanoparticles on the surface is influenced. There are researches illustrating that surface oxygen groups could decreases the hydrophobicity of the carbon, thus making surface more accessible to the metal precursor during the impregnation process[10, 29]. And the pre-treatment for carbon by thermal or chemical processes could create new nucleation sites for metals on the carbon surface[16, 17]. In view of this, it is probably there is not enough oxygen functional groups as nucleation centres to induce the deposition of Ag/Ag_2O nanoparticles over activated carbon, which leads to the diminishing effect of active sites for cyclooctane oxidation, thus explaining the limited conversion for activated carbon and Ag/AC to an extent. ii) However, the tests by ($AgNO_3$+AC) seems to conflict with the assumption i) as the presence of Ag^+ species should have exhibited a promotion effect on the oxidation but there is still no apparent conversion. It has been reported that carbon surfaces contain both hydrophobic and hydrophilic sites[13, 30]. Thus, it is possible that the abundance of hydrophobic and hydrophilic sites due to the high surface area may act as sites blockers to hinder the interaction of Ag sites and substrate. iii) Due to the existence of pores, the internal diffusion limitation could be an impacting factor. Molecular O_2 need diffuse into the pores to access the Ag sites as part of the Ag species is possibly located inside of the pores, which could slow down the reaction rate.

According to the above postulates about the inactivity of Ag/AC in cyclooctane oxidation, the tests with higher M:S ratios were carried out in the presence of Ag/AC-1

and Ag/AC-3, as shown in Fig. 7.2. Still the catalysts display inactivity or inhibiting effect during the oxidation, indicating that the amount of active site is not the main reason to explain this reaction behaviour. Meanwhile, product distribution in Fig. 7.2-b exhibits the selectivity for by-product obviously increase with the increase of M:S ratio, which is possibly related with the Brønsted acidity from the activated carbons due to the presence of oxygen functional group[16, 31]. This, however, may also be attributed to the internal diffusion of products from the pores leading to the overoxidation, as described in iii). In addition, there exist observed changes in product distribution by Ag/AC or AC, which can be attributed to the differences of physical or chemical properties of activated carbon, i.e., particle size, surface area, or the dispersion and concentration of oxygen functional groups on the surface[14]. Among the by-products, it is found that the dominating one is cyclooctene, which is obtained as a dehydration product from cyclooctanol[32].

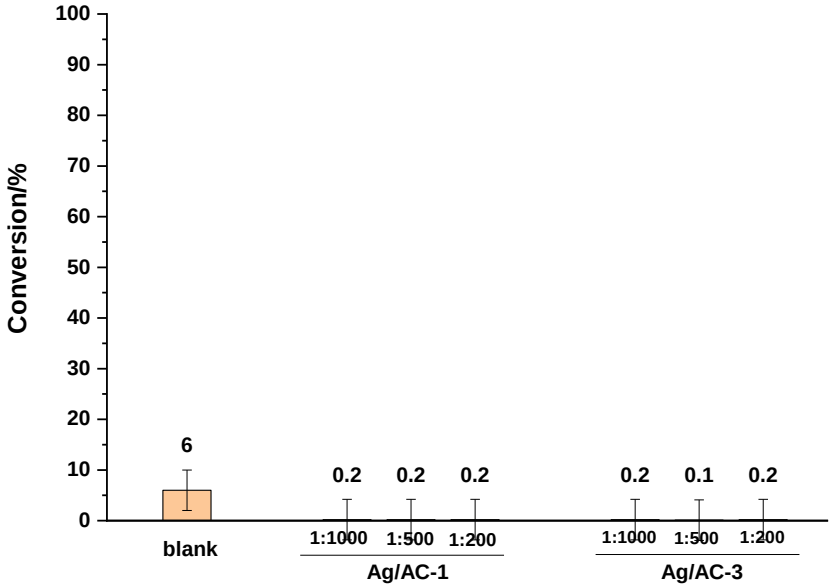

a. Conversion of cyclooctane by Ag/AC with various M:S ratios

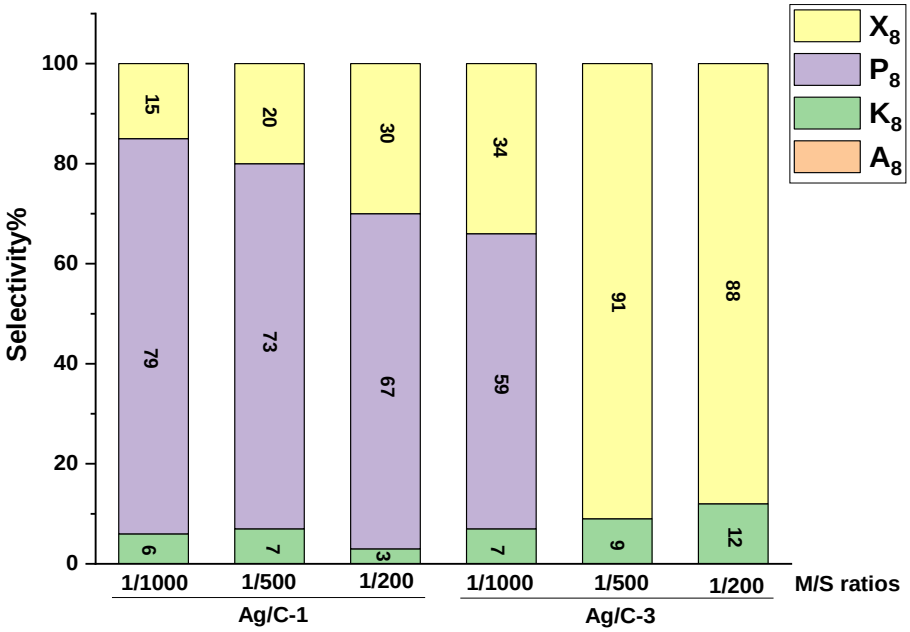

b. Product distribution by Ag/AC with various M/S ratios

Fig. 7.2 Cyclooctane oxidation by Ag/AC (1 *wt*%) prepared by wet impregnation method with various M:S ratios. a: Conversion of cyclooctane; b: Product distribution for cyclooctane oxidation. Ag/AC-1 (3) denotes the catalysts prepared by using AC-1 (3) respectively. Catalysts were calcined at 180 °C for 16 h. 3 mL cyclooctane used. T = 110 °C, $P(O_2)$ = 2 bar, t = 24 h.

7.2.2 Tests in the presence of supported Ag/AC with *tert*-butyl hydroperoxide (TBHP)

On the other hand, we speculated that the reaction could still occur in the presence of a radical initiator, as a 'standard' activation route, since that there are in literature noble metal supported on carbon catalysts that can be activated by this route[33-35], such as the oxidation of cyclohexane or alcohols like cyclohexanol, octanol in the presence of TBHP. In our case, *tert*-butyl hydroperoxide was directly used for the reaction by considering that TBHP is both a radical initiator and an oxygen donor for the free radical process[36-38]. TBHP can undergo homolytic cleavage of the O–O bond, and the process

are illustrated as scheme 7.1[28, 39]. Moreover, the role as oxygen donor is demonstrated in scheme 7.2[40], where an oxygen atom is transferred from peroxides to substrates to give oxygen containing products and a by-product is formed from the oxygen donor, e.g., in the case of TBHP, tert-butyl alcohol is formed, which can be regenerated by H_2O_2 in acid media[41]. It is found that TBHP has been applied in various reactions as oxygen donor, for example, epoxidation of cyclohexene with Ru clusters[42], styrene by supported Mn catalysts[43] or alcohols by titanium-based catalysts[36].

$(CH_3)_3$-C-OOH ⟶ $(CH_3)_3$-C-O· + ·OH **(eq. 7.1)**

$(CH_3)_3$-C-O· + $(CH_3)_3$-C-OOH ⟶ $(CH_3)_3$-C-OH + $(CH_3)_3$-C-OO· **(eq. 7.2)**

2$(CH_3)_3$-C-OO· ⟶ 2$(CH_3)_3$-C-O· + O_2 **(eq. 7.3)**

Scheme 7.1 The decomposition mechanism of TBHP.

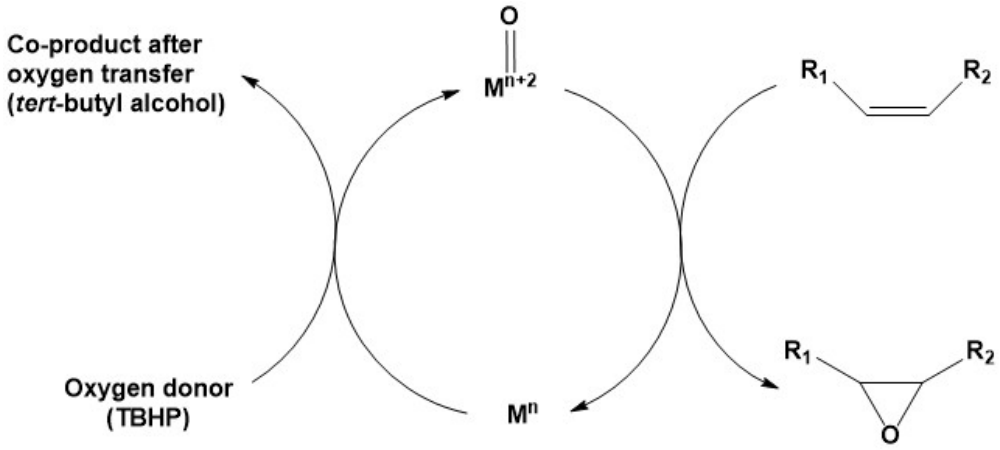

Scheme 7.2 An illustration of oxygen transfer process involves metal centre and oxygen donor. The oxygen atom is transferred by metal centre from oxygen donor to the regents.[40] Reproduced from Ref. 40 with permission from the Royal Society of Chemistry.

7.2.2.1 Tests in the presence of supported Ag/AC with 1 mol% of TBHP

When TBHP is used, the conversion of blank autoxidation by TBHP is evidently improved (Fig. 7.3), with a conversion up to 63%. If taking TBHP as oxygen donor, it is

found that the mole amount of converted cyclooctane exceeds the amount of oxygen atom given from TBHP. In view of this, TBHP is mostly likely to play the roles as initiator during the oxidation process. The formed $(CH_3)_3$-C-OO· and ·OH radicals (·OH is more reactive)[44] are reactive to abstract H atom from cyclooctane to initiate the oxidation. It is observed that the conversion in the presence of Ag/AC-1 is apparently enhanced with TBHP comparing with results from the absence of initiator and a high selectivity for ketone obtained, implying the oxidation proceeds in a selective path. In contrast, the conversion is only slightly improved (1%) with the presence of Ag/AC-2 and Ag/AC-3. The granular activated carbon we used is classified by using a series of sieves with mesh sizes of 4, 12, 40, and 60, presenting different particle ranges. And the average particle size of activated carbon in our case is AC-1>AC-2>AC-3. It is reported that the internal mass transfer could be an impacting factor in the oxidation and the external or internal mass transfer resistances should be minimized[45]. Additionally, there are studies revealing that there exists diffusive transport of H_2O_2 (oxidant in methyl-tert-butyl ether removal) and substrates in different sizes of activated carbon, indicating that the reaction performances can be influenced by the intraparticle and interparticle mass transfer to an extent[46, 47]. In view of this, it is deduced that a bigger particle size of activated carbon could dimmish the limitation of mass transfer of reactants and products, which is corresponding to the above assumption iii) in 7.2.1. From this perspective, an obvious conversion is observed in the presence of Ag/AC-1 with TBHP, not by Ag/AC-2 or Ag/AC-3. Meanwhile, the high selectivity for by-products for Ag/AC-2 and Ag/AC-3 implies the overoxidation of products, thus further corroborating the

hypothesis of the transfer limitation for the products. It is reported that diffusion limitation could result in over-oxidation, which is responsible for the over-reaction of cyclohexanol in cyclohexane oxidation[48, 49]. However, the conversion is largely decreased when using Ag/AC in comparison with that of only TBHP presented. As explained in section 7.2.1. It is possible that activated carbon can quench the radicals generated by TBHP, like cyanopropyl radicals, which have been discovered in Au/MgO catalysis system with azobis-isobutyronitrile (AIBN)[28].

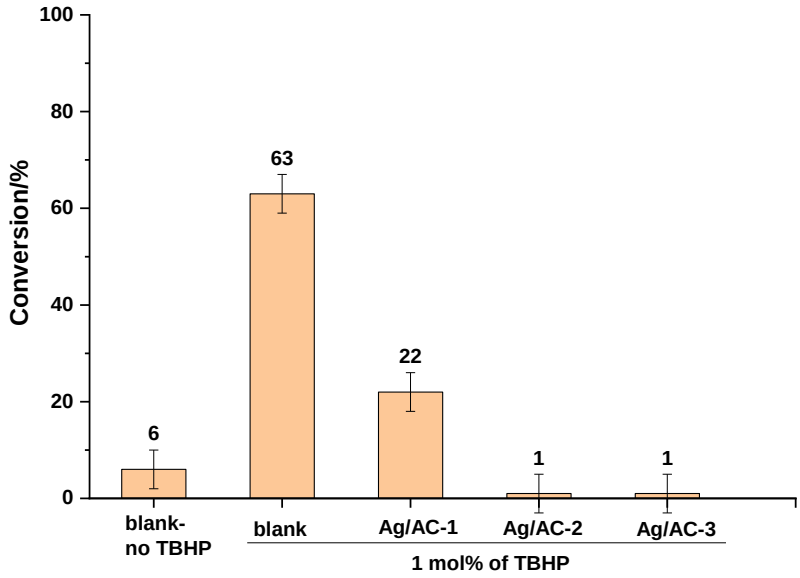

a. Conversion of cyclooctane in the presence of TBHP

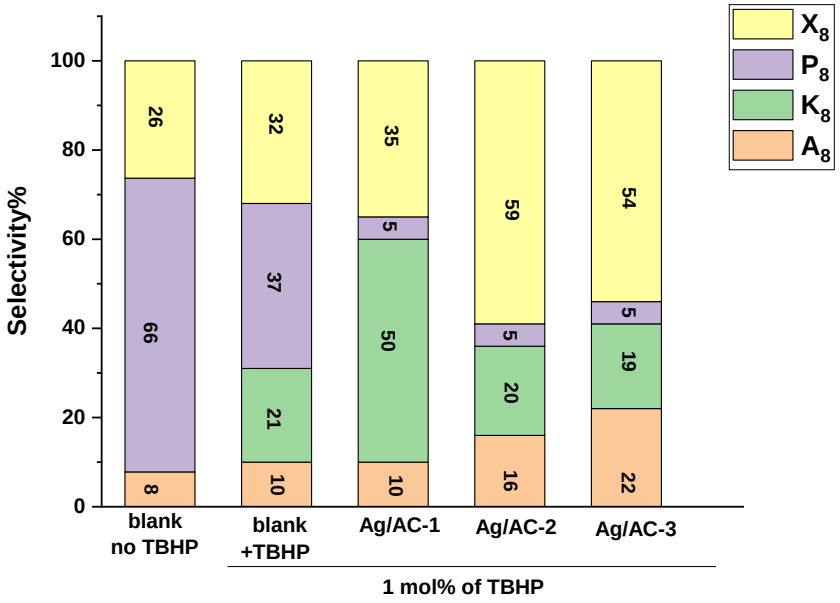

b. Product distribution of cyclooctane oxidation in the presence of TBHP

Fig. 7.3 Cyclooctane oxidation by Ag/AC (1 *wt*%) prepared by wet impregnation method in the presence of 1 mol% of TBHP. a: Conversion of cyclooctane; b: Product distribution for cyclooctane oxidation. Catalysts were calcined at 180 °C for 16 h. 3 mL cyclooctane used with M:S=1:1000. T = 110 °C, $P(O_2)$ = 2 bar, t = 24 h.

7.2.2.2 Tests in the presence of supported Ag/AC with 5 mol% of TBHP

In view of these results, we increased the amount of TBHP to 5 mol% as this was expected to enhance the oxidation in the presence of Ag/AC-1 and Ag/AC-3 with various M:S ratios (1:1000 and 1:200). As displayed in Fig. 7.4, the conversion is enhanced with the increase of TBHP concentration, especially for Ag/AC-3, as the increase in the amount of initiator results in more radicals being generated, which is expected to improve the conversion. It is found that the increasing amount of TBHP by 5 times (1 mol% to 5 mol%) does not equal to 5 times of rising in conversion, which is increased from 1% to 26% in the presence of Ag/AC-3. This similar trend is also observed for other two catalysts (Ag/AC-1 and Ag/AC-2). In view of this, furtherly we

postulate that TBHP behave as an initiator during the oxidation. Thereby, a relatively high amount of initiator is favoured in our catalytic system to dimmish the quenching effect of activated carbon on radicals for the promotion of conversion. Besides, there is slightly improvement of conversion (e.g., from (30±4)% to (36±4)% when using Ag/AC-1, identical considering the experimental error) and different product distribution is observed with the increase of M:S ratio from 1:1000 to 1:200, an implication that there might exist diffusion phenomenon.

Ultimately, it proves that the oxidation of cyclooctane by supported Ag/AC needs to be triggered with a relatively high amount of initiator (i.e., 5 mol% TBHP in our case). The mass transfer limitations and possible quenching effects of activated carbon on radicals may hinder the proceeding of this oxidation. And it should be mentioned that this catalyst system is not as efficient as that of supported Ag/Nb_2O_5 that promotes the oxidation largely with an obvious selectivity for ketone, even in the absence of initiator.

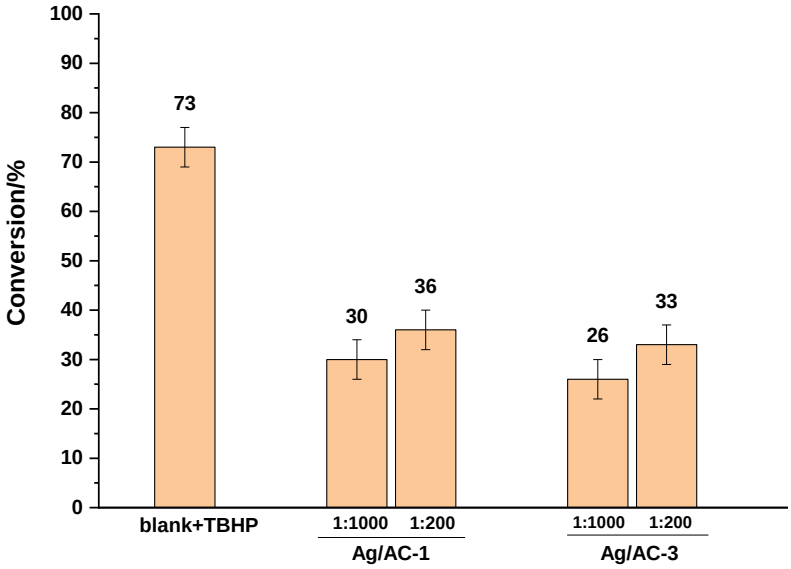

a. Conversion of cyclooctane in the presence of 5 mol% of TBHP

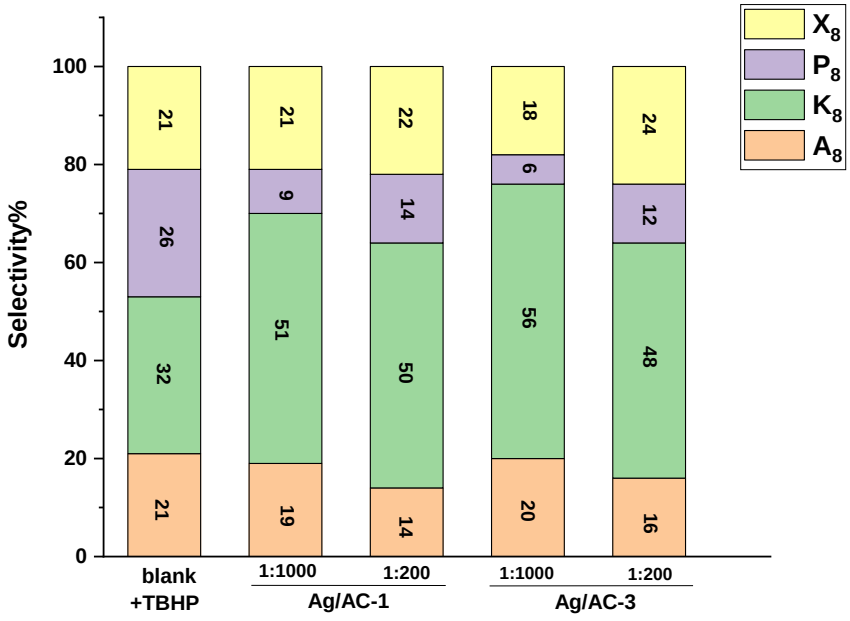

b. Product distribution of cyclooctane oxidation in the presence of 5 mol% of TBHP

Fig. 7.4 Cyclooctane oxidation by Ag/AC (1 *wt*%) prepared by wet impregnation method with 5 mol% of TBHP. a: Conversion of cyclooctane; b: Product distribution for cyclooctane oxidation. Catalysts were calcined at 180 °C for 16 h. M:S = 1:1000, T = 110 °C, $P(O_2)$ = 2 bar, t = 24 h.

7.3 Cyclohexane oxidation

Given the results obtained from cyclooctane and the relevance of cyclohexane

oxidation we were interested, the catalysts were tested for the oxidation of cyclohexane under a fixed optimized reaction condition (120 °C, 4 bar O_2, 24 h, 600 rpm).

7.3.1 Tests in the presence of supported Ag/AC prepared by wet impregnation method

Table 7.2 Reaction results about conversion and selectivity from activated carbon and supported Ag/AC in cyclohexane oxidation. All Ag/AC catalysts was loaded with nominal 1 *wt*% Ag. 3 mL cyclohexane used with M:S=1:1000. $P(O_2)$ = 4 bar. T = 120 °C, t = 24 h.

Catalysts	Preparation conditions	Conversion/ %	Selectivity/%			
			A_6	K_6	P_6	X_6
blank	--	1±1	68	0	32	0
AC-1	Parent activated carbon	0	--	--	--	--
AC-2		0	--	--	--	--
AC-3		0	--	--	--	--
Ag/AC-1	Dried at 120 °C for 24h	0	--	--	--	--
Ag/AC-2		0	--	--	--	--
Ag/AC-3		0	--	--	--	--
Ag/AC-1	Calcined at 180 °C for 24h	0	--	--	--	--
Ag/AC-2		0	--	--	--	--
Ag/AC-3		0	--	--	--	--
$AgNO_3$+AC-1	Physical mixing by grinding	0	--	--	--	--
$AgNO_3$+AC-2		0	--	--	--	--
$AgNO_3$+AC-3		0	--	--	--	--

However, as shown in table 7.2, similar with the reaction performances in cyclooctane oxidation, no apparent conversion of cyclohexane is found in the absence of initiator, implying the inert or inhibiting effect of catalysts due to the presence of activated carbon. We assume this behaviour is probably caused by the site blocking between active Ag sites and molecular of substrate, or the possible quench effect of activated carbon on radicals[27]. Additionally, tests with various M:S ratios (1:500, 1:200) also exhibits no reactivity for the oxidation of cyclohexane, furtherly clarifying that the

performance is not influenced by the amount of presented active species.

7.3.2 Tests in the presence of supported Ag/AC with *tert*-Butyl hydroperoxide (TBHP)

Hence, TBHP was also used as an initiator for the oxidation of cyclohexane in the presence of supported Ag/AC. In previous studies, TBHP was identified as an initiator in the free radical processes that enhanced the conversion with the presence of supported Au/MgO and AuPd/MgO[50, 51]. In this process, the K/A ratio is not altered but instead the formation of undesired products is enhanced. And according to the reaction results of Ag/AC in cyclooctane oxidation with TBHP, we are interested in the reactivity of Ag/AC with varied concentrations of TBHP for the oxidation of cyclohexane.

7.3.2.1 Tests in the presence of supported Ag/AC with 1 mol% of TBHP

Our results (Fig. 7.5), however, show that that there is still no conversion by supported Ag/AC with 1 mol% of TBHP and the catalysts system even acts as an inhibitor in comparison with blank tests. In view of this, the decomposition of TBHP to form reactive radicals and the activation of O_2 by Ag species is probably hindered due to the presence of activated carbon. Or it is possible that a low amount of generated radicals from TBHP decomposition due to the low concentration of initiator in reaction mixture is mainly consumed or trapped by activated carbon, leading to a no observed conversion.

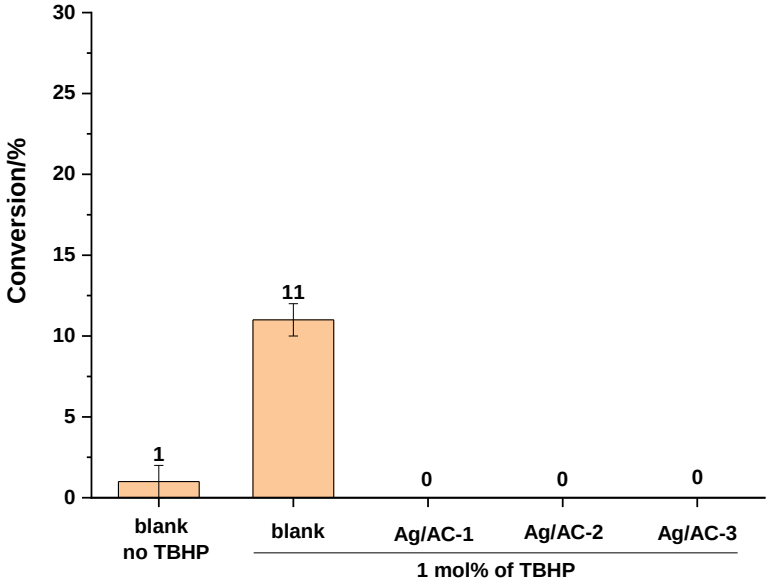

a. Conversion of cyclohexane in the presence of 1 mol% of TBHP

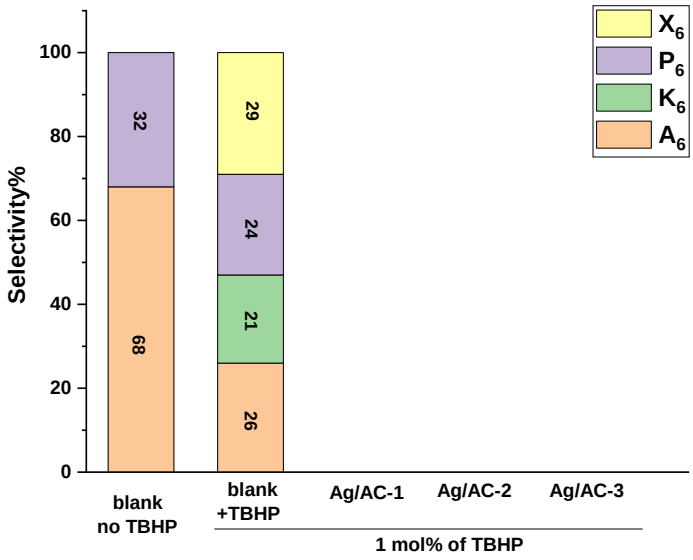

b. Product distribution of cyclohexane oxidation in the presence of 1 mol% of TBHP

Fig. 7.5 Cyclohexane oxidation by Ag/AC (1 *wt*%) prepared by wet impregnation method in the presence of 1 mol% TBHP. a: Conversion of cyclohexane; b: Product distribution for cyclohexane oxidation. Catalysts were calcined at 180 °C for 16 h. 3 mL cyclohexane was used. M:S = 1:1000, T = 120 °C, $P(O_2)$ = 4 bar, t = 24 h.

7.3.2.2 Tests in the presence of supported Ag/AC with 5 mol% of TBHP

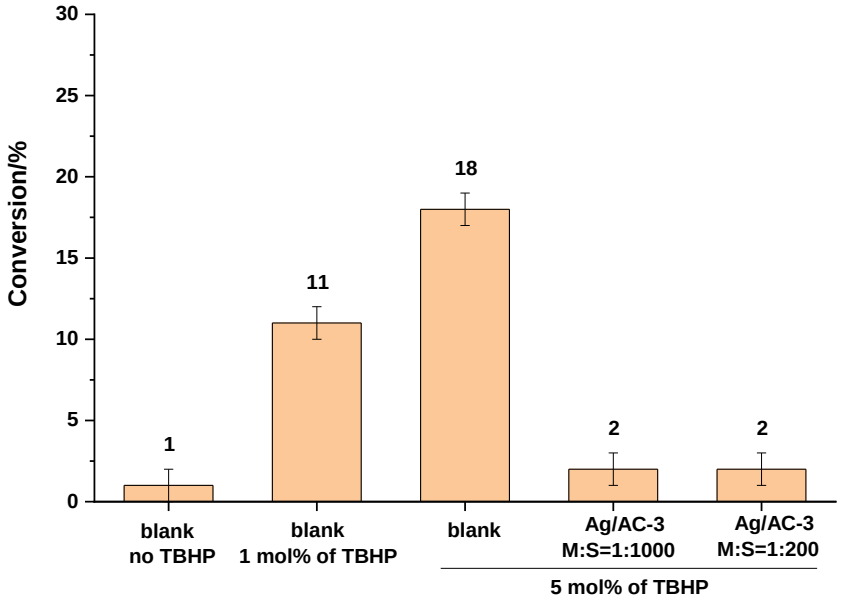

a. Conversion of cyclohexane in the presence of 5 mol% of TBHP

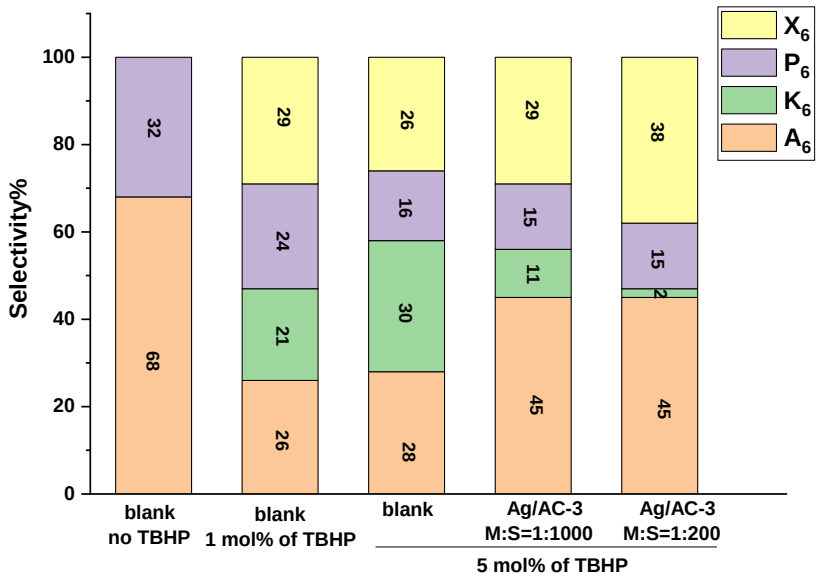

b. Product distribution of cyclohexane oxidation in the presence of 5 mol% of TBHP

Fig. 7.6 Cyclohexane oxidation by Ag/AC-3 (1 *wt*%) prepared by wet impregnation method in the presence of 5 mol% of TBHP. a: Conversion of cyclohexane; b: Product distribution for cyclohexane oxidation. Catalysts were calcined at 180 °C for 16 h. 3 mL cyclohexane was used. T = 120 °C, $P(O_2)$ = 4 bar, t = 24 h.

A higher concentration (5 mol%) of TBHP was utilised in the reaction system. As

can be seen from Fig. 7.6, the blank autoxidation was enhanced with the increase of TBHP concentration, and the product distribution implies that the oxidation path in the presence of initiator proceeds in an unselective way by following a radical mechanism with a K/A ratio close to 1.0. More importantly, there is observed conversion (~2%) of cyclohexane by Ag/AC-3 when increasing the concentration of TBHP from 1 mol% to 5 mol%, meaning that more reactive radicals from a high TBHP concentration is necessary to initiate the reaction with Ag/AC. Additionally, by comparing with blank tests in the presence of TBHP, supported Ag/AC plays a role inhibiting the oxidation. Whereas it should be noted that the selectivity for cyclohexanol is evidently improved with the decrease for cyclohexanone, suggesting that activated carbon might quench some radicals generated by the initiator leading to a low conversion, but meanwhile it promotes the O-O cleavage in TBHP decomposition, which results in a high selectivity for cyclohexanol. This behaviour is found in Au/MgO catalysts applied for cyclohexane oxidation[28]. Normally the amount of ketone is higher than that of alcohol with a K/A ratio slightly higher than 1.0 (below 1.5) in an autoxidation process, while the inverse trend of K/A ratio (obviously lower than 1.0) suggesting a catalytic process by Ag/AC[40].

To summarize this section, the oxidation of cyclohexane by Ag/AC can be enhanced with a high concentration of TBHP to generate more reactive radicals. The effect of activated carbon on oxidation can be reflected by two assumptions: i) inhibiting the oxidation by quenching radicals or acting as sites blocking to affect the interaction among active Ag sites and substrates; ii) O-O bond cleavage in TBHP is probably

promoted by activated carbon, leading to a high selectivity for cyclohexanol. Although a reasonable conversion of cyclohexane is not achieved by Ag/AC in our current research, a promising prospect is found to produce more cyclohexanol in a catalytically selective way with the presence of TBHP.

7.4 Conclusion

Based on unique textual and surface chemistry properties of activated carbon and its wide applications as support[18], the application of supported Ag over activated carbon prepared by wet impregnation method, towards the oxidation of cyclic hydrocarbons (cyclooctane, cyclohexane) was carried out. It was shown that the Ag/AC exhibits inert or inhibiting behaviour in the oxidation of cyclooctane in the absence of initiator and enhancement effect of $AgNO_3$ on cyclooctane oxidation for the generation of alkyl hydroperoxide seems to be hindered due to the presence of activated carbon. The addition of TBHP is proved to facilitate cyclooctane oxidation and an obvious conversion is only observed with the application of Ag/AC-1, implying that the reaction performance of Ag/AC tends to be influenced by the pores structure and particle size of activated carbon, which is possibly related with the interaction of active sites and substrates and diffusion process especially internal diffusion in the oxidation. A high concentration up to 5 mol% of TBHP is favoured to improve the conversion evidently with cyclooctanone and cyclooctanol as major products. Similar inert or inhibiting reaction behaviours of Ag/AC are observed in cyclohexane oxidation without initiator. An inhibiting effect is displayed with the addition of 1 mol% of TBHP in

comparing with the blank autoxidation in the presence of TBHP. This behaviour might be an implication that the presence of activated carbon can quench or trap the reactive radicals generated from TBHP decomposition to an extent or the interaction among active species and substrates are hindered. A higher concentration of 5 mol% TBHP can generate more reactive radicals in reaction system, thus the conversion of cyclohexane by Ag/AC-3 being improved. Although the conversion is still lower than that of blank tests with 5 mol% of TBHP, a trend for the production of cyclohexanol in excess of cyclohexanone is observed, suggesting a catalytic process with the participation of Ag/AC.

All in all, however, the results that we observe and the initiation effects that we detected are most likely due to an electrophilic addition of radical chain carries to the C=C double bonds that are present in large amount in a carbon matrix, which however would also indirectly prove that the oxidation mechanism is free-radical nature even if when Ag is used as an active metal species. We believe these are important consideration for the development of catalysts by design. Furthermore, different reaction behaviours are observed in comparison with Ag/Nb_2O_5, which furtherly demonstrates that Ag/Nb_2O_5 can be applied as an effective catalyst in hydrocarbons oxidation in the absence of initiator or other additives.

7.5 References

1. A. Pigamo, M. Besson, B. Blanc, P. Gallezot, A. Blackburn, O. Kozynchenko, S. Tennison, E. Crezee and F. Kapteijn, *Carbon*, 2002, **40**, 1267-1278.

2. I. Matos, M. Bernardo and I. Fonseca, *Catal. Today*, 2017, **285**, 194-203.

3. R. Schloegl, *Adv. Catal.*, 2013, **56**, 103-185.

4. Z. Li, D. Huang, R. Xiao, W. Liu, C. Xu, Y. Jiang and L. Sun, *Curr. Nanosci.*, 2012, **8**, 26-28.

5. S. Gil, L. Muñoz, L. Sánchez-Silva, A. Romero and J. L. Valverde, *Chem. Eng. J.*, 2011, **172**, 418-429.

6. S. Carabineiro, L. Martins, M. Avalos-Borja, J. G. Buijnsters, A. Pombeiro and J. Figueiredo, *Appl. Catal. A: Gen.*, 2013, **467**, 279-290.

7. G. Ertl, H. Knözinger and J. Weitkamp, *Handbook of heterogeneous catalysis*, VCH Weinheim, 1997, p 138-191.

8. M. Sadiq, M. Khan, M. Numan, R. Aman, S. Hussain, M. Sohail Ahmad, S. Sadiq, M. Abid Zia, H. Ur Rashid and R. Ali, *J. Chem.*, 2017, **2017**.

9. J. L. Figueiredo, M. F. Pereira, M. M. Freitas and J. J. Órfão, *Ind. Eng. Chem. Res.*, 2007, **46**, 4110-4115.

10. A. E. Aksoylu, M. Madalena, A. Freitas, M. F. R. Pereira and J. L. Figueiredo, *Carbon*, 2001, **39**, 175-185.

11. F. Coloma, A. Sepúlveda-Escribano, J. Fierro and F. Rodríguez-Reinoso, *Appl. Catal. A: Gen.*, 1997, **150**, 165-183.

12. E. Auer, A. Freund, J. Pietsch and T. Tacke, *Appl. Catal. A: Gen.*, 1998, **173**, 259-271.

13. E. A. Müller and K. E. Gubbins, *Carbon*, 1998, **36**, 1433-1438.

14. F. Rodriguez-Reinoso, *Carbon*, 1998, **36**, 159-175.

15. H. Boehm, *Carbon*, 1994, **32**, 759-769.

16. C. A. Wilde, Y. Ryabenkova, I. M. Firth, L. Pratt, J. Railton, M. Bravo-Sanchez, N. Sano, P. J. Cumpson, P. D. Coates and X. Liu, *Appl. Catal. A: Gen.*, 2019, **570**, 271-282.

17. M. A. Andrade and L. M. Martins, *Catalysts*, 2020, **10**, 2.

18. J. L. Figueiredo, M. Pereira, M. Freitas and J. Orfao, *Carbon*, 1999, **37**, 1379-1389.

19. A. R. Silva, V. Budarin, J. H. Clark, B. de Castro and C. Freire, *Carbon*, 2005, **43**, 2096-2105.

20. H. Jüntgen, *Fuel*, 1986, **65**, 1436-1446.

21. M. Iwanow, T. Gärtner, V. Sieber and B. König, *Beilstein journal of organic chemistry*, 2020, **16**, 1188-1202.

22. M. D. Argyle and C. H. Bartholomew, *Catalysts*, 2015, **5**, 145-269.

23. B. Nkosi, M. D. Adams, N. J. Coville and G. J. Hutchings, *J. Catal.*, 1991, **128**, 378-386.

24. M. Conte, A. F. Carley and G. J. Hutchings, *Catal. Lett.*, 2008, **124**, 165-167.

25. O. Ekpete and M. Horsfall, *Res. J. Chem. Sci.*, 2011, **1**, 10-17.

26. A.-Q. Wang, J.-H. Liu, S. Lin, T.-S. Lin and C.-Y. Mou, *J. Catal.*, 2005, **233**, 186-197.

27. J. Li, A. Zamyadi and R. Hofmann, *J. Water Supply: Res. Technol. - AQUA*, 2016, **65**, 28-36.

28. M. Conte, X. Liu, D. M. Murphy, K. Whiston and G. J. Hutchings, *Phys. Chem. Chem. Phys.*, 2012, **14**, 16279-16285.

29. M. Fraga, E. Jordao, M. Mendes, M. Freitas, J. Faria and J. Figueiredo, *J. Catal.*, 2002, **209**, 355-364.

30. A. J. Fletcher, Y. Yüzak and K. M. Thomas, *Carbon*, 2006, **44**, 989-1004.

31. Y. Liu, H. Zhang, Y. Dong, W. Li, S. Zhao and J. Zhang, *Mol. Catal.*, 2020, **483**, 110707.

32. A. Clearfield and D. S. Thakur, *J. Catal.*, 1980, **65**, 185-194.

33. S. A. Carabineiro, L. M. Martins, A. J. Pombeiro and J. L. Figueiredo, *ChemCatChem*, 2018, **10**, 1804-1813.

34. B. Li, P. He, G. Yi, H. Lin and Y. Yuan, *Catal. Lett.*, 2009, **133**, 33-40.

35. B. Li, X. Jin, Y. Zhu, L. Chen, Z. Zhang and X. Wang, *Inorganica Chim. Acta*, 2014, **419**, 66-72.

36. W. Adam and B. Nestler, *J. Am. Chem. Soc.*, 1993, **115**, 7226-7231.

37. R. Anumula, C. Cui, M. Yang, J. Li and Z. Luo, *J. Phys. Chem. C*, 2019, **123**, 21504-21512.

38. X. Liu, M. Conte, Q. He, D. Knight, D. Murphy, S. Taylor, K. Whiston, C. Kiely and G. J. Hutchings, *Chem. Eur. J.*, 2017.

39. C. Walling and L. Heaton, *J. Am. Chem. Soc.*, 1965, **87**, 38-47.

40. X. Liu, Y. Ryabenkova and M. Conte, *Phys. Chem. Chem. Phys.*, 2015, **17**, 715-731.

41. Y. F. Li, *Synlett.*, 2007, **2007**, 2922-2923.

42. G. S. Nunes, A. D. Alexiou and H. E. Toma, *J. Catal.*, 2008, **260**, 188-192.

43. Q. Zhang, Y. Wang, S. Itsuki, T. Shishido and K. Takehira, *J. Mol. Catal. A Chem.*, 2002, **188**, 189-200.

44. M. Conte, K. Wilson and V. Chechik, *Rev. Sci. Instrum.*, 2010, **81**, 104102.

45. O. Sodeinde, *Int. J. Chem. Eng. Appl.*, 2012, **3**, 67.

46. S. G. Huling, E. Kan and C. Wingo, *Appl. Catal. B: Environ.*, 2009, **89**, 651-658.

47. E. Kan and S. G. Huling, *Environ. Sci. Technol.*, 2009, **43**, 1493-1499.

48. E. V. Spinace, H. O. Pastore and U. Schuchardt, *J. Catal.*, 1995, **157**, 631-635.

49. C. Shi, B. Zhu, M. Lin, J. Long and R. Wang, *Catal. Today*, 2011, **175**, 398-403.

50. C.-C. Guo, M.-F. Chu, Q. Liu, Y. Liu, D.-C. Guo and X.-Q. Liu, *Appl. Catal. A: Gen.*, 2003, **246**, 303-309.

51. X. Liu, M. Conte, M. Sankar, Q. He, D. M. Murphy, D. Morgan, R. L. Jenkins, D. Knight, K. Whiston and C. J. Kiely, *Appl. Catal. A: Gen.*, 2015, **504**, 373-380.

Chapter 8: Conclusion and future work

This research work was centred on the preparation of novel supported nanoparticles catalysts for the selective oxidation of hydrocarbons to produce correspondingly desired products (alcohols or ketones) that are valuable building blocks for the industrial manufacture of fibres and plastics under a mild condition, i.e., low temperature (< 140 °C) and pressure below 10 bar. Given this purpose, the whole work has been carried out by involving the following aspects:

i) The qualitative and quantitative analysis for reaction mixture: a calculation method for conversion and selectivity of cyclooctane and cyclohexane oxidation by using ^{1}H-NMR was developed and verified by a close carbon mass balance within experimental error and GC-MS (discussed in chapter 3).

ii) Investigation about the effects of reaction conditions (temperature and O_2 pressure) on cyclooctane/cyclohexane oxidation with or without the presence of catalysts to determine proper conditions for the tests of catalysts and study about the autoxidation process as a benchmark, e.g., cyclooctane oxidation was conducted at 110 °C for 24 h at 2 bar O_2 (chapter 5), cyclohexane oxidation was carried out at 120 °C for 24 h at 4 bar O_2 (chapter 6).

iii) As Nb_2O_5 displays unexpected reactivity in the oxidation of cyclooctane without the addition of initiator, a systematic study about the catalytic reactivity of Nb_2O_5 in cyclooctane oxidation was conducted to investigate about the active species in Nb_2O_5 (Nb-O-Nb or other components in the parent Nb_2O_5), by which the reactivity of Nb_2O_5

was verified for this oxidation process, providing a useful background for the development of novel materials in hydrocarbons oxidation, which was also essential to discriminate the catalytic activity between supported metal nanoparticles (in our case it was Ag) and Nb_2O_5 when employing Nb_2O_5 as a support for the concept of catalyst design and mechanism study.

iv) With the validation of catalytic reactivity of Nb_2O_5 in cyclooctane oxidation by facilitating the decomposition of alkyl hydroperoxides, which is not previously reported about this effect, supported metal (mainly Ag with the incorporation of Fe) over Nb_2O_5 was designed for hydrocarbons oxidation accordingly. The catalysts exhibited a superior catalytic reactivity in the oxidation of cyclooctane and cyclohexane for the production of ketones and alcohols, especially for ketones (~60% selectivity for cyclooctanone in cyclooctane oxidation), suggesting a potential application in this field. Meanwhile, a structure activity relationship was established based on the studies about the properties of supported metal nanoparticles, e.g., metal loading, particle size, oxidation state of metal particles, by using characterization techniques like XRPD, TEM, XPS, ICP-MS.

To be specific, through a thorough studies about the catalytic reactivity of Nb_2O_5 in the oxidation of cyclooctane with a trend to produce alcohols and ketones, it was concluded that Nb_2O_5 was truly reactive in this reaction. Different media (1M HCl, concentrated HNO_3 and hot water) were utilised to abstract the possible filtrates that might take part in the oxidation process and the components in these filtrates were

analysed by ICP-MS. In addition, the possible existence of other components in the parent cyclooctane was investigated by conducting the oxidation of pretreated cyclooctane with $MgSO_4$ and 3A molecular zeolite (removed alkyl hydroperoxides and water if existed) in the presence of Nb_2O_5. Based on these control tests, the effect of other components from the parent Nb_2O_5 and cyclooctane was excluded, confirming the catalytic activity of Nb_2O_5 in cyclooctane oxidation. By the characterization using XPRD and XPS, Nb_2O_5 displayed a high stability by resisting the acid attack, and Nb element in Nb_2O_5 mainly existed in the state of Nb^{5+} instead of Nb^{4+}, ruling out the effect of Nb^{4+} species. Moreover, the decomposition of 1-phenylethyl hydroperoxide with the presence of Nb_2O_5 implied that Nb_2O_5 participated in the decomposition process of alkyl hydroperoxides. These findings suggest a potential application of Nb_2O_5 in the oxidation of hydrocarbons, which attracts limited attention before, and a sufficient understating is to be explored.

Based on the investigation about the identification of catalytic activity with Nb_2O_5, a novel supported metal material was developed and applied in the oxidation of hydrocarbons in our case, which hasn't been reported in previous research. That was, supported Ag over Nb_2O_5 prepared by using different methods (wet impregnation, deposition precipitation and sol immobilization) were applied in the oxidation of cyclooctane and cyclohexane. A synergistic effect between Ag/Ag_2O particles and Nb_2O_5 was found, by which the conversion of cyclooctane was largely enhanced (~81%) in comparison with blank autoxidation (~6%) and the selectivity for

cyclooctanone was improved obviously (~60%). These reaction results implied a promising application of Ag/Nb_2O_5 catalyst system in the oxidation of hydrocarbons for the formation of alcohols and ketones, especially for ketones, both of which are valuable precursors for the manufacture of materials like nylon or fibres. Moreover, the investigation for the identification of roles of Ag species and Nb_2O_5 in the reaction pathway pointed that Ag species (Ag^0, Ag_2O, Ag^+) were capable of activating molecular oxygen to give superoxide species that were bound to metal centres or metal oxide to abstracting H atoms from hydrocarbons to initiate the oxidation, or Ag^+ played a role as an initiator for the dissociation of C-H, as evidenced that the isolated Ag^+ in Ag/Y or Ag/ZSM-5 reacted with CH_4 to a CH_3-zeolite complex and silver hydride species for the activation of CH_4[1, 2]. The formed intermediate alkyl hydroperoxides after the initiation step can be decomposed by Nb_2O_5 to give alcohols and ketones. It should be stressed that the decomposition of O-O bond in alkyl hydroperoxides can generate alcohols[3, 4], which was likely to be related with Nb_2O_5, while the abstraction of α-H from alkyl hydroperoxides would give ketone[3, 4], which was enhanced in the presence of Ag(0) in catalysts, as it was observed that cyclooctyl hydroperoxide was the major products in the control tests by using solid $AgNO_3$ or Ag_2O while Ag/Nb_2O_5 favoured to produce cyclooctanone. Meanwhile, XPS justified that supported Ag in WI-Ag/Nb_2O_5 prepared by wet impregnation method mainly exited in the state of Ag(0), verifying the high selectivity for ketone was due to the presence of Ag(0) compared with the tests with Ag^+ ($AgNO_3$ or Ag_2O). Moreover, given the different reaction performances of Ag/Nb_2O_5 prepared by various methods, that was, a relatively lower conversion in

cyclooctane oxidation by DP- and SI-Ag/Nb_2O_5 (~68%) in comparison with WI-Ag/Nb_2O_5 (~81%) and no obviously observed catalytic activity by DP- and SI- catalysts while a 13% conversion was observed by WI-Ag/Nb_2O_5 as comparison in the oxidation of cyclohexane, we ascribed this result to a higher Ag loading in WI-Ag/Nb_2O_5 that was directly evidenced by TEM images and the existence of Ag^+ in WI-Ag/Nb_2O_5 that was verified by XPS and TEM analysis, which resulted in a higher reactivity by using WI-Ag/Nb_2O_5 in the oxidation of cyclooctane and cyclohexane. In addition, it should be noted that WI-Ag/Nb_2O_5 preserved a high stability with a very low Ag leaching (0.01%) in cyclohexane oxidation at the same time, suggesting a potential development in this reaction. Based on this, supported bimetallic catalysts based on Ag by incorporating Fe over Nb_2O_5 was developed for cyclohexane oxidation. Although the conversion remained unchanged (~13%) within the experimental error when using WI-Ag-Fe/Nb_2O_5 prepared by wet impregnation method, the selectivity for cyclohexanone was improved with the addition of Fe and this selectivity rise with the increase of Fe amount, indicating that the presence of Fe species was capable of enhancing the formation of cyclohexanone from the decomposition cyclohexyl hydroperoxide. Meanwhile, ICP-MS analysis results displayed a low leaching of Ag (0.01%) and Fe (0.002%), implying a high stability to resist the loss of active metals. Thus, a bifunctional catalyst was developed in our research for the selective oxidation of cyclohexane. Given these premises we consider our catalyst to be a promising application in the oxidation of hydrocarbons, or it can be paved for the oxidation of alcohols beyond this study.

Ultimately, to the best of our knowledge, this is the first time that supported Ag/Nb_2O_5 was applied in the oxidation of hydrocarbons. Given the reaction results with a trend for the production of alcohols and ketones, especially ketones, as important building blocks for the industrial production of plastic or fibres and the investigation to provide insight into the roles of active species (Ag^0, Ag^+, Nb_2O_5) in the oxidation process, a promising application of this catalyst is illustrated in the oxidation of hydrocarbons in the absence of initiator or other additives.

Furthermore, future work of this project can involve the aspects: i) a more clear and thorough identification of active species (Ag^+, Ag, Fe^{2+}/Fe^{3+}, Nb_2O_5) in Ag/Nb_2O_5 or $Fe\text{-}Ag/Nb_2O_5$ and investigation about their effects on the oxidation of hydrocarbons for the reaction mechanism clarification and catalyst design; ii) apply the catalysts (Ag/Nb_2O_5, $Ag\text{-}Fe/Nb_2O_5$) we developed into the oxidation of other hydrocarbons (e.g., ethylbenzene, ethylene) or alcohols; iii) design of supported silver-based catalysts by incorporating second metals for the preparation of bimetallic catalysts or selecting new economical supports, and then test their reactivity in the oxidation of hydrocarbons (cyclohexane, ethylbenzene) in comparison with the catalysts we have developed; iv) synthesize porous Nb_2O_5 or other metal oxides and explore their reactivity in the oxidation of hydrocarbons when using as active phase or support[5].

Reference

1. T. Baba, H. Sawada, T. Takahashi and M. Abe, *Appl. Catal. A: Gen.*, 2002, **231**, 55-63.

2. S. Miao, Y. Wang, D. Ma, Q. Zhu, S. Zhou, L. Su, D. Tan and X. Bao, *J. Phys. Chem. B*, 2004, **108**, 17866-17871.

3. B. P. Hereijgers and B. M. Weckhuysen, *J. Catal.*, 2010, **270**, 16-25.

4. M. Conte, X. Liu, D. M. Murphy, K. Whiston and G. J. Hutchings, *Phys. Chem. Chem. Phys.*, 2012, **14**, 16279-16285.

5. J. C. Rooke, T. Barakat, S. Siffert, B. L. Su,T, *Catal. Today*, 2012, **192**, 183-188.